Doctoral theses at NTNU, 2013:33

Songwut Krasae-in

Efficient Hydrogen Liquefaction Processes

NTNU – Trondheim
Norwegian University of
Science and Technology

Doctoral Thesis

Songwut Krasae-in

NTNU
Norwegian University of Science and Technology
Thesis for the degree of Philosophiae Doctor
Faculty of Engineering Science & Technology
Department of Energy and Process Engineering

Doctoral theses at NTNU, 2013:33

NTNU

NTNU – Trondheim
Norwegian University of
Science and Technology

ISBN 978-82-471-1869-6 (printed version)
ISBN 978-82-471-1871-9 (electronic version)
ISSN 1503-8181

Songwut Krasae-in

Efficient Hydrogen Liquefaction Processes

Thesis for the degree of Philosophiae Doctor

Trondheim, January 2013

Norwegian University of Science and Technology
Faculty of Engineering Science & Technology
Department of Energy and Process Engineering

NTNU – Trondheim
Norwegian University of
Science and Technology

NTNU
Norwegian University of Science and Technology

Thesis for the degree of Philosophiae Doctor

Faculty of Engineering Science & Technology
Department of Energy and Process Engineering

ISBN 978-82-471-1869-6 (printed version)
ISBN 978-82-471-1871-9 (electronic version)
ISSN 1503-8181

Doctoral theses at NTNU, 2013:33

Printed by Skipnes Kommunikasjon as

Preface

This dissertation is a result of a doctoral study carried out at the Department of Energy and Process Engineering (EPT), Faculty of Engineering Science and Technology, Norwegian University of Science and Technology (NTNU), during the period October 2006−January 2013.

I would like to thank my advisor, Professor Dr. *Arne M. Bredesen* at the EPT, NTNU, for all assistance during the doctoral study.

Trondheim, Thailand

January 2013

Songwut Krasae-in

II

Summary and conclusions

1. MOTIVATION AND OVERVIEW

Hydrogen is considered to be an alternative future energy carrier that can potentially facilitate the transition from fossil fuels to sources of clean energy because of its advantages such as: high energy density, variety of potential sources (for example water, biomass, organic matter), light weight, and especially low environmental impact (water is the sole combustion product). There are no CO_2 emissions from hydrogen vehicles. Therefore, irreversible global warming and climate changes would be reduced.

Hydrogen can be produced from several sources and methods both centrally and locally. In large-scale production, then, it must be distributed via several ways to storages before the end use. In some applications, liquid hydrogen is needed and transported to, e.g., hydrogen stations.

However, there remains a challenge that today efficiencies of liquefaction plants still need to be improved so that the cost of efficient and sustainable hydrogen production must be significantly reduced. Thus, the Scandinavian Research Foundation (SINTEF) Energy Research AS initials and proposes a Multi-component Refrigerant (MR) cycle as a potential system to liquefy hydrogen for large-scale efficiently; the company has a previous experience to use this MR cycle to liquefy natural gas. The author worked with this research group.

The main purpose of this dissertation work was to investigate both simulation and experiment of a small-scale laboratory MR hydrogen liquefaction plant. First, the simulation was done with a simplified 5-component composition and later with more complex 10-component composition. Next, initial experiment was performed with a measured simplified 5-component composition to compare the results with simulation data. Finally, a simulated 100 ton-per-day (TPD) liquid hydrogen large scale plant utilizing MR refrigeration system was proposed. All simulation was done by using PRO/II. In addition, a simple economic analysis of the proposed large-scale plant was also done to consider the new MR heat exchanger sizes and all compressor swept volumes and the sizes.

In summary, even though there are some little differences between simulation data and experimental data of the test rig, but they go the same direction. Then, the simulation of the

proposed large-scale plant is proposed by using the same simulation package that is done with simulation of the test rig. The trend is that the system has a high overall plant efficiency among others with possibility of smaller plant size and lower construction cost especially when comparing to current plants, e.g., at Ingolstadt and Leuna.

2. THE OBJECTIVES

Experiment:
1. To build the small-scale hydrogen liquefaction prototype that is based on multi-component refrigerant configuration.
2. To do experiment to evaluate the cycle: optimization of parameters to find method to maximize performance such as, both MR low and high side pressures, the MR charge, MR composition, setting of expansion valve, superheating, pinch temperatures, etc.
3. To do experiment to find the lowest reach attainable temperature at MR cycle to cool hydrogen gas.

Simulation:
1. A small-scale laboratory multi-component refrigerant (MR) hydrogen liquefier:
   a) To do exergy analysis to find the losses and to optimize the test rig.
   b) To find the optimized MR composition for the test rig.
   c) To compare simulation data to experimental data and to provide information on sizing the system components for maximum performance.
2. A large-scale MR hydrogen liquefaction plant:
   a) To find the right configuration for the best efficient cycle and to compare the performance of the system with other today conventional cycles.
   b) To find the optimized MR composition for the large-scale plant.
   c) To find the source of performance degradation (exergy analysis) in each component to minimize the irreversibility.

3. ABSTRACT

The problem is that today every H_2 liquefaction plant has low exergy efficiency of just between 20–30%. It is based on the pre-cooled Claude system, which is still the same as 50 years ago with little improvement. Method to resolve the challenges of the future plants is finding a completely new configuration with more efficient system. For this dissertation, a multi-component refrigerant (MR) refrigeration cycle is proposed to solve the problem. The work is divided into four parts: a literature review, a design and simulation of a small-scale laboratory plant, an experiment with the small plant, and a design and simulation of a proposed large-scale plant. First, this study investigated the simulation of a newly proposed small-scale laboratory liquid hydrogen plant with the new, innovative MR refrigeration system. The simulated test rig was capable of liquefying a feed of 2 kg/h of normal hydrogen gas at 21 bar and 25 ^{o}C to normal liquid hydrogen at 2 bar and −250 ^{o}C. The simulated power consumption for pre-cooling the hydrogen from 25 ^{o}C to −198 ^{o}C with this new MR compressor was 2.07 kWh/kg_{GH2}. This was the lowest power consumption available when compared to today's conventional hydrogen liquefaction cycles, which are approximately 4.00 kWh/kg_{GH2}. Exergy analysis of the test rig's cycle, which is required to find the losses and optimize

the proposed MR system, was evaluated for each component using the simulation data. It was found that the majority of the losses were from the compressors, heat exchangers, and expansion valves. Then, a small-scale laboratory hydrogen liquefaction plant that contains the new innovative MR refrigeration system was constructed to verify the simulation of this system. Initial experiments indicated that the rig was able to adequately cool normal hydrogen gas from 25 ^{o}C to −158 ^{o}C at a flow rate of 0.6 kg/h using a simplified 5-component MR composition refrigeration system. The power consumption of pre-cooling from the MR compressor was 1.76 kWh per kilogram of feed hydrogen gas. After two weeks, the lowest attained temperature was about −180 ^{o}C when a few additional grams of nitrogen gas were charged into the rig. There were some differences, but most of all, the simulation and experimental data were in good agreement. The primary conclusion was that pre-cooling hydrogen gas with the MR refrigeration system resulted in a lower energy consumption per kilogram of feed hydrogen gas compared to conventional refrigeration systems. Finally, a liquid hydrogen plant based on the MR refrigeration system is proposed. A cycle that is capable of producing 100 tons of liquid hydrogen per day is simulated. The MR system can be used to cool feed normal hydrogen gas from 25 ^{o}C to the equilibrium temperature of −193 ^{o}C with a high efficiency. In addition, for the transition from the equilibrium temperature of the hydrogen gas from −193 ^{o}C to −253 ^{o}C, a new proposed four H_2 Joule-Brayton cycle refrigeration system with optimization is recommended. The overall power consumption of the proposed plant for the based case is 5.91 kWh/kg_{LH2}. The current plant in Ingolstadt is used as a reference, which has an energy consumption of 13.58 kWh/kg_{LH2} and an efficiency of 21.28%. The efficiency of the proposed system is around 50% or more, where this depends on the assumed efficiency values for the compressors and expanders, together with effectiveness of heat exchangers. Importantly, the variables and constraints are preliminary studied together with how to adjust these to achieve optimal steady-state operation. The optimization problem has 23 variables and 26 constraints. A simplified 5-component composition of refrigerant suggested for the plant is found. The plant optimization was also conducted with two more pinch temperatures (1 and 3 ^{o}C). Power savings is increased with a pinch temperature of 1 ^{o}C as compared to 3 ^{o}C. This figure can have a significant impact on plants selection. In addition, pressure drops in heat exchangers are also employed in the simulation for the study, however it is shown that they don't have much significant impact on the overall plant total power consumption. The proposed system has smaller compressor motors and smaller crankcase compressors; thus, it could represent a plant with the lowest construction cost with respect to the amount of liquid hydrogen produced in comparison to today's plants, e.g., in Ingolstadt and Leuna. Therefore, the proposed system has many improvements that serves as an example for future hydrogen liquefaction plants.

4. MAIN ACHIEVEMENTS

Experiment:

1. The test rig was successfully built by a team at SINTEF Energy AS. From preliminary test run, the lowest reach attainable temperature at MR cycle was discovered to cabably cool hydrogen gas down to -180 ^{o}C. It is believed that if more volatile components such as nitrogen and hydrogen exist in the composition, the lowest reach temperature might be down to approximately -190 ^{o}C.
2. Some issues were found in order to find method to maximize performance such as, both MR low and high side pressures (2 and 18 bar), the MR charge, MR composition (4% neon (or 4%

hydrogen with the same result), 18% nitrogen, 24% methane, 28% ethane, and 26% butane by mole), setting of expansion valves, superheating (10 ^{o}C), pinch temperatures (3-10 ^{o}C), etc.
3. The primary conclusion was that pre-cooling hydrogen gas down to -193 ^{o}C with the MR refrigeration system resulted in a lower energy consumption (1.76 kWh/kg$_{LH2}$) compared to the conventional refrigeration system (4.86 kWh/kg$_{LH2}$).

Simulation:
1. The test rig:
   a) Exergy analysis was performed to find the losses that were from the compressors, heat exchangers, and expansion valves respectively.
   b) The optimized MR composition for the test rig was found that more volatile components such as nitrogen, neon, or hydrogen must exist in order to capably obtain the lowest reach temperature.
2. The large-scale plant:
   a) The optimized MR composition (4% hydrogen, 18% nitrogen, 24% methane, 28% ethane, and 26% butane by mole) for the large-scale plant was found that it should be designed according to the hydrogen gas pre-cooling curve.
   b) The right configuration recommended (MR cycle in combination with the four Joule-Brayton hydrogen cycles) for the best efficient cycle (5.98 kWh/kg$_{LH2}$) was found and compared to the today conventional cycle (Ingolstat at 13.58 kWh/kg$_{LH2}$).

5. MAIN FINDINGS AND RELATIONS AMONG THE FOUR CHAPTERS

The research project was complete with results in four chapters containing inside this dissertation. Below are the main findings and logical explanation to describe the links and relations among the four chapters:

CHAPTER 1: *Development of large-scale hydrogen liquefaction processes from 1898 to 2009*. This "CHAPTER 1" was literature survey to do before other papers. Importantly, Fig. 1.7, *Comparison of hydrogen liquefaction process efficiencies*, depicts a summary and comparison of the process efficiencies around the world, including the new proposed MR system. In this Fig. 1.7, simulation result about the efficiency of the proposed large-scale MR cycle coupled with the four hydrogen Joule-Brayton (J-B) cycles from "CHAPTER 4" is included in this "CHAPTER 1".

CHAPTER 2: *Exergy analysis on the simulation of a small-scale hydrogen liquefaction test rig with a multi-component refrigerant refrigeration system*. This is a design and optimization work of the test rig before doing experiment as described on "CHAPTER 3". This paper is very close related to "CHAPTER 3". Simulation data of the MR 5-component composition in Table 2.3, *Thermodynamic properties of each stream: enthalpy, entropy, specific exergy, and exergy flow of the proposed simplified 5-component composition*, shown on "CHAPTER 2" is the same as Fig. 3.3, *PRO/II simulation flow-sheet of the proposed 5-component composition*, found on "CHAPTER 3". It was found that the majority of the losses were from the compressors, heat exchangers, and expansion valves. About designing a large-scale system as on "CHAPTER 4", the idea of exergy analysis recommended in the last part (Section 2.4.2, *Comments on how to reduce exergy loss in each component)* of this "CHAPTER 2" is also used to reduce the exergy loss in each component of the large-scale system found on "CHAPTER 4".

CHAPTER 3: *Simulation and experiment of a hydrogen liquefaction test rig using a multi-component refrigerant refrigeration system*. After designing and optimizing work of the test rig on "CHAPTER 2", this "CHAPTER 3" is simulation and initial experiment of the rig. The data of design conditions for the test rig shown in Table 3.1, *Assumptions in the simulation model*, on "CHAPTER 3" are exactly the same as that in Table 2.1, *Boundary conditions of the test rig's simulation*, on "CHAPTER 2". The differences are that: "CHAPTER 2" is only pre-design, hydrogen flow rate in experiment is only 0.6 kg/h instead of 2.0 kg/h, the measured simplified 5-component composition consists of: 1% neon, 10% nitrogen, 33% methane, 38% ethane, and 18% butane instead of the optimized by simulation on "CHAPTER 2": 4% neon (or 4% hydrogen with similar result), 18% nitrogen, 24% methane, 28% ethane, and 18% butane. Moreover, there are other differences, between the pre-design simulation data found in "CHAPTER 2" and the experimental data, which are explained in Section 3.5.1, *Comparison of the experimental data to the simulation data*, on "CHAPTER 3". There were some differences, but most of all, the simulation and experimental data were in good agreement. This means the PRO/II simulation package can be used to verify or simulate experimental data quite well. The main discovery was that pre-cooling hydrogen gas with the MR refrigeration system resulted in a lower energy consumption compared to conventional refrigeration systems. At last, expansion on "CHAPTER 3" about small-scale laboratory plant is "CHAPTER 4" regarding the design of the future large-scale plant.

CHAPTER 4: *Simulation on a proposed large-scale liquid hydrogen plant using a multi-component refrigerant refrigeration system*. After experiencing in simulation and experiment of the small-scale plant as on "CHAPTER 3" that the trend of both simulation and experimental data go the same direction, this "CHAPTER 4" is the proposed large-scale plant with MR refrigeration system. The large-scale MR cycle is modified from small-scale MR process from the test rig described on "CHAPTER 3". The differences which can be noticed the changes from Fig. 3.9, *Simulation data of the laboratory test rig with the proposed simplified composition compared to the experimental data*, on "CHAPTER 3" to be Fig. 4.2, *PRO/II simulation flow sheet for the new modified proposed large-scale 100-TPD LH_2 plant utilizing MR and four hydrogen Joule-Brayton refrigeration cycles,* on "CHAPTER 4". Those are: ortho-para catalysts are included for ortho-para hydrogen gas conversion, single-stage to be two-stage compression to reduce power consumption, and expansion valves are replaced by expanders to reduce exergy losses. In addition, simple helium system or heat exchanger (HX5 of Fig. 3.9 on "CHAPTER 3") is replaced by the four hydrogen Joule-Brayton cycles. The simulation of the proposed large-scale plant is by using the same simulation package, PRO/II that is done with simulation of the test rig found on "CHAPTER 3". The new, optimized MR has been particularly modified for large-scale process with heat conversion by catalysts; and it has a simplified composition. The idea of exergy analysis from "CHAPTER 2" is also performed here for the analysis of the large-scale on "CHAPTER 4". It is still the same that compressors are the main components that cause greatest exergy losses. By simulation, due to substantial reduction of energy consumption compared to conventional refrigeration cycles, the new process is recommended as the future hydrogen liquefaction plant.

4. SUGGESTIONS FOR FURTHER WORK

This dissertation contains only an initial experiment of the test rig together with a preliminary design and optimization of a proposed cycle of large-scale LH_2 plant. It paves the foundation that there are a lot of works for researchers or other Master, PhD, and Post-doc students still need to be done in the future, e.g.: (1) more experiment of the proposed 5−10 component composition of MR cycle to verify the lowest attainable temperature to $-198\ ^{o}C$; (2) maybe, a research to invent a new accurate equation of state or some correction to replace Redlich-Kwong-Soave (SRK) model for simulation thermophysical data in PRO/II of the temperature below $-200\ ^{o}C$; (3) finding new more efficient cycle; (4) computer simulation work deep inside about optimization of the new more efficient cycle; (5) the theory about heat transfer and pressure drop to design MR heat exchangers (Plate-fin, Coil-wound, or Spiral-wound); and (6) dynamic modeling and control of process plant.

Finally, a single MR cycle with varied refrigerant compositions in combination with 1-5 H_2/Helium J-B cycles would also be utilized to efficiently liquefy other common industrial gases such as oxygen, argon, carbon dioxide, xenon, nitrogen, neon, and helium. All shall be further research works.

5. THE FOUR PUBLISHED PAPERS

The lastest part of dissertation is Appendix which contains the four published papers as follows:

Krasae-in S, Stang J, Neksa P. Development of large-scale hydrogen liquefaction processes from 1898 to 2009. Int J Hydrogen Energy 2010;35(10):4524-33.

Krasae-in S, Stang J, Neksa P. Exergy analysis on the simulation of a small-scale hydrogen liquefaction test rig with a multi-component refrigerant refrigeration system. Int J Hydrogen Energy 2010;35(15):8030-42.

Krasae-in S, Bredesen A, Stang J, Neksa P. Simulation and experiment of a hydrogen liquefaction test rig using a multi-component refrigerant refrigeration system. Int J Hydrogen Energy 2011;36(1):907-19.

Krasae-in S, Stang J, Neksa P. Simulation on a proposed large-scale liquid hydrogen plant using a multi-component refrigerant refrigeration system. Int J Hydrogen Energy 2010;35(22):12531-44.

Table of contents

Chapter 1. Development of large-scale hydrogen liquefaction processes from 1898 to 2009

This chapter presents a review of the development of large-scale hydrogen liquefaction processes throughout the world from 1898 to 2009. First, there is a concise literature review including numerous past, present, and future designs is given: such as the first hydrogen liquefaction device, long time ago simple theoretical processes, today actual plants with efficiencies 20–30%, a list of the capacity and location of every hydrogen liquefaction plant in the world, and some today more efficient proposed conceptual plants with efficiencies 40–50%. After that, further information about the development and improvement potential of future large-scale liquid hydrogen liquefaction plants is explained. It is found that every current plant is based on the pre-cooled Claude system, which is still the same as 50 years ago with little improvement. Methods to resolve the challenges of the future plants include proposing completely new configurations and efficient systems coupled with improved efficiencies of the main system components such as compressors, expanders, and heat exchangers. Finally, a summary and comparison of the processes' efficiencies are described, including a newly proposed multi-component refrigerant system being developed by NTNU and SINTEF Energy Research AS.

1.1. Introduction

As hydrogen has shown promise as an important energy source for use in future transportation vehicles, several hydrogen research activities have been conducted since 1980 and especially since 2000. One of the challenges in creating a hydrogen economy is the low efficiencies of the current hydrogen liquefaction plants' cycles. Since 2000, there have been several papers that have proposed conceptual plants with efficiencies up to 40–50% (Kuendig *et al* 2006; Matsuda and Nagami 1998; Quack 2002; Kuz'menko *et al* 2004; Stang *et al* 2006; Shimko and Gardiner 2007; and Valenti and Macchi 2008). This chapter chronicles the development of systems from 1898 to 2009 and gives a comparison of several cycles' efficiencies for the future hydrogen plant developer. Hydrogen was first liquefied in 1898 by a small device (Dewar, 1898). Some years later, a pre-cooled Linde-Hampson system was used as the first simple laboratory system to liquefy hydrogen. Around 1900, more efficient laboratory systems were invented including the

Claude, pre-cooled Claude, and helium refrigerated systems, arranged in order of increasing efficiency (Barron, 1966). Next, in 1957, the first few large hydrogen plants were built in the US for the growing petrochemical and aerospace industries and were based on the pre-cooled Claude cycle with more complicated systems that used liquid nitrogen as a pre-coolant to cool hydrogen gas down to −193 °C and hydrogen refrigeration systems to further cool feed hydrogen gas to −253 °C for the large scale. Up to the present, almost all of the large-scale plants in use across the world today still employ nearly the same cycle as the first few plants built in the US and have exergy efficiencies of just 20–30%. This can be seen in the Ingolstadt plant installed in Germany in 1991 (Bracha *et al*, 1994). Today, the most technologically advanced plants available in the literature are located in Leuna, Germany, and near Tokyo, Japan, were commissioned in 2008; however, only a slight improvement of efficiency was realized. Thus, there is potential to improve.

1.2. Simple hydrogen liquefaction processes

Barron (1966) illustrated the fundamental principles and how these simple processes work very well.

1.2.1. The first hydrogen liquefaction system

In 1885, Michael Faraday published a paper regarding gas liquefaction. At that time, his method was able to achieve refrigeration temperatures down to −110 °C using baths of ether and solid carbon dioxide. Gases with boiling points below that temperature, including hydrogen, were called “permanent gases” (Foerg, 2002). For the first time, the liquefaction of hydrogen was achieved by Sir James Dewar in 1898 (Dewar, 1898). This process utilized carbolic acid and liquid air for pre-cooling compressed hydrogen at 180 bar. The system was similar to the one that Linde used for the liquefaction of air.

1.2.2. Theoretical liquefaction systems for hydrogen

In 1895, Carl von Linde and William Hampson invented a simple liquefaction cycle to liquefy air. This cycle is called the “Linde-Hampson cycle”. However, according to what was explained by Barron (1966), the systems that cannot be used to liquefy hydrogen are the Linde-Hampson, Linde dual-pressure, Cascade, and Heylandt systems. A liquid nitrogen, pre-cooled Linde-Hampson system can be used to liquefy hydrogen. The cycle is shown schematically in Barron (1966).

1.2.3. Theoretical Claude system for hydrogen

In addition to liquefying air, the Claude cycle invented by Georges Claude in 1902 can also be used to liquefy hydrogen (Barron, 1966). This cycle was a development some years after the first Linde-Hampson cycle. There was an expansion engine in the Claude cycle, which produced a temperature much lower than the temperature generated by isenthalpic expansion as proposed by Linde.

1.2.4. Theoretical pre-cooled Claude system for hydrogen

The performance is somewhat improved if a pre-cooling bath of liquid nitrogen is used with the Claude system. Timmerhaus and Flynn (1989) explained that if liquid nitrogen is used for pre-cooling, one could achieve an exergy efficiency 50–70% higher than a pre-cooled Linde-Hampson cycle. Nandi and Sarangi (1993) made a comparison of the two cycles and found that the typical Figure of Merit (FOM) for the pre-cooled Linde-Hampson cycle was lower than the standard pre-cooled Claude. The Claude cycle, as explained by Nandi and Sarangi (1993), is the basis for most other conventional liquefaction cycles. An example of a modified pre-cooled Claude cycle in use today is the hydrogen liquefaction plant in Ingolstadt near Munich, Germany, as shown in Fig. 1.2, which has been in operation since 1992 (Bracha *et al*, 1994).

1.2.5. Helium-refrigerated hydrogen-liquefaction system

A secondary helium-gas refrigerator can also be used to liquefy hydrogen, as shown in Nandi and Sarangi (1993) together with Barron (1966), but this system has never been used in any actual large-scale plants.

1.3. Current plants

Table 1.1 shows a list of all of the hydrogen liquefaction plants in use around the world. In 1960, the first few liquid hydrogen plants were built to support the Apollo program. The beginning of the sixties was the demand for the US space programs. The capacity installed up to 1965 was capable of supplying the demand of NASA and others until 1977. In this period, no additional plants were built, not least because of the reduction of NASA's space activities. In 1977, this time was mainly caused by the steadily increasing commercial demand for liquid hydrogen. Today, there are more than 9 hydrogen liquefaction plants in the US with production rates of 5 to 34 ton, 4 plants in Europe with capacities of 5 to 10 TPD, and 11 plants in Asia with capacities of 0.3 to 11.3 TPD. Air Products supplies the largest liquid hydrogen capacity in North America, followed by Praxair. Today, liquid hydrogen is used to reduce the cost of hydrogen distribution (Drnevich, 2003); however, the current worldwide liquid hydrogen (LH_2) production capacity exceeds the market demand. Liquid hydrogen demand and production today is the largest in North America, which constitutes 84% of the world production. Of the total production in the US, 33.5% is used in the petroleum industry, 18.6% is for government aerospace, and the rest is for other industries. Only 0.1% is used for fuel cells today (Franser, 2003).

Table 1.1 – Commercial hydrogen liquefaction plants worldwide.

Continent/ Country	Location	Operated by	Capacity (TPD)	Commissioned in	Still in operation
America					
Canada	Sarnia	Air Products	30	1982	Yes
Canada	Montreal	Air Liquide Canada Inc.	10	1986	Yes
Canada	Becancour	Air Liquide	12	1988	Yes
Canada	Magog, Quebec	BOC	15	1989	Yes
Canada	Montreal	BOC	14	1990	Yes
French Guyane	Kourou	Air Liquide	5	1990	Yes
USA	Painsville	Air Products	3[a]	1957	No
USA	West Palm Beach	Air Products	3.2[a]	1957	No
USA	West Palm Beach	Air Products	27[a]	1959	No
USA	Mississippi	Air Products	32.7[a]	1960	No
USA	Ontario	Praxair	20	1962	Yes
USA	Sacramento	Union Carbide, Linde	54[a]	1964	No
USA	New Orleans	Air Products	34[a]	1977	Yes
USA	New Orleans	Air Products	34	1978	Yes
USA	Niagara Falls	Praxair	18	1981	Yes
USA	Sacramento	Air Products	6	1986	Yes
USA	Niagara Falls	Praxair	18	1989	Yes
USA	Pace	Air Products	30	1994	Yes
USA	McIntosh	Praxair	24	1995	Yes
USA	East Chicago, IN	Praxair	30	1997	Yes
Subtotal			300		
Europe					
France	Lille	Air Liquide	10	1987	Yes
Germany	Ingolstadt	Linde	4.4	1991	Yes
Germany	Leuna	Linde	5	2008	Yes
Netherlands	Rosenburg	Air Products	5	1987	Yes
Subtotal			24.4		
Asia					
China	Beijing	CALT	0.6	1995	Yes
India	Mahendragiri	ISRO	0.3	1992	Yes
India	India	Asiatic Oxygen	1.2	-	Yes
India	Saggonda	Andhra Sugars	1.2	2004	Yes
Japan	Amagasaki	Iwatani	1.2[a]	1978	No
Japan	Tashiro	MHI	0.6[a]	1984	No
Japan	Akita Prefecture	Tashiro	0.7	1985	Yes
Japan	Oita	Pacific Hydrogen	1.4	1986	Yes
Japan	Tane-Ga-Shima	Japan Liquid Hydrogen	1.4	1986	Yes
Japan	Minamitane	Japan Liquid Hydrogen	2.2	1987	Yes
Japan	Kimitsu	Air Products	0.3	2003	Yes
Japan	Osaka	Iwatani (Hydro Edge)	11.3	2006	Yes
Japan	Tokyo	Iwatani, built by Linde	10	2008	Yes
Subtotal			30.6		
Worldwide			355		

a Not included in the subtotal of the capacity for the year 2009.

1.3.1. Large-scale plants: Praxair, Air Products, and Air Liquide

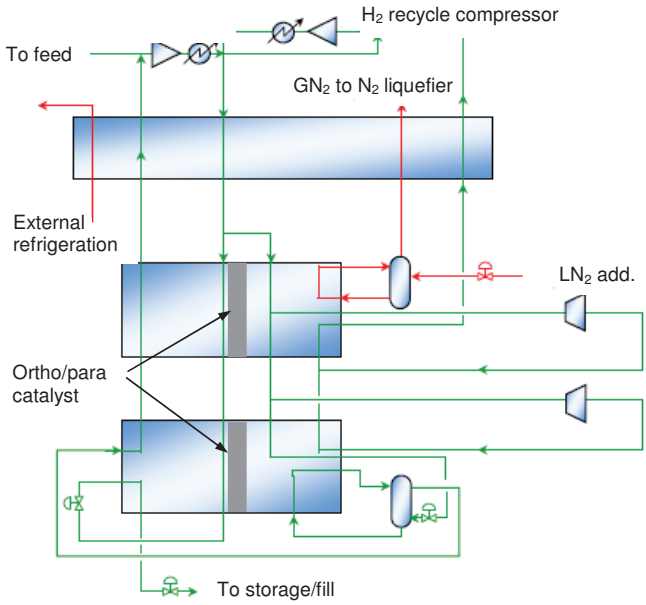

Fig. 1.1 – Praxair hydrogen liquefaction process (adapted from Drnevich, 2003).

Praxair has 5 hydrogen liquefaction plants in the US today with production rates between 6 and 35 ton LH_2 TPD. Typical specific power consumptions are between 12.5 and 15 kWh/kg_{LH2} (Drnevich, 2003). Fig. 1.1 shows a Praxair LH_2 process flow sheet. It looks like the pre-cooled Claude cycle, but is more complicated for the large-scale system. There are three heat exchangers. The first heat exchanger is cooled by nitrogen gas (GN_2) and an external refrigeration system. The second heat exchanger is cooled by liquid nitrogen (LN_2) and some of the H_2 feed. The third is cooled by a hydrogen refrigeration system that uses some of the feed to expand through turbines and Joule-Thomson (J-T) valve. The system is unique. Recently, it is the patent of Praxair invented by Schwartz *et al* (2011). Air Products has four hydrogen liquefaction plants capable of producing between 30 and 35 LH_2 TPD in use in North America today. In addition, they have two 5 TPD LH_2 plants: one in Holland and the other one in the US. Patents of Air Product's technology are found formerly by Gaumer *et al* (1988) and recently by Allam *et al* (2009). Air Liquide has a plant in France and one in Canada, and both have capacities of about 10 TPD. Both of these plants make use of the Claude cycle with hydrogen used as the cycle fluid; however, only one literature about Air Liquide's cycle can be found on a patent by Grenier (1996). The best plant in the US requires about 10 kWh/kg_{LH2} (Drnevich, 2003). The LH_2 production capacity is still greater than the demand. It seems every large-scale LH_2 plant has the cycle of LN_2 as a pre-cooling process to cool hydrogen gas from 25 °C to −193 °C and a hydrogen refrigeration system to further cool hydrogen gas to −253 °C.

1.3.2. Linde Large-scale N_2 pre-cooled Claude plant in Ingolstadt

This plant used to be the largest German hydrogen liquefier. The cycle is illustrated in Bracha *et al* (1994); more technique can be found on Bracha *et al* (2006). Feed hydrogen gas obtained from an air separation plant is generated from a steam reforming process using natural gas. Fig. 1.2 shows the actual liquefier in the plant. The big, vertical tank nearby on the left is the LN_2 tank that the nitrogen liquefaction system uses to liquefy nitrogen to pre-cool hydrogen inside the LH_2 liquefier. All of the compressors are kept inside the machinery building on the right. The leftmost tank is the LH_2 storage tank where liquefied hydrogen is kept for delivery. The tank is vacuum insulated. Fig. 1.3 (a) is the other side. To minimize the delivery cost, the hydrogen is delivered in liquid form by truck. Fig. 1.3 (b) demonstrates how LH_2 is loaded from the storage tank to the trailer.

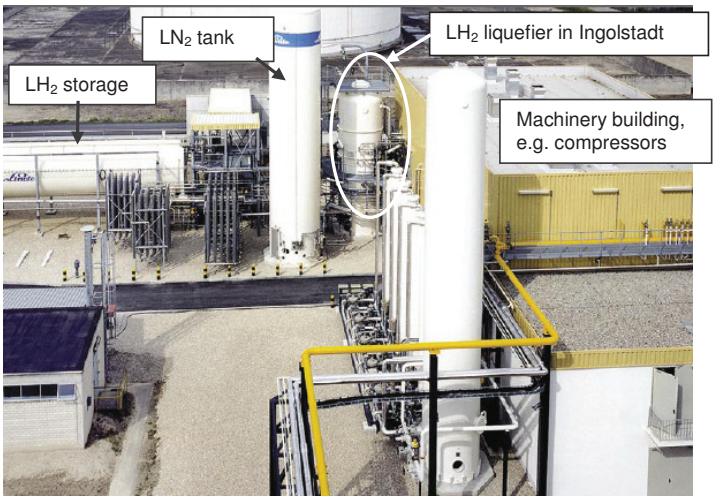

Fig. 1.2 – The location of Linde LH_2 in Ingolstadt.

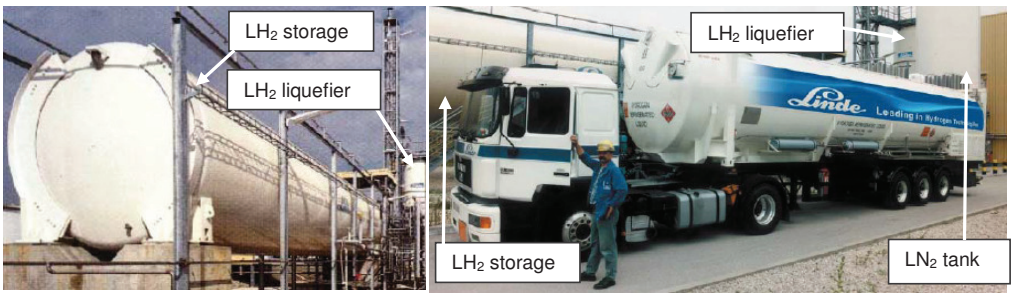

Fig. 1.3 – (a) Liquid hydrogen storage tank of Linde AG in Ingolstadt, (b) Articulated train with semi-trailer equipped for liquid hydrogen.

1.3.3. New Linde large-scale plant system in Leuna

Linde opened a second, 20 million Euro hydrogen liquefaction plant in September 2007 in Leuna, as depicted in Fig. 1.5 and Fig. 1.6. It is currently the newest and largest H_2 liquefier plant in Germany. The system with a new cycle as depicted in Fig. 1.4, is similar to the existing plant in Ingolstadt depicted in Fig. 1.2, but is more efficient. There is an important difference in the turbine arrangement between the plants in Leuna and Ingolstadt in that the plant in Leuna receives a single feed GH_2 stream from an air separation plant. There is no recycled hydrogen, and the ortho-para (O-P) conversions are put inside heat exchangers.

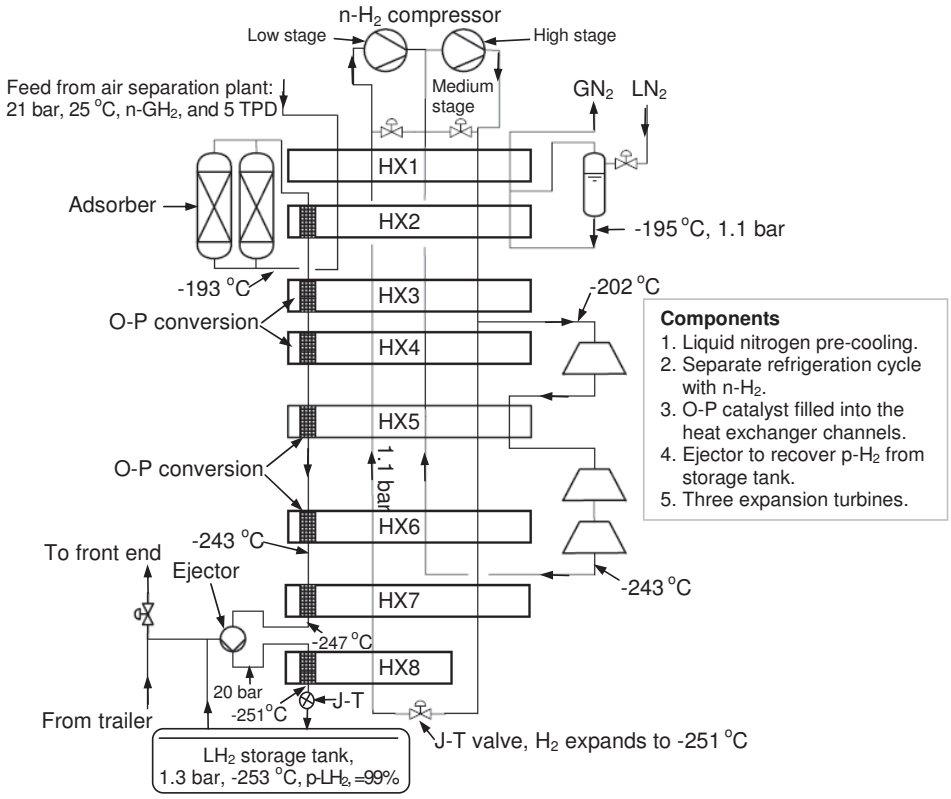

Fig. 1.4 – Process flow sheet of hydrogen liquefaction plant in Leuna (Kuendig *et al*, 2006).

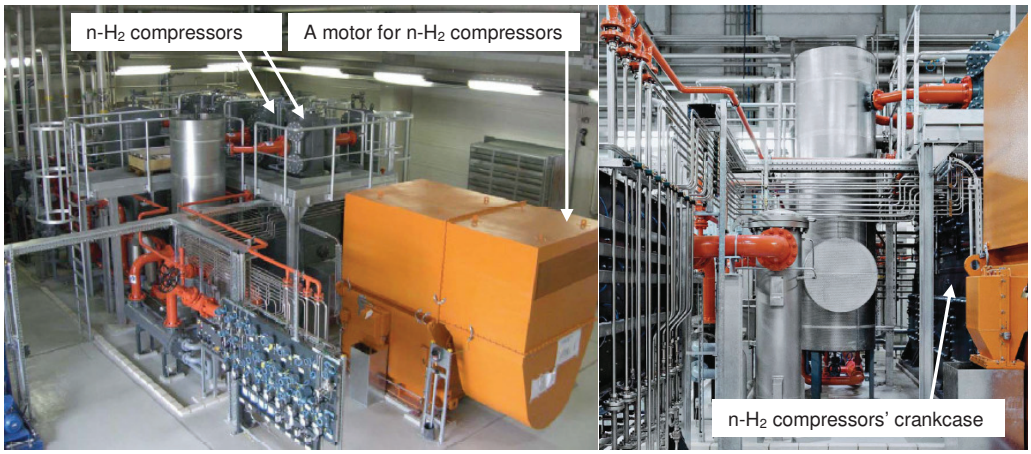

Fig. 1.5 – Piston compressors of hydrogen liquefaction plant in Leuna (adapted from Linde Group, 2008).

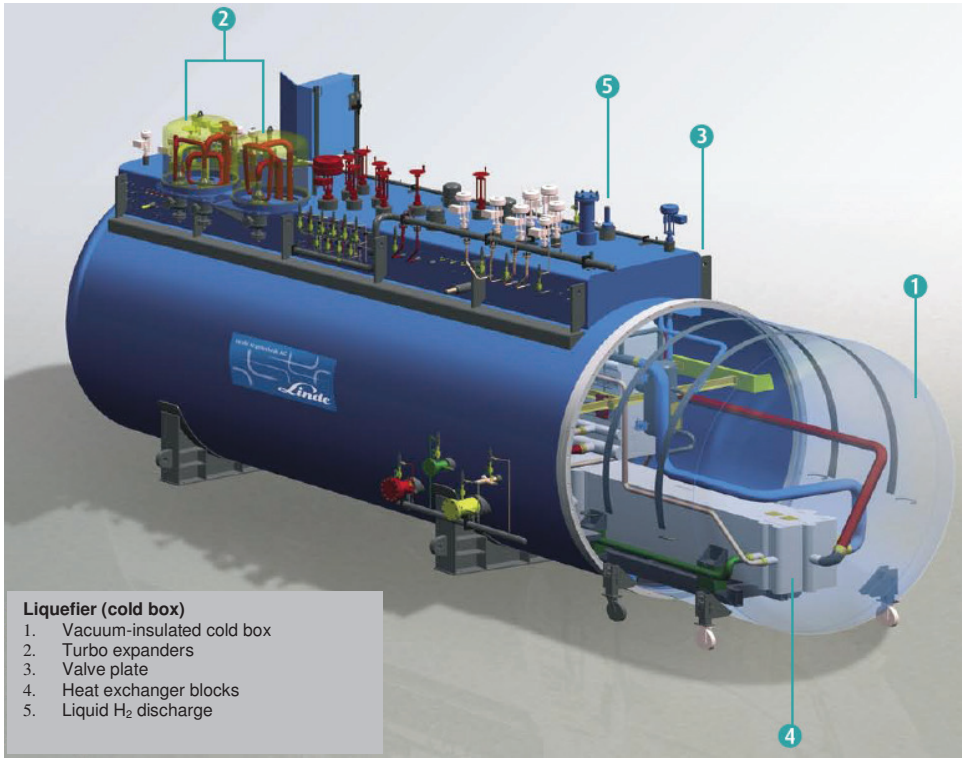

Fig. 1.6 – A Linde hydrogen (cold box) liquefier in Leuna (adapted from Linde Switzerland, 2008).

1.4. Conceptual plants

From year 2000 to 2009, some researchers have proposed new improved processes with exergy efficiencies between 40–50%. The details are given below.

1.4.1. Large-scale H_2 liquefaction in combination with liquefied natural gas pre-cooling system

Kuendig *et al* (2006) conducted a study regarding the integration of a pre-cooling liquefied natural gas (LNG) system to a new one like the Leuna N_2 pre-cooled Claude system. The study concluded that using LNG for pre-cooling in the hydrogen liquefaction process would be extremely useful to decrease the power input and the overall liquefier construction cost because the source would be free. Compared to a conventional liquefaction process, such as the one at Leuna using liquid nitrogen for pre-cooling but with compression at ambient temperature, the reduction would be from 10 to 4 kWh/kg_{LH2} (Kramer *et al*, 2006). However, this process could only be used for hydrogen gas made from LNG, and the plant would have to be located near a seaport.

1.4.2. Nitrogen pre-cooled Claude by Matsuda and Nagami (1998)

The World Energy NETwork (WE-NET) project (Mitsugi *et al*, 1998) has suggested building large-scale hydrogen liquefaction plants with liquefaction capacities of 300 TPD. The plant is based on a Claude cycle with nitrogen pre-cooling (Matsuda and Nagami, 1998). It appears that WE-NET's cycle is similar to the plant in Ingolstadt in the way that the nitrogen cycle is used to pre-cool hydrogen from 25 °C to −193 °C. Then, the hydrogen cycle is used to cool from −193 °C down to −253 °C; however, WE-NET's cycle is more complicated and is specifically designed for greater capacity. There is a large N_2 liquefaction system to reliquify GN_2 for the pre-cooling process.

1.4.3. Conceptual plant by Quack (2002)

Quack (2002) has made a conceptual design of a high-efficiency, large-capacity liquefier for hydrogen. However, internal process simulation tests run in a commercial software package, PRO/II by NTNU-SINTEF indicated that it was not able to explicitly determine whether it has a high efficiency or not because the configuration of the proposed propane refrigeration is impossible for low power consumption. The software was checked for its reliability and accuracy of process simulation. Also, the proposed helium-neon refrigeration system consumes more power due to the fact that helium-neon composition has inferior refrigerant heat transfer properties compared with hydrogen, which is commonly found in use today in actual hydrogen liquefaction plants.

1.4.4. Conceptual plant with helium refrigeration cycle by Kuz'menko (2004)

Before this, Beljakov *et al* (2000) successfully created a reliable, high-efficiency, low-capacity hydrogen liquefier with a helium refrigeration cycle. Later on, engineer Kuz'menko (2004) at Open Joint-Stock Company used this concept to design a liquefier. He made a conceptual study of building a medium-capacity hydrogen liquefier with a helium refrigeration cycle; however, it only produced a slight improvement from the Ingolstadt plant's efficiency.

1.4.5. MR Refrigeration by Stang (2005)

A hydrogen liquefaction prototype laboratory unit was developed by NTNU-SINTEF. The process was based on using a MR process for pre-cooling, as shown in the figure at Stang *et al* (2006). The experiment of the rig was complete. With the initial test, the hydrogen gas could be cooled by the MR refrigeration system from an ambient temperature of 25 °C down to near −193 °C with the highest efficiency. Detailed experimental results are reported by the author in Chapter 3.

1.4.6. Helium refrigeration cycle by Shimko (2007)

This is the design and construction of an estimated $2.6 million small-scale pilot plant (20 kg/h) that would be used for hardware demonstration (would be finished in 2011) and as a model for scaling to an estimated $39 million larger plant (50 TPD) by Shimko and Gardiner (2007). Simulations were performed using EXCEL and REFPROP. Nevertheless, the efficiency is still lower than the proposed NTNU-SINTEF system. Moreover, helium is not suitable (hydrogen has better heat transfer properties) for cooling GH_2 from −193 °C to −253 °C. If used, every component such as compressors, expanders, and heat exchangers will have to be bigger.

1.4.7. Helium Joule-Brayton cascade system by Valenti and Macchi (2008)

Valenti and Macchi (2008) proposed an innovative, high-efficiency, large-scale hydrogen liquefier that utilizes four cascaded helium Joule-Brayton cycles. However, helium is not suitable for cooling GH_2 from 25 °C to −193 °C and from −193 °C to −253 °C due to its inferior heat transfer properties compared to hydrogen. Moreover, the cycle's configuration itself to cool GH_2 from 25 °C to near −193 °C is impossible to have low exergy efficiency as reported. Also, internal simulation tests run in PRO/II by NTNU-SINTEF indicated that the system is not guaranteed to have a high efficiency.

1.5. Development potential of large-scale LH_2 plants

A potential efficiency increase in future hydrogen liquefaction plants can be realized by the following means:

- Replacement of the J-T valve at the liquefaction stage by an expansion turbine. An increase in the number and quality of expansion turbines can minimize exergy losses.
- Reduction of the circulating mass flow or using a single H_2 feed stream as used by the Leuna plant, Quack (2002), and Valenti and Macchi (2008). By doing this, the last heat exchanger must be designed to cool the hydrogen to the lowest possible temperature, e.g., near −253 °C, so there is no vapor fraction after the expansion at the last J-T valve. A small ejector is recommended to recover p-GH_2 from the storage tank the same as the plant in Leuna.
- Operating with a refrigerant composition for pre-cooling hydrogen gas from 25 °C to −193 °C. This way, pre-cooled hydrogen gas and cold MR streams get closer. This new system was studied at NTNU-SINTEF (Stang, 2006), and the results are reported in Chapter 2 to 4.
- Another major factor influencing liquefier efficiency is the feed gas input pressure. One alternative is to raise the hydrogen output pressure of the preceding hydrogen production plant, e.g., a high-pressure electrolysis process or a steam reforming plant. A good example is the 21 bar feed n-H_2 at the LH_2 plants in Ingolstadt and Leuna. The higher the feed pressure, the greater the liquefier's efficiency. The minimum liquefaction work is in conjunction with

feed pressure. The minimum feed pressure must not be below 15 bar because there could be hydrogen condensation during the cooling process. If it is below 15 bar, more energy is needed in liquefaction, and there will be more exergy loss.

- Most of the exergy losses in the hydrogen liquefaction processes are dissipated through compressors. Therefore, it is recommended for manufacturers to design new high-efficiency compressors and expanders and design all compressors in a way such that the suction temperatures are reduced as done by Quack (2002). Also, it is recommended to ventilate heat from the compressors as much as possible during the compression process to reduce the exergy loss.
- Use spiral or aluminum plate-fin heat exchangers with maximum effectiveness to reduce the exergy losses.
- If possible, construct plants near seaports for delivering LNG to be used in the pre-cooling process. This will significantly help reduce the plant size and energy consumption as recommended by Kramer *et al* (2006) and Keundig *et al* (2006).
- A cost overview for the specific investment costs of conventional liquefaction plants. When designing a large-scale plant, the cost must be compared with other existing plants. Inflation should be accounted for in current and old plants. Companies who can offer cheap, large-scale hydrogen liquefaction plants are Linde, Air Products, and Praxair. And Praxair has the largest hydrogen plant in the US with the lowest investment cost.
- Krewitt and Schmid (2005) says that costs for liquefaction are driven primarily by capital costs (today: 63%), then energy costs (29%), and finally, O&M (Drnevich, 2003). Energy costs on the other hand, are strong functions of the liquefier efficiency and are less dependent on the production rate. In small plants, energy and non-energy costs are comparable. In large-scale plants, the energy costs become more important. Krewitt and Schmid (2005) also derived the following equation for the specific investment costs: Specific investment cost for liquefier (€2,000/kg/h) = 828,313×(production capacity, kg/h)$^{-0.48}$.
- A method to decrease capital costs is to build plants on a larger scale and use the effect of building multiple plants of the same design. The following challenges for more cost effective LH_2 production systems are Drnevich (2003) system modularization for traditional sized units, large-scale equipment, higher efficiency compressors and expanders, more efficient refrigeration, and lower cost high-efficiency insulation.

The conclusions are the following:

- The problem with the current liquefaction systems is their high energy consumption. Every large-scale hydrogen liquefaction plant is based on the pre-cooled Claude system, which is still the same as 50 years ago with little improvement. If it is possible to reduce from today's energy usage of 10 kWh/kg$_{LH2}$ to around 5 kWh/kg$_{LH2}$ which will reduce electrical power consumption of the plant to be a half in the future, all of the compressors and motors in the plant, which constitute the most expensive components, could be reduced by 50%, which will also lead to cheaper plants.
- Methods to resolve the challenges include proposing completely new configurations and efficient systems coupled with improved efficiencies of the main system components such as compressors, expanders, and heat exchangers.
- The development trend is that a lot of people have tried to propose new better systems (Kuendig *et al* 2006; Matsuda and Nagami 1998; Quack 2002; Kuz'menko *et al* 2004; Stang *et al* 2006; Shimko and Gardiner 2007; and Valenti and Macchi 2008), but they are still neither more efficient nor realistic. Furthermore, compressor and expander manufacturers must invent more efficient machines.

1.6. Summary and comparison of hydrogen liquefaction processes' efficiencies

Table 1.2 is the summary and comparison. Feed hydrogen flow is normal hydrogen at 1 atm, 25 ^{o}C. FOM$\times$100% = (Ideal liquefaction power/Actual system liquefaction power)$\times$100% or Exergy efficiency. The efficiencies of systems 3, 5, and 6 are from Nandi and Sarangi (1993); the same systems have different energy consumptions and exergy efficiencies because it depends on the assumptions of the efficiencies of compressors and expanders used in the systems. When making a comparison between several different cycles and liquefiers, Berstad *et al* (2009)'s comparison method is recommended. This method, which is a direct comparison of liquefiers based on the overall exergy efficiency and specific power consumption, favors those with a higher portion of pre-compression. The feed stream was assumed and calculated at 21 bar and 25 °C before going into any cycle/liquefier, which is identical to the Ingolstadt plant. Every system is directly compared with the Ingolstadt plant at a modified feed stream pressure of 21 bar. The energy consumptions and exergy efficiencies of the Ingolstadt, WE-NET, and Quack systems as shown in Table 1.2 were calculated by Berstad *et al* (2009).

The compression power reductions of the third, fourth, fifth, and sixth hydrogen liquefaction systems in Table 1.2 are 0.9167, 0.9167, 0.2313, and 0.1026 kWh/kg$_{LH2}$, respectively. These are from the ideal H_2 feed exergy reduction of 0.55, 0.55, 0.1388, and 0.0616 kWh/kg$_{LH2}$, respectively. Make-up gas is reversibly and isothermally (ideally) compressed from the feed at 21 bar and 25 °C to each cycle's high side. This was all calculated assuming a compression exergy efficiency of 60%. For cycles 7, 8, and 9, the hydrogen feed pressure was 21 bar, the same as Ingolstadt's. Thus the energy consumption was the same. With Valenti's system, GH_2 compression must be made from 21 bar supply feed to 60 bar; therefore, there is an increased consumption of 0.72 kWh/kg$_{LH2}$ with an assumed 60% exergy efficiency from the ideal H_2 feed exergy increase of 0.43 kWh/kg$_{LH2}$. Finally, all of the system exergy efficiencies were calculated by comparing with an ideal energy consumption of 2.89 kWh/kg$_{LH2}$; however, systems 3–6 were calculated using an ideal energy consumption of 2.178 kWh/kg$_{LH2}$.

Table 1.2 – Summary and comparison of hydrogen liquefaction processes' efficiencies.

System with modified feed state: Normal hydrogen @21 bar, 25 °C	Original energy consumption (kWh/kg_{LH2})	Modified energy consumption (kWh/kg_{LH2})	Modified exergy efficiency (%)
1. The thermodynamically ideal liquefaction system			
Feed: 21 bar, 25 °C, n-GH_2			
Output: 1 bar, –253 °C, n-LH_2	-	2.178	100%
Output: 1 bar, –253 °C, 99.8% p-LH_2	-	2.890	100%
2. Theoretical simple Linde-Hampson system (Dewar, 1898) *Can't liquefy hydrogen	-	-	-
3. Theoretical pre-cooled Linde-Hampson (Dewar, 1898; Nandi and Sarangi, 1993) Output: 1 bar, –253 °C, n-LH_2	64.5-71.7	63.6-70.8	3.0-3.4%
4. Theoretical Claude system (Dewar, 1898; Nandi and Sarangi, 1993) Output: 1 bar, –253 °C, n-LH_2	Less than the pre-cooled Claude		
5. Theoretical pre-cooled Claude system (Dewar, 1898; Nandi and Sarangi, 1993) Output: 1 bar, –253 °C, n-LH_2	24.8-35.0	24.6-34.8	6.2-8.8%
6. Theoretical helium-refrigerated system (Dewar, 1898; Nandi and Sarangi, 1993) Output: 1 bar, –253 °C, n-LH_2	29.3-49.5	29.2-49.4	4.4-7.4%
7. Large-scale Praxair plant system (Drnevich, 2003) Output: ≈ 1 bar, –253 °C, 95% p-LH_2			
8. Large-scale Air Products plant system (Drnevich, 2003) Output: ≈ 1 bar, –253 °C, 95% p-LH_2	≈ 12-15		19-24%
9. Large-scale Air Linde plant system (Drnevich, 2003) Output: ≈ 1 bar, –253 °C, 95% p-LH_2			
10. Large-scale plant, Claude system in Ingolstadt on stream in 1994 by Bracha *et al* (1994) Output: 1.3 bar, –253 °C, 95% p-LH_2	13.58		21.0%
11. WE-NET: Nitrogen pre-cooled large-scale Claude plant by Matsuda and Nagami (1998) Output: 1.3 bar, –253 °C, 95% p-LH_2			
11.1) Hydrogen Claude	≈ 8.5	N/A	N/A
11.2) Helium Brayton			
11.3) Basic neon			
11.4) Neon with cold pump		7.0	41.3%
12. Large-scale conceptual plant by Quack (2002) Output: 1 bar, –253 °C, 99.8% p-LH_2			
12.1) Without pressure drop in calculation	7.0	5.49	52.6%
12.2) With pressure drop in calculation	≈ 7.3	N/A	N/A
13. Four helium Joule-Brayton cascade cycle by Valenti and Macchi (2008) Output: 1.5 bar, –253 °C, 99.8% p-LH_2	5.04	5.76	50.2%

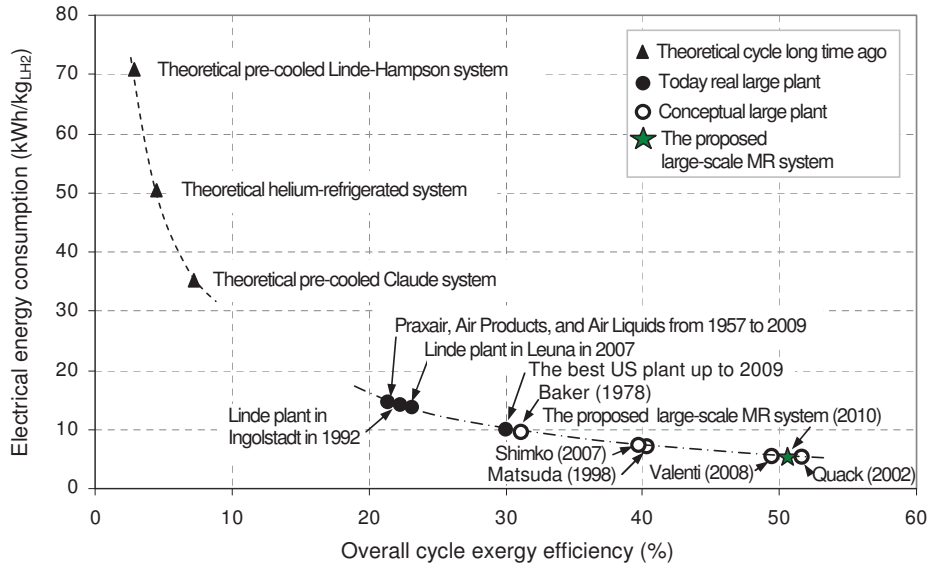

Fig. 1.7 – Comparison of hydrogen liquefaction processes' efficiencies by assuming that all processes are with uniform feed pressure equal to that of Ingolstadt plant at 21 bar.

Fig. 1.7 contains the information shown in Table 1.2. From the data, the theoretical pre-cooled Linde-Hampson system was the first imaginary system invented a long time ago, and its exergy efficiency is the lowest. After that, the second was the theoretical helium-refrigerated system, which is followed by the theoretical pre-cooled Claude system. All have a very low yield: e.g., 10% after expansion. The theoretical systems mentioned have never been used to liquefy hydrogen in large-scale production. They were just small-scale laboratory systems. Next, Ingolstadt and Praxair brought this concept to invent real plants. Today, actual large-scale hydrogen liquefaction plants, e.g., Praxair, Air Products, and Air Liquids plants in the US, energy consumptions are reported to be between 12–15 kWh/kg$_{LH2}$ (Drnevich, 2003). Baker and Shaner (1978) was the first conceptual plant, and had the lowest efficiency. The conceptual large-scale systems proposed by Matsuda and Nagami (1998), Quack (2002), and Valenti and Macchi (2008) were designed later. Recently, the efficiency of the Leuna plant (with energy consumption less than 13.58 kWh/kg$_{LH2}$) is a little better than Ingolstadt is assumed here. Quack's process reports the best cycle exergy efficiency at 5.76 kWh/kg$_{LH2}$. The best plant in the US today is reported to require 10 kWh/kg$_{LH2}$ (Drnevich, 2003), but it is not known where. A simulated 50 TPD large-scale Shimko plant, which is a helium refrigeration system with a hydrogen feed at 21 bar, is reported at 8.7 kWh/kg$_{LH2}$. The proposed large-scale MR refrigeration process with 4 J-B cycles is 5.91 kWh/kg$_{LH2}$ as depicted. The ideal theoretical minimum value is 2.89 kWh/kg$_{LH2}$. For the process with LNG for pre-cooling studied by Kuendig *et al* (2006), the power consumption is reported by Kramer *et al* (2006) to be 4 kWh/kg$_{LH2}$. Thus, the overall efficiency, compared with the ideal process, is [(2.89 kWh/kg$_{LH2}$)/(4 kWh/kg$_{LH2}$)]×100 = 72%, which is the highest with respect to all current systems. However, it is not shown in Fig. 1.7 because the process is cooled by free LNG, not by the system itself. Completely new approaches for low temperature refrigeration are magnetic refrigerators and acoustic refrigerators. Magneto caloric cooling may

reduce liquefaction energy to 5.0 kWh/kg_{LH2} (Dutton, 2003); however, this may only be for small-scale to medium-scale plants. All of the literature related to magnetic cooling has been reported on small-scale hydrogen plants. Nobody thinks such system is realistic in large-scale systems.

1.7. Conclusion

Today large hydrogen liquefaction plants have exergy efficiencies of just 20–30%; thus, there is potential to improve. From 1998 to 2008, some conceptual plants have been proposed with reported efficiencies of 40–50%. Finally, in year 2010, NTNU and SINTEF Energy Research AS proposed a new MR refrigeration process with four J-B cycles that has an efficiency greater than 50%. Details of the proposed system are reported in Chapter 4.

Chapter 2. Exergy analysis on the simulation of a small-scale hydrogen liquefaction test rig with a multi-component refrigerant refrigeration system

This study investigates the simulation of a proposed small-scale laboratory liquid hydrogen plant with a new, innovative MR refrigeration system. The simulated test rig was capable of liquefying a feed of 2 kg/h of normal hydrogen gas at 21 bar and 25 °C to normal liquid hydrogen at 2 bar and −250 °C. The simulated power consumption for pre-cooling the hydrogen from 25 °C to −198 °C with this new MR compressor was 2.07 kWh/kg_{GH2} from the ideal minimum of 0.7755 kWh per kilogram of feed hydrogen gas. This was the lowest power consumption available when compared to today's conventional hydrogen liquefaction cycles, which are approximately 4.00 kWh/kg_{GH2}. Hence, the MR cycle's exergy efficiency was 38.3%. Exergy analysis of the test rig's cycle, which is required to find the losses and optimize the proposed MR system, was evaluated for each component using the simulation data. It was found that the majority of the losses were from the compressors, heat exchangers, and expansion valves. Suggestions are provided for how to reduce exergy in each component in order to reduce the exergy loss. Finally, further improvements for better efficiency of the test rig are explained to assist in the design of a future large-scale hydrogen liquefaction plant.

2.1. Introduction

Because hydrogen has shown promise as an important energy vector for use in future transportation vehicles, several hydrogen research projects have been conducted since 1980 and in particular, since 2000. One of the challenges in creating a hydrogen economy is the low efficiencies of the current hydrogen liquefaction plants' cycles. Currently, large hydrogen liquefaction plants, e.g., the plant in Ingolstadt as described by Bracha *et al* (1994), have exergy efficiencies of just 20–30%. These efficiencies are very low. The plant consumes 4.86 kWh per kilogram of hydrogen gas using a nitrogen refrigeration system to pre-cool normal hydrogen gas from 25 °C to equilibrium hydrogen gas at −198 °C. From 1998 through 2008, some conceptual plants were proposed with reportedly improved efficiencies of 40–50% (Matsuda and Nagami 1998; Quack 2002; Kuz'menko 2004; Shimko 2007; Valenti and Macchi 2008; Berstad *et al* 2010). A literature review for the development of large-scale hydrogen liquefaction processes throughout the world from 1898 to 2009 is given in Chapter 1. Finally, in the year 2010, NTNU

and SINTEF Energy Research AS proposed a new large-scale MR system with efficiency in excess of 50%. Detailed results are reported in Chapter 4.

Refrigeration systems thermodynamically release heat into the environment. The first law governs the conservation of energy only; it gives no information on how, where, and how much the system performance is degraded. Exergy analysis is a powerful tool in the design, optimization, and performance evaluation of energy systems. The principles and methodologies of exergy analysis are well established (Gaggioli 1998; Wark 1995; Bejan 1988; Moran 1982, Bejan 1982; Kotas 1995). Exergy analysis of a complex system can be performed by analyzing the components of the system separately. Identifying the main sites of exergy destruction shows the direction for potential improvements.

Baker and Shaner (1978) studied the exergy analysis of a hydrogen liquefaction system. Dincer and Rosen (2007) together with Chiu and Newton (1980) conducted interesting discussions about the exergy analysis of cryogenic systems. Similarly, with a focus on the analysis of a hydrogen liquefaction cycle, Kanoglu (2002) together with Remeljej and Hoadley (2006) presented methodologies for the exergy analysis of refrigeration cycles and obtained the minimum work relation for the liquefaction of natural gas.

Conventional refrigeration cycles that contain single or pure refrigerant have a constant evaporating temperature as a function of the saturation pressure. Mixed refrigerant cycles do not maintain a constant evaporating temperature at a given pressure; the evaporating temperature range depends on pressure and composition. Refrigerant composition is chosen so that it has an evaporation curve that matches the cooling curve of the pre-cooled hydrogen gas with minimum temperature difference. Small temperature difference reduces entropy generation; it improves thermodynamic efficiency and reduces power consumption (Townsend and Linnhoff, 1983). Usually refrigerant compositions selection (also as performed through Chapter 2-4) has been done by trial-and-error and guided only by heuristics (Lee *et al*, 2002).

Before the initial experiment, the test rig was redesigned and optimized by simulation and exergy analysis. In this chapter, the operation of the small-scale laboratory liquid hydrogen plant is described first. Multi-component refrigerant was used in the cycle. The use of refrigerant compositions for cryogenic refrigeration was first proposed by Podbielniak (1936) in a U.S. patent. Most large base load natural gas liquefaction plants using mixed refrigerant processes derived from the basic Kleemenko (1959) process. This concept of a mixed refrigerant in gas liquefaction was developed in the past few years and has resulted in reduced energy consumption compared to conventional liquefaction cycles. This reduction is similar to what was explained by Bottura (2009), Chrz (2010), and Mafi *et al* (2009), and Bosma and Nagelvoort (2009). The differences involve the new modified cycle and the new optimized refrigerant composition that was specially designed for pre-cooling hydrogen gas from 25 ^{o}C to −198 ^{o}C. An exergy analysis was performed on the individual components in the cycle as well as on the entire cycle of the test rig. The coefficient of performance (*COP*) and the second law efficiency for the entire cycle were obtained. Finally, a process is described for how to reduce exergy loss in each component and to obtain optimization of the minimum work required for the liquefaction process of the test rig – i.e., the specific objective of this chapter.

2.2. System description

The simulation model was built in PRO/II. For the equation of state, Soave-Redlich-Kwong (SRK) was selected for use in this PRO/II simulation package because of its popularity, simplicity, and fast computation. The other popular Peng-Robinson equation of state gives quite similar results. Ortho-para conversion reactors were not included because the experimental rig could not contain the catalyst needed for the ortho-para conversion. The laboratory test rig pictured in Fig. 2.1 was designed by SINTEF Energy Research AS to use the MR containing more complex of composition. The concept of multi-component refrigerants, also known as mixed refrigerants, (Bottura 2009; Chrz 2010; Mafi *et al* 2009; Bosma and Nagelvoort 2009) has been widely used in the liquefaction of natural gas for decades because of the reduced energy consumption compared to other conventional liquefaction cycles. SINTEF has worked with this type of refrigeration cycles for several years. The novelty of this mixed refrigerant system is described very well by Flynn (1997) as well as Venkatarathnam (2008). Before the startup of the rig, a decision was made to use a less complex refrigerant during the start up period. To help obtain a theoretically optimized refrigerant-mix, a model of the liquefaction rig was made in the flow sheet of the PRO/II simulation program.

Table 2.1 contains design and assumption data. Ambient temperature, capacity, GH_2 feed, and LH_2 product were the design values. No pressure drop was assumed because the plant was a relatively small-scale system. Good low-temperature heat exchangers for cryogenic system were generally recommended by Barron (1966) to have a 1–2 ^{o}C temperature approach. The compressors' efficiencies were estimated from the manufacturers' product catalogues, which generally contained small-size gas compressors. Hydrogen gas compression ratio was higher than that of MR gas, thus lower efficiency of H_2 compressor was assumed.

Table 2.1 – Boundary conditions of the test rig's simulation.

Parameter	The test rig's process from the simulation
Ambient temperature	25 ^{o}C
Capacity of liquefied hydrogen	2 kg/h
GH_2 feed	1 bar and 25 ^{o}C
LH_2 product	2.0 bar, saturated liquid normal hydrogen
Pressure drop in system	No
Temperature approach in heat exchangers	1–2 ^{o}C (arbitrarily selected for high effectiveness)
Isentropic efficiency:	
H_2 compressor	65% (selected similar to actual machinery)
MR compressor	70% (selected similar to actual machinery)

As shown in Fig. 2.1, feed hydrogen gas was first compressed from a suction pressure in a two-stage hydrogen piston compressor with inter- and after-cooling. The outlet temperature of the aftercooler (both H_2 and MR circuit) was designed to be 25 ^{o}C. Next, the hydrogen was cooled in a series of 5 heat exchangers. In the first 4 heat exchangers, the hydrogen gas was cooled by the MR refrigeration system. In the last heat exchanger, the hydrogen gas was cooled by a liquid helium circuit. After cooling, a Joule-Thomson valve was used to throttle the hydrogen gas from

21 bar to 2 bar. Finally, most of hydrogen gas was liquefied to be 98% liquid hydrogen at stream 10 and 2% return flash hydrogen gas at stream 11.

The objective function was to minimize the MR compressor power by optimizing the following variables:

1. A suitable H_2 compressor discharge pressure:
   The discharge pressure needed to be above 15 bar (supercritical pressure) to avoid condensation. For the test rig, the discharge pressure was designed to be 21 bar, equivalent to that of the feed at Ingolstadt. High feed pressures result in minimal work liquefaction as described by Matsuda and Nagami (1998), Quack (2002), and Valenti and Macchi (2008) who used values of 50, 80, and 60 bar. On a larger scale, if the feed is 1–2 bar, it is recommended to compress the feed discharge to 21 bar instead of a higher value because of the increased energy requirement.
2. A suitable H_2 compressor suction pressure:
   This pressure must be a slightly above ambient pressure (1 bar) to be kept in a liquid tank before supply. Ingolstadt uses 1.3 bar. For this test rig, the compressor suction pressure could be anywhere between 1.3–2 bar. For control simplicity, a value of 2 bar was selected.
3. A suitable MR compressor discharge pressure:
   Several simulation trials were performed using PRO/II to determine an optimized composition for different suction pressures. An optimized and simplified 5-component composition, consisting of 4% hydrogen, 18% nitrogen, 24% methane, 28% ethane, and 26% butane, was satisfied with different suction and discharge MR pressures for all cases. Further explanation about this chosen simplified composition is detailed in Section 3.3.3, *The proposed simplified 5-component composition for the initial experiment*, in Chapter 3. The suitable MR compressor discharge pressure was 18 bar, which resulted in an MR compressor power of 4.55 kW. If the pressure was lower than that, e.g., 15, 16, or 17 bar, it was impossible for the MR system to cool the hydrogen. In addition, a solid phase of the MR flow could form inside the heat exchangers if the pressure was much lower than 18 bar. However, if the discharge pressure was higher than 18 bar, the system would work, but it would result in a higher MR compressor power. Moreover, if the pressure was too high, there would be more exergy losses at the expansion valves: EX1, EX2, and EX3.
4. A suitable MR compressor suction pressure:
   Too high or too low of a suction pressure would make it impossible to sufficiently cool down the hydrogen gas to a specified, designed temperature (−198 °C) flowing out of $\overline{HX}4$. The suitable pressure was 2 bar, which resulted in the minimum (theoretical) brake horse power (4.55 kW) of the MR compressor. The suction pressure could not be lower than 1 bar because it would result in a higher MR compressor power; additionally, it could not be higher than 2 bar because that would lead to a system that could not sufficiently cool down the hydrogen gas.
5. Hot stream hydrogen outlet temperatures from HX1, HX2, HX3, HX4, and HX5:
   Trial and error was used to find the optimum temperatures.
6. The suitable composition of the MR cycle:

Trial and error was performed to find the optimal composition. For simplicity, a reduced number of composition components were used to complete the initial experiment as explained above. Thus, simulation of the test rig with the 5-component composition was done first. After that, simulation of the test rig with a more complex 10-component composition was also done to see the difference from the simplified 5-component composition. The optimized complex MR composition, discovered through trial and error, was: 1.2% hydrogen, 25.6% nitrogen, 13.6% methane, 15.2% R14, 10% ethane, 10% propene, 5.8% propane, 1.0% Ibutane, 1.0% butane, and 10.8% pentane. Further explanation about this chosen complex composition for the test rig is similar to what proposed for the large-scale system detailed in Section 4.4, *Optimization results*, in Chapter 4. Simulation results of both 5-component and 10-component compositions of the rig, as depicted in Fig. 2.1, are shown in Tables 2.3, 2.4, and 2.5.

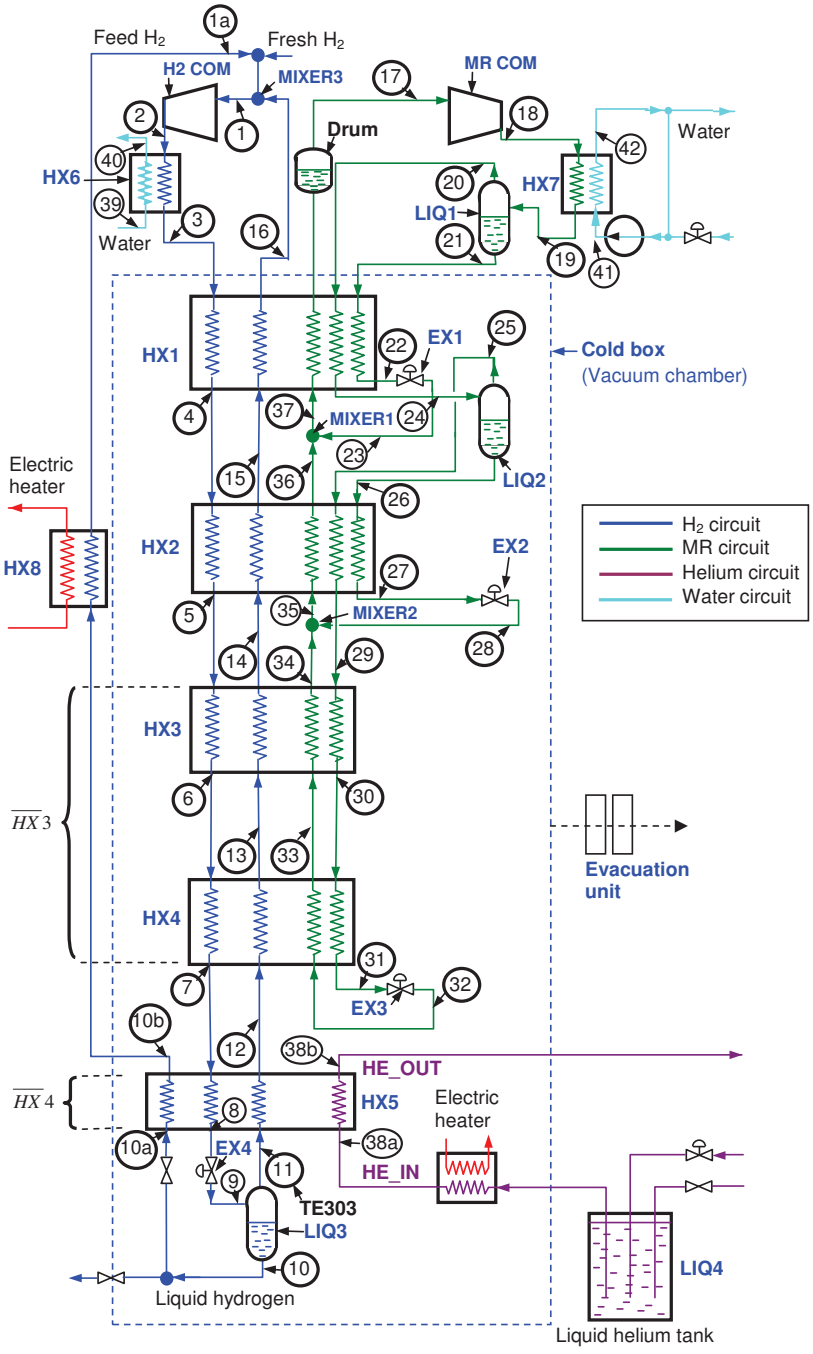

Fig. 2.1 – Schematic diagram of the laboratory MR hydrogen liquefaction system.

2.3. Analysis

All energy balance equations of all components, as depicted in Fig. 2.1, are shown in Table 2.5.

2.3.1. Heat removed from pre-cooling process

The heat removed from the hydrogen gas during the pre-cooling process from 25 °C to −198 °C in the test rig was determined by the following formula:

$$\dot{Q}_{pre-cooling} = \dot{m}_{H2}(h_{feed} - h_{pre-cooled}) = \dot{m}_{H2}(h_3 - h_7) \tag{2.1}$$

where $\dot{m}_{H2}$ is the mass flow-rate of hydrogen gas (kg/s), h_{feed} is the enthalpy of hydrogen gas at the feed (kJ/kg), which is at stream 3 (h_3), and $h_{liquefied}$ is the enthalpy of pre-cooled hydrogen (kJ/kg), which is at stream 7 (h_7). From the simulation of the test rig, $\dot{Q}_{pre-cooling}$ = 0.000571 kg/s×(175.87− −3038.81 kJ/kg) = 1.8356 kW, which was the same for both compositions. For heat removed from the hydrogen gas during the liquefaction process, $h_{liquefied}$ was the enthalpy of liquefied hydrogen (kJ/kg) which was at stream 9 (h_9).
Thus, $\dot{Q}_{liquefaction} = \dot{m}_{H2}(h_{feed} - h_{liquefied}) = \dot{m}_{H2}(h_3 - h_9) = 2.4949$ kW.

2.3.2. Energy efficiency (The first law efficiency)

Coefficient of performance (*COP*) of the test rig may be expressed as:

$$COP_{liquefaction} = \eta_I = \frac{\dot{Q}_{liquefaction}}{\dot{W}_{BH,COM}} \tag{2.2}$$

$\dot{W}_{BH,COM} = \dot{W}_{BH,MR\,COM} + \dot{W}_{BH,H2\,COM}$ was the brake horsepower of the test rig's compressors or the actual work rate input to the cycle (kW) that consisted of the compressor brake horsepower from both the MR compressor and the hydrogen compressor. Thus, *COP* of the test rig was $COP_{liquefaction} = \dot{Q}_{liquefaction} / \dot{W}_{BH,COM}$ = 2.4949 kW/7.92 kW = 0.3150 for the 5-component composition and 2.4949 kW/7.51 kW = 0.3322 for the 10-component composition. *COP* of the MR cycle only was $COP_{MR\,cycle} = \dot{Q}_{pre-cooling} / \dot{W}_{BH,MR\,COM}$ = 1.8356 kW/4.55 kW = 0.4034 for the 5-component composition and 1.8356 kW/4.1426 kW = 0.4431 for the 10-component composition.

2.3.3. Exergy efficiency (The second law efficiency)

The exergy efficiency for the liquefaction process of the test rig is maybe defined as:

$$\varepsilon = \eta_{II} = \frac{\dot{W}_{\min,cycle}}{\dot{W}_{BH,COM}} = \frac{\dot{W}_{BH,COM} - \dot{I}_{total}}{\dot{W}_{BH,COM}} = \frac{\dot{W}_{BH,COM} - (\dot{E}_{x,in} - \dot{E}_{x,out})}{\dot{W}_{BH,COM}} \tag{2.3}$$

where $\dot{W}_{\min,\,cycle}$ is the minimum work rate input to the test rig's cycle (kW). For η_{II}, the analysis is given in Section 4.1, *Results*. The ideal minimum power consumption to pre-cool normal hydrogen gas from 25 °C to −198 °C at 2 kg/h and 21 bar was the ideal minimum power consumption of the MR cycle: $\dot{W}_{\min,\,MR\,cycle} = \dot{E}_{x,\,7} - \dot{E}_{x,\,3} = 1.59$ kW. Exergy efficiency of the MR refrigeration cycle only was $\eta_{II,\,MR\,cycle} = \dot{W}_{\min,\,MR\,cycle} / \dot{W}_{BH,\,MR\,COM} = 1.59$ kW/4.55 kW = 0.3494 for the 5-component composition and 1.59 kW/4.1426 kW = 0.3838 for the 10-component composition.

2.3.4. System exergy analysis of the test rig

The easiest approach to a thermodynamic analysis of a system is to introduce exergy as additional information for each state point. Exergy, the maximal available specific work (kJ/kg), is defined as:

$$e_x = h - Ts \tag{2.4}$$

where h is the enthalpy (kJ/kg), T is the temperature (K), s is the entropy (kJ/kg-K). Otherwise:

$$de_x = dh - Tds \tag{2.5}$$

or, integrated:

$$e_x = (h - h_o) - T_o(s - s_o) \tag{2.6}$$

where e_x is the specific exergy or the maximum available specific work (kJ/kg) that can be obtained from a periodic process between a state and the ambient condition or reference state. Usually, the reference state at ambient condition is at 1 bar, 25 °C (≈300 K) for the values of h_o, T_o and s_o. In general, when substituting values into Eq. 2.6, T_o is replaced by 300 K, not 25 °C, although any conditions, temperatures, or pressures can be inserted, given the user's specifications. As shown in Tables 2.3 and 2.4, 25 °C was the ambient temperature where specific exergy (or maximum available specific work or stream exergy flow as in Eqs. 2.4 and 2.7) was assumed to be zero. This setting was used for comparison (as shown in Table 2.2) with other conventional systems that all use specified reference temperatures of 25 °C. In fact, when the reference temperature was varied, the exergy efficiency remained the same. However, if ambient temperature was increased, then exergy efficiency decreased because less heat rejection at the condenser (HX7) resulted in a higher MR compressor power consumption.

Then:

$$\dot{E}_x = \dot{m}\, e_x \tag{2.7}$$

$\dot{E}_x$ = stream exergy flow (kW) and $\dot{m}$ is the mass flow rate (kg/s) of the stream. For the whole system as well as its individual parts, thermodynamic efficiencies can be calculated as ratios of the minimum exergy necessary to the exergy actually applied. For a system analysis, however, it

was more reasonable to calculate the exergy loss occurring in a component and to compare it to the exergy input to the system. For the hydrogen liquefier test rig considered, an exergy flow diagram was plotted showing the exergy losses. Heat leaks into the liquefier were not taken into account.

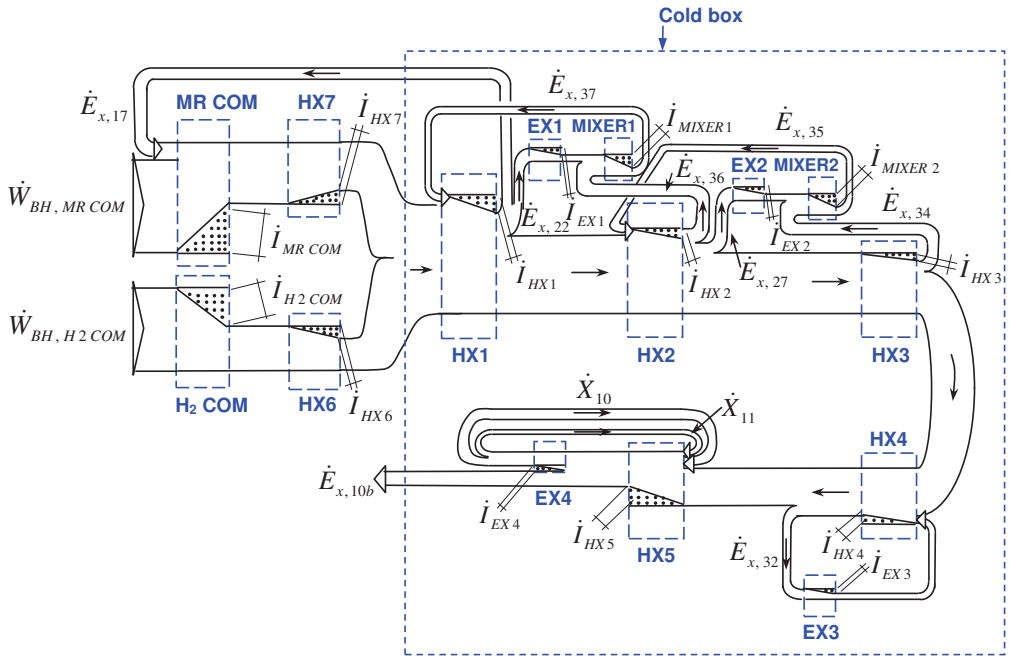

Fig. 2.2 – Exergy flow diagram of the system.

Fig. 2.2 depicts a simple exergy flow diagram of the test rig system. The power input into the electric motor drives of the H_2 compressor and the MR compressor is only part of the exergy input to the liquefier. We assumed that other electrical devices, such as fan motors, air blowers, and water pumps, were relatively small compared to the two compressors. The percentage of the total exergy input was therefore given. Additionally, there were only three throttling valves within the plant causing a small loss, namely the Joule-Thomson valve in the cooling cycle. The exergy losses in the "cold box", a vacuum chamber (as depicted in Figs. 2.1 and 2.2) that contains low-temperature heat exchangers, liquid separators, expansion valves, and mixers, are due to inefficiencies of the heat exchangers, valves, separators, mixers, and the process itself.

A large amount of the overall exergy was dissipated (see Fig. 2.2 for each component) due to inefficiencies of the following components:

1. Compressors: H_2 COM, and MR COM
2. Gas cooler: HX7
3. Liquid separators: LIQ1, LIQ2, and LIQ3
4. Heat exchangers: HX1, HX2, HX3, HX4, and HX5
5. Expansion valves: EX1, EX2, and EX3

6. Mixers: MIXER1, MIXER2, and MIXER3.

Fig. 2.2 shows that a major part of the losses was due to the process design and would occurred even if ideal heat exchangers were used. Therefore, the total exergy destruction in the cycle was simply the sum of the exergy destructions described above and can be expressed by the following equation:

$$\dot{I}_{total} = \dot{E}_{x,\,in} - \dot{E}_{x,\,out} \tag{2.8}$$

For this case, $\dot{W}_{BH,\,COM} = \dot{E}_{x,\,in}$ and for this test rig, $\dot{E}_{x,\,10b} = \dot{E}_{x,\,out}$. Thus,

$$\begin{aligned} \dot{I}_{total} = {} & (\dot{I}_{H2\,COM} + \dot{I}_{MR\,COM}) \\ & + (\dot{I}_{LIQ1} + \dot{I}_{LIQ2} + \dot{I}_{LIQ3}) \\ & + (\dot{I}_{EX1} + \dot{I}_{EX2} + \dot{I}_{EX3}) \\ & + (\dot{I}_{HX1} + \dot{I}_{HX2} + \dot{I}_{\overline{HX}3} + \dot{I}_{\overline{HX}4}) \\ & + (\dot{I}_{MIXER1} + \dot{I}_{MIXER2} + \dot{I}_{MIXER3}) \end{aligned} \tag{2.9}$$

In conclusion, the calculation of exergy losses was a very powerful means of identifying the sources of irreversibility, their portion of the total loss, the potential for improvement, and their effect on power input and operating costs of the plant.

2.4. Results and discussion

2.4.1. Results

First, the specific exergy and exergy flow were calculated from the simulation results of each stream as shown in Table 2.3 and Table 2.4. In these two tables, it is noted that the reference state of hydrogen is the feed at 2 bar and 25 °C; thus, h_o = 171.30 kJ/kg and s_o = 85.84 kJ/kg-K. The reference state of the MR side was stream 19 at 18 bar and 25 °C; thus, h_o = 348.04 kJ/kg and s_o = 9.24 kJ/kg-K. For cooling water circuit, at streams 41 and 42, and the reference state was at 1 bar and 25 °C; thus, h_o = 105.65 kJ/kg and s_o = 0.37 kJ/kg-K. Stream numbers 2, 6, 13, 30, 33, 38a, 38b, 39, and 40 were blank and were not included in the calculation because they were not needed. The calculation of irreversibility/exergy loss of each component is shown in Table 2.5.

The liquefier can be operated by making the MR refrigerant more complex. Complex composition mean that there are more components in the composition than are found with simplified components of composition. From Table 2.5, with the change from the 5-component composition to the 10- component composition, exergy losses were slightly reduced in most of the components. This reduction was especially evident in the decreased losses at the heat exchangers (HX1, HX2, and $\overline{HX}3$) due to the reduction in the temperature difference between the pre-cooling hydrogen gas and the complex MR refrigerant. This improved temperature difference allowed adaptation to the pre-cooling curve, absorption of more heat, and better

boiling heat-transfer properties than the simplified composition. The reduction in exergy loss at the MR compressor was also due to the lower complex-composition-MR flow-rate needed in the cycle. Finally, the actual work was 7.51 kW, and the liquefier exergy efficiency was 21.06%. This result demonstrates a slight improvement in exergy efficiency. Note that $\dot{W}_{BH,COM} = \dot{W}_{\min,cycle} + (\dot{I}_{total} + \dot{I}_{unknown})$, or 7.51 kW = 1.59 kW + (5.4195 kW+0.5005 kW). *In short, there was a potential improvement for the overall system efficiency when using the proposed complex 10-component composition compared to the simplified 5-component composition.*

In Table 2.4, the simulation data from PRO/II is collected. The return flash hydrogen gas stream (stream 11) was relatively small compared to the main feed (stream 3). Thus, the ideal minimum energy consumption to cool down a single feed through normal hydrogen gas from 21 bar and 25 ^{o}C to normal hydrogen gas at −193 ^{o}C at the same pressure was $w_{MR\ cycle,ideal} = e_{x,7} - e_{x,3}$ = 2,791.84 kJ/kg$_{GH2}$ = 0.7755 kWh/kg$_{GH2}$. The ideal minimum energy consumption to further cool the hydrogen down to −253 ^{o}C was $w_{Helium,ideal} = e_{x,8} - e_{x,7}$ = 7,210.20 kJ/kg$_{GH2}$ = 2.07 kWh/kg$_{GH2}$ as shown in Fig. 2.3.

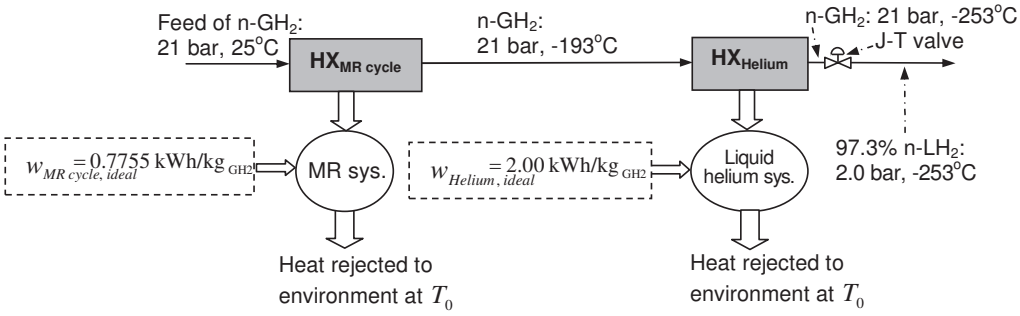

Fig. 2.3 – Ideal minimum energy consumptions calculated from the PRO/II simulation data.

Table 2.2 shows that the efficiency and energy consumption of the proposed 10-component MR system (used to pre-cool normal hydrogen gas at 21 bar from 25 ^{o}C to be −198 ^{o}C of normal hydrogen gas at the same pressure) were less than other conventional (Ingolstant, Leuna, and Praxair) and conceptual (Matsuda, Valenti, Shimko, and Quack) pre-cooling systems. The feed pressure of every refrigeration system was the same at 21 bar and 25 ^{o}C. In the table, Valenti's, Shimko's, and Quack's cycles, which were simulated in PRO/II by the author, have higher energy consumptions than 4.00 kWh/kg$_{GH2}$. The proposed MR system had a lower energy consumption (2.07 kWh/kg$_{GH2}$) and a higher exergy efficiency (38.3%) relative to the ideal minimum of 0.7755 kWh/kg$_{GH2}$ ($\eta_{II,MR\ cycle} = w_{MR\ cycle,ideal} / w_{BH,MR\ COM}$ = 0.7755 kWh/kg$_{GH2}$/2.07 kWh/kg$_{GH2}$ ≈ 0.383). This system offered the best performance when compared to the aforementioned conventional and conception systems. For example, the conventional system had an exergy efficiency of 19.4%. It was assumed that 4.00 kWh/kg$_{GH2}$ was the approximate amount of required energy as simulated in PRO/II by the author. Ortho-para conversion was not included. Actually, at the Ingolstadt plant (as reported by Bracha *et al* (1994) and recalculated by Kuz'menko *et al* (2004)), 4.86 kWh/kg$_{GH2}$ was the amount of energy required, including ortho-para conversion. Specific heat removal from the pre-cooling process was

$\dot{Q}_{pre-cooling} / \dot{m}_{H2} = (h_{feed} - h_{pre-cooled}) = (h_3 - h_7)$ = 3,214.68 kJ/kg$_{GH2}$ = 0.8929 kWh/kg$_{GH2}$. Thus, energy efficiency of the MR cycle was 44.3%, whereas the conventional cycle at the Ingolstadt plant had an efficiency of 22.3%. This result indicates that at the same refrigeration or pre-cooling load, the power consumption of the MR cycle was around half that of the conventional cycle. This finding corresponds to the energy consumptions shown in the table. In short, a comparison between energy and exergy efficiencies (as shown in Eqs. 2.2 and 2.3) highlighted the importance of exergy and showed that the exergy efficiency indicated the proximity to the ideal minimum, whereas the energy efficiency did not.

Table 2.2 – Comparison of the energy and exergy efficiencies of an MR refrigeration system with other conventional and conceptual refrigeration systems.

Refrigeration systems	Inventor	Energy consumption	Energy efficiency	Exergy efficiency
MR refrigeration	Propose in this chapter	2.07 kWh/kg$_{GH2}$	44.3%	38.3%
N_2 refrigeration	Matsuda and Nagami (1998)	≈4.00 kWh/kg$_{GH2}$	≈22.3%	≈19.4%
	Ingolstadt plant in 1992 by Bracha *et al* (1994)	4.00 kWh/kg$_{GH2}$	22.3%	19.4%
	Leuna plant in 2007 (See Chapter 1)	≈4.00 kWh/kg$_{GH2}$	≈22.3%	≈19.4%
	Praxair since 1957 (See Chapter 1)	≈4.00 kWh/kg$_{GH2}$	≈22.3%	≈19.4%
Helium refrigeration	Valenti and Macchi (2008)	A lot higher than 4.00 kWh/kg$_{GH2}$	A lot lower than 22.3%	A lot lower than 19.4%
	Shimko and Gardiner (2007)	Higher than 4.00 kWh/kg$_{GH2}$	Lower than 22.3%	Lower than 19.4%
Propane+helium refrigeration	Quack (2002)	Higher than 4.00 kWh/kg$_{GH2}$	Lower than 22.3%	Lower than 19.4%

From Table 2.5, for the 5-component composition, the majority of exergy losses were from the H_2 compressor and aftercooler, $\overline{HX}4$, the MR compressor, HX1, $\overline{HX}3$, HX7, EX3, and HX2. The large loss from $\overline{HX}4$ occurred because this was not the correct way to cool down the hydrogen gas. The temperature difference between the pre-cooling hot-stream hydrogen gas and the cold, liquid helium from LIQ4 was very large. HX1, HX2, and $\overline{HX}3$, however, performed very well and produced little exergy loss. Note that $\dot{W}_{BH,MR\,COM} = \dot{W}_{\min,cycle} + (\dot{I}_{total} + \dot{I}_{unknown})$, or 7.92 kW = 1.59 kW + (5.8490 kW + 0.491 kW). Finally, the minimum liquefaction work, $\dot{W}_{\min,cycle} = \dot{X}_{10b} - \dot{X}_{1a}$, was 1.59 kW; the actual work, $\dot{W}_{BH,COM} = \dot{W}_{BH,MR\,COM} + \dot{W}_{BH,H2\,COM}$, was 7.92 kW; and the liquefier second law or exergy efficiency, $\eta_{II} = (\dot{W}_{\min,cycle} / \dot{W}_{BH,COM}) \times 100\%$, was 20.06%.

Table 2.3 – Thermodynamic properties of each stream: enthalpy, entropy, specific exergy, and exergy flow of the proposed simplified 5-component composition.

Stream number	Pressure P (bar)	Temp. T (°C)	Flow rate $\dot{m}$ (kg/s)	Enthalpy h (kJ/kg)	Entropy s (kJ/kg-K)	Exergy e_x (kJ/kg)	Exergy flow $\dot{E}_x$ (kW)	Phase	Description
1	2	24.6	0.000571	165.79	85.82	0.04	0.00	Superheated vapor	H_2 cool gas
1a	2	25.0	0.000556	171.30	85.84	0.00	0.00	Superheated vapor	H_2 gas
2	- - -								
3	21	25.0	0.000571	175.87	76.12	2921.68	1.67	Superheated vapor	H_2 cool gas
4	21	-46.1	0.000571	-837.64	72.23	3073.19	1.75	Superheated vapor	H_2 cold gas
5	21	-103.1	0.000571	-1650.18	68.11	3497.42	2.00	Superheated vapor	H_2 cold gas
6	- - -								
7	21	-198.1	0.000571	-3038.81	56.09	5713.52	3.26	Superheated vapor	H_2 cold gas
8	21	-250.0	0.000571	-4193.52	28.21	12923.72	7.38	Superheated vapor	H_2 cold gas
9	2	-250.2	0.000571	-4193.52	29.30	12596.59	7.19	Mixture	H_2 cold mixture
10	2	-250.2	0.000556	-4206.16	28.75	12749.28	7.09	Saturated liquid	H_2 cold liquid
10a	2	-250.2	0.000556	-4206.16	28.75	12749.28	7.09	Saturated liquid	H_2 cold liquid
10b	2	-201.8	0.000556	-3038.81	65.60	2860.63	1.59	Superheated vapor	H_2 cold gas
11	2	-250.2	0.000016	-3744.47	48.88	7172.87	0.11	Superheated vapor	H_2 cold gas
12	2	-201.8	0.000016	-3038.81	65.59	2866.19	0.04	Superheated vapor	H_2 cold gas
13	- - -								
14	2	-107.2	0.000016	-1678.36	77.68	599.29	0.01	Superheated vapor	H_2 cold gas
15	2	-53.8	0.000016	-945.19	81.49	187.96	0.00	Superheated vapor	H_2 cold gas
16	2	10.9	0.000016	-29.66	85.15	6.18	0.00	Superheated vapor	H_2 cold gas
17	2	10.9	0.016818	319.52	8.98	51.62	0.87	Superheated vapor	MR cold gas
18	18	158.7	0.016818	590.32	9.21	253.08	4.26	Superheated vapor	MR hot gas
19	18	25.0	0.016818	213.14	8.12	202.12	3.40	Saturated liquid	MR warm liquid
20	18	25.0	0.011543	282.90	8.59	130.02	1.50	Saturated vapor	MR warm gas
21	18	25.0	0.005274	60.46	7.08	359.91	1.90	Saturated liquid	MR warm liquid
22	18	-46.1	0.005274	-106.68	6.45	384.08	2.03	Compressed liquid	MR cold liquid
23	2	-50.4	0.005274	-106.68	6.47	378.67	2.00	Mixture	MR cold mixture
24	18	-46.1	0.011543	-40.51	7.36	175.93	2.03	Superheated vapor	MR cold mixture
25	18	-46.1	0.005505	54.06	8.29	-9.30	-0.05	Mixture	MR cold gas
26	18	-46.1	0.006038	-126.74	6.51	344.81	2.08	Saturated liquid	MR cold liquid
27	18	-103.1	0.006038	-256.73	5.85	412.34	2.49	Compressed liquid	MR cold liquid
28	2	-106.3	0.006038	-256.73	5.87	405.76	2.45	Mixture	MR cold mixture
29	18	-103.1	0.005505	-209.91	6.95	130.69	0.72	Superheated vapor	MR cold gas
30	- - -								
31	2	-198.1	0.005505	-579.65	3.94	664.32	3.66	Saturated liquid	MR cold liquid
32	2	-199.7	0.005505	-579.65	4.03	635.38	3.50	Mixture	MR mixture
33	- - -								
34	2	-105.8	0.005505	-69.70	8.40	-163.28	-0.90	Superheated vapor	MR cold gas
35	2	-102.8	0.011543	-167.53	7.08	132.66	1.53	Mixture	MR cold gas
36	2	-53.8	0.011543	65.57	8.30	0.32	0.00	Superheated vapor	MR cold gas
37	2	-53.4	0.016818	11.55	7.73	118.90	2.00	Mixture	MR cold mixture
38a, b	- - -								
39, 40	- - -								
41	1	25.0	0.002229	105.65	0.37	0.00	0.00	Compressed liquid	Liquid water
42	1	150.0	0.002229	2775	7.619	494.65	0.50	Superheated vapor	Hot water

Table 2.4 – Thermodynamic properties of each stream: enthalpy, entropy, specific exergy, and exergy flow of the proposed 10-component mixture.

Stream number	Pressure P (bar)	Temp. T (°C)	Flow rate $\dot{m}$ (kg/s)	Enthalpy h (kJ/kg)	Entropy s (kJ/kg-K)	Exergy e_x (kJ/kg)	Exergy flow $\dot{E}_x$ (kW)	Phase	Description
1	2	25.0	0.000571	171.14	85.84	0.00	0.00	Superheated vapor	H_2 cool gas
1a	2	25.0	0.000556	171.30	85.84	0.00	0.00	Superheated vapor	H_2 gas
2		- - -							
3	21	25.0	0.000571	175.87	76.12	2921.68	1.67	Superheated vapor	H_2 cool gas
4	21	-46.1	0.000571	-837.64	72.23	3073.19	1.76	Superheated vapor	H_2 cold gas
5	21	-103.1	0.000571	-1650.18	68.11	3497.42	2.00	Superheated vapor	H_2 cold gas
6		- - -							
7	21	-198.1	0.000571	-3038.81	56.09	5713.52	3.26	Superheated vapor	H_2 cold gas
8	21	-250.0	0.000571	-4193.52	28.21	12923.72	7.38	Superheated vapor	H_2 cold gas
9	2	-250.2	0.000571	-4193.52	29.30	12596.59	7.20	Mixture	H_2 cold mixture
10	2	-250.2	0.000556	-4206.16	28.75	12749.28	7.08	Saturated liquid	H_2 cold liquid
10a	2	-250.2	0.000556	-4206.16	28.75	12749.28	7.08	Saturated liquid	H_2 cold liquid
10b	2	-201.9	0.000556	-3038.81	65.59	2866.19	1.59	Superheated vapor	H_2 cold gas
11	2	-250.2	0.000016	-3744.47	48.88	7172.87	0.11	Superheated vapor	H_2 cold gas
12	2	-201.9	0.000016	-3038.81	65.59	2866.19	0.04	Superheated vapor	H_2 cold gas
13		- - -							
14	2	-107.2	0.000016	-1698.12	77.56	615.10	0.01	Superheated vapor	H_2 cold gas
15	2	-58.5	0.000016	-1011.20	81.19	213.23	0.00	Superheated vapor	H_2 cold gas
16	2	24.5	0.000016	165.39	85.82	0.04	0.00	Superheated vapor	H_2 cold gas
17	2	24.5	0.019929	263.40	6.66	37.68	0.75	Superheated vapor	MR cold gas
18	18	166.1	0.019929	471.27	6.84	193.37	3.85	Superheated vapor	MR hot gas
19	18	25.0	0.019929	173.77	5.99	149.08	2.97	Saturated liquid	MR warm liquid
20	18	25.0	0.015497	207.69	5.81	238.31	3.69	Saturated vapor	MR warm gas
21	18	25.0	0.004432	55.18	6.64	-162.90	-0.72	Saturated liquid	MR warm liquid
22	18	-46.1	0.004432	-101.74	6.04	-140.21	-0.62	Compressed liquid	MR cold liquid
23	2	-50.4	0.004432	-101.74	6.06	-145.17	-0.64	Mixture	MR cold mixture
24	18	-46.1	0.015497	-33.68	4.89	273.69	4.24	Superheated vapor	MR cold mixture
25	18	-46.1	0.008085	32.83	4.67	403.77	3.26	Mixture	MR cold gas
26	18	-46.1	0.007412	-106.23	5.12	131.80	0.98	Saturated liquid	MR cold liquid
27	18	-103.1	0.007412	-215.16	4.57	188.27	1.40	Compressed liquid	MR cold liquid
28	2	-106.3	0.007412	-215.16	4.58	182.79	1.35	Mixture	MR cold mixture
29	18	-103.1	0.008085	-139.35	3.79	497.69	4.02	Superheated vapor	MR cold gas
30		- - -							
31	2	-198.1	0.008085	-349.49	2.09	798.29	6.45	Saturated liquid	MR cold liquid
32	2	-198.4	0.008085	-349.49	2.11	789.59	6.38	Mixture	MR mixture
33		- - -							
34	2	-107.2	0.008085	-43.84	4.69	323.87	2.62	Superheated vapor	MR cold gas
35	2	-105.0	0.015497	-125.78	4.64	255.69	3.96	Mixture	MR cold gas
36	2	-58.3	0.015497	45.41	5.53	158.93	2.46	Superheated vapor	MR cold gas
37	2	-55.6	0.019929	12.69	5.65	90.62	1.81	Mixture	MR cold mixture
38a, b		- - -							
39, 40		- - -							
41	1	25.0	0.002229	105.65	0.37	0.00	0.00	Compressed liquid	Liquid water
42	1	150.0	0.002229	2775.00	7.62	494.65	0.50	Superheated vapor	Hot water

Table 2.5 – Calculation of exergy loss in each process's component of the 5-component and the 10-component mixtures.

Component	Energy equation	Exergy equation	5-component mixture		10-component mixture	
			$\dot{I}$	Percent loss	$\dot{I}$	Percent loss
			(kW)	%	(kW)	%
MR COM	$\dot{W}_{BH,\ MR\ COM} = \dot{m}_{17}(h_{18} - h_{17})$	$\dot{I}_{MRCOM} = \dot{E}_{x,17} - \dot{E}_{x,18} + \dot{W}_{BH,MRCOM}$	1.1662	19.94	1.0392	19.18
H_2 COM	$\dot{W}_{BH,\ H2\ COM} = \dot{m}_1(h_2 - h_1)$	$\dot{I}_{H2\ COM} = \dot{E}_{x,1} - \dot{E}_{x,3} + \dot{W}_{BH,H2\ COM}$	1.7012	29.09	1.7012	31.39
HX1	$\dot{m}_3 h_3 + \dot{m}_{15} h_{15} + \dot{m}_{37} h_{37} + \dot{m}_{20} h_{20} + \dot{m}_{21} h_{21} = \dot{m}_4 h_4 + \dot{m}_{16} h_{16} + \dot{m}_{17} h_{17} + \dot{m}_{24} h_{24} + \dot{m}_{22} h_{22}$	$\dot{I}_{HX1} = (\dot{E}_{x,3} + \dot{E}_{x,15} + \dot{E}_{x,37} + \dot{E}_{x,20} + \dot{E}_{x,21}) - (\dot{E}_{x,4} + \dot{E}_{x,16} + \dot{E}_{x,17} + \dot{E}_{x,24} + \dot{E}_{x,22})$	0.3905	6.68	0.3228	5.96
HX2	$\dot{m}_4 h_4 + \dot{m}_{14} h_{14} + \dot{m}_{35} h_{35} + \dot{m}_{25} h_{25} + \dot{m}_{26} h_{26} = \dot{m}_5 h_5 + \dot{m}_{15} h_{15} + \dot{m}_{36} h_{36} + \dot{m}_{29} h_{29} + \dot{m}_{27} h_{27}$	$\dot{I}_{HX2} = (\dot{E}_{x,4} + \dot{E}_{x,14} + \dot{E}_{x,35} + \dot{E}_{x,25} + \dot{E}_{x,26}) - (\dot{E}_{x,5} + \dot{E}_{x,15} + \dot{E}_{x,36} + \dot{E}_{x,29} + \dot{E}_{x,27})$	0.1133	1.94	0.0856	1.58
$\overline{HX}3$	$\dot{m}_5 h_5 + \dot{m}_{12} h_{12} + \dot{m}_{32} h_{32} + \dot{m}_{29} h_{29} = \dot{m}_7 h_7 + \dot{m}_{14} h_{14} + \dot{m}_{34} h_{34} + \dot{m}_{31} h_{31}$	$\dot{I}_{\overline{HX}3} = (\dot{E}_{x,5} + \dot{E}_{x,12} + \dot{E}_{x,32} + \dot{E}_{x,29}) - (\dot{E}_{x,7} + \dot{E}_{x,14} + \dot{E}_{x,34} + \dot{E}_{x,31})$	0.2290	3.92	0.1043	1.93
$\overline{HX}4$	$\dot{m}_{10a} h_{10a} + \dot{m}_7 h_7 + \dot{m}_{11} h_{11} + \dot{m}_{38a} h_{38a} = \dot{m}_{10b} h_{10b} + \dot{m}_8 h_8 + \dot{m}_{12} h_{12} + \dot{m}_{38b} h_{38b}$	$\dot{I}_{\overline{HX}4} = (\dot{E}_{x,10a} + \dot{E}_{x,7} + \dot{E}_{x,11} + \dot{E}_{x,38a}) - (\dot{E}_{x,10b} + \dot{E}_{x,8} + \dot{E}_{x,12} + \dot{E}_{x,38b})$	1.4483	24.76	1.4395	26.56
HX7	$\dot{m}_{18} h_{18} + \dot{m}_{41} h_{41} = \dot{m}_{19} h_{19} + \dot{m}_{42} h_{42}$	$\dot{I}_{HX7} = (\dot{E}_{x,18} + \dot{E}_{x,41}) - (\dot{E}_{x,19} + \dot{E}_{x,42})$	0.3570	6.10	0.3827	7.06
LIQ1	$\dot{m}_{19} h_{19} = \dot{m}_{20} h_{20} + \dot{m}_{21} h_{21}$	$\dot{I}_{LIQ1} = \dot{E}_{x,19} - (\dot{E}_{x,20} + \dot{E}_{x,21})$	0.0002	0.00	0.0000	0.00
LIQ2	$\dot{m}_{24} h_{24} = \dot{m}_{25} h_{25} + \dot{m}_{26} h_{26}$	$\dot{I}_{LIQ2} = \dot{E}_{x,24} - (\dot{E}_{x,25} + \dot{E}_{x,26})$	0.0001	0.00	0.0000	0.00
LIQ3	$\dot{m}_9 h_9 = \dot{m}_{10} h_{10} + \dot{m}_{11} h_{11}$	$\dot{I}_{LIQ3} = \dot{E}_{x,9} - (\dot{E}_{x,11} + \dot{E}_{x,10})$	0.0078	0.13	0.0000	0.00
EX1	$h_{22} = h_{23}$	$\dot{I}_{EX1} = \dot{E}_{x,22} - \dot{E}_{x,23}$	0.0285	0.49	0.0220	0.41
EX2	$h_{27} = h_{28}$	$\dot{I}_{EX2} = \dot{E}_{x,27} - \dot{E}_{x,28}$	0.0397	0.68	0.0406	0.75
EX3	$h_{31} = h_{32}$	$\dot{I}_{EX3} = \dot{E}_{x,31} - \dot{E}_{x,32}$	0.1593	2.72	0.0703	1.30
EX4	$h_8 = h_9$	$\dot{I}_{EX3} = \dot{E}_{x,8} - \dot{E}_{x,9}$	0.1868	3.19	0.1868	3.45
MIXER1	$\dot{m}_{23} h_{23} + \dot{m}_{36} h_{36} = \dot{m}_{37} h_{37}$	$\dot{I}_{MIXER\ 1} = \dot{E}_{x,36} + \dot{E}_{x,23} - \dot{E}_{x,37}$	0.0011	0.02	0.0135	0.25
MIXER2	$\dot{m}_{28} h_{28} + \dot{m}_{34} h_{34} = \dot{m}_{35} h_{34}$	$\dot{I}_{MIXER\ 2} = \dot{E}_{x,34} + \dot{E}_{x,28} - \dot{E}_{x,35}$	0.0199	0.34	0.0110	0.20
MIXER3	$\dot{m}_{1a} h_{1a} + \dot{m}_{16} h_{16} = \dot{m}_1 h_1$	$\dot{I}_{MIXER\ 3} = \dot{E}_{x,1a} + \dot{E}_{x,16} - \dot{E}_{x,1}$	0.0001	0.00	0.0000	0.00
Total		$\dot{I}_{total}$	**5.8490**	**100.00**	**5.4195**	**100.00**

2.4.2. Comments on how to reduce exergy loss in each component

1. Hydrogen compressor and MR compressor (shown in numbers by PRO/II in Table 2.6):
   - Reduce the suction temperature. From experience, (which can also be verified by calculations) the compressor power is also reduced when the suction temperature is reduced. In this test rig, the hydrogen feed temperature was decreased by turning off the HX8 electric heater. The hydrogen recycled temperature and MR suction temperature were reduced by designing the right MR composition. The right composition, e.g., enough ethane inside the MR cycle, requires enough to boil and cool down HX2 and finally, HX1. Sufficient methane and neon are needed to cool down HX4 and HX3. If all heat exchangers can be cooled down low enough, then the temperature of the suction compressors will be low. Moreover, discharge temperature will also decrease, resulting in the reduction of compressor fatigue, corrosion, and temperature, thereby extending compressor life.
   - Reduce or increase the term of equation: $\dot{I}_{MR\,COM} = \dot{E}_{x,17} - \dot{E}_{x,18} + \dot{W}_{BH,\,MR\,COM}$. From the equation, when the suction temperature is reduced, $\dot{E}_{x,17}$ is reduced. Reduction of the suction temperature causes a reduction in $\dot{W}_{BH,\,MR\,COM}$. For the reasons mentioned above, irreversibility (or loss) is decreased.
   - Decrease the mass flow rate. Because the largest exergy loss (compared to other losses) is at the compressor, reducing the mass flow rate or making a smaller compressor will reduce the power consumption and exergy loss. For this test rig, reducing the MR compressor rotational speed will reduce the MR mass flow rate. But it should also be noted that too low of a MR mass flow rate will cause an insufficient flow to pre-cool the hydrogen gas.
   - Additionally, there is the exergy flow due to heat transfer from the compressor. Cooling down the compressor by any means (water-cooled or air-cooled) is recommended before the compressed gas comes out of the compressor. For this test rig, a two-stage hydrogen compressor was already designed by the manufacturer to include water cooling between the stages. For the MR compressor, heat was ventilated from the compressor by an aircooled fan system.
   - For a large liquefaction system, a good example is the arrangement of hydrogen compressors and pre-cooling propane compressors connected in series. This setup is the same as Quack (2002)'s conceptual plant, which cools down both the suction and discharge gas temperatures by cooling and exchanging heat with a low-temperature propane heat exchanger. Therefore, the suction temperature of a hydrogen compressor and propane compressor is around 0 ^{o}C. Moreover, it is highly recommended for a large compressor manufacturer to design a product with a water cooling system that wraps around the compressor case to transfer heat or make the outer surface temperature as low as possible (the same as a car engine water cooling system). Alternatively, high-flow oil injection cooling can be used in a screw refrigeration compressor. In short, any means of ventilating as much heat as possible somewhere around the compressor is highly recommended. A high efficiency compressor can also be used. The final recommendation is to avoid designing a system that results in too large of a difference between the suction and discharge pressure.

Table 2.6 – Methods to reduce MR compressor's exergy loss/irreversibility of the test rig's 5 components.

Numbers in bold italics are the changed values. Numbers in bold were simulated from PRO/II.	Suction			Discharge			$\dot{W}_{BH,MR\ COM}$	$\dot{I}_{MR\ COM}$
	P_{17}	T_{17}	$\dot{E}_{x,17}$	P_{18}	T_{18}	$\dot{E}_{x,18}$		
Unit	(bar)	(°C)	(kW)	(bar)	(°C)	(kW)	(kW)	(kW)
Suppose that the reference state is at: =>	1.4	25	**-2.94**	22	**194**	**1.74**	**6.09**	**1.41**
1. Reduce suction temperature	1.4	***10.9***	**-2.92**	22	**178**	**1.49**	**5.81**	**1.40**
2. Increase suction pressure	***2.0***	25	**-2.49**	22	**173**	**1.42**	**5.15**	**1.24**
3. Reduce discharge pressure	1.4	25	**-2.94**	***18***	**181**	**1.32**	**5.58**	**1.32**
4. Reduce mass flowrate from 1.8 to 1.58 kg-mole/h	1.4	25	***-2.58***	22	**194**	**1.52**	**5.34**	**1.24**
5. Ventilate heat from compressor	1.4	25	**-2.94**	22	**190**	**1.70**	**6.00**	**1.36**

2. Gas coolers: HX6 and HX7
   - For HX6 and HX7: Increase or make the size of the heat exchanger as large as possible to reduce the temperature difference between the two streams and between the inlet and outlet. However, this will increase the cost of material, so the appropriate size should be considered. For this test rig, gas coolers were already selected and installed. Alterations were not possible.
   - For HX6, *Hydrogen after-cooler*:
     Consider the equation: $\dot{I}_{HX6} = (\dot{E}_{x,2} + \dot{E}_{x,39}) - (\dot{E}_{x,3} + \dot{E}_{x,40})$ and $(T_2 - T_{40})$ should be as close as possible to transfer all heat or to have high heat exchange effectiveness. For example, at HX6, the temperature of stream 40 should be close to or the same as that of stream 2. Likewise, the temperature of stream 39 should be close to or the same as that of stream 3. Also, the cooling water flow rate should be increased as much as possible, but the inlet and the outlet water should not be colder than the outlet hydrogen discharge or the inlet hydrogen suction.
   - For HX7, *MR water-cooled condenser*:
     The following equation, $\dot{I}_{HX7} = (\dot{E}_{x,18} + \dot{E}_{x,41}) - (\dot{E}_{x,19} + \dot{E}_{x,42})$, indicates that the term $(\dot{E}_{x,18} + \dot{E}_{x,41})$ must be a low value, while the term $(\dot{E}_{x,19} + \dot{E}_{x,42})$ must be a high value. Thus, it is recommended to have a low discharge MR temperature, a low water inlet temperature, a high outlet MR temperature (close to water inlet temperature), and a high water outlet temperature (close to MR discharge temperature). The temperature of stream 42 should be close to or the same as that of stream 18, and the temperature of stream 41 should be close to or the same as that of stream 19. In short, a high effectiveness *MR water-cooled condenser* is recommended. A large heat exchanger with a lower water-cool flow rate is better than a small heat exchanger with a high water-cool flow rate and a very low water inlet temperature.

3. Expansion valves: EX1, EX2, and EX3
   - From equations: $\dot{I}_{EX1} = \dot{E}_{x,22} - \dot{E}_{x,23}$, $\dot{I}_{EX2} = \dot{E}_{x,27} - \dot{E}_{x,28}$, and $\dot{I}_{EX3} = \dot{E}_{x,31} - \dot{E}_{x,32}$; a decrease in exergy loss means making the difference between the inflow and outflow exergy rate, $\dot{E}_x$ as small as possible.
   - The only way to reduce exergy loss in the expansion device is by reducing the pressure difference. This reduction may involve avoiding too large of a pressure difference between the suction and discharge pressure of the MR cycle. Also, this may mean trying

to maintain the suction MR pressure at the designed 2.0 bar, with a low discharge MR pressure.

- The last way to reduce exergy loss is to reduce the temperature difference between an incoming fluid temperature and an out-going fluid temperature.

4. Heat exchangers: HX1, HX2, HX3, HX4, and HX5 (shown in numbers by PRO/II in Table 2.7)
   - Increase heat transfer or increase the size of the heat exchanger as much as possible to enhance the surface area between the two streams (hydrogen and MR) and the decreased temperature difference between the inlet and outlet. For example, from HX3, consider the equation: $\dot{I}_{\overline{HX}3} = (\dot{E}_{x,5} + \dot{E}_{x,12} + \dot{E}_{x,32} + \dot{E}_{x,29}) - (\dot{E}_{x,7} + \dot{E}_{x,14} + \dot{E}_{x,34} + \dot{E}_{x,31})$; $(T_5 - T_{14})$, $(T_6 - T_{13})$, $(T_{29} - T_{34})$, and $(T_{30} - T_{33})$ should be as close as possible to transfer all heat or to have a high heat exchange effectiveness (an almost perfect heat exchanger). For example, at $\overline{HX}3$, the temperatures of stream 14 and 34 should be close to those of stream 5 and 29, and the temperatures of stream 12 and 32 should be close to those of stream 5 and 29. Other heat exchangers, HX1, HX2, HX4, and HX5, are all the same. The results from attempting to make the temperature difference between the hydrogen and MR as low as possible while pre-cooling are shown in Fig. 2.4. Finally, it is recommended that more components of the MR composition, e.g., a complex composition instead of simplified one, have a smaller temperature gap between the pre-cooled hydrogen and the MR cooling mixture. This is to increase the heat exchanger size or enhanced surface area; however, this will increase the cost of material, so the appropriate size should be considered. In the actual large plant design, the heat exchanger should be inside a vacuum chamber to attempt to reduce the temperature difference. However, a vacuum will cause it to be too big to fit inside. Therefore, consultations should be made with the heat exchanger manufacturer. From the energy and exergy balances above, it should be noted that the amount of heat transfer from the feed hydrogen gas to the MR cold stream in HX1 to HX4 was not directly related to how much exergy was lost.
   - The right substance, capable of both flowing and boiling (to take heat away from each heat exchanger) is recommended. Because boiling involves latent heat of phase change, it can absorb more heat per kg of mass flow. Thus, only a small amount of fluid flow is needed. Less energy is required to drive the smaller fluid flow, which results in a smaller compressor size. Thus, the heat exchanger size is reduced. Moreover, a small temperature difference between the two fluid streams reduces the exergy loss in the heat exchanger. It should be noted that the author tried to have a high concentration of methane in $\overline{HX}3$, ethane in HX2, and butane in HX1 to boil and thus take heat away from each heat transfer. This boiling heat transfer method is the best way to remove as much heat as possible. In short, the right MR composition will make this successful.

5. Mixers: MIXER1 and MIXER2
   Reducing the exergy loss at fluid mixer is difficult. It should be noted that trying to avoid too large of temperature difference between the two incoming-mixing streams and the exit stream will reduce exergy loss at the fluid mixer. On the test rig, this can be done by adjusting the MR compressor speed and modifying the MR composition.

6. Liquid separators: LIQ1, LIQ2, and LIQ3
   Reduce the pressure drop by avoiding pressure differences, temperature differences, and a high liquid level over the inlet. Reducing the exergy loss at the fluid gas separators is

important. Insulation must be made for the low-temperature LIQ2 and LIQ3 segments of the test rig to prevent heat. Finally, it should be noted that the separation of two phases in equilibrium is nearly reversible.

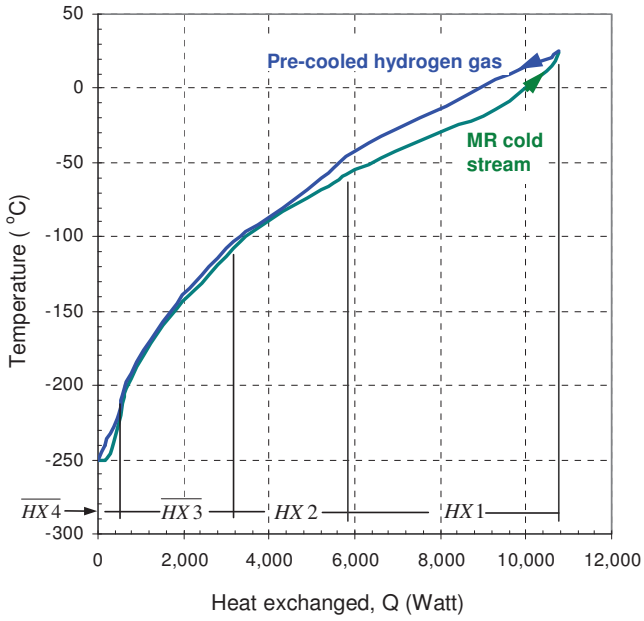

Fig. 2.4 – Hydrogen pre-cooling curve of the proposed 10-component composition.

Before designing a large system, improvements must be made. For the exergy analysis, some development must be done to reduce the exergy loss in each component as recommended. A concise conclusion of these recommendations are as follows:

1. H_2 compressor and MR compressor: use the highest efficiency compressor, e.g., 80–95 percent.
2. More improvement to reduce exergy loss at HX1, e.g., a better MR composition to cool down HX1.
3. No $\overline{HX}4$ in a real large system.
4. For a real large system, use turbines to replace EX3 and EX4 (and maybe EX1 and EX2).
5. Use an additional liquid separator, e.g., LIQ4, after EX3 as a buffer to maintain volatile components.
6. More improvements in MIXER1 and MIXER2, if possible.
7. Use a complex composition, if possible.
8. In MR composition, replace neon with hydrogen because of its higher specific heat capacity.
9. Improvements to reduce exergy loss at HX7.

In short, in order to improve the test rig to be a more highly efficient future large-scale plant, replace the components with higher efficiency compressors, almost perfect heat exchangers with complex MR refrigerant compositions, and higher efficiency expanders.

Table 2.7 – Methods to reduce HX3 and HX4's exergy loss/irreversibility of the test rig's 5 components of composition.

Numbers in bold italics are the changed values. Numbers in bold were simulated from PRO/II.	Inlet flow				Outlet flow				$\dot{Q}_{\overline{HX}3}$	$\dot{I}_{\overline{HX}3}$
	T_5	T_{12}	T_{29}	T_{32}	T_7	T_{14}	T_{31}	T_{34}		
Unit	(°C)	(°C)	(°C)	(°C)	(°C)	(°C)	(°C)	(°C)	(kW)	(kW)
Reference state	-103	-201	-103	-199	-198	-105	-198	-105	**2.828**	**3.92**
1. High HXs effectiveness	-103	***-199***	-103	***-199***	-198	***-104***	-198	***-104***	**2.880**	**1.50**
2. MR 10 components instead of 5	-103	-201	-103	-198	-198	-107	-198	***-107***	**2.489**	**1.93**

2.5. Conclusion

Because of its higher efficiency, a new innovative MR refrigeration system is proposed in this chapter as a pre-cooling system to cool down hydrogen gas in a small-scale laboratory hydrogen liquefaction plant. This chapter presents a simulation of a test rig capable of liquefying 2 kg/h of normal hydrogen gas at 21 bar and 25 °C to normal liquid hydrogen at 2 bar and −250 °C. The simplified 5-component composition suggested for the test rig was found consisting of 4% hydrogen, 18% nitrogen, 24% methane, 28% ethane, and 26% butane by mole. The mixed refrigerant composition is adjusted from trial and error to match the cooling curve of feed hydrogen gas. Whereas, the complex 10-component composition yields slight improvement of efficiency; it is considered the same as the simplified 5-component composition. The simulated power consumption of the MR compressor in the MR refrigeration system was 2.07 kWh per kilogram of feed hydrogen gas (to pre-cool it from 25 °C to −198 °C), which was the lowest power consumption compared to today's conventional hydrogen liquefaction cycles (with power consumptions around 4 kWh per kilogram of feed hydrogen gas). The energy efficiency of the MR cycle was 44.3%, compared to 22.3% for the conventional cycle such as the Ingolstadt plant. The proposed MR system had a higher exergy efficiency at 38.3% from the ideal minimum at 0.77 kWh/kg_{GH2}, whereas the conventional system had a lower exergy efficiency of 19.4%. The main purpose of this chapter was to find where and how exergy losses occurred and to optimize the test rig's overall performance through a reduction in exergy loss in each component. It was found that major losses resulted from the compressors, heat exchangers, and expansion valves. To highlight the importance of exergy, the exergy efficiency indicated the proximity to the ideal minimum, whereas energy efficiency did not. Importantly, exergy analysis was needed to find the losses and optimize the MR system proposed in this chapter. Finally, comparison of the simulation data presented in this chapter to experimental data of the test rig is reported in Chapter 3.

Chapter 3. Simulation and experiment of a hydrogen liquefaction test rig using a multi-component refrigerant refrigeration system

A small-scale laboratory hydrogen liquefaction plant that contains a new innovative MR refrigeration system is proposed. A test rig was constructed to verify the simulation of this system. Initial experiments indicated that the rig was able to adequately cool normal hydrogen gas from 25 ^{o}C to −158 ^{o}C at a flow rate of 0.6 kg/h using a simplified 5-component MR composition refrigeration system. The power consumption of pre-cooling from the MR compressor was 1.76 kWh per kilogram of feed hydrogen gas. After two weeks, the lowest temperature was about −180 ^{o}C when a few additional grams of nitrogen gas were charged into the rig. There were some differences, but most of all, the simulation and experimental data were in good agreement. The primary conclusion was that pre-cooling hydrogen gas with the MR refrigeration system resulted in a lower energy consumption per kilogram of feed hydrogen gas compared to conventional refrigeration systems.

3.1. Introduction

Hydrogen has good potential as an energy vector for future use in transportation vehicles, and several hydrogen research activities have been conducted since 1980 and especially since 2000. One of the major obstacles for the future hydrogen economy is the large amount of hydrogen liquefaction work. There are several existing simple hydrogen liquefaction processes (Dewar 1898; Barron 1966; Timmerhaus and Flynn 1989; Nandi and Sarangi 1993). Baker *et al* (1978) proposed the first conceptual plant with the lowest efficiency. Today, large hydrogen liquefaction plants, such as the Ingolstadt plant described by Bracha *et al* (1994), have exergy efficiencies of only 20–30%, which is considered to be very low. The plant consumes 4.86 kWh per kilogram of hydrogen gas using a nitrogen refrigeration system to pre-cool normal hydrogen gas from 25 ^{o}C to equilibrium hydrogen gas at −198 ^{o}C. Therefore, it is possible to improve this efficiency. From 1998 until 2008, some conceptual plants were proposed that reported improved efficiencies of 40–50%: Matsuda (1998) under WE-NET's project (Mitsugi *et al*, 1998), Quack (2002), Kuz'menko *et al* (2004), Shimko and Gardiner (2007), and Valenti and Macchi (2008). Different cycles were compared by Berstad *et al* (2010). Later on, a literature review for the development of large-scale hydrogen liquefaction processes throughout the world from 1898 to 2009 is in Chapter 1. Finally, in 2009, NTNU and SINTEF Energy Research AS proposed a new large-scale MR refrigeration system with an efficiency greater than 50%.

Multi-component refrigerant was used in the test rig cycle. This concept of mixed refrigerant in gas liquefaction which was developed in recent years results in reduced energy consumption compared to conventional liquefaction cycles. It is in agreement with the work by Bottura (2009), Chrz (2010), Mafi *et al* (2009), and Bosma and Nagelvoort (2009). In this chapter, the differences are as follows: a new modified cycle and a new optimized refrigerant composition designed for pre-cooling hydrogen gas from 25 ^{o}C to −198 ^{o}C were used, as proposed by Stang *et al* (2006).

In this chapter, simulations and experiments of a small-scale laboratory test rig were performed. The simulation was conducted to design the rig, whereas the experiments were performed to verify the simulation data. First, a determination of the correct simplified composition and the operation of the small-scale laboratory liquid hydrogen plant are described. Then, the simulation, optimization, experiment, comparison, and discussion of the results are presented.

3.2. Test rig description

A schematic diagram of the test rig is shown in Fig. 3.9, and the rig is further explained in Section 3.3.2. Fig. 3.1 (a) shows the outside of the test room, i.e., an overview of the test rig. All of the compressors, heat exchangers, and instruments were located inside of the test room. The room is designed to protect personnel in case of a fire, hydrogen leak, or explosion.

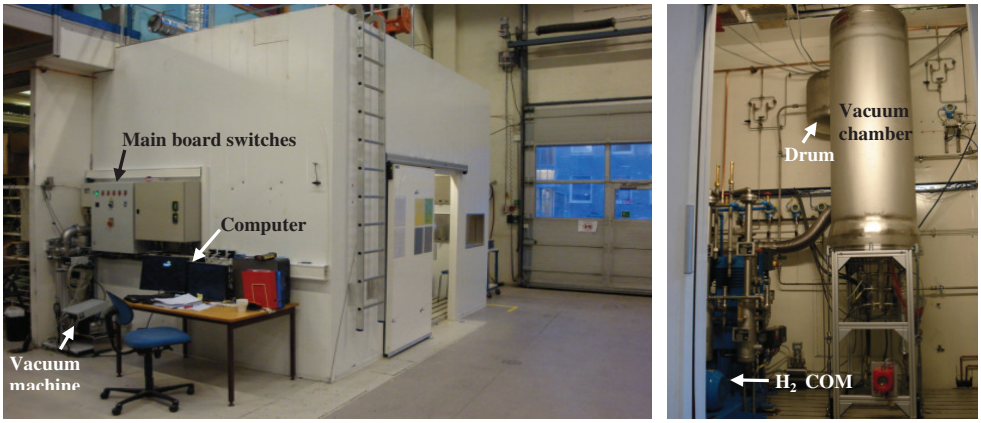

Fig. 3.1 – Complete construction of: (a) the test room, and (b) inside the test room.

Fig. 1 (b) shows a portion of the inside of the test room. The vacuum chamber contains all of the heat exchangers: HX1, HX2, HX3, HX4, and HX5. The heat exchangers are handmade copper spiral tube-in-tube type that were internally designed and manufactured. The vacuum chamber also contains LIQ2, EX1, EX2, and EX3. The hydrogen compressor unit (bottom left of Fig. 3.1 (b)) is equipped with a Mehrer TZL 20/80/65/S4-4Ex compressor, which is an open-type two-stage reciprocating unit with two cylinders with a rotational speed of 485 RPM. The compressor is used to compress hydrogen gas from 25 ^{o}C at a suction pressure of 2 (abs) bar to an outlet pressure of 21 (abs) bar, and the expected hydrogen flow rate is 2 kg/h. The unit is water cooled between stages. The power of the motor is 4 kW. The MR compressor unit is a Blackmer HD162C compressor, which is an open-type single-stage reciprocating unit with one cylinder.

The rotational speed is 350/825 RPM. The compressor is used to compress MR gas at 25 ^{o}C at a suction pressure of 2.0 (abs) bar to an outlet pressure of 20 (abs) bar, and the expected gas flow rate is 44 kg/h. The compressor always operates at its maximum speed; thus, the maximum braking horsepower is 7.5 kW. The hydrogen flow-rate meter is a Brook Instruments 5863E (with an accuracy of ±1%), and the mass flow meter for the MR circuit is an Endress+Hauser – Promass 83F (with an accuracy of ±0.35%). The temperature sensors are Lake Shore Silicon diodes DT-470-CO-13 (with an accuracy of ±0.5 K for a temperature range of 2 K to 30 K, ±0.25 K for 30 K to 60 K, and ±0.15 K for 60 K to 345 K). The liquid level sensors are Endress PMD75 (with accuracy ±0.05%), and the pressure sensors are Endress PMD71 (with an accuracy up to ±0.075% of the set span).

3.3. Preliminary rig simulation

3.3.1. Determination of the correct components

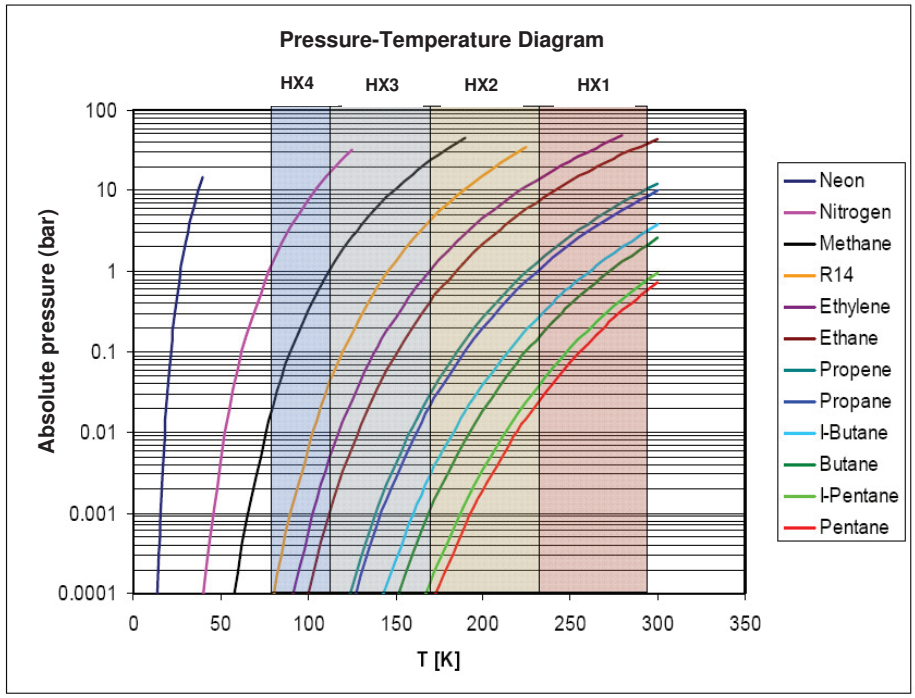

Fig. 3.2 – Boiling curves for different components simulated from PRO/II version 8.1.

Fig. 3.2 presents the boiling curves for arbitrarily selected components: neon, nitrogen, methane, R14, ethylene, ethane, propene, propane, I-butane, butane, I-pentane, and pentane. These curves were obtained from the boiling temperature and pressure of each substance and were plotted using PRO/II. The designed working temperatures of the four heat exchangers are shown as dashed blue lines, whereas the boiling pressure of the MR composition in the MR cycle at 2.0 bar is shown as a red horizontal line. For each of the selected components in the composition, the

partial pressure (0.1−1 bar) at the boiling point temperature is slightly below this value. Although it is difficult to use these curves to directly calculate the optimal composition of the MR, they were used to indicate the components that must be included. For example, at heat exchanger 1 (HX1), one or two volatile substances such as propane, I-butane, butane, I-pentane, or pentane should be selected. At HX3 and HX4, methane and nitrogen should be selected to boil and transfer heat from the hydrogen gas. Additionally, the flow rate of each substance should be high enough to boil and transfer heat in each of the heat exchangers. Neon was also used in the refrigerant because its lower temperature could be used to cool HX4.

3.3.2. Design conditions

The simulation model was built in PRO/II. Ortho-para conversion reactors were not included because the experimental rig did not contain a catalyst for ortho-para conversion. The laboratory test rig shown in Fig. 3.9 was designed to use a complex multi-component refrigerant with 10 components. The concept of multi-component refrigerants or mixed refrigerants (Bottura 2009; Chrz 2010; Mafi *et al* 2009; Bosma and Nagelvoort 2009) are widely used in the liquefaction of natural gas because of their reduced energy consumption compared to conventional liquefaction cycles. SINTEF Energy Research AS has worked with these types of refrigeration cycles for several years. During the startup period of the rig, a less complex 5-component composition of the MR was used. To obtain a theoretically optimized refrigerant-mix, a flow chart was used to model the liquefaction rig using the PRO/II simulation program. The design conditions for the test rig are shown in Table 3.1.

Table 3.1 – Assumptions in the simulation model.

Hydrogen flow rate	2 kg/h	-	-	-
Compressors	**Inlet abs. pressure (bar)**	**Outlet abs. pressure (bar)**	**Isentropic efficiency**	**Outlet temperature (^{o}C)**
H_2 compressor	2 bar at stream 1	21 bar at stream 2	0.65	25
MR compressor	2 bar at stream 18	18 bar at stream 18	0.70	25
Heat exchangers	**Hot stream outlet temperature (^{o}C)**	**Cold stream outlet temperature (^{o}C)**	**Pressure drop (bar)**	**Heat leak (W)**
HX1	–46.15 ^{o}C at stream 4	-	0	0
HX2	–103.15 ^{o}C at stream 5	-	0	0
HX3	–163.15 ^{o}C at stream 6	-	0	0
HX4 ($\overline{HX}3$)	–198.15 ^{o}C at stream 7	-	0	0
HX5 ($\overline{HX}4$)	–250.00 ^{o}C at stream 8	-	0	0
JT valves	**Outlet pressure (bar)**	-	-	-
H_2: (EX4)	2	-	-	-
MR: (EX1, EX2, EX3)	2	-	-	-
Flash drums	**Pressure drop (bar)**	**Duty (W)**	-	-
LIQ1	0	0	-	-
LIQ2	0	0	-	-
LIQ3	0	0	-	-

From Fig. 3.3 and Fig. 3.9, feed hydrogen gas was first compressed from a suction pressure in a two stage hydrogen piston compressor with inter- and after-cooling. The outlet temperature of the aftercooler (both H_2 and MR circuit) was set to 25 ^{o}C. The hydrogen gas was subsequently cooled in five heat exchangers. In the first four heat exchangers, the hydrogen was pre-cooled by the MR circuit and hydrogen flash gas from the Joule-Thomson valve. In the last heat exchanger, the

hydrogen flash gas and product were used to cool the hydrogen feed, but no helium was used in the simulation. For the final cooling of the hydrogen to −251 °C, a Joule-Thomson valve was used to throttle the hydrogen down to the suction pressure. In a large-scale hydrogen liquefaction plant, an expansion machine can be used; however, its use was not economically feasible for this small-scale laboratory plant. The SRK equation of state was selected as the fluid package for the simulation software because of its popularity, simplicity, and computational efficiency. The goal was to minimize the MR compressor power by optimizing the following variables:

1. Suitable H_2 compressor discharge pressure:
   The discharge pressure must be greater than 15 bar (supercritical pressure) to avoid condensation. For the test rig, the discharge pressure was designed to be 21 bar, which is equivalent to the pressure of the feed at Ingolstadt. Higher feed pressures result in minimal work liquefaction, which was reported by Matsuda and Nagami (1998), Quack (2002), and Valenti and Macchi (2008) who used values of 50, 80, and 60 bar, respectively. At the large-scale, if the feed is 1–2 bar, then it is recommended to compress the feed discharge to 21 bar instead of a higher value because of the increased energy requirement.
2. Suitable H_2 compressor suction pressure:
   The suction pressure must be a slightly above the ambient pressure (1 bar) to be stored in a liquid tank before it is supplied. Ingolstadt uses 1.3 bar. For this test rig, the pressure could be anywhere between 1.3 and 2 bar. For the simplicity of the controls, a value of 2 bar was selected.
3. Suitable MR compressor discharge pressure:
   Several simulation trials were performed using PRO/II to determine the optimal composition for different suction pressures. An optimized, simplified, 5-component composition that consisted of 4% hydrogen, 18% nitrogen, 24% methane, 28% ethane, and 26% butane by mole was adequate with different suction and discharge MR pressures for all of the cases. A suitable MR compressor discharge pressure was 18 bar, which resulted in a MR compressor power of 4.55 kW. If the pressure was lower than 18 bar, e.g., 15, 16, or 17 bar, then it was impossible for the MR system to cool the hydrogen. In addition, solid phase MR flow could form inside of the heat exchangers if the pressure was much lower than 18 bar. However, if the discharge pressure was higher than 18 bar, then the system would function, but it would result in an increase in MR compressor power. Furthermore, if the pressure was too high, then there would be more exergy losses at expansion valves EX1, EX2, and EX3.
4. Suitable MR compressor suction pressure:
   A very high or low suction pressure would not be allowed. The hydrogen gas can be cooled sufficiently to the specified design temperature (−198 °C) flowing out of $\overline{HX}4$. A suitable pressure was 2 bar, which resulted in the minimum (theoretical) brake horsepower (4.55 kW) of the MR compressor. The suction pressure should not be lower than 1 bar because that would increase the MR compressor power; additionally, the pressure should not be higher than 2 bar because this would result in a system that could not sufficiently cool the hydrogen gas.
5. Hot stream hydrogen outlet temperatures from HX1, HX2, HX3, HX4, and HX5:
   Trial and error was used to determine the optimal temperatures.
6. Suitable composition of the MR cycle:
   Trial and error was used to determine the optimal composition as shown in Table 3.2.

3.3.3. The proposed simplified 5-component composition for the initial experiment

For simplicity, a reduced number of components for the composition were required to perform the initial experiment as aforementioned in Chapter 2. The simulation results proposed an optimized composition of 4% hydrogen, 18% nitrogen, 24% methane, 28% ethane, and 26% butane by mole with 66.4 kg/h, as shown in Table 3.2. The new composition was changed by trial and error; it was adjusted to match the cooling curve of feed hydrogen gas to avoid cross over between hot and cold streams as depicted in Fig. 3.5 and importantly in Fig. 3.6. Neon could be replaced by hydrogen or helium with similar results. The experiments were performed on the test rig, and trial and error was used to obtain the composition. Finally, the simulation result for this composition is shown in Fig. 3.3 and is detailed below:

More amount of hydrogen which is increased a little is needed to cool $\overline{HX}3$ to prevent the cross over. As in Fig. 3.9, *Simulation data of the laboratory test rig with the proposed simplified composition compared to the experimental data*, it can be noticed here that why the rig couldn't produce very low temperature at TE106 to −198 °C as required with the measured 5-component composition; it seemed it still lacked a lot of nitrogen. In the new composition, neon is replaced by hydrogen because hydrogen has better heat transfer property than neon. Moreover, it is likely that hydrogen is cheaper and easier affordable. The new flowrate is the minimum value; it is increased a little to make sure there is positive temperature difference every where at the *Q-T* and *h-T* curves shown in Figs. 3.5 and 3.6.

Table 3.2 – Choice of the proposed 5-component MR composition.

Option No.	1	2	3
Component	**%Mole**	**%Mole**	**%Mole**
Hydrogen	-	4	-
Helium	-	-	4
Neon	4		-
Nitrogen	18	18	18
Methane	24	24	24
Ethylene	-	-	-
Ethane	28	28	28
Propene	-	-	-
Butane	26	26	26

The possibility of having three components of the composition, e.g., 26% methane, 30% ethane, and 28% butane, without nitrogen was investigated. In this case, the pre-cooled hydrogen gas at stream 7 leaving $\overline{HX}3$ could only be cooled to −150 °C but not to the designed −198.15 °C. Therefore, the presence of nitrogen in the composition was required to sufficiently cool the hydrogen gas because nitrogen has a lower boiling temperature than methane after expanding at EX3. In conclusion, the composition must have at least five components, and more components result in a little better liquefier. The simulation results are shown in Fig. 3.3 for an energy consumption of 3.96 kWh/kg of the hydrogen liquefied/feed. The MR flow rate was 66.4 kg/h, which is the minimum flow rate. The flow rate must be maintained above this minimum rate; otherwise, the low-temperature liquefaction system cannot be produced because there would not be enough MR fluid flowing to transfer heat.

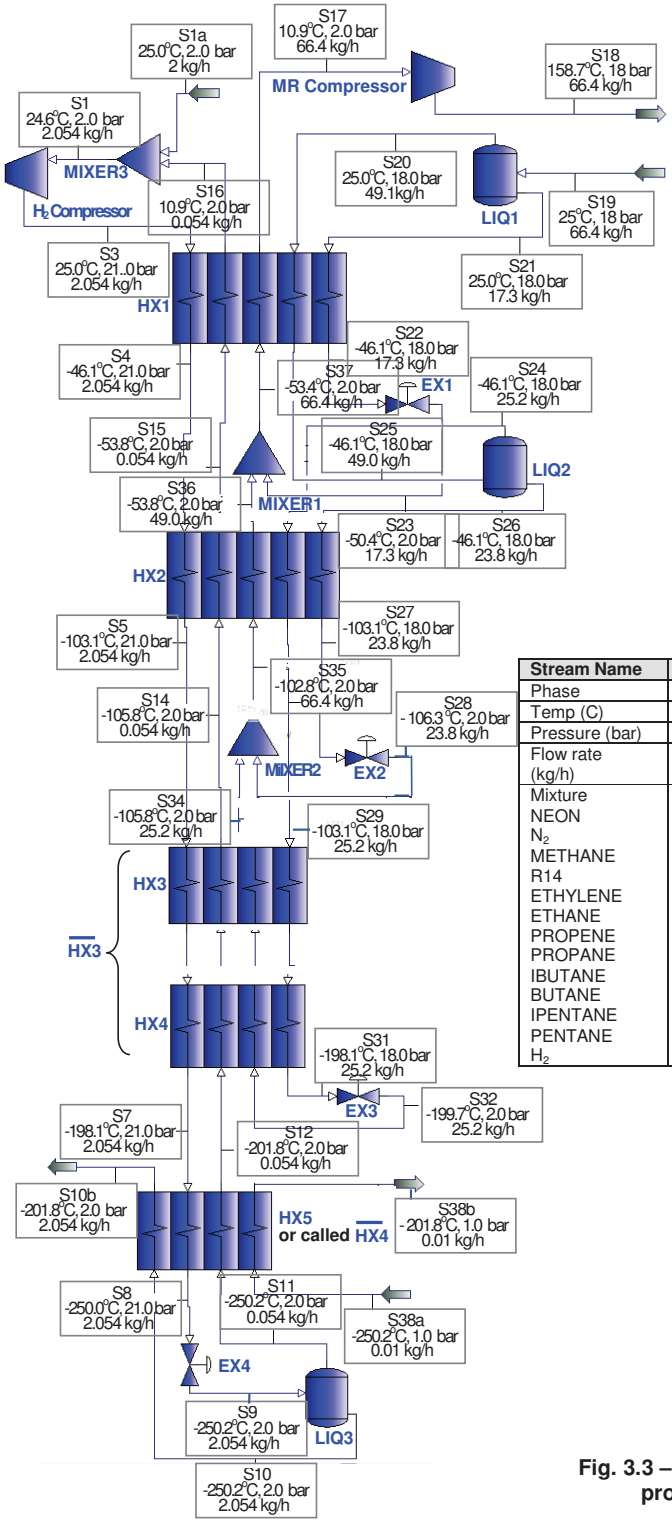

H_2 compressor power	= 3.37 kW
MR compressor power	= 4.55 kW
All compressor power	= 7.92 kW
System energy consumption	= 14,267 kJ/kg_{LH2}
	= 3.96 kWh/kg_{LH2}

Stream Name	S19	S20	S21	S23	S28	S31
Phase	Mixed	Vapor	Liquid	Mixed	Mixed	Mixed
Temp (C)	25	25	25	- 50.3	-105.6	-198.1
Pressure (bar)	18	18	18	2.0	2.0	18
Flow rate (kg/h)	66.4	49.1	17.3	17.3	23.8	25.2
Mixture						
NEON	0.040	0.048	0.001	0.001	0.001	0.073
N_2	0.180	0.214	0.008	0.013	0.013	0.323
METHANE	0.240	0.282	0.031	0.080	0.080	0.391
R14	0.000	0.000	0.000	0.000	0.000	0.000
ETHYLENE	0.000	0.000	0.000	0.000	0.000	0.000
ETHANE	0.280	0.305	0.157	0.484	0.484	0.208
PROPENE	0.000	0.000	0.000	0.000	0.000	0.000
PROPANE	0.000	0.000	0.000	0.000	0.000	0.000
IBUTANE	0.000	0.000	0.000	0.000	0.000	0.000
BUTANE	0.260	0.151	0.804	0.422	0.422	0.005
IPENTANE	0.000	0.000	0.000	0.000	0.000	0.000
PENTANE	0.000	0.000	0.000	0.000	0.000	0.000
H_2	0.000	0.000	0.000	0.000	0.000	0.000

The proposed mixture

Fig. 3.3 – PRO/II simulation flow-sheet of the proposed 5-component mixture.

Fig. 3.3 shows a hydrogen pre-cooling curve. Table 3.3 shows that most of the heat from the MR hot stream is transferred to the MR cold stream.

Table 3.3 – Amount of heat transfer from the two hot streams to the MR cold stream (Q), Watts.

HX	From H_2 gas hot stream (W)	From MR hot stream (W)	Total (W)
HX 1	578	3,760	4,338
HX 2	464	1,783	2,247
HX 3	793	1,625	2,418

Fig. 3.4 indicates that the MR pre-cooling performs better than N_2 pre-cooling because, in the latter case, a large amount of heat is transferred to the N_2 at a constant temperature (roughly 80 K), whereas, in the former case, heat is transferred to the MR at a variable temperature. In addition, the MR can better track the H_2 cooling curve.

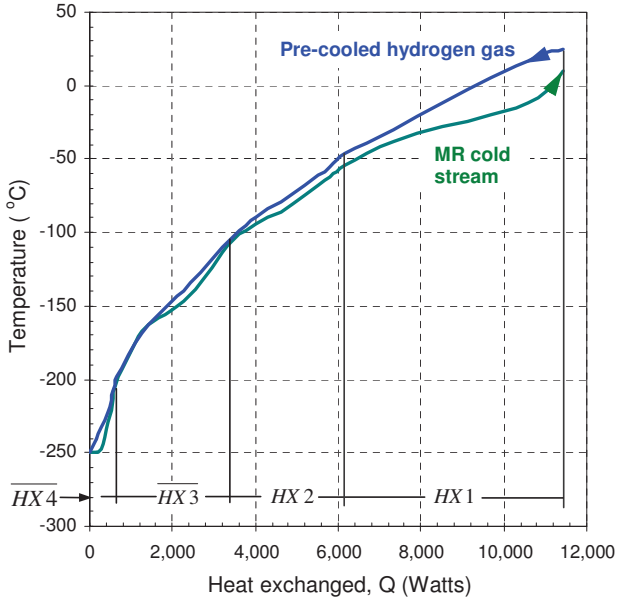

Fig. 3.4 – Hydrogen pre-cooling curve for the proposed 5-component composition depicted in Table 3.2 and Fig. 3.3.

Around 84% of the worldwide LNG produced today comes from the plant utilizing propane pre-cooled, mixed refrigerant technology that all contained in the order of 20% propane more or less (Jensen 2008, p. 155; Alabdulkarem *et al* 2011; Mortazavi *et al* 2011; and Linde Engineering 2011). According to Fig. 3.2, *Boiling curves for different components*, propane has boiling curve near butane and ethane. Therefore, propane can be in the new proposed 5-component composition by substituting either butane or ethane:

- Suppose butane is replaced by propane to consist of the following composition: 4% hydrogen, 18% nitrogen, 24% methane, 28% ethane, and 26% propane. Because propane is more volatile than butane. In this case, the composition at 25 ^{o}C and 18 bar entering LIQ1 at Stream 19 (S19) is all vapor as depicted in Fig. 3.3, *PRO/II simulation flow-sheet of the proposed 5-component composition*. Location of LIQ1 of the test rig can be read from the figure. By simulation, 28% propane in the composition will be in vapor at S19 and S20. Thus, there will be no liquid at S21 leaving LIQ1 to cool HX1 of the rig for making the possible MR refrigeration cycle. For that reason, propane is not suitable for this case.
- Suppose ethane is replaced by propane to consist of the following composition: 4% hydrogen, 18% nitrogen, 24% methane, 28% propane, and 26% butane. Due to the fact that propane is heavier than ethane. If the composition as mentioned flows in S19 passing LIQ1, propane containing in the composition exists both in liquid and vapor phase will be separated. S21 with high flow rate as in the Fig. 3.3 consists mostly of liquid propane and liquid butane in order to flow to cool HX1. But the amount of the liquid mixture flowing at S21 is too much than what is needed to cool down HX1. In other words, there is less gas mixture flowing at S20 out causing no enough refrigerant gas flowing pass LIQ1 to cool down HX2 and HX3. Thus, there will be crossover of *h-T* curves between hot and cold curves in HX2 and HX3.

All possible MR compositions with every component were tried resulting with only the best new proposed 5-component MR composition aformentioned. But that was just simulation. 20% propane in the composition was simulated but the new proposed 5-component MR composition was better. However, the best way to verify the best composition must be from experiment. In conclusion, propane is not appropriate to contain in the proposed 5-component composition because of the reasons explained aforementioned.

Fig. 3.5: (a), (b), and (c) show here the simulated *Q-T* curves (Heat transfer, kW and temperature, ^{o}C) for HX1, HX2, and $\overline{HX}3$ respectively. The *Q-T* curves belong to the new proposed 5-component composition: 4% hydrogen, 18% nitrogen, 24% methane, 28% ethane, and 26% butane with 66.4 kg/h at S19. There is positive temperature difference every where. Fig. 3.4, *Hydrogen pre-cooling curve for the proposed 5-component composition*, shows the *Q-T* curves of all the HXs. All are just simulation. However, more big gap of the positive temperature difference everywhere along the lines between the hot and cold streams can be seen, it is recommended increasing the MR flow rate in the simulation of the rig. The simulated 5-component composition of the rig will be the same that it will depend mostly on assumptions in Table 2.1, *Boundary conditions of the test rig's simulation.* After that, there will be more temperature difference between the hot and cold streams. But the power consumption of MR compressor will be a little higher.

Fig. 3.6: (a), (b), and (c) depict *h-T* curves (scaled enthalpy in % with temperature in ^{o}C) of all streams in each heat exchanger: HX1, HX2, and $\overline{HX}3$. The *h-T* curves belong to the new proposed 5-component composition. Each figure, each stream of *h-T* data is first scaled from the unit of enthalpy in kJ/kg by setting zero at enthalpy value at the lowest temperature which is at the lowest end, and the modified value is then scaled from minimum to maximum enthalpy with

value 0-100%. In each figure, there is positive difference every where between the "Cold MR" stream that cools other hot streams ("Subcooled MR" and "Feed GH_2"). It is except the lowest end between "Cold MR" and "Subcooled MR" streams in Fig. 3.6 (c) are at the same value of enthalpy because the flow passes through throttle valve results in equivalent enthalpy. And there is a cross over in each Fig. 3.6: (a), (b) and (c), but that is between two cold streams ("Cold MR" and "Return GH_2"); thus it is not important because they don't transfer heat each other. In each Fig. 3.6: (a), (b) and (c), the cold "Return GH_2" stream has trivial flow rate with only 2% by mass compared to the "Feed GH_2" stream and approximately 0.02% or less by mass compared to the "Subcooled MR" streams; hence it doesn't affect all other *Q-T* and *h-T* curves. What more is with or without the cold "Return GH_2" stream, it is not important; nothing will be changed regarding *Q-T* and *h-T* curves together with temperatures, pressures, or others at steady state run simulation result. This is because its trivial and very little flow rate generates trivial/extremely little heat transfer to other hot streams. In short, the trivial little cold "Return GH_2" flow stream doesn't cool MR evaporators because it has very little amount of flow rate compared to other hot streams.

Regarding the cross over's problem of *h-T* curves in heat exchangers in Fig. 3.6: (a), (b), and (c) and how to handle them, the explanation is step by step as explained below:

- Let's first consider PRO/II simulation flow sheet of the rig cycle shown in Fig. 3.3. The right composition is determined by trial and error.
- After that check if there is temperature difference every where at *Q-T* curves that belong to the chosen proposed 5-component composition if there is no problems about the cross over at *Q-T* curves.
- Next, look at the *h-T* curves. Check with the chosen proposed 5-component composition if there is the crossover between the hot streams and the cold streams of *h-T* curves at heat exhangers: HX1, HX2, and $\overline{HX}3$.
- Finally, after trial and error, the new proposed 5-component composition is: 4% hydrogen, 18% nitrogen, 24% methane, 28% ethane, and 26% butane by mole with 66.4 kg/h at S19. The MR flow at S19 is increased a little from 59.8 kg/h to be 66.4 kg/h to make sure there is volatile component such as nitrogen and hydrogen to cool down HX3 for the temperature difference.
- The variables are the composition and the flowrate to be adjusted to trace and to prevent the crossover (which is the constrain) of the "Cold MR" stream *h-T* line/curves to the hot "Subcooled MR" and "Feed GH_2" *h-T* line/curves to minimize MR compressor power. The other constraints are minimum approach temperatures at MR heat exchangers of the rig. The idea is that if there is a cross over in $\overline{HX}3$, it means volatile components are not enough, just increase hydrogen and nitrogen in the composition. If there is a cross over in HX2, just increase methane or ethane. And if there is a cross over in HX1 it means heavy component is not enough, just increase butane in the composition. The increasing much flowrate helps a little to widen the gap difference between the hot and cold *h-T* lines/curves, while the composition is more important.
- The new proposed 5-component composition contains more nitrogen in the composition. This means experimental result of the rig as shown in Fig. 3.9, *Simulation data of the laboratory test rig with the proposed simplified composition compared to the experimental data*, and Fig. 3.10 have only around 10% nitrogen. The rig will need additional nitrogen and the other volatile component such as neon (or hydrogen will be better) in order to cool all MR evaporators and hydrogen gas further lower down to −198 ^{o}C as required.

Both Figs. 3.5 and 3.6 show that there is positive difference everywhere along the curves between the hot streams ("Subcooled MR" and "Feed GH_2") and cold streams ("Cold MR" and "Return GH_2") of the cycle in Fig. 3.3, *PRO/II simulation flow-sheet of the proposed 5-component composition*. It means the new proposed 5-component composition: 4% hydrogen, 18% nitrogen, 24% methane, 28% ethane, and 26% butane by mole as mentioned in Section 3.3.3, *The proposed simplified 5-component composition for the initial experiment*, is possibly acceptable. It is the design that the temperature difference in the evaporators approach a practical minimum; small temperature difference mean low irreversibility and therefore lower power consumption.

(a)

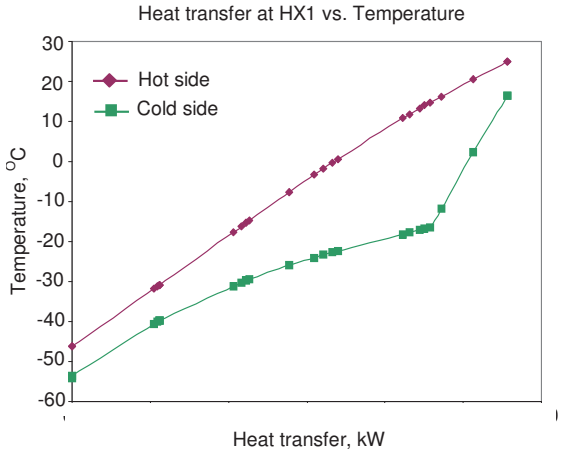

(b)

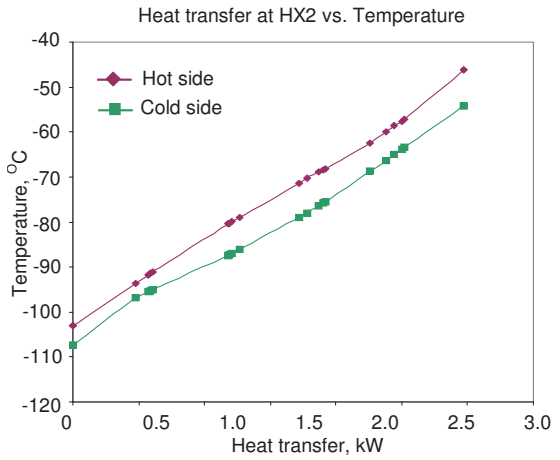

(c)

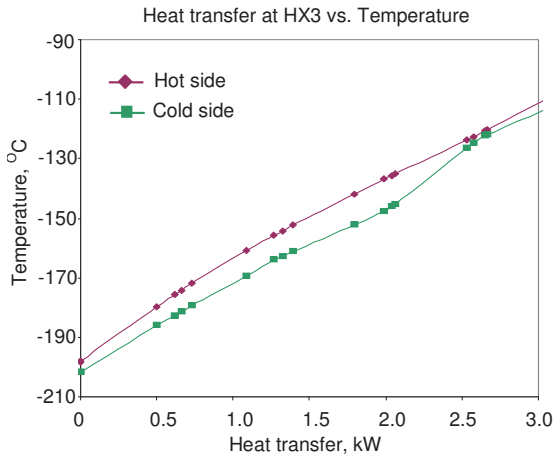

Fig. 3.5 – Adapted *Q-T* curves for the new proposed 5-component composition: *4% hydrogen, 18% nitrogen, 24% methane, 28% ethane, and 26% butane* by mole for the test rig at: (a) HX1, (b) HX2, and (c) $\overline{HX}3$**.**

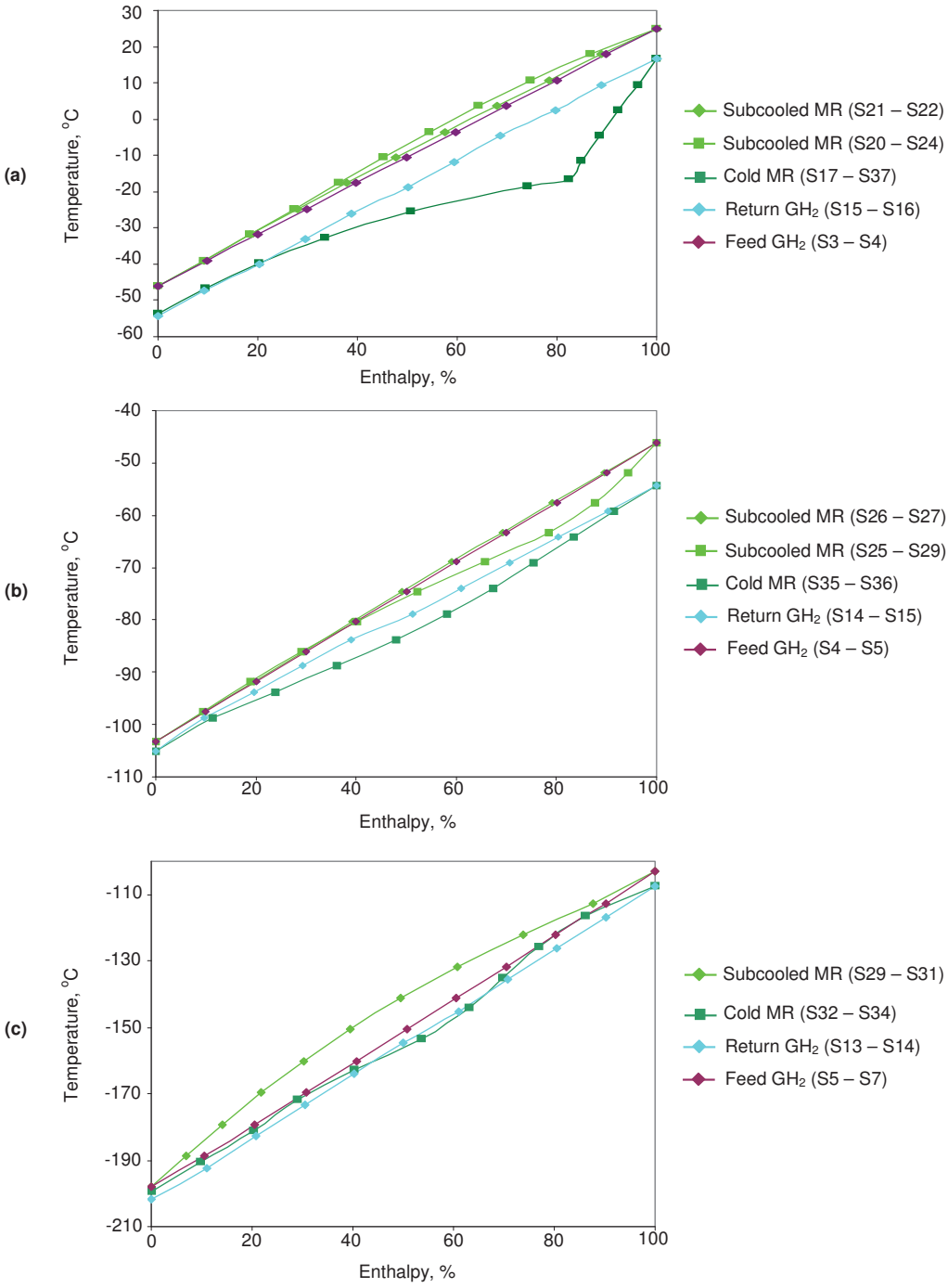

Fig. 3.6 – Adapted *h-T* curves for the new proposed 5-component composition: *4% hydrogen, 18% nitrogen, 24% methane, 28% ethane, and 26% butane* by mole for the test rig at: (a) HX1, (b) HX2, and (c) $\overline{HX}3$.

3.4. Initial experimental results

This section expands on Section 3.3, *Preliminary rig simulation*; it provides a detailed description of the experimental procedure, experimental results, and analysis of the test rig. All of the data were automatically collected using LABVIEW while running the experiments.

3.4.1. Initial experiment

Table 3.4 provides a detailed composition of the MR mixture used in the initial experiments; the simulated and experimental compositions are compared. Initially, neon was selected to contain in the simplified composition instead of hydrogen because it was what first discovered before. Butane has the highest molecular weight, which causes the flow to be heavier at a higher flow rate.

Table 3.4 – Composition of the mixture.

Component	Molecular weight (kg/kmole)	%Mole by simulation	Measured %mole by experiment
Neon	20.18	4.0	1.0
Nitrogen	28.01	12.0	10.0
Methane	16.04	26.0	33.0
Ethane	30.07	30.0	38.0
Butane	58.12	28.0	18.0
Total		**100.0**	**100.0**

First, each component (neon, nitrogen, methane, ethane, and butane) contained in the high pressure cylinder tank was discharged directly into the test rig at the MR cycle. This discharge was done by measuring the mass reduction of the gas tank, which is equivalent to the amount of the gas filled in the rig at the MR cycle. The simulated and measured compositions shown in Table 3.4 are located in the MR flow at stream 19. Each component was then charged into the rig at the suction of the MR compressor when it was switched on. Each cylinder tank had a higher pressure than the suction pressure of the MR compressor. Thus, the gas composition was forced to flow from the inside of the tank into the MR circuit of the rig until it achieved a satisfactory MR composition. The measured composition shown in Table 3.4 (at stream 19) can be achieved directly by reading the gas chromatography instrument, which can be positioned at three different points, as shown in Fig. 3.9. This process describes the process for creating the MR composition in the test. Before the last initial experiment of the cycle was performed, as shown in Figs. 3.7, 3.8, and 3.9, a preliminary test run was performed, which included several tests. Some experiments were performed multiple times to allow the rig to cool the temperature of the flowing hydrogen gas as much as possible. This cooling was done by adjusting the MR composition, suction and discharge pressures, and MR flow rate until the temperature was optimized. The final total amounts of neon, nitrogen, methane, ethane, and butane completely charged into the rig were 0.080, 0.330, 0.900, 2.160, and 4.790 kg, respectively. However, these values are not exact due to the presence of multiple leakages. As a result, the exact composition inside the test rig remained unknown.

3.4.2. Initial experimental results

Fig. 3.7 shows the pressure and temperature characteristics of the MR cycle side. Fig. 3.8 shows the pressure and temperature characteristics of the H_2 cycle side. As shown on the x-axis of the two figures, the experiment began on 08.09.2009 at 10:08:01 and ended at 17:10:03.

- At 10:08:01, logging began on all of the measuring instruments. The computer then began to collect the temperatures, pressures, flow rates, and other parameters.
- At 10:30:03, the MR compressor was switched on. In Fig. 3.7 (a), the MR discharge pressure was raised to 8 bar within a few minutes. The low-side pressure decreased to 2 bar within a few minutes.
- Between 11:30:03 and 14:10:03, ethane, methane, and nitrogen were charged into the MR side. This increased both the MR discharge and the suction pressures. However, the MR suction pressure was maintained at 2 bar by an additional closure of expansion valves EX1, EX2, and EX3. Therefore, the MR discharge pressure gradually increased to 18 bar, as shown in Fig. 3.7 (a).
- At 14:50:03, the helium side was turned on, as shown in Fig. 3.7 (a). Helium gas at −256 ^{o}C and 1 bar was used to cool down HX5. Each temperature reading began to decrease, especially on the H_2 side, as shown in Figs. 3.8 (c) and (d). This decrease was due to the helium cooling HX5, which was connected to and near HX4. Furthermore, the helium gas cooled the hydrogen gas that was leaving HX4 towards HX5. The cold recycled hydrogen gas that returned to the H_2 compressor from HX5 cooled HX4, HX3, HX2, and HX1.
- At 15:10:03, the H_2 compressor was turned on, as shown in Fig. 3.8 (b).
- From 15:50:03 until 16:50:03, particularly at 16:30:03, a steady state was reached, as shown in Fig. 3.9. The MR side, H_2 side, and helium side were all opened, and all of the temperatures and pressures were stable. The most interesting temperature was TE106, *H_2 pre-cooled cold gas temperature leaving HX4*, as shown in Fig. 3.8 (d). At TE106, hydrogen could only be cooled to −158 ^{o}C, whereas the simulation predicted a temperature of −198 ^{o}C, as shown in Fig. 3.3. It was assumed that an inadequate amount of the MR composition was charged into the system (particularly the volatile components such as nitrogen and neon) in the initial experiment and that the two hours opening of the system were insufficient. However, the final experiment exhibited an improvement over the first experiment that was performed several months prior; the hydrogen gas could be cooled to a lower temperature. When helium was used, more refrigerant was charged into the rig at appropriate MR suction and discharge pressures. The other interesting temperatures were cooling the MR flow at, for example, TE206, TE209, TE210, TE211, and TE212 as shown in Figs. 3.7 (c), 3.7 (d), and 3.8 (a). In Fig. 3.7 (a): the MR high side pressure (PE215) was maintained at 18 bar, which is the same as the simulation result. The MR compressor speed was maintained at the highest speed. The low side pressure (PE214) was set to 2 bar, which is the same as the simulation result, by the further closure of expansion valves EX1, EX2, and EX3 to maintain the MR suction pressure at 2 bar.
- At 16:50:03, the H_2 compressor was switched off, as shown in Fig. 3.8 (b).
- At the same time, 16:50:03, the MR compressor was finally switched off, as shown in Fig. 3.7 (a).

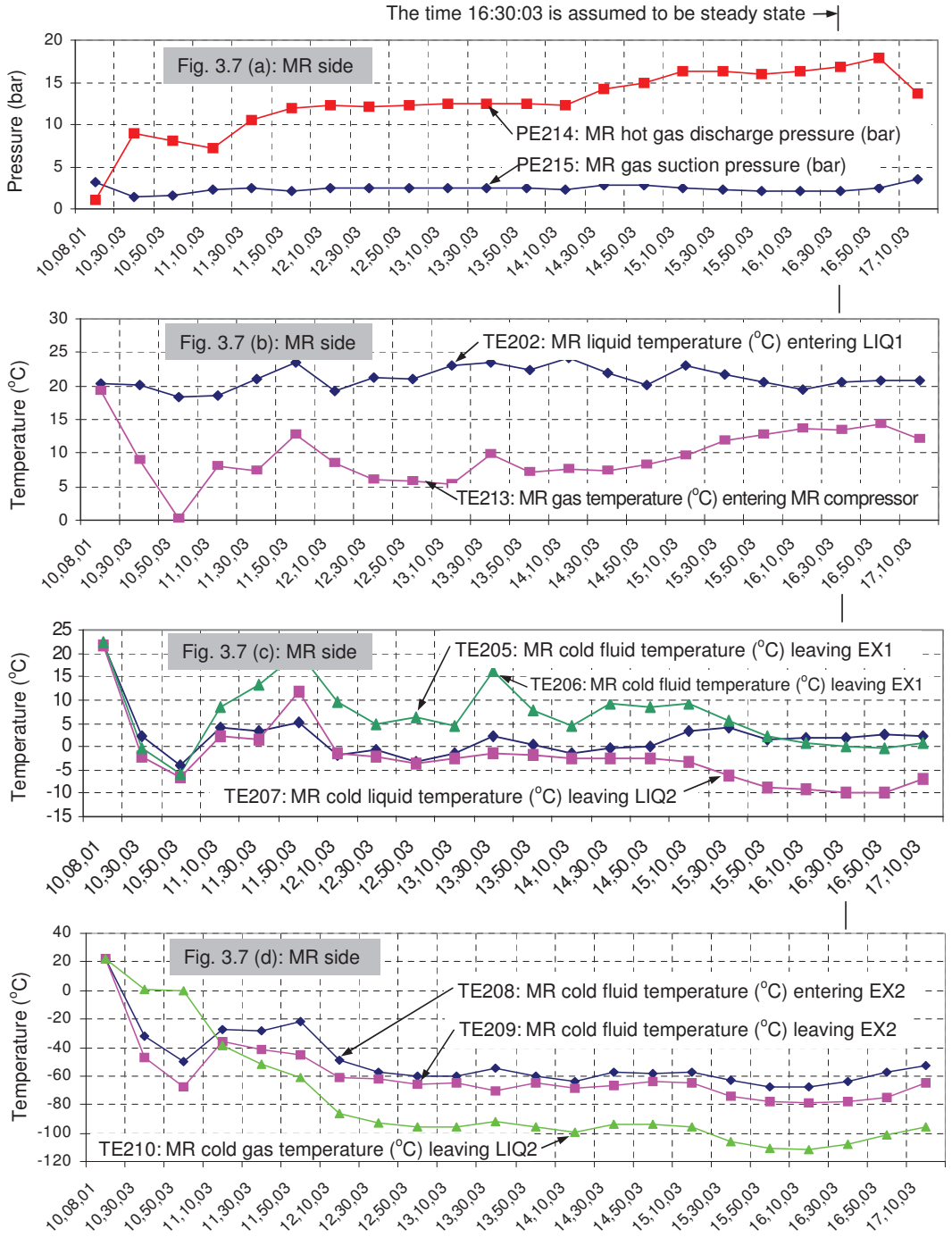

Fig. 3.7 – Final transient experimental results of the MR side: pressures and temperatures as a function of time.

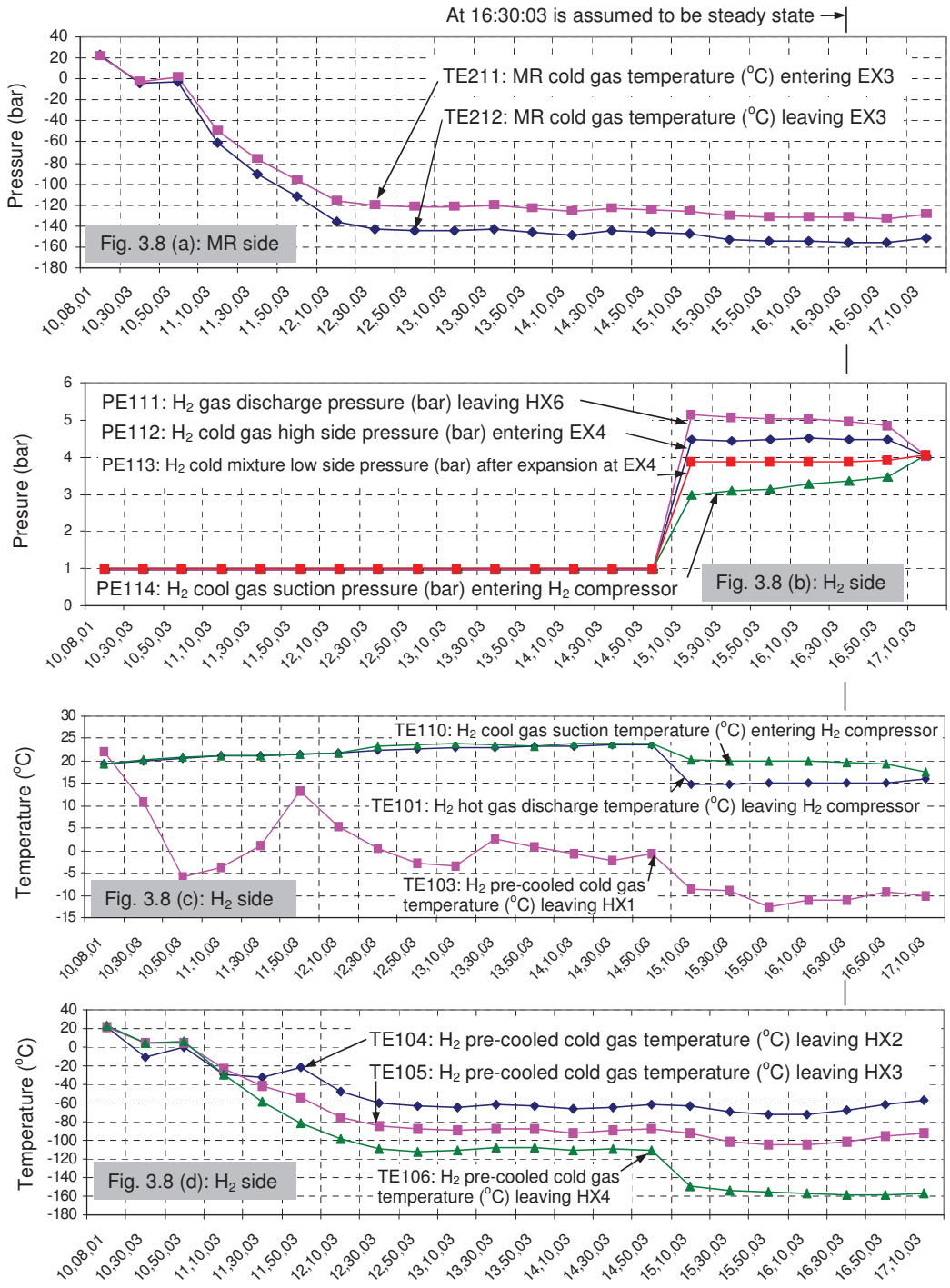

Fig. 3.8 – Final transient experimental results of the H_2 side: pressures and temperatures as a function of time.

3.5. Comparison

3.5.1. Comparison of the experimental data to the simulation data

Fig. 3.9 shows the steady-state experimental data at 16:30:03 when both the H_2 and helium sides were on. The simulation was used to design the rig (i.e., to select a composition) and to compare the results; thus, the simulation was used at two different times (as illustrated in Fig. 3.3 for the preliminary design of the rig and Fig. 3.9 for comparison to the experimental results). After both the H_2 and MR sides were switched on, the helium circuit was opened to allow cold helium gas from the liquid helium storage tank to cool HX5. This was an important time to record and compare the measured experimental data to the simulation data. Cold helium gas was flowing to cool HX5. As a result, all of the temperatures, especially TE211 and TE212, decreased further. Thus, the feed hydrogen gas could be cooled to −158 ^{o}C after leaving HX4 and remain at the same temperature at LIQ3. If more time was available, then HX5 could almost cool to the feed helium temperature, and liquid hydrogen would exist at LIQ3. As shown in Fig. 3.9, changes in the simulation data were required to obtain the measured hydrogen flow rate from the experiment. The simulated H_2 flow rate shown in Fig. 3.3 was adjusted from 2.0 kg/h (i.e., every 2 kg of hydrogen requires 50 kg of MR flow rate) to 0.6 kg/h, and the MR flow rate was set to 18 kg/h. From the simulation, 18 kg/h of MR flow rate was required to cool 0.6 kg/h of hydrogen gas. The hydrogen flow rate was too low because all of the expansion valves were closed to maintain a low suction pressure of 2 bar. All of the simulated temperatures were still the same as in Fig. 3.3. The final composition that was measured using gas chromatography in the rig also remained the same; it consisted of: 1% neon, 10% nitrogen, 33% methane, 38% ethane, and 18% butane. The neon content appeared to be too low, which prevented a further decrease in the temperature at TE212 following the expansion at EX3. In summary, the simulation and experimental data are nearly equivalent.

Table 3.5 indicates that the simulation and experimentally measured power consumptions of the two compressors were equal because the simulation data was calculated using the experimental data. The compressor power was calculated from the flow rate, inlet and outlet pressures, and temperatures. According to the law of conservation of energy, the calculated brake horsepower was the same as the measured one. The hydrogen gas flow rate from the measurement was only 0.6 kg/h instead of the initially designed 2.0 kg/h, as shown in Fig. 3.3. The flow rate was adjusted to account for the small flow of the MR, which enabled the liquefier to cool the hydrogen gas. The measured MR suction gas flow rate was only 18 kg/h at the maximum MR compressor speed instead of the designed 55 kg/h. However, this is not significant because the flow rate can be increased by increasing the rotational speed of the motor. There may have also been solidification of the MR after expansion, e.g., at EX3. Therefore, more time and experiments were performed to correct these problems. Another possibility was freezing due to moisture; in this case, a refrigeration filter dryer should be installed after the condenser. However, freezing was not a problem because the refrigerant was high quality and there was no moisture. It is important to note that the measured MR compressor power consumption should be the same as the simulation value. Compressor powers of 0.067 kW for the hydrogen compressor and 1.06 kW for the MR compressor were obtained from the measured pressures and temperatures of both the suction and discharge together with the measured flow rate. The isentropic efficiencies of the two compressors were 90%, which are quite high; this may have been due to the small mass flow rates. The final overall test rig power consumption was 1.12 kW.

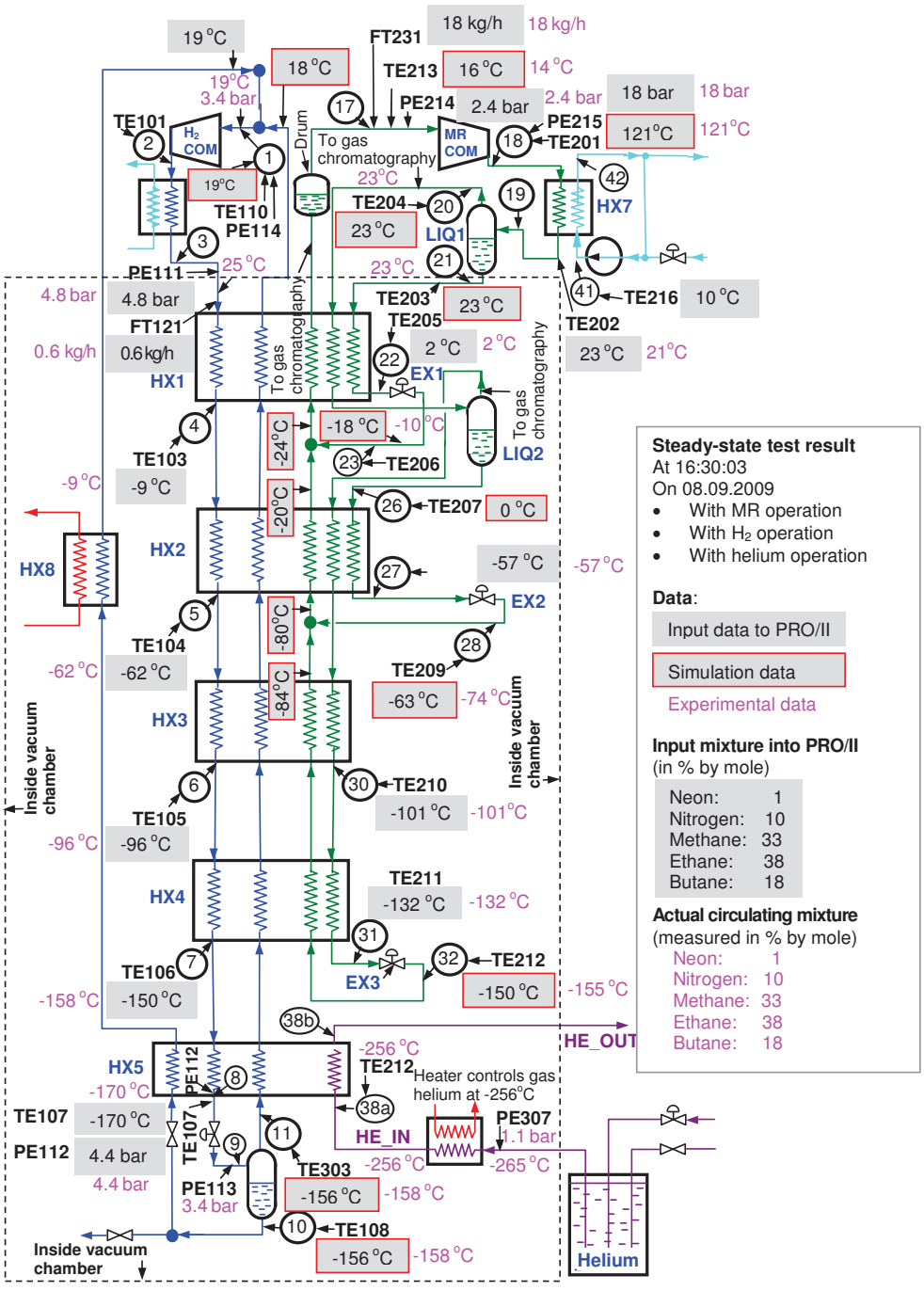

Fig. 3.9 – Simulation data of the laboratory test rig with the proposed simplified composition compared to the experimental data with H_2 and helium operation at steady state. The experimental data reached steady state at 14:50:03 on 08.09.2009.

In Fig. 3.9, regarding the flow rate of the MR and hydrogen streams, the simulation and experimental results are exactly the same because the experimental data were input into the simulation software. In contrast, there are small discrepancies in the temperatures because the SRK model used in the commercial software is only an approximation.

Table 3.5 – Simulation and initial experimental data of the proposed simplified 5-component composition from Fig. 3.9.

Parameter	Equations/Symbols	[a]Simulation data	[a]Experimental data
H_2 mass flow rate at S3	$\dot{m}_{H2}$ in kg/h	[c]0.6 kg/h	[d]0.6 kg/h
MR mass flow rate at S17	$\dot{m}_{MR}$ in kg/h	[c]18.0 kg/h	[d]18.0 kg/h
H_2 compressor power	$\dot{W}_{H2\,COM,\,BH}$	[a]0.067 kW	[d]0.067 kW
Isentropic efficiency of H_2 compressor	$\eta_{ISEN,\,H2\;COM}$	[b]80%	[b]80%
MR compressor power	$\dot{W}_{MR\,COM,\,BH}$	[b]1.06 kW	[b]1.06 kW
Isentropic efficiency of MR compressor	$\eta_{ISEN,\,MR\;COM}$	[b]85%	[b]85%
Actual work	$\dot{W}_{COM,\,BH} = \dot{W}_{MR\,COM,\,BH} + \dot{W}_{H2\,COM,\,BH}$	[c]1.127 kW = 1.06 kW + 0.067 kW	[b]1.127 kW = 1.06 kW + 0.067 kW

a From Fig. 3.9, *Simulation data of the laboratory test rig with the proposed simplified composition compared to the experimental data with H_2 and helium operation at steady state.*
b Experimental data: mass flow rates, inlet and outlet pressures, and temperatures of compressors were used to simulate the values in PRO/II.
c Values assumed to be the same as in the experiment.
d Values measured directly from the experiment at the test rig.

3.5.2. Uncertainty analysis

3.5.2.1. Simulation data

The main thermophysical properties of hydrogen gas at 4.8 bar and between −150 °C and 0 °C, as shown in Fig. 3.9, were compared to REFPROP 8 by NIST (2010) as a reference. The average uncertainties for n-H_2 of some important properties such as ρ, h, s, and c_P were found to be 0.7%, 2.2%, 0.6%, and 7.1%, respectively. However, the MR side is very complicated; thus, an uncertainty analysis is difficult to perform due to its complex composition.

3.5.2.2. Parameters calculated from the simulation data

An uncertainty analysis for the calculated parameters of the proposed system was performed using the method by Moffat (1988). According to that method, the function R is calculated from a set of N simulated data (independent variables), which is represented

by $R = R(X_1, X_2, X_3,..., X_N)$. Then, the uncertainty of the result R can be determined by combining the uncertainties of individual terms by using a root-sum-square method, i.e.,

$$\delta R = \left\{ \sum_{i=1}^{N} \left(\frac{\partial R}{\partial X_i} \delta X_i \right)^2 \right\}^{1/2}$$

Using the accuracies as simulation variables, the uncertainties of the parameters calculated by PRO/II, such as $\dot{W}_{H2\,COM,\,BH}$, and $\eta_{ISEN,\,H2\,COM}$ as shown in Table 3.5, estimated by the analysis are 0.3% and 0.3%, respectively.

3.5.2.3. Measured data

The uncertainty of the measured data, such as temperatures, pressures, and flow rates of both hydrogen and MR sides, due to errors in the measuring devices are reported and were given above in Section 3.2, *Test rig description*.

3.5.3. Differences betweem simulation and experimental data

The main conclusion is that the compressor power and liquefier efficiency were the same as the simulation data. Although the test rig was capable of cooling hydrogen gas using the MR refrigeration system, it was only able to reach a temperature of −158 °C instead of the designed value of −198 °C. Even for the final experimental results, the MR cycle was not well adjusted, meaning it was very successful. However, additional experimental work is required to study, identify, and resolve the problems. Several factors can explain why the temperature could not be decreased to −198 °C, and some differences between the simulation and experimental data are as follows:

- Correct MR composition:
  Most of the flow was directed to EX3; therefore, the composition consisted of methane and nitrogen. It was not known if there was an adequate amount of liquid methane and nitrogen after EX3 to boil and cool HX3 and HX4 or if a LIQ (liquid separator) was present after EX3. Thus, the temperature at TE212 could not reach −198 °C. The chromatography measured the composition of the test rig, which was compared to the simulated composition. However, that was not more important than determining if there was an adequate amount of liquid in each liquid separator to boil, absorb heat, and cool each heat exchanger. Additionally, before steady state, the temperature of the MR flow was higher after expanding at EX3. According to the simulation, this indicates that more volatile components such as methane, nitrogen, and especially neon were required in the composition. If the MR composition was not correct, then it would not be able to reach the desired temperature, regardless of the flow rate of the MR refrigerant.
- Correct amount of MR refrigerant charged into the rig:
  If the quantity of refrigerant is not sufficient, then both the suction and discharge pressures will be low. In the opposite case, both pressures will be high. Therefore, it is difficult to control the appropriate pressures.
- Correct MR compressor suction and discharge pressures:

The discharge pressure should be about 18 bar or higher, and higher pressures are more favorable because they result in lower temperatures after the expansion valves. The pressure could be as high as 22 to 24 bar according to the simulation results. This higher pressure could be achieved by using a faster compressor speed, closing more expansion valves, and charging more refrigerant. However, more power consumption is required for the MR compressor for a high discharge pressure. Additionally, according to the simulation, the MR compressor suction pressure should be about 2 bar. However, the simulation can only predict the qualitative behavior; the actual values could be slightly lower or higher. Additional experiments should be performed to determine the optimal suction and discharge pressures of the MR cycle.

- Correct flow rate of the MR refrigerant:
  If there is not sufficient flow, it will not transfer heat, and the liquefier will be too warm. The control must to be adjusted during the experiment to ensure that the flow is sufficient to produce the desired temperature.
- Helium must be in operation:
  The helium was always turned on to cool HX5, which was the lowest temperature heat exchanger. Because HX5 was connected to HX4, heat conduction occurred to HX4. If there was no helium flow to cool it down, then it would be too warm. Also, the recycled hydrogen that flowed back from HX5 would be warm. Therefore, the other heat exchangers, HX1, HX2, HX3, and HX4, would be warmer. For HX5, it always had to be cooled by helium to produce the coolest exchanger as explained above.
- Flow rate of feed hydrogen gas:
  If the MR flow rate was too low, but the feed hydrogen gas was too high, then there would not be enough MR flow to cool the heat exchangers. The correct hydrogen flow rate should correspond to the correct MR flow rate.

Beside aforementioned, the other differences of experimental to simulation results are as below:

3.5.3.1. The chosen composition of the 5-component refrigerant

All possible MR compositions with every component were later tried resulting the best proposed 5-component MR composition: 4% neon (or 4% hydrogen with the same result), 18% nitrogen, 24% methane, 28% ethane, and 26% butane as in Table 3.2. But that was just simulation. There is difference in the simulated MR composition when comparing to the measured MR composition: 1% neon, 10% nitrogen, 33% methane, 38% ethane, and 18% butane. But the trend goes the same direction. It seemed the measured composition has too much methane and ethane, but it lacked much nitrogen compared to the proposed 5-component MR composition. It was the reason why the MR cycle at the rig could cool hydrogen gas to only −150 ^{o}C, not −198 ^{o}C as required. When the information from experiment including the measured composition is used to simulate in PRO/II to verify the software as in Fig. 3.9, even though it is not exactly the same, but the software can predict the trend quite well. However, all it is not important than simulation power consumption at MR compressors by PRO/II that it would be correct. With given flows of MR and hydrogen gas compressed by compressors simulated by the software, as the information shown in Table 3.6, fluid properties' models could be acceptable.

3.5.3.2. About helium gas used to cool down HX5

According to schematic diagram of the test rig as in Fig. 3.9, *Simulation data of the laboratory test rig with the proposed simplified composition compared to the experimental data*, helium gas system was used to cool down HX5, not J-T section. If without the on of helium system, the whole HX5 which is connected to HX4 is always hot at ambient temperature. For that reason, it is difficult to lower the whole temperature of HX4 down. Even though there is a return cold hydrogen gas with temperature equivalent to S7 from HX5 to HX4, but that is just relatively small. Thus it is not significant. In fact it is a wrong design to have the return hydrogen stream. Moreover, there is a shut-off switch that there is no return hydrogen according to experiment data in Chapter 3. Thus, the experiment with MR-cycle was not the distraction.

3.5.3.3. Some further differences between simulation and experimental data

Table 3.6 is the comparison between the reference fluid data belongs to NIST (2011) and the popular SRK equation of state used in PRO/II. In the software, pressure and temperature are required to compute density by SRK model. Then, other properties such as enthalpy and entropy are calculated by using pressure, temperature, and density correlation. According to the Table 3.6, there are hydrogen, nitrogen, methane, ethane, and butane as main components used in simulation of the feed hydrogen and the 5-component MR composition at the rig. For every fluid: densities are exact the same; specific heat constants and thermal conductivities are quite the same with trivial differences. Enthalpies and entropies are different because they are based on different references; however, when substituting SRK data such as enthalpies and entropies into equations to calculate heat and exergy balances, they are quite the approximation as using data from NIST. Moreover, SRK model was used by Hammer *et al* (2003), Jensen (2008), Myklebust (2010), and Nogal *et al* (2008) in design, simulation, and optimization of multi-component system in LNG processes. For all aforementioned, SRK in PRO/II are used to predict the trend what happens in the rig and the simulation large-scale plant.

In Chapter 3, Section 3.5.3, *Differences between simulation and experimental data*, there is the discussion there. Several reasons why it is different between simulation at Fig. 3.3 and experiment at Fig. 3.9 in Chapter 3 is because experiment didn't entirely follow the assumptions in Table 2.1, *Boundary conditions of the test rig's simulation*, in Chapter 2 and Table 3.6, *Assumptions in the simulation model*, in Chapter 3 especially the assumption of all MR heat exchangers are in high effectiveness which is different from experiment.

This means MR and hydrogen streams leaving each heat exchanger together with heat exchanger effectivenesses assumed are not the same as occuring in real case resulting different composition of MR mixture. Moreover, composition of only at Stream 17 is known by gas chromatography, but the rest in MR cycle are not known. Thus, temperatures at some points are not the same, e.g., at S28 and S32.

Table 3.6 – Comparison between the standard-reference NIST and the SRK models used in PRO/II.

PARA hydrogen (21 bar)

T (°C)	h (kJ/kg)		s (kJ/kg-°C)		ρ (kg/m^3)		c_p (kJ/kg-°C)		k (W/m-°C)	
	NIST	SRK	NIST	SRK	NIST	SRK	NIST	SRK	NIST	SRK
-250	47.2	-2883.7	0.87	31.21	70.26	70.84	10.50	20.42	0.1111	0.1000
-240	196.1	-2640.6	6.09	39.82	52.61	53.34	23.60	32.22	0.0942	0.0800
-200	963.2	-1728.3	22.86	59.34	7.24	7.33	12.64	16.22	0.0614	0.0600
-150	1663.3	-948.5	30.08	67.49	4.10	4.13	15.60	15.26	0.1081	0.1000
-100	2479.3	-191.7	35.63	72.65	2.90	2.91	16.54	15.05	0.1454	0.1600
-50	3290.8	558.4	39.75	76.46	2.25	2.26	15.84	14.96	0.1666	0.2200
0	4063.6	1305.4	42.88	79.45	1.84	1.84	15.13	14.92	0.1842	0.2700
25	4439.0	1678.3	44.19	80.78	1.68	1.68	14.90	14.91	0.1932	0.3000

Normal hydrogen (21 bar)

T (°C)	h (kJ/kg)		s (kJ/kg-°C)		ρ (kg/m^3)		c_p (kJ/kg-°C)		k (W/m-°C)	
	NIST	SRK	NIST	SRK	NIST	SRK	NIST	SRK	NIST	SRK
-250	46.2	-4193.5	0.82	28.21	70.35	70.57	10.32	19.79	0.1113	0.1000
-240	192.5	-3957.2	5.96	36.59	53.02	53.09	23.17	31.57	0.0949	0.0800
-200	958.8	-3067.4	22.74	55.71	7.24	7.33	11.98	15.49	0.0583	0.0600
-150	1555.0	-2324.6	28.94	63.47	4.10	4.13	12.28	14.52	0.0873	0.0900
-100	2195.3	-1605.1	33.29	68.37	2.90	2.91	13.28	14.30	0.1186	0.1200
-50	2876.9	-892.4	36.75	71.99	2.25	2.26	13.92	14.22	0.1480	0.1400
0	3582.5	-181.7	39.60	74.86	1.84	1.84	14.26	14.27	0.1743	0.1700
25	3940.4	175.9	40.85	76.12	1.69	1.69	14.36	14.34	0.1865	0.1800

Nitrogen (1 bar)

T (°C)	h (kJ/kg)		s (kJ/kg-°C)		ρ (kg/m^3)		c_p (kJ/kg-°C)		k (W/m-°C)	
	NIST	SRK	NIST	SRK	NIST	SRK	NIST	SRK	NIST	SRK
-200	-130.6	-451.9	2.720	2.39	824.94	827.96	2.02	2.02	0.1549	0.1400
-150	126.5	-192.3	5.915	5.61	2.77	2.77	1.06	1.05	0.0121	0.0100
-100	179.0	-139.9	6.273	5.97	1.95	1.95	1.05	1.05	0.0165	0.0200
-50	231.2	-87.7	6.537	6.23	1.51	1.51	1.04	1.04	0.0204	0.0200
0	283.2	-35.6	6.748	6.44	1.23	1.23	1.04	1.04	0.0240	0.0200
25	309.3	-9.6	6.839	6.53	1.13	1.13	1.04	1.04	0.0257	0.0300

Methane (1 bar)

T (°C)	h (kJ/kg)		s (kJ/kg-°C)		ρ (kg/m^3)		c_p (kJ/kg-°C)		k (W/m-°C)	
	NIST	SRK	NIST	SRK	NIST	SRK	NIST	SRK	NIST	SRK
-180	-63.4	-749.5	-	5.64	448.25	448.18	3.38	3.57	0.2084	0.2200
-150	536.0	-133.3	4.796	11.20	1.61	1.61	2.16	2.12	0.0129	0.0100
-100	642.2	-28.0	5.520	11.92	1.13	1.13	2.11	2.10	0.0188	0.0200
-50	747.6	77.2	6.055	12.45	0.87	0.87	2.12	2.12	0.0247	0.0200
0	854.8	184.3	6.488	12.88	0.71	0.71	2.18	2.18	0.0309	0.0300
25	910.0	239.4	6.681	13.08	0.65	0.65	2.23	2.23	0.0343	0.0300

Ethane (1 bar)

T (°C)	h (kJ/kg)		s (kJ/kg-°C)		ρ (kg/m^3)		c_p (kJ/kg-°C)		k (W/m-°C)	
	NIST	SRK	NIST	SRK	NIST	SRK	NIST	SRK	NIST	SRK
-150	-144.5	-415.7	-	4.52	615.86	624.18	2.34	2.44	0.2274	0.2300
-100	-27.4	-293.4	-	5.35	558.12	567.49	2.38	2.48	0.1782	0.1800
-50	545.2	289.2	2.930	8.48	1.65	1.65	1.50	1.49	0.0127	0.0100
0	624.0	367.5	3.249	8.80	1.34	1.34	1.66	1.65	0.0179	0.0200
25	667.0	410.1	3.398	8.95	1.22	1.22	1.76	1.75	0.0210	0.0200

Butane (1 bar)

T (°C)	h (kJ/kg)		s (kJ/kg-°C)		ρ (kg/m^3)		c_p (kJ/kg-°C)		k (W/m-°C)	
	NIST	SRK	NIST	SRK	NIST	SRK	NIST	SRK	NIST	SRK
-120	-53.6	-250.1	-	5.57	717.99	715.10	1.98	2.02	0.1700	0.1800
-100	-13.5	-209.9	0.031	5.82	699.35	696.67	2.01	2.01	0.1617	0.1700
-50	89.5	-109.2	0.55	6.33	651.78	651.67	2.12	2.07	0.1384	0.1400
0	585.5	392.2	2.42	8.21	2.67	2.65	1.64	1.60	0.0142	0.0100
25	627.6	433.5	2.56	8.36	2.42	2.41	1.73	1.71	0.0166	0.0200

3.5.3.4. The lowest attainable temperature of pre-cooled hydrogen gas by MR refrigeration system.

In Section 3.4.2, *Initial experimental results*, the lowest reached temperature was −158 °C, but that was just the initial experiment. Section 3.4.2 reports only the initial data saying only −158 °C. But after two weeks from 9:19 to 15:05 o'clock on 17 September 2010, the lowest attained temperature was −180 °C as depicted in Fig. 3.10 shown below when a few additional grams of nitrogen gas were charged into the rig. The amount was not known. The measured 5-component composition was the same. The MR compressor runs with the same power consumption. The feed hydrogen gas was cooled by MR refrigeration cycle to −180 °C.

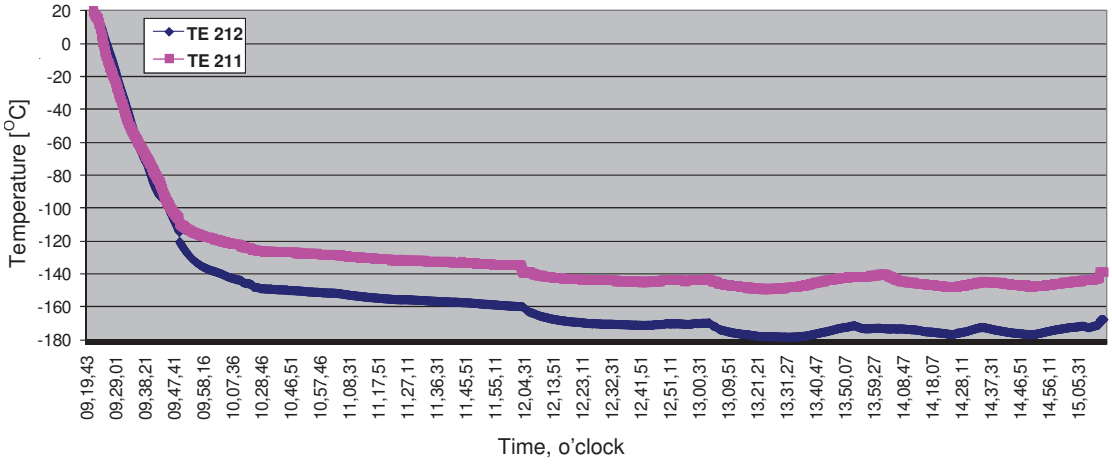

Fig. 3.10 – Transient temperatures at TE212 and TE211 as a function of time, Drescher (2010).

If there were more time and more experiment to adjust the composition, the temperature would have reached down −198 °C (80 K) as expected. This can be done by increasing more volatile components such as neon and nitrogen. Also, more time would be needed for cooling down HX5 by using helium gas cycle. The theory can be used to predict the trend. And the experiments follow the same trend. Without the commercial computer program, the approximate MR composition can't be predicted and the test rig can't be designed.

3.6. Conclusion

From the simulation, a simplified 5-component composition that consisted of 4% neon (or 4% hydrogen with the same result), 18% nitrogen, 24% methane, 28% ethane, and 26% butane by mole was developed for the new MR refrigeration system. Suitable MR compressor suction and discharge pressures were found as 2 bar and 18 bar, respectively, which yielded the lowest MR compressor power of 4.55 kW. Initial experiments showed that the test rig could cool 0.6 kg/h normal hydrogen gas from 25 °C to −158 °C with a measured simplified 5-component composition similar to the simulated composition: 1% neon, 10% nitrogen, 33% methane, 38% ethane, and 18% butane by mole. The power consumption required to pre-cool the feed hydrogen

gas was 1.76 kWh per kilogram. After two weeks, the lowest temperature was about −180 °C with a few more grams of nitrogen gas charged into the rig. More volatile components such as neon and nitrogen must be charged into the rig to further decrease the temperature to −200 °C. The resulting power consumption was nearly equal to that of the initial experiment, and the simulated and experimental power consumption were nearly equal. The main conclusion was that pre-cooling hydrogen gas with the new MR refrigeration system resulted in a lower energy consumption compared to conventional refrigeration systems. This lower energy consumption was due to the higher heat transfer coefficient of boiling MR for a lower mass flow rate of compression at the MR compressor. Currently, an actual hydrogen liquefaction plant at Ingolstadt consumes 4.86 kWh per kilogram using a nitrogen refrigeration system. Therefore, it is highly recommended to design this new refrigeration system to pre-cool feed normal hydrogen gas from an ambient temperature of 25 °C down to equilibrium hydrogen gas at −200 °C in the future large-scale hydrogen liquefaction plant.

Chapter 4. Simulation on a proposed large-scale liquid hydrogen plant using a multi-component refrigerant refrigeration system

A proposed liquid hydrogen plant using a MR refrigeration system is explained in this chapter. A cycle that is capable of producing 100 tons of liquid hydrogen per day is simulated. The MR system can be used to cool feed normal hydrogen gas from 25 ^{o}C to the equilibrium temperature of −193 ^{o}C with a high efficiency. In addition, for the transition from the equilibrium temperature of the hydrogen gas from −193 ^{o}C to −253 ^{o}C, a new proposed four H_2 J-B cycle refrigeration system with optimization is recommended. The overall power consumption of the proposed plant is 5.91 kWh/kg_{LH2}, with an ideal minimum of 2.89 kWh/kg_{LH2}. The current plant in Ingolstadt is used as a reference, which has an energy consumption of 13.58 kWh/kg_{LH2} and an efficiency of 21.28%. The efficiency of the proposed system is around 50% or more, where this depends on the assumed efficiency values for the compressors and expanders, together with effectiveness of heat exchangers. Importantly, the variables and constraints are preliminary studied together with how to adjust these to achieve optimal steady-state operation. The optimization problem has 23 variables and 26 constraints. A simplified 5-component composition of refrigerant suggested for the plant is found. The plant optimization was also conducted with two more pinch temperatures (1 and 3 ^{o}C). Power savings is increased with a pinch temperature of 1 ^{o}C as compared to 3 ^{o}C. Moreover, the proposed system has some smaller-size heat exchangers, much smaller compressor motors, and smaller crankcase compressors. Thus, it could represent a plant with the lowest construction cost with respect to the amount of liquid hydrogen produced in comparison to today's plants, e.g., in Ingolstadt and Leuna. Therefore, the proposed system has many improvements that serves as an example for future hydrogen liquefaction plants. Pressure drops in heat exchangers are also employed in the simulation for the study, but it is shown that they don't have much significant impact on the overall plant total power consumption.

4.1. Introduction

Because hydrogen has shown promise as an important energy vector for use in future transportation vehicles, several hydrogen research projects have been conducted since 1980 and in particular, since 2000. One of the challenges in creating a hydrogen economy is the low efficiencies of the current hydrogen liquefaction plant cycles. Currently, large hydrogen liquefaction plants, e.g., the plant in Ingolstadt as described by Bracha *et al* (1994), have exergy efficiencies of just 20−30%. These efficiencies are very low. The plant consumes 4.86 kWh per kilogram of hydrogen gas using

a nitrogen refrigeration system to pre-cool normal hydrogen gas from 25 °C to equilibrium hydrogen gas at −198 °C. From 1998 through 2008, some conceptual plants were proposed with reportedly improved efficiencies of 40–50% (Matsuda and Nagami 1998; Quack 2002; Kuz'menko 2004; Shimko and Gardiner 2007; Valenti and Macchi 2008; Berstad *et al* 2010). A literature review for the development of large-scale hydrogen liquefaction processes throughout the world from 1898 to 2009 is given in Chapter 1. Finally, in the year 2010, NTNU and SINTEF Energy Research AS proposed a new large-scale MR system with efficiency approximately or in excess of 50%. The details of this new system are reported in this chapter.

4.2. The proposed 100 ton-per-day LH_2 plant with the MR refrigeration system

For a larger metropolitan area with 100,000–200,000 hydrogen vehicles, the automotive consumption rate will be in the magnitude of 100 tons per day (Kramer *et al*, 2006). Therefore, a large-scale LH_2 plant of that size will be proposed in this section. From a preliminary study, single MR refrigeration alone cannot be used to cool down n-GH_2 from 25 °C to −253 °C because there will be solidification of the mixed heavy component between −193 °C and −253 °C. MR refrigeration can be used with a very high efficiency to cool down the gas from 25 °C to only −193 °C, as shown in Fig. 4.1. Then, to cool equilibrium hydrogen gas from −193 °C to −253 °C, a four H_2 J-B cycle system is recommended in this chapter. It is noted that w_A is the net power for system A, while w_B is the net power for system B.

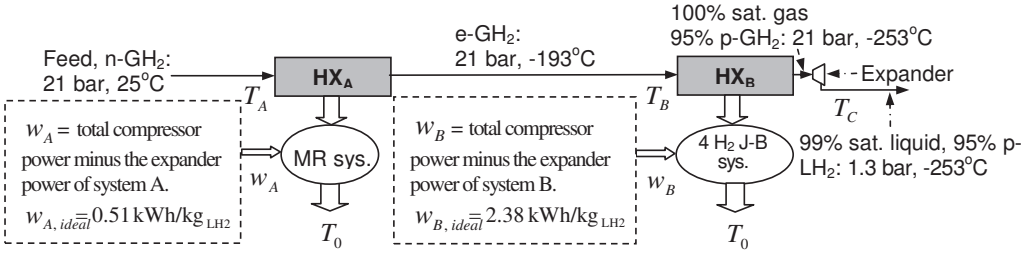

Fig. 4.1 – MR refrigeration system in combination with the four H_2 Joule-Brayton cycle refrigeration system.

4.2.1. Choice of refrigeration systems for the proposed plant

As aforementioned in Chapter 2 that the first person who introduces MR cycle is Podbielniak (1936). Later on Kleemenko (1959) teaches from the Podbielniak's patent that the cycle's efficiency depends on small temperature differences between the fluid being cooled and the multi-component refrigerants which is related to the irreversibility of the heat transferring between the two streams. After that there are several US patents about this technology for LNG. One of interesting cycles recommended is maybe for example by Gaumer et al. (1972).

Refrigeration systems such as MR, nitrogen, helium, and propane can be used to cool hydrogen gas from 25 °C to −193 °C (see Table 4.1). MR, which is a cycle under research at NTNU-SINTEF, was selected first because it has the lowest power consumption.

MR cycle has been used for decades in the LNG sector. This concept of mixed refrigerant in gas liquefaction (Bottura 2009; Chrz 2010; Mafi *et al* 2009; Bosma and Nagelvoort 2009) developed in the past few years results in reduced energy consumption compared to conventional liquefaction. The novelty of this mixed refrigerant system is described very well by Flynn (1997) as well as Venkatarathnam (2008). Until today, some large-scale LNG plants are employed with more complicated MR cycles such as naming "Dual" and "Cascade" MR processes previously from Newton (1985), Etzbach et al. (1976), also Rentler and Sproul (1983) that recently invented by Kimble (2001) as well as Robert and Agrawal (2001), together with Cole and Bowen (2000) respectively; the processes are suitable only for extremely large-scale plants, but not appropriate for the proposed 100-TPD plant due to the complexity. The differences involve the new modified cycle and the new optimized refrigerant composition that was specially designed for pre-cooling hydrogen gas from 25 ^{o}C to −198 ^{o}C explained in Section 4.2.3, *MR refrigeration system for cooling feed normal hydrogen gas from 25 ^{o}C to the equilibrium temperature of −193 ^{o}C*.

Today, large-scale plants that use nitrogen refrigeration systems (Bracha *et al*, 1994) have a power consumption of 4.86 kWh/kg_{LH2}. From a simulation test run in a commercial software package, SimSci-PRO/II, the helium system of Valenti and Macchi (2008) has a very high energy consumption. Propane in combination with a helium refrigeration system (Quack, 2002) cannot achieve a high efficiency because it only has one or two refrigerants and its own system cycle. For cooling hydrogen gas from −193 ^{o}C to −253 ^{o}C, either hydrogen or helium can be used as a refrigerant in refrigeration systems because they do not freeze in this low temperature range. Hydrogen freezes at temperatures below −259 ^{o}C, while helium freezes below −272 ^{o}C. Helium is widely used as a refrigerant in cryocoolers because it remains in the gas phase at extremely low temperatures.

Table 4.1 – Choice of refrigeration systems for the proposed 100-TPD H_2 liquefaction plant.

System	Refrigeration system	Inventor	Energy consumption
HX_A	MR refrigeration	Propose in this chapter	1.38 kWh/kg_{LH2}
	N_2 refrigeration	Matsuda and Nagami (1992)	≈4.86 kWh/kg_{LH2}
		Ingolstadt plant in 1992 (Bracha *et al*, 1994)	4.86 kWh/kg_{LH2}
		Leuna plant in 2007 (See Chapter 1)	≈4.86 kWh/kg_{LH2}
		Praxair since 1957 (See Chapter 1)	≈4.86 kWh/kg_{LH2}
	Helium refrigeration	Valenti and Macchi (2008)	Extremely higher than 4.86 kWh/kg_{LH2}
	Propane+helium refrigeration	Shimko and Gardiner (2007)	Higher than 4.86 kWh/kg_{LH2}
		Quack (2002)	Higher than 4.86 kWh/kg_{LH2}
HX_B	H_2 refrigeration	Matsuda and Nagami (1992)	A little ≤8.65 kWh/kg_{LH2}
		Ingolstadt plant in 1992 (Bracha *et al*, 1994)	8.65 kWh/kg_{LH2}
		Leuna plant in 2007 (See Chapter 1)	A little ≤8.65 kWh/kg_{LH2}
		Praxair since 1957 (Chapter 1)	A little ≤8.65 kWh/kg_{LH2}
	Helium refrigeration	Valenti and Macchi (2008)	Higher than 8.65 kWh/kg_{LH2}
		Shimko and Gardiner (2007)	Higher than 8.65 kWh/kg_{LH2}
		Quack (2002)	Higher than 8.65 kWh/kg_{LH2}
		Kuz'menko *et al* (2004)	7.84 kWh/kg_{LH2}
	Reversed helium/neon Brayton cycle	Berstad *et al* (2010)	≈ 5.18 kWh/kg_{LH2}
	Four H_2 J-B cycle refrigeration	Propose in this chapter	4.24 kWh/kg_{LH2}

The Matsuda and Nagami (1998) under a Japanese hydrogen program (Mitsugi 1998) and Praxair cycles are quite similar to the Ingolstadt and Leuna cycles. Since they are all hydrogen refrigeration systems; in particular, Ingolstadt's cycle requires 8.65 kWh/kg_{LH2} of power to cool hydrogen gas from −193 ^{o}C to −253 ^{o}C (Kuz'menko, 2004), which is a high power consumption. Thus, we will now consider the helium system (Quack, 2002), which is too simple. However, from a simulation test that was run with a 64-bar discharge and a 2.7-bar suction pressure in the J-B cycle, it is impossible to have a high efficiency system. Kuz'menko *et al* (2004)'s helium system has a power consumption of 7.84 kWh/kg_{LH2}, which is a little better than the hydrogen refrigeration's power consumption of 8.65 kWh/kg_{LH2}. However, it is still very high due to the complexity of the helium liquefaction process. For Shimko and Gardiner (2007)'s helium system, the preliminary simulation/test run in PRO/II indicates that it is still not good in comparison to the proposed four H_2 J-B cycle system. Finally, the performance of the reversed helium/neon Brayton cycle by Berstad *et al* (2010) is maybe lower because helium gas has inferior heat transfer properties to hydrogen gas used in the cycle proposed in this chapter. The researchers aforementioned have developed the systems with plenty of the best efforts; more explanations of remodeling those conceptual plants are given in Chapter 1. This chapter proposes completely new configurations and systems. The MR refrigeration system is selected to cool from 25 ^{o}C to −193 ^{o}C in combination with the four H_2 J-B cycle system, which cools from −193 ^{o}C to −253 ^{o}C. The proposed MR system consumes only 1.38 kWh/kg_{LH2} in comparison to the ideal of 0.51 kWh/kg_{LH2}. In addition, the proposed four H_2 J-B cycle system consumes 4.24 kWh/kg_{LH2} in comparison to the ideal of 2.38 kWh/kg_{LH2}. Finally, comparison of the energy consumption of the proposed MR refrigeration system and the proposed four H_2 J-B cycle system to other conventional and the conceptual refrigeration systems, is detailed in Table 4.1.

4.2.2. The whole process plant

In Fig. 4.2, the flow sheet was developed from the PRO/II simulation flow-sheet that was modified from a laboratory test rig based on research at NTNU-SINTEF. Experiments were conducted. The simulation data and experimental data matched well, and the main discovery was that pre-cooling hydrogen gas with this new MR refrigeration system resulted in a lower energy consumption per kilogram of feed hydrogen gas compared to conventional refrigeration systems. Details of the results are reported in Chapter 3.

For simplicity, it is assumed that there is no pressure drop in the simulation because the exact components' sizes of heat exchangers and pipings are not known. The single hydrogen feed through stream is at: a pressure of 21 bar which is the same condition as the Ingolstadt plant (Bracha *et al*, 1994), a temperature of 25 ^{o}C, and a flow rate of 1.157 kg/s for 24 hours a day in operation or 100 TPD. The large-scale isentropic efficiency for every compressor and expander is assumed to be 90% and 80% respectively (usually 90% found in large-scale refrigeration compressors) for the worst case; thus, it has already compensated for the no pressure drop assumption and the temperature difference, which is too small, between the pre-cooled hydrogen gas stream and the MR pre-cooling stream. Moreover, if the three or more number of stages required in compression are used which means more number of compressors, the overall system's efficiency will be better. However, it will be more expensive than a single compression (only single big compressor) and two-stage compression (two compressors). It is not known how much it costs for each compressor. This information is needed to investigate the number of stages required in the compressors as well as in the expanders to think of the payback period of

investment. Initially, a frequently applied approximation for optimum intermediate pressure of ideal gas compression or expansion, in this case which possibly applicable to MR and hydrogen gases that for simplicity are assumed to be ideal, is given by: $P_{opt\,\mathrm{int}} = \sqrt{P_L P_H}$. Where $P_{opt\,\mathrm{int}}$ represents an estimate of the optimum intermediate pressure, P_L is the low pressure, and P_H is the high pressure. In addition, due to the large volume of mass flow rates and low compression ratios, MR compressors and hydrogen compressors must be dynamic. On the other hand, because of lower mass flow rates at expanders in the MR cycle proposed have two-phase inlets and outlets, thus volumetric machines that have margin for two-phase flows are recommended. The manufacturers should be consulted about the machinery. In this chapter, at least two-stage compression with inter-cooling between stages is recommended as an example. More than two-stage compression of MR is used just because lower compression power. But, compression of hydrogen gas in the four H_2 J-B cycle system, more than two-stage compression must be used, because, besides lower energy consumption, a single stage compression results in very high outlet temperature. The condensers must be evaporative cooling towers. Mechanical conversion of work from the expander is assumed to be 98%. For cooling n-H_2 from 25 ^{o}C to e-H_2 around −193 ^{o}C, the MR refrigeration system is proposed. For cooling from −193 ^{o}C to −253 ^{o}C, as a preliminary design, a combination of the four H_2 J-B cycle system is proposed due to the improved efficiency.

Table 4.2 lists the boundary conditions that were initially used to simulate the process depicted in Fig. 4.2. It contains design and assumption data. Ambient temperature, capacity, GH_2 feed, and LH_2 product were the design values. For simplicity, no pressure drop was assumed. Realistic large-scale low-temperature heat exchangers for cryogenic system were generally recommended by Alabdulkarem *et al* (2011) to have 3 ^{o}C temperature approach. The compressors' efficiencies were estimated from the manufacturers' product catalogues, which generally contained large-size gas compressors. The process was simulated with the PRO/II software package. In addition, other commercially available process simulation programs can be used to simulate, including for example HYSYS, HYSIM, and ASPEN PLUS, are all similar. For the equation of state, SRK was selected for use because of its popularity, simplicity, and fast computation.

Table 4.2 – Boundary conditions.

Parameter	The proposed 100-TPD process plant from the simulation
Ambient temperature	25 ^{o}C
Capacity	100 TPD (in 24 hours) = 4,166 kg/h = 1.157 kg/s
GH_2 feed	21 bar and 25 ^{o}C
LH_2 product	1.3 bar, saturated liquid with 95% para
Ortho-para conversion	Stepwise
Pressure drop in system	No
Temperature approach in heat exchangers	3 ^{o}C or above
Isentropic efficiency:	
Compressors	90% (selected similar to actual machinery)
Expanders	80% (selected similar to actual machinery)

In PRO/II simulation software, the component models of heat exchangers, compressors, and expanders are absolutely correct. But investigation the accuracy of the modeling of all the working fluids in the cryogenic region of interest must be performed. The thermodynamic model must be validated first. Regarding hydrogen, one may use as a comparison either the monography

R. McCarty, J. Hord, H. Roder, selected properties of hydrogen (Engineering Design Data), Tech. Rep. Monograph 168, U.S. National Bureau of Standards (now NIST) or the software REFPROP 8. Recently, the best paper about hydrogen properties is given by Leachman *et al* (2009). All data about thermo-physical properties of fluid hydrogen from the same researchers mentioned, found at the software REFPROP 8, can also be checked at NIST (2010).

However, after investigating the accuracy of the modeling of all the working fluids in the region of interest especially hydrogen gas at temperature between −193 °C to −253 °C, it is found that SRK model is quite the same as that of the model from REFPROP 8. This is also in temperature range between 25 °C to −193 °C. It is especially the given values of pressure and temperature, then the simulated density will be exactly the same. Even though there are some differences regarding simulated enthalpy and entropy, this is because the references used in the two models are not the same; but the simulated enthalpy and entropy increments (Δh and Δs) are the same which indicate the two values are correct. These two values are important in energy and exergy analyses of the overall plant. Moreover, even if there are some extremely small deviations of specific heat coefficients, but this is acceptable. The other thermo-physical properties are not important. In short, the SRK model is adequate for the cryogenic region and the simulation results could be near the reality.

According to Bracha *et al* (1994), purity of hydrogen from real large plant is 99%. It is high. Thus, it is assumed here that the impurities may not play a significant role for energy intensity of the plant.

After experiencing in simulation and experiment of the small-scale plant as in Chapter 3 that the trend of both simulation and experimental data go the same direction, this paper is the proposed large-scale plant with MR refrigeration system. The large-scale MR cycle is modified from small-scale MR process from the test rig described aforementioned. The differences which can be noticed the changes from Fig. 3.9, *Simulation data of the laboratory test rig with the proposed simplified composition compared to the experimental data*, in Chapter 3 to be Fig. 4.2, *PRO/II simulation flow sheet for the new modified proposed large-scale 100-TPD LH_2 plant utilizing MR and four hydrogen Joule-Brayton refrigeration cycles,* on this chapter. Those are: ortho-para catalysts are included for ortho-para hydrogen gas conversion, single-stage to be two-stage compression to reduce power consumption, and expansion valves are replaced by expanders to reduce exergy losses. In addition, simple helium system or heat exchanger (HX5 of Fig. 3.9 in Chapter 3) is replaced by the four H_2 J-B cycles. The simulation of the proposed large-scale plant is by using the same simulation package, PRO/II that is done with simulation of the test rig found in Chapter 3. The new, optimized MR has been particularly modified for large-scale process with heat conversion by catalysts; and it has a simplified composition. The idea of exergy analysis from Chapter 2 is also performed here for the analysis of the large-scale on this Chapter.

Brief refrigeration explanation of the whole process plant, Fig. 4.2 is a simplified schematic diagram illustrating quite a complete liquefaction facility. Tables 4.4 and 4.5 contain pressure, temperature, and flowrate data of each stream detailed in Fig. 4.2. Beginning with the hydrogen feed gas to be liquefied with high purity and free of moisture process is first supplied to the liquefaction plant through pipeline S3 as a vapor phase. Then, the gaseous feed flowing at 21 bar 25 ^{o}C is cooled at HX1, HX2, and HX3 by MR cycle and at the same time passing two o-p converters to be equilibrium hydrogen gas at −198 ^{o}C in line S7. Later on, it is cooled by the four H_2 J-B cycles together with o-p catalysts at HX4, HX5, HX6, and HX7 to be −253 ^{o}C equilibrium

gas at S8e. Finally, the gas is expanded by the expander EX8 to be 99% liquid hydrogen and supplied to LIQ4 for use at S8h. The trivial fraction at line S8f which is vapor is pumped by ejector to line S8d and finally cooled back to be liquid again at HX7. For the MR system, beginning with line S17 contains a single gaseous refrigerant which is a mixture of gases. This multi-component refrigerant is compressed in low-stage compressor COM1 and cooled in inter-stage water cooler so that a portion is condensed and then separated in separator. The condensate S17c is withdrawn from the bottom of the separator and pumped directly into the separator LIQ1. The gaseous fraction of the refrigerant is withdrawn from the top of separator at line S17b, compressed in high stage compressor COM2, cooled in water cooler EVAP1 and joined with the previously mentioned condensate. In the first stage of MR separator LIQ1, the liquid fraction rich at line S21 is first sub-cooled at HX1, then expanded at EX1 lower down temperature to be vapor-liquid mixture in line S23, next supplied to line S23 mixed with upward flowing MR line S36, finally vaporized at HX1 to cool most of refrigeration load at feed hydrogen gas S3 and partly MR condensate and gas in line S21 and S20 together with returned hydrogen gas streams at the four H_2 J-B cycles. In a similar manner, the second, and the third fractional condensation steps are performed by passing vapor refrigerant from the phase separators LIQ1 and LIQ2 to provide the second condensate S26 and the last high liquid sub-cooled stream S31. The first condensate S21 contains much of high boiling point components. The intermediate condensate S26 has decreasing high boiling point components and increasing low boiling point components. The last stream S31 is rich in low boiling point components, but it doesn't contain the highest boiling point components. The condensates S22, S27, and S31 after being sub-cooled are reduced in pressure by expanders EX1, EX2, and EX3 in order to reduce temperatures to vaporize and cool the downwardly flowing warm fluid streams. Regarding the four H_2 J-B cycles, beginning with normal hydrogen gas from line S12a flowing downwardly becoming S12d is mostly cooled by counter flow line S12f to S12i and partly by MR cycle. The MR cycle cools the streams to make sure the temperatures at lines S12d as well as S11d, S10d, and S9d get down to $-198\ ^{o}C$. Then, the gas from line S12d is expanded through expander EX4 to reduce temperature according to the rule of positive Joule-Thompson effect in order to cool mostly e-hydrogen feed S7a to S7b and partly n-hydrogen in other H_2 J-B cycles. Finally, other H_2 J-B cycles perform the same way as the first cycle aforedescribed.

The idea, reason, and rules for selecting the cycle as in Fig. 1 why it is superior to conventional ones is explained and clarified here. To cool normal hydrogen gas from $25\ ^{o}C$ to equilibrium temperature of $-193\ ^{o}C$ by MR cycle, the reason is given in the experiment by Chapter 3. The system is more efficient, simple, reliable in comparison to pure refrigerant ones; because the mixture of refrigerants is evaporated isobarically, not at a single but in a range of temperatures. And to cool the equilibrium ortho-para hydrogen gas from $-193\ ^{o}C$ to $-253\ ^{o}C$ by the new proposed configuration four H_2 J-B cycle refrigeration system; it is better to replace helium gas by hydrogen gas a refrigerant. This can be explained in the following sections.

4.2.3. MR refrigeration system for cooling feed normal hydrogen gas from 25 ^{o}C to the equilibrium temperature of −193 ^{o}C

When designing a large MR refrigeration system, there are various ways to improve efficiency. Briefly, these improvements include the following: to use 21-bar single n-GH_2 feed-through, to use a high isentropic efficiency MR compressor, to replace every expansion valve with a high

efficiency expander, to use a 10-component composition of MR refrigerant, to add another liquid separator after EX3, to improve the condenser. The flow sheet is depicted in Fig. 4.2.

The MR compressor power must be minimized. Thus, the variables that must be optimized were determined from trial and error in PRO/II and are arranged as below:

1. First, the suitable feed pressure of the H_2 compressor must be determined:
   The feed pressure must be above 15 bar, which is the supercritical pressure to avoid condensation. The pressure of 18 bar may still be too close to 15 bar. For the proposed plant, the discharge pressure is designed to be 21 bar, which is equal to the feed at Ingolstadt (see Fig. 4.1). However, for the real large-scale process, if the feed is 1–2 bar, it is recommended to compress it to 21 bar.

   It is right that the higher feed hydrogen pressure, e.g., raising it to 40 or 60 bar, the better liquefier is as stated by Quack (2002) and Berstad *et al* (2010). This is because less ideal work of liquefaction. But due to the additional high compression power in order to raise to that high feed pressure makes the liquefier with that additional compressors consumes more energy. So this method is not attractive.

   Moreover, with the same system and configuration as proposed in Fig. 4.2, no matter how much high feed pressure (S3) between 14–60 bar as simulated by trial in PRO/II, energy consumption from MR and hydrogen compressors is the same; it is because the same compressors and heat exchangers' configuration of the MR and the four H_2 J-B cycles generate the same irreversibilities. Moreover, specific heat constant and thermal conductivity don't change much with the increased pressure resulting no change in heat transfer. Therefore, maintaining above 14 bar just a little higher than critical point pressure (12.9 bar) of feed hydrogen pressure is recommended in actual large-scale plant as depicted in Fig. 4.2. Cooling feed hydrogen gas both at 14 bar above the critical pressure and 2–3 bar below the critical pressure from 25 ^{o}C to −253 ^{o}C release heat quite the same amount. But feeding at 2–3 bar at −253 ^{o}C is still the saturated gas, while at 14 bar is the entire hydrogen liquid, thus more heat is transferred to be entire liquid through condensation. Therefore hydrogen releases more heat if the feed is maintained at lower than critical pressure at 12.9 bar during condensation process below the saturation curve. In addition, the critical temperature of hydrogen is −240 ^{o}C. This means that hydrogen can only be liquefied below that temperature regardless of the pressure applied.

   However in the proposed cycle as in Fig. 4.2, hydrogen feed is maintained at 21 bar absolute to be cooled down from 25 ^{o}C to −253 ^{o}C by the MR and the four H_2 J-B cycles in order to avoid condensation before expansion to have liquefied hydrogen for minimum liquefaction power consumption; importantly, the other reason is also because it is used to compare the same feed pressure but different cycle to the referenced Ingolstadt plant's by Bracha *et al* (1994).

2. Then, the hot stream hydrogen outlet temperatures from HX1, HX2, and HX3 should be determined:
   This is determined from trial and error for the minimum MR compressor in the simulation software. In addition, the MR mass flow rate at HX1 is the largest, while HX3 is the smallest. Thus, HX1 should cool and remove heat from the hydrogen gas more than HX3.
3. Next, a suitable discharge pressure for the MR compressor should be determined:

The discharge pressure cannot be lower than 18 bar because it will be impossible to cool the system. In addition, it should not be more than 22 bar because there will be too much compression power.

4. After that, a suitable suction pressure for the MR compressor must be determined:
   The suction pressure cannot be lower than 1 bar because of the MR compressor's high power. The suction should not be more than 2 bar because it will be insufficient or impossible to cool the hydrogen gas.
5. The arrangement of the 2-stage MR compression similar to Linde Engineering (2011)'s:
   All pressures reported herein all through out this thesis are absolute pressures. As seen in Fig. 4.2, compression by the first stage MR compressor from 2 bar to intermediate pressure at 9.3 bar, the intermediate pressure is optimized by writing a small source code in PRO/II to find it. This is to minimize power consumption from the two compressors: COM1 and COM2. The hot discharge MR gas is cooled by condenser to 30 ^{o}C, 5 degree higher than ambient. At this temperature and pressure, MR flow (S17a) is a composition. Then it is separated at a separation tank to be vapor and liquid. After that, the vapor (S17b) is compressed by the second stage MR compressor. And the liquid from the separation tank at intermediate pressure (S17c) is pumped to mix with high pressure discharge (S18).
6. Finally, a suitable composition for the MR mixture and the flow rate should be determined:
   This is also found from trial and error. This step is more complex, e.g., up to a 10-component composition is needed for the large-scale plant's process.

Previously, Chapter 2 is the design and simulation of a small-scale test rig. The new, optimized MR has been particularly modified for large-scale processes with heat conversion by catalysts and has the following composition: 1.2% hydrogen, 25.6% nitrogen, 13.6% methane, 15.2% R14, 10% ethane, 10% propene, 5.8% propane, 1.0% Ibutane, 1.0% butane, and 10.8% pentane by mole. A better efficiency is attained when neon is replaced with 1.2% hydrogen. All of these results were determined from trial and error by the simulation in PRO/II. In fact, the catalysts should be filled inside of the heat exchangers to improve efficiency, but this cannot be simulated in the PRO/II software. There is a liquid separator, LIQ3, that acts as a buffer to maintain enough volatile components, such as nitrogen, methane, R14, and hydrogen (or not). They are almost in the liquid phase after expansion at stream 32 (S32). If they are not charged enough, the HX3 will not be able to cool the hydrogen gas to the designed value at −193 ^{o}C. There will not be enough of the volatile component to cool down the HX3. If they are charged too much, there is no problem; they will be kept in the liquid phase while in operation at LIQ4. Moreover, there is no energy loss from having the liquid separator, LIQ3. A surge drum acts as a buffer to keep liquid MR refrigerant when the plant stops for maintenance and to protect MR compressors while in operation. The simulation's net power, w_A is 1.36 kWh/kg$_{LH2}$ in comparison to the ideal of 0.51 kWh/kg$_{LH2}$. In Fig. 4.2, electricity consumptions for the cooling loads due to water pumps and air-cooled fans in the after coolers and evaporative condensers are very relatively small compared to compressors and expanders. However, they are assumed to be around 5% of power consumption from compressors as calculated in Table 4.9. From the simulation's calculations, the second law analysis was conducted. The exergy losses are dissipated mainly through the following components: compressors 55%, evaporative condenser 19%, heat exchangers 18%, expanders 5%, mixers 1%, and liquid separator 1% as calculated in Table 4.6. In fact, the loss due to evaporative condenser may not be included because it seems not important to know. It is impossible to avoid all those losses aforementioned. However, this proposed MR cycle is the best system in comparison to the nitrogen, helium, and propane refrigeration systems, as shown in Table 4.1.

The proposed MR system is quite mature now with respect to process configuration. A little more research is needed for small improvements. This is just a preliminary design; it is not really a real one. More information from future studies on the MR 10-component composition or the more complex compositions is needed to better simulate the size of each MR heat exchanger. The information is as follows:

- The temperature of each pre-cooled hydrogen gas stream that leaves each heat exchanger, e.g., HX1, HX2, and HX3 from the experiment. Those temperatures depend on the information below.
- The optimized MR composition for the complex composition from the test rig experiment.

4.2.4. Cooling the feed equilibrium hydrogen gas from −193 °C to −253 °C by the four H_2 Joule-Brayton cycle refrigeration system

Initially, Brayton Quack's (2002) together with Valenti and Macchi's (2008) helium systems with optimized discharge and suction pressures were selected by a preliminary test run in PRO/II. However, from trial and error, it was found that replacing helium with hydrogen as a refrigerant in the four J-B cycle system that was proposed by Valenti and Macchi (2008) is better than helium when cooling hydrogen gas from −193 °C to −253 °C. One disadvantage of helium is the high discharge temperature when it is compressed, which is due to the lower heat transfer properties. Hydrogen has much better heat transfer properties than helium. For that reason, the size of the heat exchangers will be smaller. In addition, the power consumption from the compressor is less when using hydrogen because of less mass flowrate compared to helium. To cool hydrogen from −243 °C to −253 °C, the hydrogen Brayton cycle is better. Currently, all large-scale plants use hydrogen refrigeration systems; nobody uses helium. Thus, it is recommended to use hydrogen. To improve efficiency, the four cycles may also be replaced by up to six cycles: −193 to −203 °C, −203 to −213 °C, −213 to −223 °C, −223 to −233 °C, −233 to −243 °C, and −243 to −253 °C. However, it's not recommended that a larger number of heat exchangers results in a greater exergy loss; there will be more compressors and the system will be more complicated; thus, having only four cycles is enough. The choice of pressure levels or temperature levels in the hydrogen J-B cycle sub plant is all from trial and error to get optimum.

A better flow sheet was found and simulated in PRO/II as depicted in Fig. 4.2, some improved modification by trial and error to get optimum at all compressors. It is made to be different from the previously proposed cycle described in Fig. 2, *PRO/II simulation flow sheet for the proposed large-scale 100-TPD LH_2 plant with MR and four H_2 Joule-Brayton cascade cycles*, on Krasae-in *et al* (2010) as explained below:

- In Fig. 4.2, there is integration of heat exchangers of the "four hydrogen J-B cycles" to the MR cycle. This is to make sure that all discharges: S9d, S10d, S11d, and S12d of the high side pressures at the "four H_2 J-B cycles" are cooled down to −193 °C and all the returns: S9o, S10m, S11k, S12i of the low side pressures are realistic temperatures at approximately 0−10 °C before suction to all hydrogen compressors. The MR refrigeration cycle does very good job efficiently to bring heat from −193 °C source to 25 °C atmosphere. Then, the further cooling of feed hydrogen gas by the new improved system as proposed in Fig. 4.2 from −193 °C down to −253 °C would be realistic. This is importantly why the new proposed cycle is superior to the

old flowsheet.

- The proposed 5- or 10-component composition can be used with quite the same result. The MR flow rate which can be noticed from S18 or S19 is 36.11 kg/s to cool MR heat exchangers: HX1, HX2, and HX3. There is additional heat transfer from hydrogen gas flows in the new proposed "four H_2 J-B cycles".
- It is very important to note here that every MR heat exchanger and every hydrogen heat exchanger must be realistic high effectiveness heat exchangers to specify 3 ^oC temperature difference at the cold and hot end in the heat exchangers. It is especially those at the four H_2 J-B cycles to obtain overall cycle to be realistic high efficient hydrogen liquefaction plant. But HX1, HX2, and HX3 don't need to be big because they are designed for the real size heat exchangers that 5−10 ^oC temperature difference at the cold and hot end in the heat exchangers. For that reason, the heat exchangers need to be big. It is repeated here that high efficient hydrogen liquefaction plant must have every high effectiveness heat exchanger resulting in the big size of every heat exchanger. Therefore, the proposed high efficient hydrogen cycle might have smaller or bigger heat exchangers than today conventional plant especially when comparing to the pre-cooled Claude cycles as depicted in Fig. 1.4, *Process flow sheet of hydrogen liquefaction plant in Leuna*, in Chapter 1. It depends. According to the figure, the cycle with given temperatures and pressures, e.g., 32 bar at high, 9 bar at intermediate, and 1.1 bar at low stages are the input for simulation at PRO/II. The outcome is that the pre-cooled Claude cycles use high flowrate hydrogen gas to circulate in order to take heat resulting in high power consumption of low-stage and high-stage hydrogen compressors. The system uses hydrogen cycles to cool feed hydrogen gas from −193 ^oC to −253 ^oC; the proposed four H_2 J-B cycles are quite the same, the differences are the high effectiveness of heat exchangers and the four instead of three Joule-Brayton cycles. Thus hydrogen flowrates in the proposed four H_2 J-B cycles are less resulting less energy consumption.
- In Fig. 4.2, there are only four cycles of the H_2 J-B cycle to cool feed hydrogen from −193 ^oC to −253 ^oC. This is because from trial and error in the software, five or a little more cycles consume quite the same power consumption; this is due to the fact that more cycles mean more numbers of compressors and heat exchangers that generate more irreversibilities. As seen in Fig. 4.2, no direction solution about the arrangement of each H_2 J-B cycle, temperatures, and pressures. It is all about trial and error to get optimum at the power consumption of hydrogen compressor. The design and arrangement of HX4, HX5, and HX6 is that the expansion of hydrogen gas at EX4, EX5, EX6 to lower down the tempeatures of the gas to cool down all streams to designed values that flowing and leaving HX4, HX5, and HX6; this is of course as the rule, all expanded streams: S9h, S10g, S11f, and S12e are below inversion curve and have positive Joule Thompson's effect.
- It is impossible to have only one or two H_2 J-B cycles to cool feed hydrogen from −193 ^oC to −253 ^oC. This is because the return cooling hydrogen gas to cool down feed hydrogen in each cycle has higher temperature to further cool normal hydrogen gas at regenerator for obtaining Joule-Brayton cycle possible.
- In Fig. 4.2, proposing the system with two or three H_2 J-B cycles are possible but that will look like somewhat presenting quite the same cycle as Leuna's. As depicted in Fig. 1.4, *Process flow sheet of hydrogen liquefaction plant in Leuna*, the Leuna system has high, intermediate, and low H_2 J-B cycles which are well arranged to eliminate the numbers of stages those have a lot of heat exchangers and compressors. This is by coupling all together in a whole operated and compressed by less numbers of low side and high side hydrogen compressors. However, by trial and error in simulation in PRO/II, the system like this must

have higher hydrogen flowrates with small size hydrogen heat exchangers. Thus, it consumes more power consumption.
- The arrangement of compressors that two stage compression of both MR and H_2 J-B cycles is enough because three stage compression yields only slight improvement for this size of the plant.
- The intermediate pressures at streams (at S9p, S10, S11l, and S12j) in Fig. 4.2 by two-stage hydrogen compression are optimized and found by writing a small source code in PRO/II. This is to minimize power consumption from the two low-stage and high-stage compressors.

Finally, the feed hydrogen gas at −253 °C is depressurized by the expander from 21 bar to 1.3 bar. By simulation, this is a 100% yield 95% p-LH_2. But in reality there might be a small fraction of vapor, thus 99% liquid (stream 8h) and 1% vapor (stream 8g) is assumed. Actually, para content at 95% of LH_2 output is enough to be kept for use, the same as Ingolstadt plant's. If it is more than this value, more conversion energy is needed which is not necessary. By doing this, the last heat exchanger must be designed to cool the hydrogen to the lowest possible temperature, e.g., near −253 °C, so there is no vapor fraction after the expansion at the last expander. A small ejector is recommended to recover p-GH_2 from the storage tank (LIQ4), the same as the plant in Leuna. In short, the sum of the simulation's net power, w_B, for the proposed system is 3.39 kWh/kg_{LH2} in comparison to the ideal of 2.38 kWh/kg_{LH2}. According to the second law analysis, the exergy losses are dissipated through the following: compressors 24%, expanders 28%, heat exchangers 38%, and evaporative condensers 10% as calculated in Table 4.6. Exergy losses are much especially at expanders that two-stage expanders might be used. The losses due to evaporative condensers may also not be included because it seems not important to know. This proposed four H_2 Joule-Brayton cycle system is the best compared to the nitrogen and helium refrigeration systems, as shown in Table 4.1. However, if anyone has suggestions or different opinions for more improvement, they can be proposed later. Unfortunately, the proposed four H_2 Joule-Brayton cycle system is still not the best; each H_2 Joule-Brayton cycle system is the Linde-Hampson system, which is the world's first air liquefaction system, but with the expander to replace the J-T valve for work recovery. Moreover, the helium-refrigerated or hydrogen-refrigerated hydrogen systems may be good as well. However, the system with pre-cooling needs an additional nitrogen pre-cooled system that makes the overall system complicated due to the additional compressors and heat exchangers for the nitrogen liquefaction system. The Claude system may also be good since it has a compressor power reduction around 5–10%, which was found in a preliminary test run in PRO/II; however, a greater number of heat exchangers and a high-priced expander are needed. For simplicity, it can be a J-T valve instead of an expander. Thus, it depends on the overall liquefier's size, suitability, cost, etc. The proposed system (see Fig. 4.2) is an optimistic preliminary design process. However, it is still not very mature. The designer should take this into account when in the design process. Finally, more time and work is needed to find the best system to cool hydrogen gas from −193 °C to −253 °C. *In short, it is possible to obtain a cycle that has a better efficiency than what is mentioned. However, a better efficiency means a more complicated and more expensive system. Thus, the following information is needed to design the real plant: machinery from the manufacturers, cost of the materials, size of the heat exchangers, and so on.*

4.3. Optimal operation of the new modified proposed large-scale 100-TPD LH_2 plant

For the review of literature, there are some interesting papers about optimization of MR cycle recommended to read for understanding, for example: Alabdulkarem *et al* (2011) and Tak *et al* (2011) explain how to optimize MR cycles with different pinch temperatures. Nogal *et al* (2008) gives an idea how to optimize the MR composition showing no crossovers or minimum temperature approach violations, that the hot and cold temperature profiles (composite curves) are checked for feasibility. Jensen and Skogestad (2006) propose a method how to optimize MR cycle.

This section contains a preliminary study on the optimum operation of a proposed cycle as the flow sheet given in Fig. 4.2. The optimization's idea of mixed refrigerant cycle in this chapter is from Jensen (2006) who studied about the optimum operation of refrigeration and LNG processes. The optimization model is solved on the platform of commercial software PRO/II mostly by trial-and-error and some with small source-code program writing through the internal software's calculator and an optimizer.

4.3.1. Objective function

The objective function for optimal operation is simpler than for optimal design, discussed by Jensen (2006), because the investment costs, the capital costs, and others are not considered. The simplified cost function to reduce total compressor consumption to be minimized then becomes:

$$\begin{aligned} &\min \quad \dot{W}_S \\ &\text{subject to } \dot{m}_{feed} = \text{given (or } \dot{m}_{GH_2} = \text{given} = 1.157 \text{ kg/s)} \\ &c \le 0 \end{aligned}$$

Here, $\dot{W}_S$ is the sum of all compressor powers (kW): COM1, COM2, COM3, COM4, COM5, COM6, COM7, COM8, COM9, and COM10 shown in Fig. 4.2. $c \le 0$ represents the mathematical formulation of the operational constraints and the model equations. And $\dot{m}_{feed}$ is maintained at the nominal feed rate.

4.3.2. Nominal conditions

Feed hydrogen gas stream:

- Feed: normal hydrogen gas enters with P = 21 bar and T = 25 ^{o}C after gas purification equivalent to the feed at Ingolstadt plant by Bracha *et al* (1994). Nominal flow rate (S3) is 100 TPD = 100,000 kg/24 hours = 4,166 kg/hour = 1.157 kg/s.
- Product: 95% para-liquid hydrogen is at P = 1.3 bar and T = −253 ^{o}C equivalent to the product at Ingolstadt plant by Bracha *et al* (1994).

MR cycle:

- The mixed refrigerant vapour to the suction of low-stage MR compressor (COM1) is super-heated 0–10 ^{o}C because this usually happens in real case in refrigeration system.
- Pressure drops inside HX1, HX2, and HX3 are assumed to be zero because the information about design criteria of all heat exchangers is not known. And it is assumed to be not much significant.

Four H_2 J-B cycles:

- In every hydrogen compressor after discharge, the hydrogen gas is cooled to 25 ^{o}C atmospheric temperature either by air-cooler or evaporative condenser (assumed maximum cooling).
- Pressure drops inside HX1, HX2, HX3, HX4, HX5, HX6, and HX7 are assumed to be zero because the information about design criteria of all heat exchangers is not known. It is also assumed to be not much significant.

The SRK equation of state is used both for feed GH_2, the mixed refrigerant in MR cycle, and the GH_2 in four H_2 J-B cycles. The heat exchangers are distributed models with constant heat transfer coefficients. All MR and hydrogen compressors are isentropic with 90% constant efficiencies.

For the equation of state, SRK was selected for use in this PRO/II simulation package because of the reason aforediscribed. It is used both for feed GH_2, the mixed refrigerant in MR cycle, and the GH_2 in four H_2 J-B cycles. The accuracy of this model was vertified and explained. Moreover, SRK model was used by Hammer *et al* (2003), Jensen (2008), Myklebust (2010), and Nogal *et al* (2008) in design, simulation, and optimization of multi-component system in LNG processes. For all aforementioned, SRK in PRO/II are used to predict the trend what happens in the rig and the simulation large-scale plant. The other popular Peng-Robinson equation of state gives quite similar results. The heat exchangers are distributed models with constant heat transfer coefficients. All MR and hydrogen compressors are isentropic with 90% constant efficiencies.

4.3.3. Manipulated variables

For the cycles, the number of manipulated variables are the number of compressors and valves plus one active charge for each cycle.

From the discussion aforementioned it is found that there are 23 manipulated variables:

MR cycle:

- MR compressor powers: COM1, and COM2.
- 3 expander openings: EX1, EX2, and EX3.
- MR compositions.
- 1 active charge.

Four H_2 J-B cycles:

- Hydrogen compressor powers: COM3, COM4, COM5, COM6, COM7, COM8, COM9, and COM10.
- 4 expander openings: EX4, EX5, EX6, and EX7.
- 4 active charges (one for each cycle).

In actual commission and operation of real large plant, openings of MR 3-expanders/valves and the MR active charge will result in the control of low side (S17) and high side (S18) pressures of MR cycle. Openings of J-B 4-expanders/valves and the J-B active charge will result in the control of low side and high side pressures of each H_2 J-B cycle. In the PRO/II software, pressures can be controlled by setting values at the outlets of compressors and expanders. The increase in MR flowrate at S19 in PRO/II will increase MR compressor powers: COM1, and COM2. And adjusting the increase in hydrogen flowrate in PRO/II of each H_2 J-B cycle will increase hydrogen compressor powers: COM3, COM4, COM5, COM6, COM7, COM8, COM9, and COM10.

The active charge is defined as the total mass accumulated in the process equipment in the cycle, mainly in the condenser and evaporator, but excluding any adjustable mass in liquid receivers/accumulators (tanks).

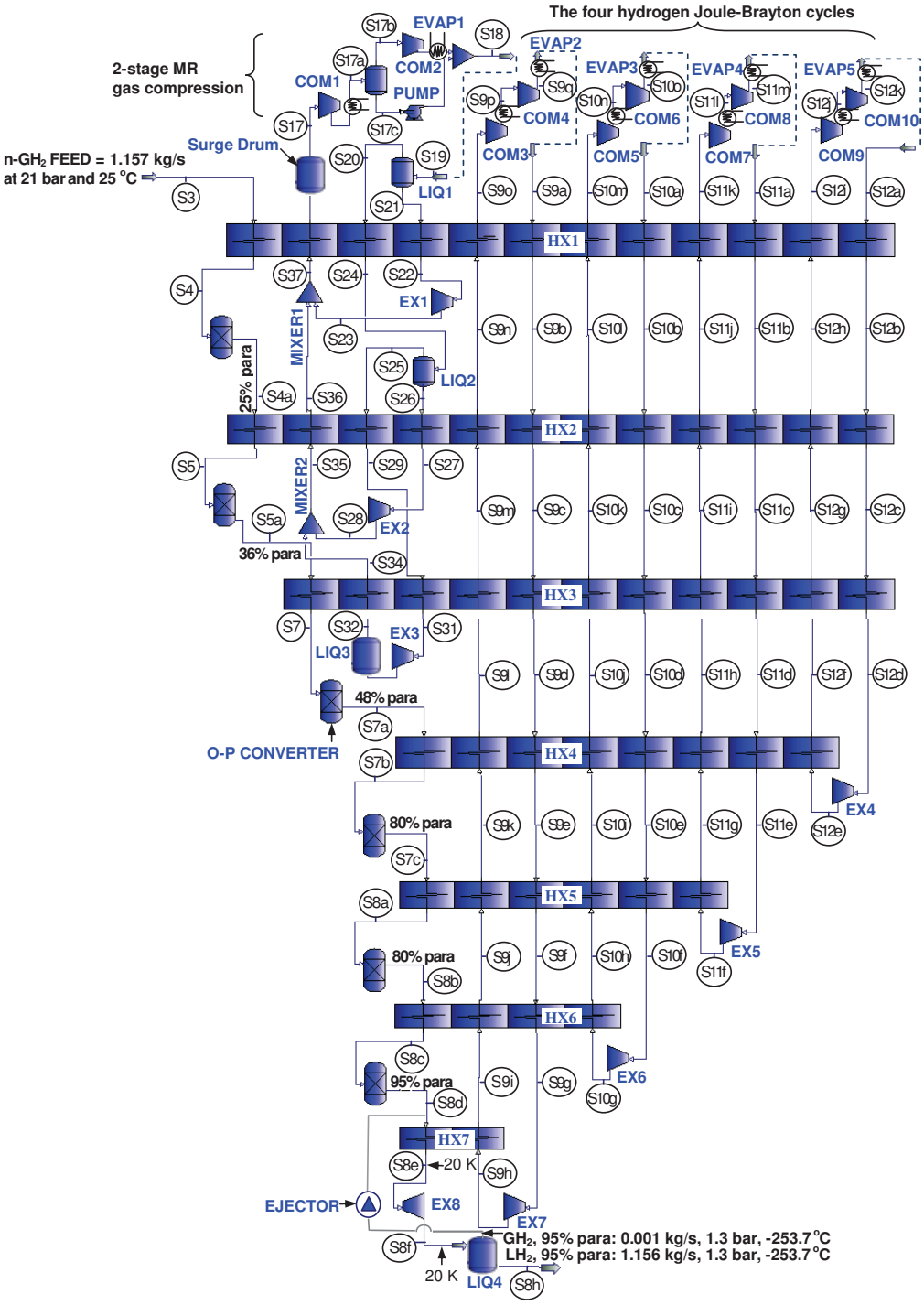

Fig. 4.2 – PRO/II simulation flow-sheet for the new modified proposed large-scale 100-TPD LH_2 plant utilizing MR and four hydrogen Joule-Brayton refrigeration cycles.

4.3.4. Constraints during operation

There are 26 constraints must be satisfied during operation:

Feed hydrogen gas stream:

- Feed: normal hydrogen gas (S3) enters with P = 21 bar and T = 25 ^{o}C.
- Feed hydrogen gas temperature leaving HX3 cooled by MR cycle at T = −198 ^{o}C. The reason to specify this temperature in simulation is because from preliminary experimental experience by the author as stated in Chapter 3, the MR cycle at the rig could cool hydrogen gas to -180 ^{o}C even though it was not every well adjusted to achieve lower temperature. The mixture still lacked hydrogen and nitrogen to achieve the desired −198 ^{o}C. Thus specifying near at −198 ^{o}C would be possible in reality.
- Product: 95% para-liquid hydrogen (S8h) is at P = 1.3 bar and T = −253 ^{o}C.

MR cycle:

- The mixed refrigerant vapour (S17) to the suction of low-stage MR compressor (COM1) is superheated 0−10 ^{o}C to avoid the damage in compressor because this value usually happens in real case in refrigeration systems.
- The temperature after the refrigerant condenser (S18 or S19) is 25 ^{o}C by assuming that it is very good evaporative condenser heat exchanger. Price and Mortko (1996) report 29 ^{o}C and 32 ^{o}C, respectively.
- Heat exchanger minimum approach temperature for HX1 and HX2 is: 5 ^{o}C ≤ ΔT_{min} ≤ 10 ^{o}C.
- Heat exchanger minimum approach temperature for HX3 only at location between S7 and S32 is: ΔT_{min} = 3 ^{o}C.

Four H_2 J-B cycles:

- Hydrogen vapour (S9o, S10m, S11k, and S12j) to the suction of low-stage hydrogen compressors (COM3, COM5, COM7, and COM9) is between 0−10 ^{o}C because this usually happens in real case in refrigeration systems.
- The temperature after the refrigerant condenser (S9a, S10a, S11a, and S12a) is 25 ^{o}C by assuming that it is very good heat exchanger.
- Heat exchanger minimum approach temperature for HX1, HX2, and HX3 is: 5 ^{o}C ≤ ΔT_{min} ≤ 10 ^{o}C.
- Heat exchanger minimum approach temperature for HX4, HX5, and HX6 is ΔT_{min} = 3 ^{o}C.
- Heat exchanger minimum approach temperature for HX7 only at loation between S8e and S9h is: ΔT_{min} = 3 ^{o}C.

According to Jensen (2006), there are two methods in design of processes with heat exchangers. The one common method is specifying ΔT_{min} for individual heat exchangers. The other alternative recommended is the simplified Total Annualized Cost (TAC). However TAC method is complicated that it needs to know overall heat transfer coefficients and exact heat exchangers'

sizes which is the research of the future work. It is impossible at this preliminary optimization work. Thus, ΔT_{min} method is preferred to mention here.

The idea is that the heat exchanger minimum approach temperature, ΔT_{min}, gives a balance between low operating cost (favored by low ΔT_{min}) and low capital cost (favored by high ΔT_{min}). A small value of ΔT_{min} means that a lot of the energy is recovered, but it requires a large heat exchanger. On the other hand, a larger value of ΔT_{min} requires less area, but the outlet temperature will be higher and less energy is recovered; thus the higher refrigerant flows is needed resulting in higher energy consumption from compressors. There is rule of thumb for the value of ΔT_{min} such as Turton *et al* (2002, p.250) recommends 10 ^{o}C for fluids and 5 ^{o}C for refrigerants. It is very important to note that heat exchanger effectiveness must get close to unity as recommended by Barron (1966, p.155). This means almost perfect heat exchanger is needed when designing cryogenic system. It reflects the exergy loss and overall cycle efficiency.

The reason to arbitrary avoid specifying ΔT_{min} in the temperature within the range 1–2 ^{o}C for the constraints aforementioned because the heat exchanger sizes will be very big. This is to make the proposed cycle possible in realistic. It also doesn't exaggerate the report of good efficiency of the proposed plant. It is except the locations at HX3 (between S7 and S32) and HX7 (S8e and S9h). Because, by simulation, it is difficult about the control to further lower down the temperatures of cooling streams (S32 and S9h) by further lower expansion pressures. However, if the plant owner doesn't care about the construction cost due to the big size of heat exchangers, thus specifying ΔT_{min} in the temperature range 1–2 ^{o}C for all heat exchangers will result in a great deal of improved overall plant energy efficiency. However, that's not realistic.

4.3.5. Unconstraints during operation

Below are variables that can be designed, optimized, and controlled while making simulation in PRO/II software, but they can't be controlled to be exact during operation of the real-large plant due to discrepancy of simulation from real case:

Feed hydrogen gas stream:

- Feed hydrogen gas temperatures cooled by MR cycle after leaving HX1 and HX2.

This can be noticed at the differences of simulation from experiment on Chapter 3.

MR cycle:

- MR streams' temperatures subcooled after leaving HX1, HX2, and HX3.

Four H_2 J-B cycles:

- Hydrogen gas streams' temperatures after leaving HX4, HX5, HX6, and HX7.

4.4. Optimization results

In this section, total compressor consumption is optimized by variables aforementioned to locate the optimal operation of a given hydrogen flowrate of LH_2 plant. Some key values are given in Tables 4.3, 4.4, and 4.5 which are the simulation data of Fig. 4.2.

Some remarks:

- The total shaft work from all compressors is 25,190 kW.
- The optimal GH_2 temperatures out of HX1, HX2 and HX3 are: −46 °C, −103 °C, and −198 °C respectively.
- The proposed refrigerant is a mix of 4% hydrogen, 18% nitrogen, 24% methane, 28% ethane, and 26% butane by mole.

The mixed refrigerant composition mentioned above is chosen so that it has an evaporation curve that matches the cooling curve of the pre-cooled hydrogen gas with minimum temperature difference. Small temperature difference reduces entropy generation; it improves thermodynamic efficiency and reduces power consumption (Townsend, 1983). Usually refrigerant compositions selection has been done by trial-and-error and guided only by heuristics (Lee, 2002).

The proposed simplified 5-component composition from trial and error is adjusted to match the cooling curve of feed hydrogen gas. It is similar to output of a proposed 10-component composition: 1.2% hydrogen, 25.6% nitrogen, 13.6% methane, 15.2% R14, 10% ethane, 10% propene, 5.8% propane, 1.0% Ibutane, 1.0% butane, and 10.8% pentane. The total power consumption from MR compresors due to the 10-component composition is quite the same as the 5-component composition. Therefore, the proposed 5-component composition is selected for the large-scale plant instead of the possible complicated 6- to 10- or more-component compositions because of its simplicity reason.

Fig. 4.3 shows adapted *h-T* curves for the new proposed 5-component composition in the proposed large-scale plant. Fig. 4.4 shows adapted *h-T* curves for the 10-component composition that maybe used in the proposed large-scale plant. With a chosen MR flowrate, the MR compositions as variables are chosen from trial and error to have positive temperature difference (as constraints) everywhere all along the curves between the hot streams ("Subcooled MR" and "Feed GH_2") and the "Cold MR" stream. Minimum approach temperature differences at the hot and cold ends of all the three MR heat exchangers are also the constraints. Both Figs. 4.3 and 4.4 have quite similar curves that have all positive difference between the hot and cold streams but the complex 10-component composition has smoother curves.

The assumption in this section is the same as in Table 4.2 except that all compressor efficiencies are assumed to be 90% similar to actual large-scale machinery. No pressure drop in all heat exchangers are still assumed here. Because it is considered to be small and not significant in actual system.

In Table 4.3, MR compressors' total power is 5,896 kW from COM1 and COM2. Total power of hydrogen compressors in the four H_2 J-B cycles is 19,294 kW which is the sum of COM3, COM4, COM5, COM6, COM7, COM8, COM9, and COM10. Total miscellaneous power consumption from all pumps and fans in cooling towers, air condensers, and others is 1,100 kW. It is estimated around 5% the same as in Fig. 1.2, *The location of Linde LH_2 in Ingolstadt*, in Chapter 4 from overall plant energy consumption. Thus, energy consumption of MR cycle is 1.38 kWh/kg_{LH2} and the four H_2 J-B cycles is 4.24 kWh/kg_{LH2}. At last, the overall plant energy consumption is 5.91 kWh/kg_{LH2}.

Table 4.3 – Simulation data of the system's energy consumption in Fig. 4.2.

MR compressors' power	= 5,896	kW
Hydrogen compressors' power	= 19,294	kW
Expanders' total power	= 1,245	kW
Miscellaneous	= 1,100	kW
Overall cycle energy consumption	= 5.91	kWh/kg_{LH2}

Table 4.4 – Simulation data of the modified proposed MR cycle.

Stream number	Pressure	Temp.	Flow rate	Specific enthalpy	Specific entropy	Phase	Description
	P	T	$\dot{m}$	h	s		
	(bar)	(°C)	(kg/s)	(kJ/kg)	(kJ/kg- °C)		
3	21	25	1.157	175.87	76.12	Superheated vapor	H_2 cool gas
4	21	-46.00	1.157	-837.64	72.23	Superheated vapor	H_2 cold gas
4a	21	-46.00	1.157	-552.78	75.14	Superheated vapor	H_2 cold gas
5	21	-103.00	1.157	-1,377.43	70.95	Superheated vapor	H_2 cold gas
5a	21	-103.00	1.157	-1,373.83	70.98	Superheated vapor	H_2 cold gas
7	21	-198.00	1.157	-2,776.45	58.84	Superheated vapor	H_2 cold gas
7a	21	-194.75	1.157	-2,183.80	61.75	Superheated vapor	H_2 cold gas
7b	21	-213.15	1.157	-2,481.86	57.42	Superheated vapor	H_2 cold gas
17	2	15.00	36.11	317.25	9.12	Superheated vapor	MR cool gas
17a	6	25.00	36.11	327.80	8.89	Superheated vapor	MR cool gas
17b	6	25.00	36.11	327.80	8.89	Superheated vapor	MR cool gas
17c	6	25.00	0.00	-	-	-	-
18	18	25.00	36.11	220.82	8.28	Saturated liquid	MR cool liquid
19	18	25.00	36.11	220.82	8.28	Saturated liquid	MR cool liquid
20	18	25.00	26.49	279.01	8.71	Saturated vapor	MR cool gas
21	18	25.00	9.62	60.61	7.08	Saturated liquid	MR cool liquid
22	18	-46.00	9.62	-105.59	6.446	Compressed liquid	MR cool liquid
23	2	-50.86	9.62	-108.80	6.450	Mixture	MR cold mixture
24	18	-46.00	26.49	-35.79	7.52	Mixture	MR cold mixture
25	18	-46.00	13.258	51.66	8.536	Saturated vapor	MR cool gas
26	18	-46.00	13.235	-123.403	6.502	Saturated liquid	MR cool liquid
27	18	-103.00	13.235	-215.557	5.853	Compressed liquid	MR cool liquid
28	2	-106.62	13.235	-254.48	5.857	Mixture	MR cold mixture
29	18	-103.00	13.258	-198.98	7.257	Mixture	MR cold mixture
31	18	-198.00	13.258	-579.402	4.125	Mixture	MR cold mixture
32	2	-201.08	13.258	-585.116	4.145	Mixture	MR cold mixture
34	2	-111.04	13.258	-113.33	8.408	Mixture	MR cold mixture
35	2	-107.10	26.49	-183.84	7.142	Mixture	MR cold mixture
36	2	-55.71	26.49	50.136	8.383	Mixture	MR cold mixture
37	2	-54.96	36.11	7.785	7.868	Mixture	MR cold mixture

Table 4.5 – Simulation data of the modified proposed four H_2 Joule-Brayton cycles.

Stream number	Pressure P (bar)	Temp. T (°C)	Flow rate $\dot{m}$ (kg/s)	Specific enthalpy h (kJ/kg)	Specific entropy s (kJ/kg-°C)	Phase	Description
8a	21	-233.00	1.157	-2,618.52	48.45	Supercritical	H_2 cold liquid
8b	21	-232.47	1.157	-2,470.36	48.28	Supercritical	H_2 cold liquid
8c	21	-243.00	1.157	-2,858.25	38.15	Superheated vapor	H_2 cold liquid
8d	21	-243.00	1.157	-2,752.54	37.46	Superheated vapor	H_2 cold liquid
8e	21	-253.00	1.157	-2,969.72	28.79	Superheated vapor	H_2 cold liquid
8f	21	-253.71	1.157	-3,023.10	28.88	Mixture: 99% liquid	H_2 mixture
8g	21	-253.71	0.001	-2,509.85	53.07	Superheated vapor	H_2 cold gas
8h	21	-253.57	1.156	-2,993.99	28.79	Superheated vapor	H_2 cold liquid
9a	2.2	25.00	2.099	171.35	85.44	Superheated vapor	H_2 cold gas
9b	2.2	-46.00	2.099	-834.67	81.59	Superheated vapor	H_2 cold gas
9c	2.2	-103.00	2.099	-1,639.41	77.51	Superheated vapor	H_2 cold gas
9d	2.2	-198.00	2.099	-2,984.25	65.94	Superheated vapor	H_2 cold gas
9e	2.2	-213.00	2.099	-3,198.23	62.76	Superheated vapor	H_2 cold gas
9f	2.2	-233.00	2.099	-3,486.78	56.92	Superheated vapor	H_2 cold gas
9g	2.2	-243.00	2.099	-3,635.08	52.67	Superheated vapor	H_2 cold gas
9h	0.25	-254.92	2.099	-3,785.10	54.85	Superheated vapor	H_2 cold gas
9i	0.25	-246.55	2.099	-3,665.38	60.26	Superheated vapor	H_2 cold gas
9j	0.25	-235.90	2.099	-3,514.26	66.04	Superheated vapor	H_2 cold gas
9k	0.25	-214.26	2.099	-3,208.21	71.52	Superheated vapor	H_2 cold gas
9l	0.25	-197.79	2.099	-2,975.71	75.00	Superheated vapor	H_2 cold gas
9m	0.25	-111.04	2.099	-1,751.82	85.81	Superheated vapor	H_2 cold gas
9n	0.25	-55.71	2.099	-971.53	89.95	Superheated vapor	H_2 cold gas
9o	0.25	15.07	2.099	29.32	93.93	Superheated vapor	H_2 cold gas
9p	0.8	25	2.099	171.03	89.66	Superheated vapor	H_2 cold gas
9q	2.2	115.23	2.099	1,470.10	89.25	Superheated vapor	H_2 cold gas
10a	20	25.00	2.240	175.62	76.32	Superheated vapor	H_2 cold gas
10b	20	-46.00	2.240	-835.48	72.44	Superheated vapor	H_2 cold gas
10c	20	-103.00	2.240	-1,647.62	68.32	Superheated vapor	H_2 cold gas
10d	20	-198.00	2.240	-3,033.84	56.35	Superheated vapor	H_2 cold gas
10e	20	-213.00	2.240	-3,270.18	52.84	Superheated vapor	H_2 cold gas
10f	20	-233.00	2.240	-3,657.11	43.95	Superheated vapor	H_2 cold gas
10g	6	-245.04	2.240	-3,759.49	44.85	Superheated vapor	H_2 cold gas
10h	6	-235.90	2.240	-3,561.73	51.14	Superheated vapor	H_2 cold gas
10i	6	-214.26	2.240	-3,232.07	58.14	Superheated vapor	H_2 cold gas
10j	6	-197.80	2.240	-2,992.14	61.73	Superheated vapor	H_2 cold gas
10k	6	-111.04	2.240	-1,755.22	72.67	Superheated vapor	H_2 cold gas

Table 4.5 (Cont.) – Simulation data of the modified proposed four H_2 Joule-Brayton cycles.

Stream number	Pressure	Temp.	Flow rate	Specific enthalpy	Specific entropy	Phase	Description
	P	T	$\dot{m}$	h	s		
	(bar)	(^{o}C)	(kg/s)	(kJ/kg)	(kJ/kg-^{o}C)		
10l	6	-55.71	2.240	-972.26	76.82	Superheated vapor	H_2 cold gas
10m	6	15.07	2.240	30.44	80.82	Superheated vapor	H_2 cold gas
10n	11.82	25.00	2.240	173.58	78.30	Superheated vapor	H_2 cold gas
10o	20	74.05	2.240	881.68	78.51	Superheated vapor	H_2 cold gas
11a	40	25.00	1.736	181.06	73.43	Superheated vapor	H_2 cold gas
11b	40	-46.00	1.736	-835.26	69.54	Superheated vapor	H_2 cold gas
11c	40	-103.00	1.736	-1,654.87	65.38	Superheated vapor	H_2 cold gas
11d	40	-198.00	1.736	-3,083.13	53.00	Superheated vapor	H_2 cold gas
11e	40	-213.00	1.736	-3,344.42	49.11	Superheated vapor	H_2 cold gas
11f	6	-236.72	1.736	-3,575.15	50.77	Superheated vapor	H_2 cold gas
11g	6	-214.26	1.736	-3,232.07	58.14	Superheated vapor	H_2 cold gas
11h	6	-197.80	1.736	-2,992.14	61.74	Superheated vapor	H_2 cold gas
11i	6	-111.04	1.736	-1,755.22	72.67	Superheated vapor	H_2 cold gas
11j	6	-55.71	1.736	-972.26	76.82	Superheated vapor	H_2 cold gas
11k	6	15.07	1.736	30.44	80.82	Superheated vapor	H_2 cold gas
11l	16.18	25.00	1.736	174.65	77.19	Superheated vapor	H_2 cold gas
11m	40	123.40	1.736	1,606.16	77.56	Superheated vapor	H_2 cold gas
12a	40	25.00	1.232	181.05	73.43	Superheated vapor	H_2 cold gas
12b	40	-46.00	1.232	-835.26	69.54	Superheated vapor	H_2 cold gas
12c	40	-103.00	1.232	-1,654.87	65.38	Superheated vapor	H_2 cold gas
12d	40	-198.00	1.232	-3,038.13	53.00	Superheated vapor	H_2 cold gas
12e	14	-215.56	1.232	-3,286.24	53.90	Superheated vapor	H_2 cold gas
12f	14	-197.80	1.232	-3,014.47	58.02	Superheated vapor	H_2 cold gas
12g	14	-111.00	1.232	-1,759.04	69.14	Superheated vapor	H_2 cold gas
12h	14	-55.73	1.232	-973.33	73.31	Superheated vapor	H_2 cold gas
12i	14	15.05	1.232	31.79	77.31	Superheated vapor	H_2 cold gas
12j	25.5	25.00	1.232	177.03	75.31	Superheated vapor	H_2 cold gas
12k	40	71.18	1.232	847.99	75.51	Superheated vapor	H_2 cold gas

Table 4.6 – Calculation of exergy loss in each process's component of the proposed 100-TPD H_2 liquefaction plant.

Component	Energy equation	Exergy equation	$\dot{I}$ (kW)	Percent loss %
COM1	$\dot{W}_{BH,COM1} = \dot{m}_{17}(h_{17,disc} - h_{17})$	$\dot{I}_{COM1} = \dot{E}_{x,17} - \dot{E}_{x,17,disc} + \dot{W}_{BH,COM1}$	631.05	7.37
COM2	$\dot{W}_{BH,COM2} = \dot{m}_{17b}(h_{17b,disc} - h_{17b})$	$\dot{I}_{COM2} = \dot{E}_{x,17b} - \dot{E}_{x,17b,disc} + \dot{W}_{BH,COM2}$	504.84	5.90
COM3	$\dot{W}_{BH,COM3} = \dot{m}_{9o}(h_{9o,disc} - h_{9o})$	$\dot{I}_{COM3} = \dot{E}_{x,9o} - \dot{E}_{x,9o,disc} + \dot{W}_{BH,COM3}$	181.85	2.12
COM4	$\dot{W}_{BH,COM4} = \dot{m}_{9o}(h_{9q} - h_{9p})$	$\dot{I}_{COM4} = \dot{E}_{x,9p} - \dot{E}_{x,9q} + \dot{W}_{BH,COM4}$	200.25	2.34
COM5	$\dot{W}_{BH,COM5} = \dot{m}_{10m}(h_{10m,disc} - h_{10m})$	$\dot{I}_{COM5} = \dot{E}_{x,10m} - \dot{E}_{x,10m,disc} + \dot{W}_{BH,COM5}$	357.41	4.17
COM6	$\dot{W}_{BH,COM6} = \dot{m}_{10m}(h_{10o} - h_{10n})$	$\dot{I}_{COM6} = \dot{E}_{x,10n} - \dot{E}_{x,10o} + \dot{W}_{BH,COM6}$	100.20	1.17
COM7	$\dot{W}_{BH,COM7} = \dot{m}_{11k}(h_{11k,disc} - h_{11k})$	$\dot{I}_{COM7} = \dot{E}_{x,11k} - \dot{E}_{x,11k,disc} + \dot{W}_{BH,COM7}$	286.99	3.35
COM8	$\dot{W}_{BH,COM8} = \dot{m}_{11k}(h_{11m} - h_{11l})$	$\dot{I}_{COM8} = \dot{E}_{x,11l} - \dot{E}_{x,11m} + \dot{W}_{BH,COM8}$	300.09	3.50
COM9	$\dot{W}_{BH,COM9} = \dot{m}_{12i}(h_{12i,disc} - h_{12i})$	$\dot{I}_{COM9} = \dot{E}_{x,12i} - \dot{E}_{x,12i,disc} + \dot{W}_{BH,COM9}$	399.26	4.66
COM10	$\dot{W}_{BH,COM10} = \dot{m}_{12i}(h_{12k} - h_{12j})$	$\dot{I}_{COM10} = \dot{E}_{x,12j} - \dot{E}_{x,12k} + \dot{W}_{BH,COM10}$	453.76	5.30
EX1	$\dot{m}_{22}h_{22} = \dot{m}_{23}h_{23} + \dot{W}_{EX1}$	$\dot{I}_{EX1} = \dot{E}_{x,22} - \dot{E}_{x,23} - \dot{W}_{EX1}$	48.25	0.56
EX2	$\dot{m}_{27}h_{27} = \dot{m}_{28}h_{28} + \dot{W}_{EX2}$	$\dot{I}_{EX2} = \dot{E}_{x,27} - \dot{E}_{x,28} - \dot{W}_{EX2}$	30.34	0.35
EX3	$\dot{m}_{31}h_{31} = \dot{m}_{32}h_{32} + \dot{W}_{EX3}$	$\dot{I}_{EX3} = \dot{E}_{x,31} - \dot{E}_{x,32} - \dot{W}_{EX3}$	30.16	4.09
EX4	$\dot{m}_{9b}h_{9b} = \dot{m}_{9c}h_{9c} + \dot{W}_{EX4}$	$\dot{I}_{EX4} = \dot{E}_{x,12d} - \dot{E}_{x,12e} - \dot{W}_{EX4}$	350.21	7.78
EX5	$\dot{m}_{10b}h_{10b} = \dot{m}_{10b}h_{10c} + \dot{W}_{EX5}$	$\dot{I}_{EX5} = \dot{E}_{x,11e} - \dot{E}_{x,11f} - \dot{W}_{EX5}$	666.16	5.46
EX6	$\dot{m}_{11b}h_{11b} = \dot{m}_{11c}h_{11c} + \dot{W}_{EX6}$	$\dot{I}_{EX6} = \dot{E}_{x,10f} - \dot{E}_{x,10g} - \dot{W}_{EX6}$	467.52	10.00
EX7	$\dot{m}_{12b}h_{12b} = \dot{m}_{12c}h_{12c} + \dot{W}_{EX7}$	$\dot{I}_{EX7} = \dot{E}_{x,9g} - \dot{E}_{x,9h} - \dot{W}_{EX7}$	856.36	0.00
EX8	$\dot{m}_{8c}h_{8e} = \dot{m}_{8f}h_{8f} + \dot{W}_{EX8}$	$\dot{I}_{EX8} = \dot{E}_{x,8e} - \dot{E}_{x,8f} - \dot{W}_{EX8}$	≈ 0.01	4.58
EVAP1	$\dot{m}_{17b}h_{17b,disc} + \dot{m}_{air}h_{air,in} = \dot{m}_{17b}h_{18} + \dot{m}_{air}h_{air,out}$	$\dot{I}_{EVAP1} = (\dot{E}_{x,17b} + \dot{E}_{x,air,in}) - (\dot{E}_{x,17b,disc} + \dot{E}_{x,air,out})$	392.62	1.35
EVAP2	$\dot{m}_{9q}h_{9q} + \dot{m}_{air}h_{air,in} = \dot{m}_{9a}h_{9a} + \dot{m}_{air}h_{air,out}$	$\dot{I}_{EVAP2} = (\dot{E}_{x,9q} + \dot{E}_{x,air,in}) - (\dot{E}_{x,9a} + \dot{E}_{x,air,out})$	115.35	3.69
EVAP3	$\dot{m}_{10o}h_{10o} + \dot{m}_{air}h_{air,in} = \dot{m}_{10a}h_{10a} + \dot{m}_{air}h_{air,out}$	$\dot{I}_{EVAP3} = (\dot{E}_{x,10o} + \dot{E}_{x,air,in}) - (\dot{E}_{x,10a} + \dot{E}_{x,air,out})$	316.06	1.98

Table 4.6 (Cont.) – Calculation of exergy loss in each process's component of the proposed 100-TPD H_2 liquefaction plant.

Component	Energy equation	Exergy equation	$\dot{I}$ (kW)	Percent loss %
EVAP4	$\dot{m}_{11\,m} h_{11\,m} + \dot{m}_{air} h_{air,in} = \dot{m}_{11\,a} h_{11\,a} + \dot{m}_{air} h_{air,out}$	$\dot{I}_{EVAP\,4} = (\dot{E}_{x,11m} + \dot{E}_{x,air,in}) - (\dot{E}_{x,11a} + \dot{E}_{x,air,out})$	169.49	4.44
EVAP5	$\dot{m}_{12\,k} h_{12\,k} + \dot{m}_{air} h_{air,in} = \dot{m}_{12\,a} h_{12\,a} + \dot{m}_{air} h_{air,out}$	$\dot{I}_{EVAP\,5} = (\dot{E}_{x,12k} + \dot{E}_{x,air,in}) - (\dot{E}_{x,12a} + \dot{E}_{x,air,out})$	380.44	2.20
HX1	$\sum_{i=1}^{n} \dot{m}_{in} h_{in} = \sum_{i=1}^{n} \dot{m}_{out} h_{out}$	$\dot{I}_{HX1} = \sum_{i=1}^{n} \dot{E}_{in} - \sum_{i=1}^{n} \dot{E}_{out}$	188.82	0.68
HX2	$\sum_{i=1}^{n} \dot{m}_{in} h_{in} = \sum_{i=1}^{n} \dot{m}_{out} h_{out}$	$\dot{I}_{HX2} = \sum_{i=1}^{n} \dot{E}_{in} - \sum_{i=1}^{n} \dot{E}_{out}$	57.83	1.26
HX3	$\sum_{i=1}^{n} \dot{m}_{in} h_{in} = \sum_{i=1}^{n} \dot{m}_{out} h_{out}$	$\dot{I}_{HX3} = \sum_{i=1}^{n} \dot{E}_{in} - \sum_{i=1}^{n} \dot{E}_{out}$	108.01	0.16
HX4	$\sum_{i=1}^{n} \dot{m}_{in} h_{in} = \sum_{i=1}^{n} \dot{m}_{out} h_{out}$	$\dot{I}_{HX4} = \sum_{i=1}^{n} \dot{E}_{in} - \sum_{i=1}^{n} \dot{E}_{out}$	13.46	1.77
HX5	$\sum_{i=1}^{n} \dot{m}_{in} h_{in} = \sum_{i=1}^{n} \dot{m}_{out} h_{out}$	$\dot{I}_{HX5} = \sum_{i=1}^{n} \dot{E}_{in} - \sum_{i=1}^{n} \dot{E}_{out}$	151.75	6.67
HX6	$\sum_{i=1}^{n} \dot{m}_{in} h_{in} = \sum_{i=1}^{n} \dot{m}_{out} h_{out}$	$\dot{I}_{HX6} = \sum_{i=1}^{n} \dot{E}_{in} - \sum_{i=1}^{n} \dot{E}_{out}$	571.22	2.17
HX7	$\sum_{i=1}^{n} \dot{m}_{in} h_{in} = \sum_{i=1}^{n} \dot{m}_{out} h_{out}$	$\dot{I}_{HX7} = \sum_{i=1}^{n} \dot{E}_{in} - \sum_{i=1}^{n} \dot{E}_{out}$	185.72	0.12
LIQ1	$\dot{m}_{19} h_{19} = \dot{m}_{20} h_{20} + \dot{m}_{21} h_{21}$	$\dot{I}_{LIQ1} = \dot{E}_{x,19} - (\dot{E}_{x,20} + \dot{E}_{x,21})$	10.35	0.00
LIQ2	$\dot{m}_{24} h_{24} = \dot{m}_{25} h_{25} + \dot{m}_{26} h_{26}$	$\dot{I}_{LIQ2} = \dot{E}_{x,24} - (\dot{E}_{x,25} + \dot{E}_{x,26})$	12.14	0.00
LIQ3	$\dot{m}_{32} h_{32} = \dot{m}_{33} h_{33}$	$\dot{I}_{LIQ3} = \dot{E}_{x,32} - \dot{E}_{x,33} = 0$	0.00	0.00
MIXER1	$\dot{m}_{23} h_{23} + \dot{m}_{36} h_{36} = \dot{m}_{37} h_{37}$	$\dot{I}_{MIXER\,1} = \dot{E}_{x,23} + \dot{E}_{x,36} - \dot{E}_{x,37}$	0.33	0.00
MIXER2	$\dot{m}_{28} h_{28} + \dot{m}_{34} h_{34} = \dot{m}_{35} h_{35}$	$\dot{I}_{MIXER2} = \dot{E}_{x,28} + \dot{E}_{x,34} - \dot{E}_{x,35}$	25.39	0.30
Total		$\dot{I}_{total}$	**8,563.00**	**100.00**

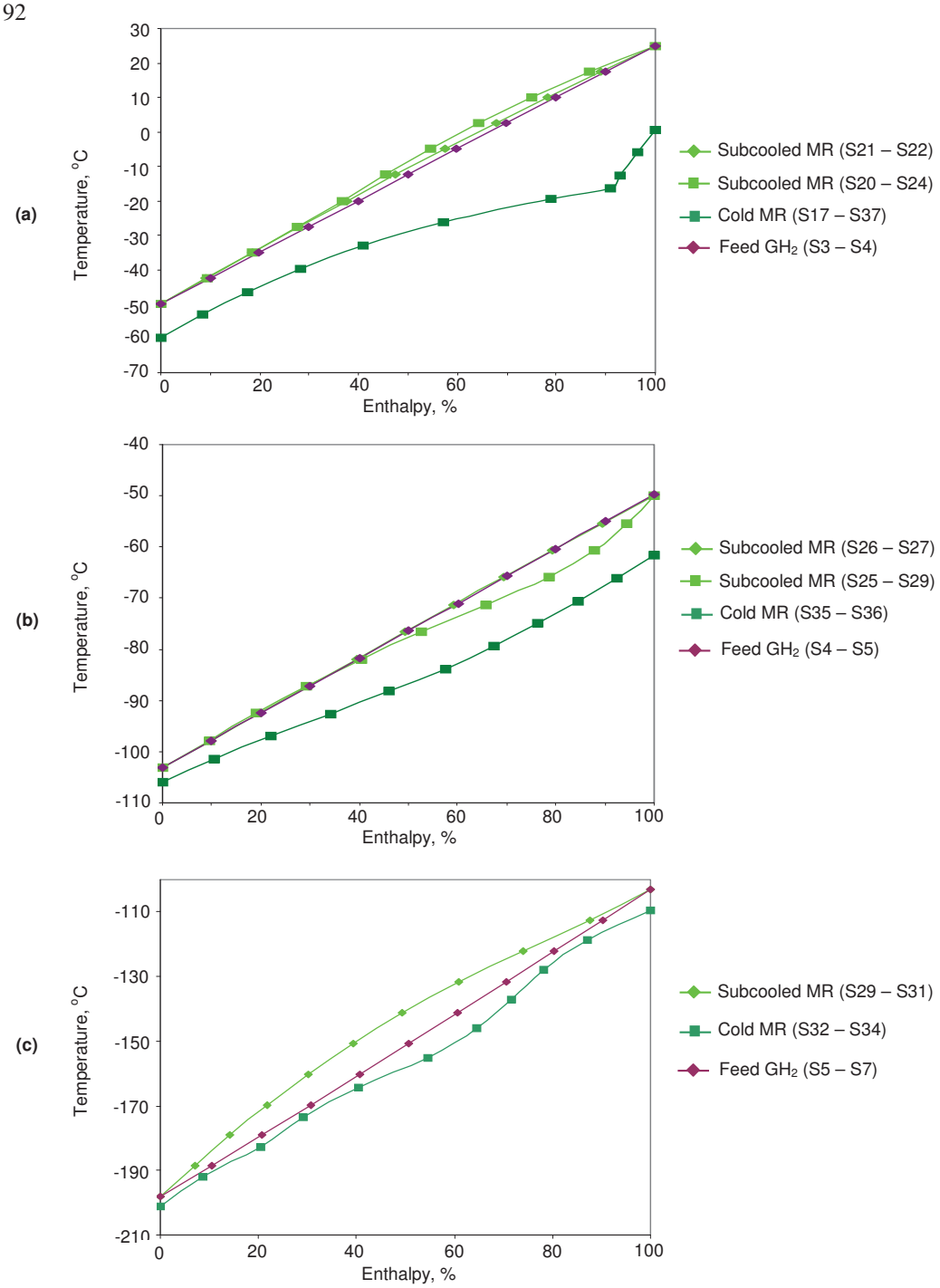

Fig. 4.3 – Adapted *h-T* curves for the new proposed 5-component composition: *4% hydrogen, 18% nitrogen, 24% methane, 28% ethane, and 26% butane* by mole in the proposed large-scale plant at: (a) HX1, (b) HX2, and (c) HX3.

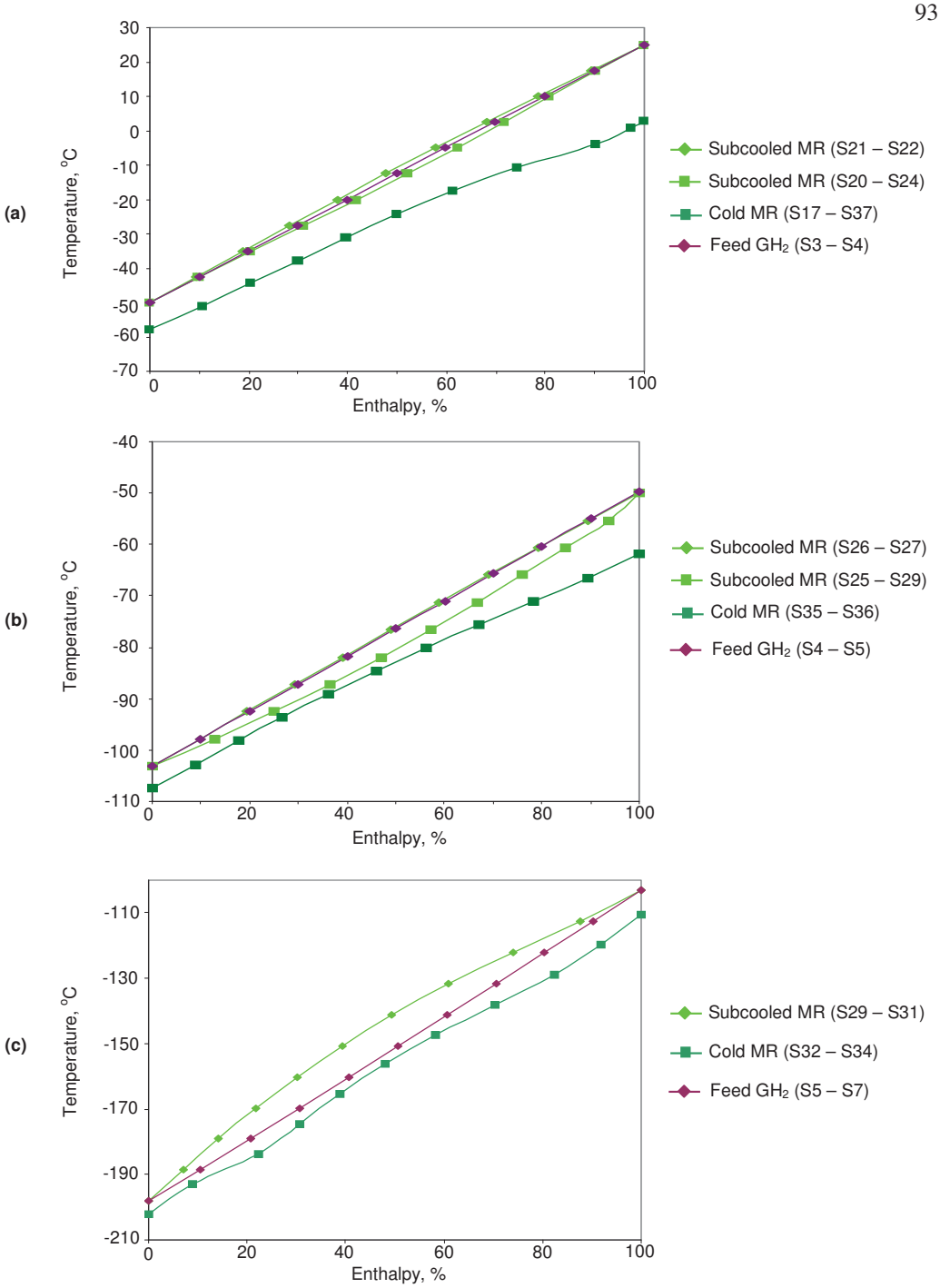

Fig. 4.4 – Adapted *h-T* curves for the 10-component composition: *1.2% hydrogen, 25.6% nitrogen, 13.6% methane, 15.2% R14, 10% ethane, 10% propene, 5.8% propane, 1.0% Ibutane, 1.0% butane, and 10.8% pentane* that maybe used in the proposed large-scale plant at: (a) HX1, (b) HX2, and (c) HX3.

4.5. Control structure design

Section aforediscribed is the discussion about the optimum for the process that can be identified, but how should this optimum be implemented in practice? First the *active constraints* such as pressures and temperatures at locations depicted in Fig. 4.5 need to be controlled:

- Low side pressures of MR cycle and each cycle of the H_2 J-B system must be controlled to be exact according to simulated values such as at positions: S17, S9o, S10n, S11l, and S12j. The low side pressure must be low enough in order to produce low temperature after expansion at the expansion valve/expander. To do this, the active charge can be used.
- High side pressures of MR cycle and each cycle of the H_2 J-B system don't need to be controlled to be exact, but just approximately around simulated values such as at positions: S18, S9a, S10a, S11a, and S12a. But the care should be handled that the higher discharge pressure, the higher compressor energy consumption.
- Optimum intermediate pressure of each two-stage compression both MR and hydrogen compression such as at positions: S17a, S9p, S10n, S11l, and S12j.
- The feed GH_2 outlet temperature at S7 is attained at −198 ^oC: This is controlled by the right MR composition, enough active charge, right low and high side pressures, and enough MR flowrate in MR cycle to cool the GH_2.
- The cooling stream after expansion of each H_2 J-B cycle, e.g., at positions: S9h, S10g, S11f, and S12e must be controlled approximately at the simulated temperature values as in Table 4.5. This is by controlling low side pressure and increasing flowrate of hydrogen by higher speed compressor in each cycle if required.

Then, based on physical insight, the following *variables* may be suggested:

- Compressor speeds to increase MR and hydrogen flowrate of each MR and H_2 J-B cycle. Therefore, compressor power should be 10–20% over designed and the speed can be adjusted especially those belong to the H_2 J-B cycles. This is to make sure that there is enough hydrogen in each cycle to cool the feed hydrogen gas from −198 ^oC to −253 ^oC.

Assume maximum cooling in coolers after compression in every compressor. The ejector is to control pressure inside LH_2 tank: If the pressure is higher than a set value, the hydrogen gas from LH_2 tank will be pumped to mix with the hydrogen feed stream and cooled by HX7. The sequence of switching on the plant is by: first turning on the cooler pumps, then MR compressors, after that hydrogen compressors. Finally, if such simplified 5-component composition would be favourable for the MR-plant, there must be a discussion about the needed skills to keep the composition behaving well in practice. Chapter 3 explains about charging of the simplified 5-component MR-composition and doing the commissioning of the test rig. To keep the 5-component composition behaving well in practice for the MR-plant, the procedure should be the same as doing with the rig. The plant manager or maintenance engineer must have a quarterly or annually check-up. It depends on how much the leak. This can be done by reading the gas chromatography instrument measured at the suction of MR compressor if the composition is right. If not, manually charging will be performed with the missing component. However, the new proposed 5-component composition is nearly the same as the complex 10-component composition. Thus, it seems it is more suitable for the large-scale plant due to its simplicity.

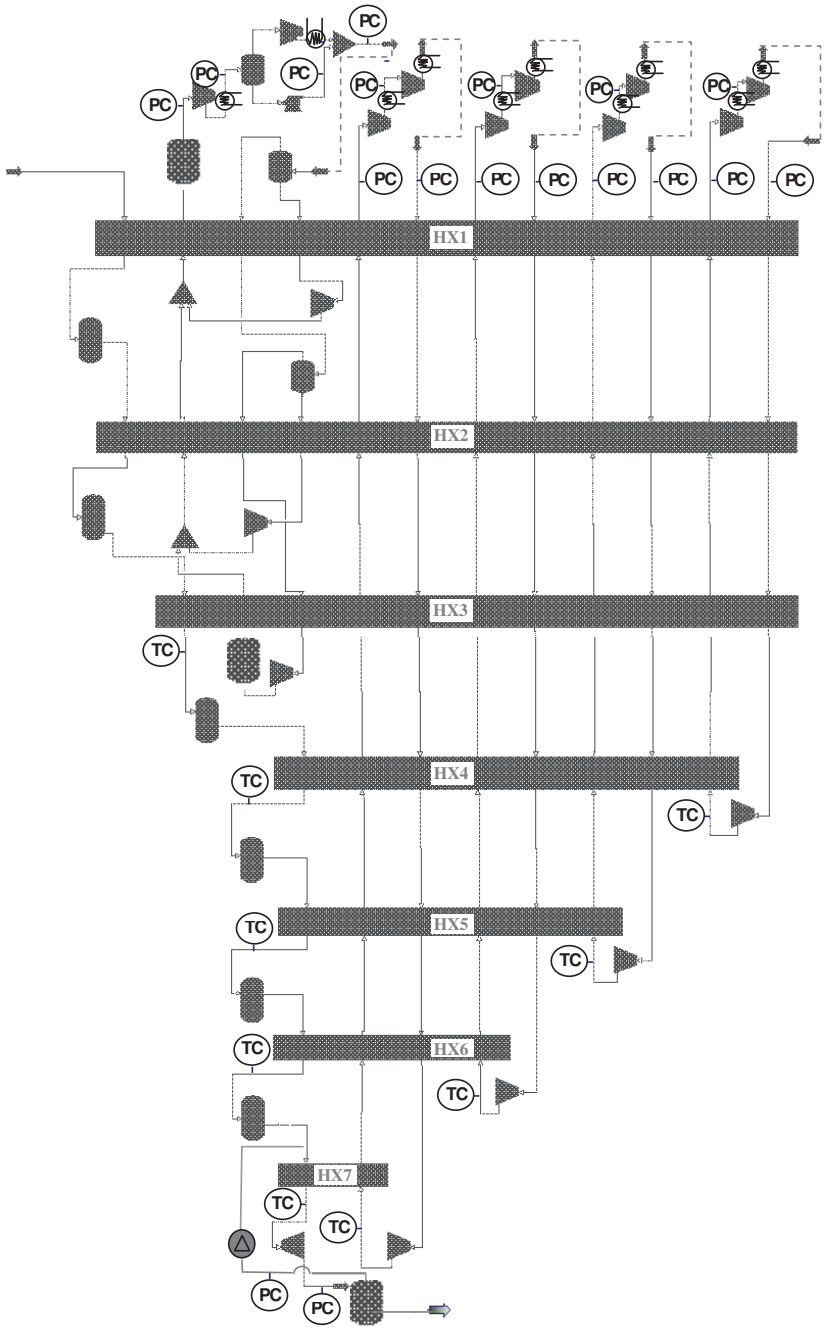

Fig. 4.5 – Suggested control structure for the LH_2 process. PC and TC are pressure and temperature controllers respectively. Pressure controller is on the low pressure side using the active charge in each cycle.

4.6. Pinch temperatures and pressure drops that affect plant power consumption

The effect of pinch temperatures (PT, temperature differences at the cold ends of heat exchangers) on the H_2 liquefaction plant power consumption were investigated. Mostly by trial-and-error and some with the optimizer in PRO/II was run with two pinch temperatures: approximately 1 and 3 ^oC. Usually, most of current spiral wound heat exchangers found in world wide large-scale MR cycles used to liquefy natural gas have pinch temperature with a range as small as 1–3 ^oC (Hasan, 2009); at 3 ^oC is the most realistic. It is recommended that the design of H_2 liquefaction plant's heat exchangers would probably be the same. In contrast, low pinch temperature such as 0.01 ^oC represents extremely large heat exchangers that do not exist, thus it is not considered here. Alabdulkarem (2011) also found that there was little improvement with 0.01 ^oC compared to the others'. While high pinch temperature, such as 5 ^oC or more, is not popular in cryogenic processes because of extremely high plant operating or energy consumption cost.

Table 4.7 contains the simulation data with varied pinch temperatures for economic evaluation of different H_2 liquefaction plants selection. Based case is particulary the PT specified in Section 4.3.4 yielding in what simulated and detailed shown in Tables 4.3, 4.4, and 4.5. It is that PT for HX1, HX2, and HX3 is: $5\,^oC \le \Delta T_{min} \le 10\,^oC$, but for HX4, HX5, and HX6 is: $\Delta T_{min} = 3\,^oC$. This results in the plant power consumption at 5.91 kWh/kg_{LH2}. New modifications are made to study the PT effect that while pinch temperature around 3 and 1 ^oC, the same in every heat exchanger; thus, the plant power consumption is reduced to be 5.2 and 5.0 kWh/kg_{LH2} respectively. In addition, for the near actual case prediction that pressure drop in all streams both MR and hydrogen flow passing each heat exchanger are assumed to be 0.1 bar. By guessing, it is approximately close to 1 bar for pressure drop (e.g. between lines S17–S19 in MR cycle together with S9a–S9o, S10a–S10m, S11a–S11k, and S12a–S12i in H_2 J-B cycles) which is considered extremely high entirely in each MR cycle and H_2 J-B cycle. This is assumed to be a huge size plant. Then, the plant power consumption will be 5.24, 5.56, and 6.29 kWh/kg_{LH2} as shown in Table 4.7. The conclusion here can be made that the pressure drops in all heat exchangers don't have much significant impact on the overall plant total power consumption. In fact, the design, optimizing, and sizing of all heat exchangers must be performed by the expert to find the right pressure drop information, but that will be too complicated task for further work. Thus, preliminary prediction here would be compromised.

Table 4.7 – Optimized total plant compressors power and overall plant total power consumption at different heat exchanger pinch temperatures.

Cycle	Variables are flow rates at the streams of the proposed plant in Fig. 1, $\dot{m}$ (kg/s)					Objective function	Overall plant total power consumption (kWh/kg_{LH2})	
	S19	S9a	S10a	S11a	S12a	Total compressors' power consumption without pressure drop in HXs (kW)	Without pressure drop in all HXs	With assumed pressure drop in all HXs
Based case	36.1	2.0	2.2	1.7	1.2	25,190	5.91	6.29
Optimized, PT ≈ 3 ^oC	25.2	1.9	2.1	1.7	1.2	21,863	5.20	5.56
Optimized, PT ≈ 1 ^oC	24.3	1.7	2.0	1.7	1.2	20,989	5.00	5.24

4.7. Comparison of the proposed system to Ingolstadt liquefier

In Table 4.8, the types of hydrogen liquefiers are the following: 1. Ingolstadt system, 2. the proposed system (MR system + four H_2 Joule-Brayton cycle system). The Ingolstadt system is from a paper by Kuz'menko *et al* (2004), *Comparison of thermodynamic efficiencies with Ingolstadt liquefier*. The proposed plant is from a simulation that is shown in Fig. 4.2. The system's net power consumptions to cool n-GH_2 from 25 ^{o}C to e-GH_2 at −193 ^{o}C and then e-GH_2 at −193 ^{o}C to e-GH_2 at −253 ^{o}C are w_A = 1.38 and w_B = 4.24 kWh/kg_{LH2}, respectively. Therefore, the overall power is $w_A + w_B$ = 5.91 kWh/kg_{LH2}. Finally, the efficiency of the proposed plant is 50%, in comparison to the ideal liquefaction power of 2.89 kWh/kg_{LH2}; this efficiency is a lot better than Ingolstadt's, which is used as a reference (21.28%). Moreover, it is better than WE-NET's hydrogen liquefaction project (Mitsugi *et al*, 1998) by Matsuda and Nagami (1998). However, Quack's (2002), and Valenti and Macchi's (2008) systems do not explicitly mention whether they have high efficiencies. If not, the proposed system is the most efficient. Therefore, the proposed system has a great potential for improvement and can be used as a reference for future hydrogen liquefaction plants.

Table 4.8 – Comparison of the proposed system's to Ingolstadt liquefier's thermodynamic efficiency.

Parameter		System	
		[a]Ingolstadt	[b]The new proposed cycle
Capacity referred to liquid hydrogen	TPD	4.4	100
	kg/h	180	4,166
	kg/s	0.05	1.1572
Para form content in the product, %		95	95
Pressure of liquid hydrogen, bar		1.3	1.3
Flow rates of streams in the cycle, kg/h:			
MR		-	190,152
hydrogen		1,440	7,556/8,064/6,249/4,435
helium		-	-
nitrogen (liquid nitrogen requirement, kg/h)		1,750	-
Compression pressure in the cycle, bar:			
MR		-	18/2
hydrogen		22	40/14/6/20/2.2/0.3
helium		-	-
nitrogen		1.4	-
Power consumption, kW:			
of MR compressor		-	5,896
of all hydrogen compressors		1,557	19,294
of all helium compressors		-	-
of all nitrogen compressors		-	-
of other equipments[f]		-	[f]1,100
All expander power, kW:		N/A	[c]1,245
Total energy consumption with due regard for the consumption for liquid nitrogen from an air separation plant at the rate of 0.5 kWh/kg of liquid nitrogen, kWh		2,432	-
Net $\dot{W}_A$, kW		875	5,896
Net $\dot{W}_B$, kW		1,557	19,294
Net w_A, kWh/kg$_{LH2}$		**4.86**	**1.38**
Net w_B, kWh/kg$_{LH2}$		**8.65**	**4.24**
Overall cycle specific energy consumption for liquefaction, kWh/kg$_{LH2}$		**≈ [d]13.58**	**5.91**
The thermodynamically ideal liquefaction system, kWh/kg$_{LH2}$		[e]2.89	[e]2.89
Thermodynamic efficiency with due regard for ortho-para conversion, %		**21.28**	**≈ 50.00**

a Information is from Kuz'menko *et al* (2004).
b Info from Fig. 4.2, *PRO/II simulation flow-sheet of the proposed large-scale 100-TPD LH_2 plant with MR and four H_2 Joule-Brayton cycles*.
c The sum of all expander powers, kW: mechanical conversion is 98% from the expanders.
d This is modified from Kuz'menko *et al* (2004): 4.86 + 8.65 = 13.51 kWh/kg$_{LH2}$.
e Minimum theoretical exergy consumption from feed 21 bar, 25 °C, n-GH_2 to: 1.3 bar, –253 °C, 95% p-LH_2.
f Electricity consumptions for the cooling loads due to water pumps and air-cooled fans in the after coolers and evaporative condensers. They are assumed to be around 5% of power consumption from compressors.

4.8. Economic analysis of the proposed plant with MR refrigeration

The cost of liquid hydrogen production consists of the following:

Drnevich *et al* (2003) states that:
LH_2 manufacturing cost ($/kg) = Capital cost + Energy cost + Operation and maintenance.

Kramer *et al* (2006) also states that:
Hydrogen cost ($/kg) = LH_2 manufacturing cost + Distribution cost + Retail site operations.

The energy cost is measured by the overall liquefier efficiency. The low efficiency liquefier consumes a lot of electrical power. In addition, when constructing a LH_2 plant, the capital cost should also be considered. It must be determined how the MR pre-cooling process is superior to the other pre-cooling cycles of Ingolstadt, Leuna, Quack, and Valenti. Similarly, it must be determined how cooling hydrogen gas with multi-component refrigerant is different from the others, e.g., nitrogen and hydrogen (Ingolstadt, Leuna, Praxair, and WE-NET), propane (Quack), and helium (Valenti). The overall size of the compressor and the heat exchanger is a measure. It reflects the capital or construction cost of the entire plant.

Table 4.9 – Comparison of the proposed large-scale plant to the MR refrigeration system's overall compressor swept volume, together with the overall heat exchanger's size in comparison to the Ingolstadt/Leuna liquefier (nitrogen refrigeration) and the Valenti liquefier (helium refrigeration).

Parameter	Unit	Refrigerant				
		[a]MR_{HX1}	G-Hydrogen	[b]G-Nitrogen	L-Nitrogen	[c]G-Helium
$\dot{m}_i / \dot{m}_{H2}$	-	25.70	1	$\frac{1{,}750 kg/h}{180 kg/h} = 9.70$	9.70	$\frac{27.35 kg/s}{10.00 kg/s} = 2.75$
$\dot{V}_i / \dot{V}_{H2}$	-	129	1	$\frac{1{,}400 m^3/hr}{100 m^3/hr} = 14.31$	14.31	$\frac{161.83 m^3/s}{5.43 m^3/s} = 29.80$
α_i / α_{H2}	-	Gas MR: 0.522 Liquid MR: 1.26 Boiling MR: 1.89	Gas: 1	Gas: 0.2892	0.2490 Boiling: ≈0.28-0.4	Gas: 0.9723
$A_{HX,i} / A_{HX,MR}$	-	The smallest	Bigger than MR	The largest	Bigger than G-Helium	Bigger than G-Hydrogen
Thermo-physical properties below are at 1 bar and 0 °C. Data are from SRK simulation model in PRO/II.						
c_P	kJ/kg-K	[d]1.02/2.01	14.34	1.04	[e]2.04	5.19
k	kW/m-K	[d]0.02/0.13	0.16	0.02	[e]0.02	0.142
Latent heat of vaporization	kJ/kg	N/A	446	-	[e]199	20
ρ	kg/m^3	[d]4.5/655	0.085	1.25	[e]808	0.169
μ	Pa.s	[d]0.00001/0.00033	0.00001	0.00002	[e]0.00018	0.00002
Pr	-	[d]0.51/5.10	0.89625	1.04	18.36	0.73098
Gas price	-	Most expensive	Expensive	The cheapest		Very expensive

a The proposed large-scale plant with MR refrigeration system; in particular, the analysis is at the top MR heat exchanger. b Ingolstadt liquefier. c Valenti liquefier. $\dot{m}_{H2}$ is the mass flow rate of the feed hydrogen gas into the liquefier at 21 bar and 25 °C. d Properties of the MR at stream 37 between gas/liquid at 2 bar and –50 °C. e Properties of liquid nitrogen at 1 bar and –200 °C. $\dot{V}_{H2}$ is the volumetric flow rate (m^3/s) of the feed hydrogen gas into the liquefier at 21 bar and 25 °C. α_i / α_{H2} is the ratio between the refrigerant heat transfer coefficient (kW/m^2-°C) and the hydrogen gas coefficient (kW/m^2-°C). A_i / A_{MR} is the ratio between the refrigerant heat transfer area (m^2) and the MR heat transfer area (m^2).

4.8.1. Comparison of compressor's size to other refrigeration systems

This section compares the compressor's swept volumes. From Table 4.9, the ratio between the suction volumetric flow rate of the MR and the hydrogen, $\dot{V}_{MR}/\dot{V}_{H2}$ is less than with nitrogen, $\dot{V}_{N2}/\dot{V}_{H2}$. Ingolstadt uses both gas and liquid nitrogen to cool the hydrogen feed stream. Even though hydrogen has the smallest suction volumetric flow rate when it is used in refrigeration systems to cool hydrogen gas, it is impossible to use because of its high power consumption. Therefore, the overall MR compressor's size for the proposed large-scale MR system is smaller than closed liquid nitrogen system with recondensation such as WE-NET's nitrogen refrigeration system.

4.8.2. Comparison of the heat exchanger's size to other refrigeration systems

The right way to size the heat exchanger is by (1) using the LMTD or NTU to find the approximate size, or by (2) dividing the whole heat exchanger into many small finite volumes/pieces together with the computational balance equations (mass, momentum, and energy) to find the actual size. The plate fin heat exchangers are widely used in cryogenic applications due to their compactness, low weight, and high effectiveness, and their use is proposed here. Spiral heat exchangers are generally widely used in large-scale cryogenic plants, but it's not mentioned here. Aluminium is the most commonly used material, but stainless steel construction is employed for high pressure and high temperature applications. Fin geometries can be plain, offset strip, perforated, wavy, pin, or louvered. Among these, the offset strip fin is frequently adopted for its high heat transfer coefficient. It is the most widely used finned surface, particularly in high effectiveness heat exchangers that are employed in cryogenic applications.

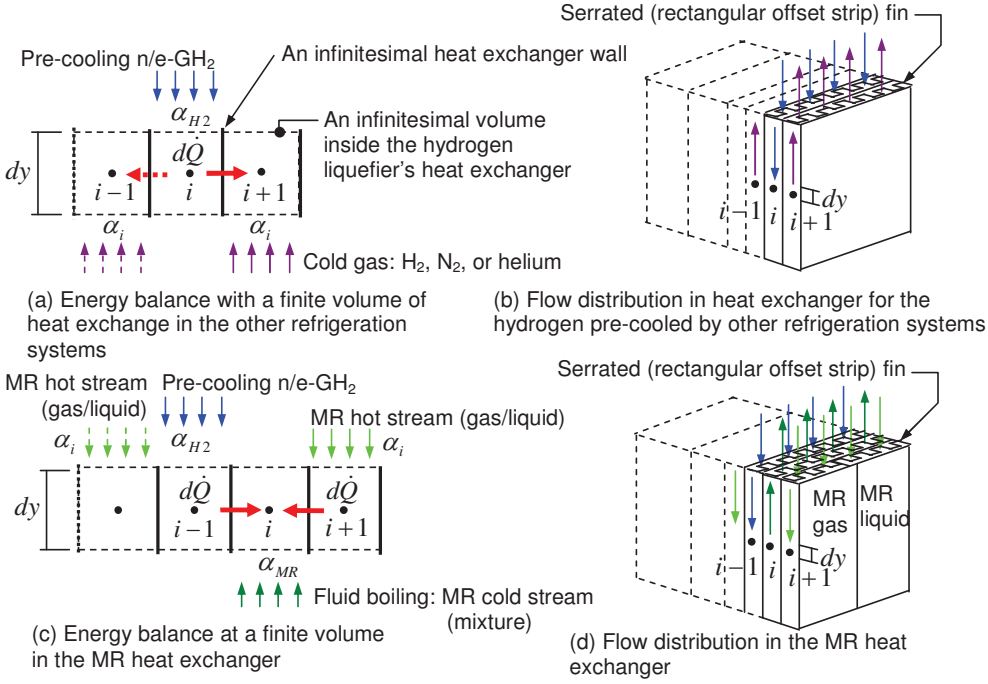

Fig. 4.6 – Proposed plate fin heat exchanger for the proposed hydrogen liquefaction system.

Fig. 4.6 (a) explains that a small heat transfer $d\dot{Q}$ from the hot stream hydrogen gas (node i to $i+1$ and $i-1$) can be cooled with a cold gas that is generally in the liquefaction process, e.g., hydrogen, nitrogen, or helium. It is a small finite volume inside of the heat exchanger, as depicted in Fig. 4.6 (b). The heat exchanger has a stack arrangement. The gases are compared with the MR to determine which one can best reduce the heat exchanger's size. In Fig. 4.6 (c), the heat transfer is from both the hot stream hydrogen and the MR hot stream to the MR cold composition stream (node to $i+1$ and $i-1$ to i). Fig. 4.6 (d) depicts the possible arrangement of the streams in the MR heat exchangers (HX1, HX2, and HX3) for the proposed large-scale system, as in Fig. 4.2. The heat transfer and flow friction characteristics of the plate fin surfaces are presented in terms of the Colburn factor, j, and the Fanning friction factor, f, versus the Reynolds number, Re; the relationships are different for the different surfaces. Usually, turbulent flow (approximately 3,000 to 10,000) is mandatory for most heat exchangers to attain a better heat transfer coefficient and for a compact size. However, with more turbulence, the pressure drop increases. Thus, an optimization should be done to compute the velocity, pressure, and temperature fields to determine the over appropriate range of the Reynolds number and the geometric dimensions. In order to compare the size of the heat exchanger for different fluids, we will first start with the heat transfer coefficient for any flow in a channel:

$$\alpha = \frac{jGc_P}{\mathrm{Pr}^{2/3}} \tag{4.1}$$

Manglik and Bergles (1995) proposed the Colburn factor, j, in Eq. 4.1 to describe the right trend of the heat transfer behavior for a single-phase flow and a channel with offset strip fins in the laminar, transition, and turbulent flow regimes:

$$\begin{aligned} j = {} & 0.6522\mathrm{Re}_{Dh}^{-0.5403}\beta^{-0.1541}\delta^{0.1499}\gamma^{0.0678} \\ & \times\left[1+5.269\times10^{-5}\,\mathrm{Re}_{Dh}^{1.34}\beta^{0.504}\delta^{0.456}\gamma^{-1.055}\right]^{0.1} \end{aligned} \tag{4.2}$$

where $Re_{Dh} = \frac{GD_h}{\mu}$. β, δ, and γ are geometrical descriptions of the typical offset strip fin core inside of the heat exchanger's channel. Then, the ratio of the heat transfer coefficient (α_i) for a flowing gas (hydrogen, nitrogen, or helium) to that of hydrogen's (α_{H2}) is used as a comparison. It is assumed that all of the channel sizes and fin dimensions of the pre-cooled hydrogen and cooling medium are the same. By eliminating the offset strip fin's geometrical descriptions that are all assumed to be the same, Eq. 4.1 can be expressed as follows:

$$\frac{\alpha_i}{\alpha_{H2}} = \left(\frac{\mu_{H2}}{\mu_i}\cdot\frac{\dot{m}_i}{\dot{m}_{H2}}\right)^{-0.5403}\left(\frac{\dot{m}_i}{\dot{m}_{H2}}\right)\left(\frac{c_{Pi}}{c_{PH2}}\right)\left(\frac{\mathrm{Pr}_{H2}}{\mathrm{Pr}_i}\right)^{2/3} \tag{4.3}$$

where $\dot{m}_i/\dot{m}_{H2}$, μ, c_P, and Pr are from Table 4.9. For simplicity, it is assumed that the fluid's thermo-physical properties at different temperatures (from −250 °C to 0 °C) are quite the same at 0 °C. Thus, the comparison of the heat transfer coefficients for flowing hydrogen, nitrogen, or helium gas to that of hydrogen's in the heat exchanger is calculated and shown in Table 4.9. It seems that hydrogen gas has the highest heat transfer coefficient in comparison to hydrogen gas

itself. Then, it is followed by helium gas, liquid nitrogen, and nitrogen gas ($\alpha_{H2} > \alpha_{Helium} > \alpha_{LN2} > \alpha_{GN2}$).

Next, the analysis compares the heat exchanger's size or area, A_{HX}. Actually, the LMTD is used if all of the outlet and inlet stream temperatures are known as below:

$$\dot{Q}_{HX} = FU_{HX} A_{HX} (LMTD_{HX}) \tag{4.4}$$

where $\dot{Q}_{HX}$ is the overall heat transfer for the whole heat exchanger (kW). F is the correction factor. When the fin efficiency and the wall resistance are neglected for simplicity, U_{HX} can be expressed in dominant terms, e.g., α_{H2} and α_i, as follows:

$$\frac{1}{U_{HX}} = \frac{1}{\alpha_{H2}} + \frac{1}{\alpha_i} \tag{4.5}$$

α_i is a cold fluid (hydrogen gas, helium gas, liquid nitrogen, or nitrogen gas) that cools hydrogen gas in a heat exchanger. Finally, Eq. 4.5 in combination with Eq. 4.4 gives a comparison of the heat transfer area of the gas (hydrogen gas, helium gas, liquid nitrogen, or nitrogen gas) as a cooling media to that of the MR, which is expressed in an inverse relation between its heat transfer coefficient as follows:

$$\frac{A_{HX,i}}{A_{HX,MR}} \propto \frac{\alpha_{MR}}{\alpha_i}$$

The MR fluid in the MR refrigeration system and the liquid nitrogen at Ingolstadt and Leuna, which flows inside of the heat exchanger, are two-phase flows. The others are single phase flows. Boiling inside of the heat exchanger is dominated by two phenomena: convective boiling and nucleated boiling. Thus, the local boiling heat transfer coefficient, as in this case, can be formulated by using superposition (which includes both nucleated and convective boiling effects) and is commonly represented as follows (Kim and Sohn, 2006):

$$\alpha_{TP} = \alpha_{nb} + \alpha_{cb} \tag{4.7}$$

where α_{TP} is the local two phase flow heat transfer coefficient (kW/m^2-^{o}C). α_{nb} is the nucleated heat transfer coefficient (kW/m^2-^{o}C) and α_{cb} is the heat transfer coefficient (kW/m^2-^{o}C). It seems to have been accepted that at high heat fluxes or low qualities, nucleated boiling has a larger influence than convective boiling. For the considered condition, the effect of nucleated boiling is small and the dominant heat transfer mechanism is two-phase forced convection. If noticed from Eq. 4.1 for the same flow rate of any fluid, in most cases, a single-phase flow of liquid has a higher heat transfer coefficient than that of the gas due to the higher c_P. A study from Feldman *et al* (2000) seems to imply that boiling heat transfer inside of the plate fin heat exchanger usually has a boiling coefficient around 1.5–2 times greater than the liquid flow.

At last, the values of $A_{HX,i} / A_{HX,MR}$ are calculated in Table 4.9. In the table, the most important thing is boiling heat transfer coefficient of MR refrigerant in the MR cycle is the highest when compared to feed hydrogen gas's as a reference (Eq. 4.3: $\alpha_{MR} / \alpha_{H2} = 1.89$ of Boiling MR). For that reason, it can be concluded that if the feed hydrogen gas is cooled by hydrogen gas, helium gas, liquid nitrogen, or nitrogen gas; the size of the heat transfer area or heat exchanger is the smallest when using hydrogen gas because it has the highest heat transfer coefficient. It is then followed by helium gas and liquid nitrogen. Eq. 4.6 proves this statement. *In summary, it seems that MR has the highest heat transfer coefficient due to boiling; thus, the trend is that it may offer the smallest heat exchanger size in comparison to using other fluids to cool the hydrogen liquefaction system.*

4.9. Future work about efficient hydrogen liquefaction process

The work of this dissertation is a preliminary study about efficient liquefaction process of hydrogen concerning initial literature, initial experimental rig, and an initial proposed efficient large-scale plant. There is a large amount of work must be done in the future in the way similar to efficient liquefaction processes of LNG, e.g.:

As referenced the most in this chapter about optimization of refrigeration cycle is from Jansen (2006). Other interesting works are also at NTNU regarding LNG such as Fredheim *et al* (1994), Neeraas (1994), and Aunan (2000) did measurements on the shell and tube side of a coil-wound heat exchanger. Owren (1998), Melaaen (1993), Jorstad (1993) and Grini (1994) worked with thermodynamic properties and equations of states. Melaaen (1994) produced a thesis on the dynamic modelling of the liquefaction in a LNG plant. NTNU together with SINTEF Energy Research, have worked in close cooperation with Statoil R&D on LNG research since 1985. This cooperation has produced three applications for LNG simulation: CryoPro, SCoil, and DCoil. Fredheim *et al* (2000) invents thermal design tools for LNG heat exchangers and static simulation tools. CryoPro simulates an entire liquefaction process. SCoil simulates the spiral wound heat exchanger. The DCoil application by Vist *et al* (2003) and Hammer *et al* (2003) dynamically describe the spiral-wound heat exchanger. All these applications use heat transfer and pressure drop correlations based on the measurements made at the Department of Energy and Process Engineering, NTNU. The academic work on dynamic LNG simulation is limited; the only work found and studied are by Zaim (2002) and Melaaen (1993).

In summary, the future works about efficient hydrogen liquefactions maybe are:

1. According to the last experiment as in Fig. 3.10, the rig was able to cool hydrogen gas to only around −180 ^{o}C, not −198 ^{o}C as required. More additional grams of nitrogen, neon or hydrogen is required to achieve the temperature. The future work maybe that more experiment would be done with the new proposed 5-component composition of MR cycle to verify the lowest attainable temperature to −198 ^{o}C if possible.

   However, from preliminary simulation test run of the large-scale plant if the MR cycle can cool hydrogen gas to only −180 ^{o}C, the whole plant energy consumption will be 6.19

kWh/kg_{LH2}, just a little increase from the based case that is 5.91 kWh/kg_{LH2} as in Table 4.7. In the case, the MR cycle that cools equilibrium hydrogen gas from 25 °C to −180 °C consumes (at 1.11 kWh/kg_{LH2} from 1.38 kWh/kg_{LH2}) a little less energy; and the four H_2 J-B cycles that cools equilibrium hydrogen gas from −180 °C to −250 °C consumes (at 4.82 kWh/kg_{LH2} from 4.24 kWh/kg_{LH2}) a little more energy.

2. It seems maybe there is some deviation of SRK model used to predict hydrogen gas and others between temperature range −200 °C to −250 °C. Hence, maybe, there is a need for a research to invent a new accurate equation of state or some correction to replace SRK for simulation in PRO/II of fluid properties in the temperature range below −200 °C.
3. The proposed MR cycle for the large-scale is quite mature, but the four H_2 J-B cycles maybe not. So there will be a need to find a new better efficient cycle.
4. Optimization of the proposed large-scale plant explained is simplified and it is just a preliminary one. A lot more information is still required for more complicated work. It is a must that there is a study about computer simulation work deep inside about optimization of the new more efficient cycle.
5. The theory about heat transfer and pressure drop to design MR heat exchangers (Plate-fin or Coil-wound) needs to be studied. The work is to find: the exact sizes of MR evaporators, which type is appropriate, pressure drop information used in large-scale system's optimization, and others.
6. The study about dynamic modeling and control of large-scale process plant to understand both transient and steady state operations may also be needed.

Finally, besides the proposed MR and four H_2 J-B cycles that can be used to efficiently liquefy hydrogen, MR cycle alone with varied refrigerant compositions would also be utilized to efficiently liquefy other common industrial gases whose boiling point temperatures at ambient pressure are above −193 °C, such as oxygen (−182.95 °C), argon (−185.85 °C), carbon dioxide (−78.5 °C), and xenon (−111.70 °C). Moreover, MR cycle and a single H_2 J-B cycle could be in use with nitrogen (−195.79 °C). Also, MR cycle together with four H_2 J-B cycles would be manipulated with neon (−248.6 °C). Lastly, the plant process that consists of MR cycle, three-five H_2 J-B cycles, and a single helium J-B cycle would probably be employed to efficiently liquefy helium (−268.93 °C). All aforementioned shall be further research works. Preliminary simulation data are tabulated below:

Table 4.10 – Preliminary simulation of the proposed MR and J-B cycles to efficiently liquefy some common industrial gases.

Fluid	Boiling temp. at 1 bar.		Ideal minimum liquefaction energy consumption		Today existing processes	The proposed MR + J-B processes
	K	°C	kJ/kg	kWh/kg	kWh/kg	kWh/kg
Helium	4.22	-269	6,823	1.8952	7.0000	6.1720
Nitrogen	77.31	-196	770	0.2138	0.3602	0.3000
Argon	87.28	-186	477	0.1325	N/A	0.2089
Oxygen	90.19	-183	635	0.1764	N/A	0.2363

4.10. Conclusion

A 100 TPD large-scale hydrogen liquefaction plant by simulation is proposed with preliminary optimal study. The optimization problem has 23 variables and 26 constraints. For cooling feed n-GH_2 from 25 ^oC to be e-GH_2 around −193 ^oC, the MR refrigeration system is recommended with the simulation's net power at 1.38 kWh/kg_{LH2}, in comparison to the ideal of 0.51 kWh/kg_{LH2}. The compressor and expander efficiencies are assumed to be 90%, which is close to the actual values for general large sizes that are available in the general market. With 100% efficiencies for ideal compression and expansion, the power consumption of the MR system is 1.07 kWh/kg_{LH2}. The largest loss is from the compressors and expanders. The other loss is from the heat exchangers of the MR system. More complex, e.g., from 6- to 10-component composition, yields slight improvement of efficiency, thus, a simplified 5-component composition suggested for the plant is found consisting of: 4% hydrogen, 18% nitrogen, 24% methane, 28% ethane, and 26% butane by mole. The mixed refrigerant composition is adjusted from trial and error to match the cooling curve of feed hydrogen gas. It is the best in comparison to the nitrogen, helium, and propane refrigeration systems. In addition, for further cooling down equilibrium hydrogen gas from −193 ^oC e-GH_2 to be liquid hydrogen at −253 ^oC (e-LH_2), the four H_2 Joule-Brayton cycle refrigeration system is recommended due to its improved efficiency. The net power for the proposed 4 J-B system is 4.24 kWh/kg_{LH2}, in comparison to the ideal of 2.38 kWh/kg_{LH2}. Similarly, the losses are from the compressors, expanders, and heat changers. It is the best in comparison to the nitrogen and helium refrigeration systems. The overall power consumption of the whole system is 1.38 kWh/kg_{LH2} + 4.24 kWh/kg_{LH2} = 5.91 kWh/kg_{LH2} which is a half compared to the current plant. Usually, the liquefier at Ingolstadt is a reference with an energy consumption of 13.58 kWh/kg_{LH2} and an efficiency of 21.28%. *While the proposed system is 50% or more, it depends on the assumption of the compressor and expander efficiencies together with all heat exchangers' effectiveness.* The plant optimization was also conducted with two more pinch temperatures (1 ^oC and 3 ^oC) yielding less plant energy consumption. But 3 ^oC is recommended for actual plant. Pressure drops in heat exchangers are also studied, but the result reveals that they don't have much significant impact on the overall plant total power consumption. The efficiency of the proposed system can reach very close to the ideal's if the compressors, expanders, and heat exchangers are ideal; and if there is no pressure drop. Moreover, the system has some smaller size heat exchangers, a much smaller compressor motor, and a smaller crankcase compressor for both the MR and the four H_2 Joule-Brayton cycles, which is due to the smaller energy consumption and hydrogen mass flow rates in the heat exchangers. Nitrogen pre-cooled systems that are designed for very large-scale systems (like Ingolstadt's) will require an additional nitrogen liquefaction cycle to liquefy nitrogen gas back (like WE-NET's). It will be a much larger size plant. Thus, the proposed new system could possibly be the lowest specific construction cost plant in comparison to Ingolstadt and Leuna. Therefore, the proposed system has a great potential for improvement and is recommended as a reference for future hydrogen liquefaction plants.

Nomenclature

1. Symbols

A	area/ heat transfer area, m^2
c	mathematical formulation of the operational constraints and the model equations
c_P	specific heat, kJ/kg-K
$\dot{E}$	rate of exergy (stream flow exergy) when used with subscript x, kW
e_x	specific exergy when used with subscript x, kJ/kg
$\dot{E}_x$	rate of exergy flow = $\dot{m}e_x$, kW
F	correction factor, -
f	friction factor, -
G	mass flowrate, kg/m^2-s
h	enthalpy, kJ/kg
$\dot{I}$	exergy loss/irreversibility, kW
j	Colburn factor, $j = St.Pr^{2/3}$ or $Nu/(Re.Pr^{1/3})$, -
k	thermal conductivity, kW/m-^oC
$\dot{m}$	mass flow rate, kg/s
$\dot{m}_{feed}$	nominal feed rate, kg/s
$\dot{m}_{GH2}$	hydrogen gas mass flowrate, kg/s
N	total number of independent variables in the function R, -
P	pressure, bar
Pr	Prandtl number, -
$\dot{Q}$	refrigeration load/the heat removed from the hydrogen gas during the pre-cooling process of the test rig, kW
R	function of independent variables, -
Re	Reynolds number, -
s	entropy, kJ/kg-K
T	temperature, K or ^oC
U	overall heat transfer coefficient, kW/m^2-^oC
v	specific volume, m^3/kg
V	volume, m^3

$\dot{V}$	volumetric flow rate, m^3/s
w	specific work/energy requirement, kJ/kg_{LH2} or kWh/kg_{LH2}
$\dot{W}$	power/rate of work, kW
X	independent variable, -
$\dot{X}$	stream exergy flow, W

2. Abbreviations

COM	compressor, -
COP	coefficient of performance, -
EVAP	evaporative condenser, -
EX	expander, -
FOM	Figure of Merit, -
GH_2	gas hydrogen, -
HX	heat exchanger, -
J-B	Joule-Brayton, -
J-T	Joule-Thomson
LH_2	liquid hydrogen, -
LIQ	liquid separator, -
LNG	liquefied natural gas, -
LMTD	Log Mean Temperature Difference, ^oC
n-	normal, -
MIXER	mixer of streams, -
MR	multi-component refrigerant/multi-mixed refrigerant, -
NTU	number of transfer units, -
O-P	ortho-para, -
p-	para, -
PT	pinch temperature
RH	relative humidity, -
SRK	Redlich-Kwong-Soave equation of state, -
TPD	ton per day, -

3. Greek letters

ε	exergy efficiency, -
η	efficiency, -
ρ	density, kg/m^3
α	heat transfer coefficient, $kW/m^2\text{-}^oC$
β , δ , γ	fin geometric parameters, -
μ	viscosity, Pa.s

4. Subscripts

I	of the first law, -
II	of the second law, -
0	at reference/dead state, -
1 up to 38	stream number of the test rig process depicted in Fig. 4.2, -

air	of flowing air, -
A	of system A, -
B	of system B, -
BH	brake/shaft horse, -
cb	convective boiling, -
disc	stream at discharge of compressor
elec	electrical, -
D_h	hydraulic diameter, m
EX	at expansion valve/expander, -
feed	of the feed flow at 21 bar and 25 ^{o}C, -
GH_2	hydrogen gas, -
i	of a single phase fluid: nitrogen, hydrogen, helium, or MR, -
in	input or at inlet, -
isen	isentropic, -
H	high, -
*H*2	of hydrogen/feed hydrogen, -
*H*2 *COM*	of hydrogen compressor, -
Helium	of liquid helium system, -
HX	of heat exchanger, -
ISEN	isentropic, -
L	low, -
LIQ	at liquid separator, -
liquefaction	due to hydrogen liquefaction process of the test rig, -
liquefied	liquefied hydrogen, -
min	minimum, -
MIXER	at mixer, -
MR	of MR, -
MR COM	of MR compressor, -
MR cycle	of MR refrigeration cycle, -
nb	of nucleate boiling, -
net	net cycle power consumption = compressors – expanders, -
opt int	optimum intermediate, -
out	at outlet, -
pre-cooled	of pre-cooled hydrogen gas, -
pre-cooling	of hydrogen gas pre-cooling process from 25 to -198 ^{o}C, -
s	summation, -
total	of total, -
TP	of two phase flow, -
V	volumetric, -

References

Alabdulkarem A, Mortazavi A, Hwang Y, Radermacher R, Rogers P. 2011. Optimization of propane pre-cooled mixed refrigerant LNG plant. *Applied Thermal Engineering*;31(6-7):1091-98.

Allam RJ, James PS. 2009. *Process and apparatus for liquefying hydrogen*. U.S. Patent 7,559,213. Available from: http://www.google.com/patents [accessed 28.07.2012].

Aunan B. 2000. *Shell-side heat transfer and pressure drop in coil-wound LNG heat exchangers, Laboratory measurements and modelling*. PhD dissertation, Norwegian University of Science and Technology.

Barron RF. 1966. *Cryogenic systems*. Oxford, United Kingdom: Oxford University Press; 1966.

Baker CR, Shaner RL. 1978. A study of the efficiency of hydrogen liquefaction process. *Int J Hydrogen Energy*;3(3):321-34.

Beljakov V, Krakovsky BD, Popov OM. 2000. Low capacity hydrogen liquefier with helium cycle. *In: Proc Cryogenics*; Praha: 158-61.

Bejan A. 1982. *Entropy generation through heat and fluid flow*. Willey, New York.

Bejan A. 1988. *Advanced engineering thermodynamics*. Wiley, New York.

Berstad D, Stang J, Neksa P. 2009. Comparison criteria for large-scale hydrogen liquefaction processes. *Int J of Hydrogen Energy*;34(3):1560-68.

Berstad D, Stang J, Neksa P. 2010. Large-scale hydrogen liquefier utilising mixed-refrigerant pre-cooling. *Int J Hydrogen Energy*;35(10):4512-23.

Bosma P, Nagelvoort RB. 2009. Liquefaction technology; developments through history. *Proceedings of the 1st Annual Gas Processing Symposium*, 10-12 January 2009, Doha, Qatar 2009, pp. 19-31.

Bottura L. 2009. Cryogenic mixed refrigerant processes. *Cryogenics*;49(12):745-46.

Bracha M, Lorenz GA, Wanner M. 1994. Large-scale hydrogen liquefaction in Germany. *Int J Hydrogen Energy*;19(1):53-59.

Bracha M, Trill R, Wolf J. 2006. *Method and device for liquefying hydrogen*. U.S. Patent 7,040,119 B2. Available from: http://www.google.com/patents [accessed 28.07.2012].

Chrz V. 2010. Cryogenic mixed refrigerant processes. *Int J Refrigeration*;33(3):648-49.

Cole ET, Bowen RR. 2000. *Cascade refrigeration process for liquefaction of natural gas*. U.S. Patent 6,016,665. Available from: http://www.google.com/patents [accessed 28.07.2012].

Dewar J. 1898. Liquid hydrogen. *Science*;8(183):3-6.

Dincer I, Rosen MA. 2007. Exergy analysis of cryogenic systems. *Exergy Energy, Environment and Sustainable Development*; 277-89.

Drnevich R. 2003. *Hydrogen delivery - liquefaction & compression*. Praxair, Strategic Initiatives for Hydrogen Delivery Workshop - May 7, 2003. Available from: http://www1.eere.energy.gov/hydrogenandfuelcells/pdfs/liquefaction_comp_pres_praxair.pdf [accessed 20.5.2009].

Dutton G. 2003. Hydrogen transitions- a UK perspective; 2003.

Etzbach V, Forg W, Grimm P. 1976. *Cascaded refrigeration cycles for liquefying low-boiling gaseous mixtures*. U.S. Patent 3,970,441. Available from: http://www.google.com/patents [accessed 28.07.2012].

Feldman A, Marvillet C, Lebouche M. 2000. Nucleate and convective boiling in plate fin heat exchangers. *Int J Heat and Mass Transfer*;43(18):3433-42.

Flynn TM. 1997. *Cryogenic engineering*. 2nd ed. NY: Marcel Dekker Press.

Foerg W. 2002. History of cryogenics: the epoch of the pioneers from the beginning to the year 1911. *Int J Refrigeration*;25(3):283-92.

Franser D. 2003. *Solutions for hydrogen solutions for hydrogen storage and distribution by dynetek industries Ltd*. The PEI Wind-Hydrogen Symposium June 22 to 24, 2003. Available from: http://www.gov.pe.ca/photos/original/dev_solutions.pdf [accessed 04.3.2008].

Fredheim AO. 1994. *Thermal design of coil-wound LNG heat exchangers, shell-side heat transfer and pressure drop*. PhD dissertation, Norwegian University of Science and Technology.

Fredheim AO, Owren G, Vist S, Neeraas BO. 2000. Coil, a model for simulation of spiral wound LNG heat exchangers. *World Gas Conference 2000*, Nice.

Gaggioli RA. 1998. Available energy and exergy. *Int J Appl. Thermodyn*;1(1-4):1-8.

Gaumer LS, Newton CL. 1972. *Process for liquefying natural gas employing a multicomponent refrigerant for obtaining low temperature cooling*. U.S. Patent 3,645,106. Available from: http://www.google.com/patents [accessed 28.07.2012].

Gaumer LS, Winter AR. 1988. *Hydrogen liquefaction using a dense fluid expander and neon as a precoolant refrigerant*. U.S. Patent 4,765,813. Available from: http://www.google.com/patents [accessed 28.07.2012].

Grenier M. 1996. *Process and apparatus for the liquefaction of hydrogen*. U.S. Patent 5,579,655. Available from: http://www.google.com/patents [accessed 28.07.2012].

Grini PG. 1994. *Flow calorimetry and enthalpy increment measurements for natural gas*. PhD dissertation, Norwegian University of Science and Technology.

Hasan M, Karimi I, Alfadala H, Grootjans H. 2009. Operational modeling of multistream heat exchangers with phase changes. *AIChE Journal*;55(1):150-171.

Hammer M, Vist S, Nordhus H, Sperle IL, Owren G. 2003. Dynamic modelling of spiral wound LNG heat exchangers - comparison to experimental results. *AIChE Spring Meeting 2003*, New Orleans.

Jensen JB, Skogestad S. 2006. Optimal operation of a mixed fluid cascade LNG plant. *Computer Aided Chemical Engineering*;21:1569-74.

Jensen JB. 2008. *Optimal operation of refrigeration cycles*. PhD dissertation, Norwegian University of Science and Technology.

Jorstad O. 1993. *Equation of state for hydrocarbon mixtures*. PhD dissertation, Norwegian University of Science and Technology.

Kanoglu M. 2002. Exergy analysis of multi-stage cascade refrigeration cycle used for natural gas liquefaction. *Int J Energy Res*.;26:763-74.

Kim B, Sohn B. 2006. An experimental study of flow boiling in a rectangular channel with offset strip fins. *Int J Heat and Fluid Flow*;27(3):514-21.

Kimble EL. 1999. *Dual multi-component refrigeration cycles for liquefaction of natural gas*. U.S. Patent 6,250,105. Available from: http://www.google.com/patents [accessed 28.07.2012].

Kleemenko AP. 1959. One flow cascade cycle. *Proceedings of the 10th international congress of refrigeration*;1:34-39.

Kramer GJ, Huijsmans J, Austgen D. 2006. Clean and green hydrogen. *In: 16th World hydrogen energy conference*. 16/13-16 June 2006 – Lyon, France. Available from: http://www.shell.com/static/hydrogen-en/downloads/speeches/speech_clean_green_hydrogen_1.pdf [accessed 05.06.2009].

Krasae-in S, Stang J, Neksa P. 2010. Simulation on a proposed large-scale liquid hydrogen plant using a multi-component refrigerant refrigeration system. *Int J Hydrogen Energy*;35(22):12531-44.

Krewitt W, Schmid S. 2005. *Common information database – Fuel cell technologies and hydrogen production/distribution options*. Available from: http://www.dlr.de/fk/Portaldata/40/Resources/dokumente/publikationen/2005-09-02_CASCADE_D1.1_fin.pdf [accessed 14.06.2009].

Kuendig A, Loehlein K, Kramer GJ, Huijsmans J. 2006. *Large scale hydrogen liquefaction in combination with LNG re-gasification*. Available from: http://www.cder.dz/A2H2/Medias/Download [accessed 05.06.2009].

Kuz'menko IF, Morkovkin IM, Gurov EI. 2004. Concept of building medium-capacity hydrogen liquefiers with helium refrigeration cycle. *Chem and Petro Eng*;40(1):94-98.

Kotas TJ. 1995. *The exergy method of thermal plant analysis*. Florida: Kreiger.

Leachman JW, Jacobsen RT, Penoncello S, Lemmon EW. 2009. Fundamental equations of state for para hydrogen, normal hydrogen, and ortho hydrogen. *J Physical and Chemical Reference Data*;38(3):721-48.

Lee GC, Smith R, Zhu XX. 2002. Optimal synthesis of mixed-refrigerant systems for low-temperature processes. *Industrial & Engineering Chemistry Research*;41:5016-5028.

Linde Engineering, 2011. *Small to Midscale LNG Plants – Process Plant – Liquefaction of Natural Gas*. Available from: http://www.linde-engineering.com/en/process_plants/liquefied_natural_gas/small_to_midscale_lng_plants/index.html [accessed 24.08.2011].

Linde Group. Available from: http://www.linde.com [accessed 02.03.2008].

Linde Switzerland. Available from: http://www.linde-kryotechnik.ch [accessed 02.03.2008].

Mafi M, Amidpour M, Mousavi Naeynian SM. 2009. Development in mixed refrigerant cycles used in olefin plants. *Proceedings of the 1st Annual Gas Processing Symposium*. 10–12 January 2009, Doha, Qatar 2009, pp. 154-161.

Manglik RM, Bergles AE. 1995. Heat transfer and pressure drop correlations for the rectangular offset strip fin compact heat exchangers. *Experimental Thermal and Fluid Sci*;10(2):171-80.

Matsuda H, Nagami M. 1998. *Study of large hydrogen liquefaction process*. Kanagawa, Japan: Nippon Sanso Corp. WE-NET: Summary of annual reports 1998. Available from: http://www.enaa.or.jp/WE-NET/ronbun/1997/e5/sanso1997.html [accessed 05.06.2009].

Melaaen IS. 1993. *Probabilistic modelling on the influence of inaccuracies in the thermodynamic properties on process olant design*. PhD dissertation, Department of Refrigeration Engineering, Norwegian University of Science and Technology.

Melaaen E. 1994. *Dynamic simulation of the liquefaction section in baseload LNG plants*. PhD dissertation, Department of Refrigeration Engineering, Norwegian University of Science and Technology.

Mitsugi C, Harumi A, Kenzo F. 1998. WE-NET: Japanese hydrogen program. *Int J Hydrogen Energy*;23(3):159-65.

Moffat RJ. 1988. Describing the uncertainties in experimental results. *Experimental Thermal and Fluid Science*;1(1):3-17.

Moran MJ. 1982. *Availability analysis: a guide to efficient energy use*. Prentice-Hall, Englewood Cliffs, NJ.

Mortazavi A, Somers C, Hwang Y, Radermacher R. 2011. Performance enhancement of propane pre-cooled mixed refrigerant LNG plant. *Applied Thermal Engineering*; In Press, Corrected Proof.

Myklebust J. 2010. *Techno-economic modelling of value chains based on natural gas – with consideration of CO_2 emissions*. PhD dissertation, Norwegian University of Science and Technology.

Nandi TK, Sarangi S. 1993. Performance and optimization of hydrogen liquefaction cycles. *Int J Hydrogen Energy*;18(2):131-39.

National Institute of Standards and Technology (NIST). 2010. *Thermophysical properties of hydrogen*. Thermophysical Properties Division, Chemical Science and Technology Laboratory. 2010. Available from: http://www.boulder.nist.gov/div838/Hydrogen/Properties/Properties.htm [accessed 19.5.2010].

Neeraas BO. 1994. *Condensation of hydrocarbon mixtures in coil wound LNG heat exchangers, shellside heat transfer and pressure drop*. PhD dissertation, Norwegian University of Science and Technology.

Newton CL. 1985. *Dual mixed refrigerant natural gas liquefaction with staged compression*. U.S. Patent 4,525,185. Available from: http://www.google.com/patents [accessed 28.07.2012].

Nogal FD, Kim J, Perry S, Smith R. 2008. Optimal design of mixed refrigerant cycles. *Ind. Eng. Chem. Res.*;47:8724-40.

Owren GA. 1998. *Condensation of multi-component mixtures*. PhD dissertation, Norwegian University of Science and Technology.

Podbielniak WJ. 1936. *Art of refrigeration*. U.S. Patent 2,041,725. Available from: http://www.google.com/patents [accessed 28.07.2012].

Price BC, Mortko RA. 1996. PRICO - a simple, flexible proven approach to natural gas liquefaction. *GASTECH, LNG, Natural Gas, LPG International Conference 1996*, Vienna".

Quack H. 2002. Conceptual design of a high efficiency large capacity hydrogen liquefier. *Adv Cry Eng*;47:255-63.

Remeljej CW, Hoadley AFA. 2006. An exergy analysis of small-scale liquefied natural gas (LNG) liquefaction processes. *Energy*;31(12):2005-19.

Rentler RJ, Sproul DD. 1983. *Combined cascade and multicomponent refrigeration method with refrigerant intercooling*. U.S. Patent 4,404,008. Available from: http://www.google.com/patents [accessed 28.07.2012].

Roberts MJ, Agrawal R. 2001. *Dual mixed refrigerant cycle for gas liquefaction*. U.S. Patent 6,269,655. Available from: http://www.google.com/patents [accessed 28.07.2012].

Schwartz JM, Drnevich RF, Barrett PA, Neu BT. 2011. *Hydrogen liquefaction method and liquefier*. U.S. Patent 8,042,357 B2. Available from: http://www.google.com/patents [accessed 28.07.2012].

Shimko M, Gardiner M. 2007. *Innovative hydrogen liquefaction cycle*. Available from: http://www.hydrogen.energy.gov/pdfs/progress08/iii_7_shimko.pdf [accessed 14.06.2009].

Stang J, Neksa P, Brendeng E. 2006. On the design of an efficient hydrogen liquefaction process. *WHEC*; 16 / 13-16 June 2006 – Lyon France.

Tak K, Lim W, Choi K, Ko D, Moon I. 2011. Optimization of mixed-refrigerant system in LNG liquefaction process. *21st European Symposium on Computer Aided Process Engineering*: 1824-28.

Timmerhaus KD, Flynn TM. 1989. *Cryogenic process engineering*. New York: Springer.

Townsend DW, Linnhoff B. 1983. Heat and power networks in process design, *AIChE Journal*; 29(15):742-48.

Turton R, Bailie RC, Whiting WB, Shaeiwitz JA. 2002. *Analysis, synthesis, and design of chemical processes*. 2nd ed.: Prentice Hall.

Valenti G, Macchi E. 2008. Proposal of an innovative, high-efficiency, large-scale hydrogen liquefier. *Int J Hydrogen Energy*;33(12):3116-21.

Venkatarathnam G. 2008. *Cryogenic mixed refrigerant processes*. New York: Springer.

Vist S, Hammer M, Nordhus H, Sperle IL, Owren G. 2003. Dynamic modelling of spiral wound LNG heat exchangers – model description. *AIChE Spring Meeting 2003*, New Orleans.

Wark KJ. 1995. *Advanced thermodynamics for engineers*. McGraw-Hill, New York.

Zaim A. 2002. *Dynamic optimization of an LNG plant, Case study: GL2Z LNG plant in Arzew, Algeria*. PhD dissertation, RWTH Aachen University.

Appendix

Krasae-in S, Stang J, Neksa P. Development of large-scale hydrogen liquefaction processes from 1898 to 2009. Int J Hydrogen Energy 2010;35(10):4524-33.

Krasae-in S, Stang J, Neksa P. Exergy analysis on the simulation of a small-scale hydrogen liquefaction test rig with a multi-component refrigerant refrigeration system. Int J Hydrogen Energy 2010;35(15):8030-42.

Krasae-in S, Bredesen A, Stang J, Neksa P. Simulation and experiment of a hydrogen liquefaction test rig using a multi-component refrigerant refrigeration system. Int J Hydrogen Energy 2011;36(1):907-19.

Krasae-in S, Stang J, Neksa P. Simulation on a proposed large-scale liquid hydrogen plant using a multi-component refrigerant refrigeration system. Int J Hydrogen Energy 2010;35(22):12531-44.

Krasae-in S, Stang J, Neksa P. Development of large-scale hydrogen liquefaction processes from 1898 to 2009. Int J Hydrogen Energy 2010;35(10):4524-33.

INTERNATIONAL JOURNAL OF HYDROGEN ENERGY 35 (2010) 4524–4533

Available at www.sciencedirect.com

ScienceDirect

journal homepage: www.elsevier.com/locate/he

Review

Development of large-scale hydrogen liquefaction processes from 1898 to 2009

Songwut Krasae-in [a,*], *Jacob H. Stang* [b,1], *Petter Neksa* [b,2]

[a] *Norwegian University of Science and Technology, Kolbjorn Hejes vei 1d, NO-7491 Trondheim, Norway*
[b] *SINTEF Energy Research AS, Kolbjorn Hejes vei 1d, NO-7465 Trondheim, Norway*

ARTICLE INFO

Article history:
Received 22 December 2009
Received in revised form
15 February 2010
Accepted 21 February 2010
Available online 26 March 2010

Keywords:
Liquid hydrogen
Hydrogen liquefier
Large hydrogen liquefaction
Exergy efficiency
Comparison

ABSTRACT

This paper presents a review of the development of large-scale hydrogen liquefaction processes throughout the world from 1898 to 2009. First, there is a concise literature review including numerous past, present, and future designs given such as the first hydrogen liquefaction device, long time ago simple theoretical processes, today's actual plants with efficiencies 20–30%, a list of the capacity and location of every hydrogen liquefaction plant in the world, and some modern more efficient proposed conceptual plants with efficiencies 40–50%. After that, further information about the development and improvement potential of future large-scale liquid hydrogen liquefaction plants is given. It is found that every current plant is based on the pre-cooled Claude system, which is still the same as was 50 years ago with little improvement. Methods to resolve the challenges of the future plants include proposing completely new configurations and efficient systems coupled with improved efficiencies of the main system components such as compressors, expanders, and heat exchangers. Finally, a summary and comparison of the process efficiencies are described, including a newly proposed Multi-component Refrigerant (MR) system being developed by NTNU and SINTEF Energy Research AS.

1. Introduction

As hydrogen has shown promise as an important energy source for use in future transportation vehicles, several hydrogen research activities have been conducted since 1980 and especially since 2000. One of the challenges in creating a hydrogen economy is the low efficiency of the current hydrogen liquefaction plant cycles. Since 2000, there have been several papers that have proposed conceptual plants with efficiencies up to 40–50% [1–7]. This paper chronicles the development of systems from 1898 to 2009 and gives a comparison of several cycle efficiencies for the future hydrogen plant developer. Hydrogen was first liquefied in 1898 by a small device [8]. Some years later, a pre-cooled Linde–Hampson system was used as the first simple laboratory system to liquefy hydrogen. Around 1900, more efficient laboratory systems were invented including the Claude, pre-cooled Claude, and helium-refrigerated systems, arranged in order of increasing efficiency [9]. Next, in 1957, the

* *Corresponding author*. Tel.: +47 735 92991; fax: +47 735 97214.
E-mail addresses: songwut.krasaein@ntnu.no, krasaein@hotmail.com (S. Krasae-in), jacob.stang@sintef.no (J.H. Stang), petter.neksa@sintef.no (P. Neksa).
[1] Tel.: +47 735 98109.
[2] Tel.: +47 735 93923.
0360-3199/$ – see front matter © 2010 Professor T. Nejat Veziroglu. Published by Elsevier Ltd. All rights reserved.
doi:10.1016/j.ijhydene.2010.02.109

first few large hydrogen plants were built in the USA for the growing petrochemical and aerospace industries and were based on the pre-cooled Claude cycle with more complicated systems that used liquid nitrogen as a pre-coolant to cool hydrogen gas down to −193°C and hydrogen refrigeration systems to further cool feed hydrogen gas to −253°C on a large scale. Up to the present, almost all the large-scale plants in use across the world today still employ nearly the same cycle as the first few plants built in the US and have exergy efficiencies of just 20–30%. This can be seen in the Ingolstadt plant installed in Germany in 1991 [10]. Today, the most technologically advanced plants available in the literature are located in Leuna, Germany, and near Tokyo, Japan, which were commissioned in 2008; however, only a slight improvement of efficiency was realized. Thus, there is potential for improvement.

2. Simple hydrogen liquefaction processes

Barron [9] illustrated the fundamental principles and how these simple processes work very well.

2.1. *The first hydrogen liquefaction system*

In 1885, Michael Faraday published a paper regarding gas liquefaction. At that time, his method was able to achieve refrigeration temperatures down to −110°C using baths of ether and solid carbon dioxide. Gases with boiling points below that temperature, including hydrogen, were called ''permanent gases'' [11]. For the first time, the liquefaction of hydrogen was achieved by Sir James Dewar in 1898 [8]. This process utilized carbolic acid and liquid air for pre-cooling compressed hydrogen at 180bars. The system was similar to the one that Linde used for the liquefaction of air.

2.2. *Theoretical liquefaction systems for hydrogen*

In 1895, Carl von Linde and William Hampson invented a simple liquefaction cycle to liquefy air. This cycle is called the 'Linde–Hampson cycle'. However, according to what was explained by Barron [9], the systems that cannot be used to liquefy hydrogen are the Linde–Hampson, Linde dual-pressure, Cascade, and Heylandt systems. A liquid nitrogen, pre-cooled Linde–Hampson system can be used to liquefy hydrogen. This cycle is shown schematically by Barron [9].

2.3. *Theoretical Claude system for hydrogen*

In addition to liquefying air, the Claude cycle invented by Georges Claude in 1902 can also be used to liquefy hydrogen [9]. This cycle was a development some years after the first Linde–Hampson cycle. There was an expansion engine in the Claude cycle, which produced a temperature much lower than the temperature generated by isenthalpic expansion as proposed by Linde.

2.4. *Theoretical pre-cooled Claude system for hydrogen*

The performance is somewhat improved if a pre-cooling bath of liquid nitrogen is used with the Claude system. Timmerhaus and Flynn [12] explained that if liquid nitrogen is used for pre-cooling, one could achieve an exergy efficiency 50–70% higher than a pre-cooled Linde–Hampson cycle. Nandi and Saragni [13] made a comparison of the two cycles and found that the typical Figure of Merit (FOM) for the pre-cooled Linde–Hampson cycle was lower than the standard pre-cooled Claude. The Claude cycle, as explained by Nandi et al. [13], is the basis for most other conventional liquefaction cycles. An example of a modified pre-cooled Claude cycle in use today is the hydrogen liquefaction plant in Ingolstadt near Munich, Germany, as shown in Fig. 2, which has been in operation since 1992 [10].

2.5. *Helium-refrigerated hydrogen liquefaction system*

A secondary helium-gas refrigerator can also be used to liquefy hydrogen, as shown in Nandi and Sarangi [13] and Barron [9], but this system has never been used in any actual large-scale plants.

3. Current plants

Table 1 shows a list of all of the hydrogen liquefaction plants in use around the world. In 1960, the first few liquid hydrogen plants were built to support the Apollo program. In the beginning of the 1960s there was a demand for US space programs. The capacity installed up to 1965 was capable of supplying the demand of NASA and others until 1977. In this period, no additional plants were built, not least because of the reduction of NASA's space activities. Since 1977, this time was mainly caused by the steadily increasing commercial demand for liquid hydrogen. Today, there are more than 9 hydrogen liquefaction plants in the US with production rates of 5–34 tons per day (TPD), 4 plants in Europe with capacities of 5–10 TPD, and 11 plants in Asia with capacities of 0.3–11.3 TPD. Air Products supplies the largest quantity of liquid hydrogen in North America, followed by Praxair. Today, liquid hydrogen is used to reduce the cost of hydrogen distribution [14]; however, the current worldwide liquid hydrogen (LH_2) production capacity exceeds the market demand. Liquid hydrogen demand and production today is the largest in North America, which constitutes 84% of the world production. Of the total production in the US, 33.5% is used in the petroleum industry, 18.6% is for government aerospace, and the rest is for other industries. Only 0.1% is used for fuel cells today [15].

3.1. *Large-scale plants: Praxair, Air Products, and Air Liquide*

Praxair has five hydrogen liquefaction plants in the US today with production rates between 6 and 35 TPD LH_2. Typical specific power consumptions are between 12.5 and 15 kW h/kg_{LH2} [14]. Fig. 1 shows a Praxair LH_2 process flow sheet. It looks like the pre-cooled Claude cycle, but is more complicated for the large-scale system. There are three heat exchangers. The first heat exchanger is cooled by nitrogen gas (GN_2) and an external refrigeration system. The second heat exchanger is cooled by liquid nitrogen (LN_2) and some of the H_2 feed. The third is cooled by a hydrogen refrigeration system

Table 1 – Commercial hydrogen liquefaction plants worldwide.

Continent/Country	Location	Operated by	Capacity (TPD)	Commissioned in	Still in operation
America					
Canada	Sarnia	Air Products	30	1982	Yes
Canada	Montreal	Air Liquide Canada Inc.	10	1986	Yes
Canada	Becancour	Air Liquide	12	1988	Yes
Canada	Magog, Quebec	BOC	15	1989	Yes
Canada	Montreal	BOC	14	1990	Yes
French Guyane	Kourou	Air Liquide	5	1990	Yes
USA	Painsville	Air Products	3[a]	1957	No
USA	West Palm Beach	Air Products	3.2[a]	1957	No
USA	West Palm Beach	Air Products	27[a]	1959	No
USA	Mississippi	Air Products	32.7[a]	1960	No
USA	Ontario	Praxair	20	1962	Yes
USA	Sacramento	Union Carbide, Linde Div.	54[a]	1964	No
USA	New Orleans	Air Products	34	1977	Yes
USA	New Orleans	Air Products	34	1978	Yes
USA	Niagara Falls	Praxair	18	1981	Yes
USA	Sacramento	Air Products	6	1986	Yes
USA	Niagara Falls	Praxair	18	1989	Yes
USA	Pace	Air Products	30	1994	Yes
USA	McIntosh	Praxair	24	1995	Yes
USA	East Chicago, IN	Praxair	30	1997	Yes
Subtotal			300		
Europe					
France	Lille	Air Liquide	10	1987	Yes
Germany	lngolstadt	Linde	4.4	1991	Yes
Germany	Leuna	Linde	5	2008	Yes
Netherlands	Rosenburg	Air Products	5	1987	Yes
Subtotal			24.4		
Asia					
China	Beijing	CALT	0.6	1995	Yes
India	Mahendragiri	ISRO	0.3	1992	Yes
India	India	Asiatic Oxygen	1.2	–	Yes
India	Saggonda	Andhra Sugars	1.2	2004	Yes
Japan	Amagasaki	Iwatani	1.2[a]	1978	No
Japan	Tashiro	MHI	0.6[a]	1984	No
Japan	Akita Prefecture	Tashiro	0.7	1985	Yes
Japan	Oita	Pacific Hydrogen	1.4	1986	Yes
Japan	Tane-Ga-Shima	Japan Liquid Hydrogen	1.4	1986	Yes
Japan	Minamitane	Japan Liquid Hydrogen	2.2	1987	Yes
Japan	Kimitsu	Air Products	0.3	2003	Yes
Japan	Osaka	Iwatani (Hydro Edge)	11.3	2006	Yes
Japan	Tokyo	Iwatani, built by Linde	10	2008	Yes
Subtotal			30.6		
Worldwide			355		

a Not included in the subtotal of the capacity for the year 2009.

that uses some of the feed to expand through turbines and the Joule–Thomson (J–T) valve. The system is unique. Air Products has four hydrogen liquefaction plants capable of producing between 30 and 35 TPD LH_2 in use in North America today. In addition, they have two 5 TPD LH_2 plants: one in Holland and the other one in the USA. However, there is no literature about Air Product's technology. Air Liquide has a plant in France and one in Canada, and both have capacities of about 10 TPD. Both of these plants make use of the Claude cycle with hydrogen used as the cycle fluid; however, there are no papers about Air Liquide's cycle. The best plant in the USA requires about 10 kW h/kg_{LH2} [14]. The LH_2 production capacity is still greater than the demand. It seems that every large-scale LH_2 plant has the cycle of LN_2 as a pre-cooling process to cool hydrogen gas from 25 °C to −193 °C and a hydrogen refrigeration system to further cool hydrogen gas to −253 °C.

3.2. *Linde large-scale N_2 pre-cooled Claude plant in Ingolstadt*

This plant used to be the largest German hydrogen liquefier. The cycle is illustrated in Bracha et al. [10]. Feed hydrogen gas obtained from an air separation plant is generated from a steam reforming process using natural gas. Fig. 2 shows the

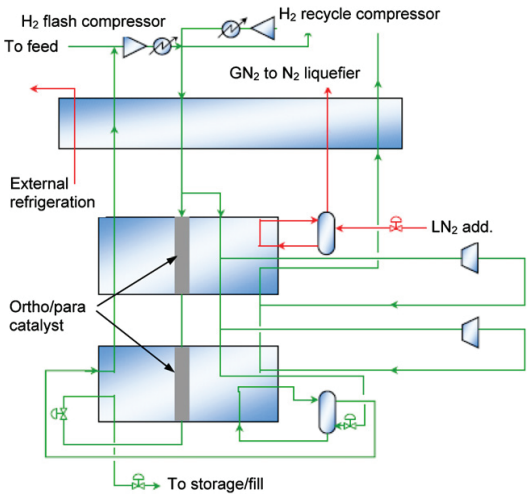

Fig. 1 – Praxair hydrogen liquefaction process (adapted from [14]).

actual liquefier in the plant. The big, vertical tank nearby on the left is the LN_2 tank that the nitrogen liquefaction system uses to liquefy nitrogen to pre-cool hydrogen inside the LH_2 liquefier. All of the compressors are kept inside the machinery building on the right. The leftmost tank is the LH_2 storage tank where liquefied hydrogen is kept for delivery. The tank is vacuum insulated. Fig. 3(a) is for the other side. To minimize the delivery cost, the hydrogen is delivered in liquid form by truck. Fig. 3(b) demonstrates how LH_2 is loaded from the storage tank to the trailer.

3.3. *The new Linde large-scale plant system in Leuna*

Linde opened a second, 20 million Euro hydrogen liquefaction plant in September 2007 in Leuna, as depicted in Figs. 5 and 6. It is currently the newest and largest H_2 liquefier plant in Germany. The system with a new cycle as depicted in Fig. 4 is similar to the existing plant in Ingolstadt depicted in Fig. 2, but

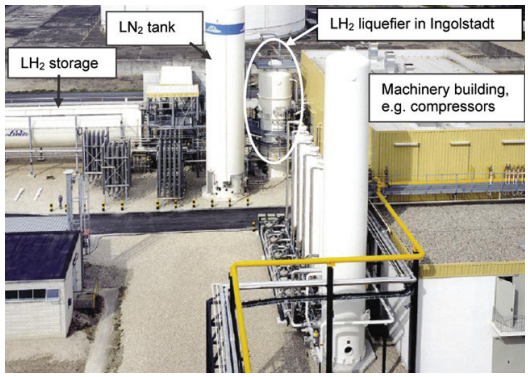

Fig. 2 – The location of Linde LH_2 in Ingolstadt.

is more efficient. There is an important difference in the turbine arrangement between the plants in Leuna and Ingolstadt in that the plant in Leuna receives a single feed GH_2 stream from an air separation plant. There is no recycled hydrogen, and the ortho–para (o–p) conversions are put inside heat exchangers.

4. Conceptual plants

From year 2000 to 2009, some researchers have proposed new improved processes with exergy efficiencies between 40 and 50%. The details are given below.

4.1. *Large-scale H_2 liquefaction in combination with liquefied natural gas (LNG) pre-cooling system*

Kuendig et al. [1] conducted a study regarding the integration of a pre-cooling LNG system to a new one like the Leuna N_2 pre-cooled Claude system. The study concluded that using LNG for pre-cooling in the hydrogen liquefaction process would be extremely useful to decrease the power input and the overall liquefier construction cost because the source would be free. Compared to a conventional liquefaction process, such as the one at Leuna using liquid nitrogen for pre-cooling but with compression at ambient temperature, the reduction would be from 10 to 4 kW h/kg_{LH2} [16]. However, this process could only be used for hydrogen gas made from LNG, and the plant would have to be located near a seaport.

4.2. *Nitrogen pre-cooled Claude by Matsuda and Nagami [2]*

The World Energy NETwork (WE-NET) project [17] has suggested building large-scale hydrogen liquefaction plants with liquefaction capacities of 300 TPD. The plant is based on a Claude cycle with nitrogen pre-cooling [2]. It appears that WE-NET's cycle is similar to the plant in Ingolstadt in that the nitrogen cycle is used to pre-cool hydrogen from 25 to −193 °C. Then, the hydrogen cycle is used to cool from −193 °C down to −253 °C; however, WE-NET's cycle is more complicated and is specifically designed for greater capacity. There is a large N_2 liquefaction system to reliquify GN_2 for the pre-cooling process.

4.3. *Conceptual plant by Quack [3]*

Quack [3] has made a conceptual design of a high-efficiency, large-capacity liquefier for hydrogen. However, internal process simulation tests run in a commercial software package; SimSci/PROII by NTNU-SINTEF indicated that it was not able to explicitly determine whether it has a high-efficiency or not because the configuration of the proposed propane refrigeration is impossible for low power consumption. The software was checked for its reliability and accuracy of process simulation. Also, the proposed helium–neon refrigeration system consumes more power due to the fact that helium–neon mixture has inferior refrigerant heat transfer properties compared with hydrogen, which is commonly found in use today in actual hydrogen liquefaction plants.

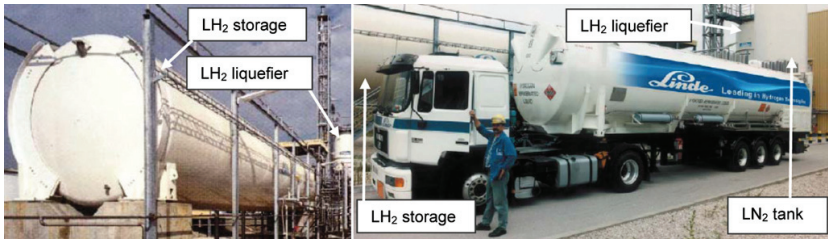

Fig. 3 – (a) Liquid hydrogen storage tank of Linde AG in Ingolstadt, (b) articulated train with semi-trailer equipped for liquid hydrogen.

4.4. *Conceptual plant with helium refrigeration cycle by Kuzmenko et al. [4]*

Before this, Beljakov et al. [18] successfully created a reliable, high-efficiency, low-capacity hydrogen liquefier with a helium refrigeration cycle. Later on, engineer Kuzmenko et al. [4] at Open Joint-Stock Company used this concept to design a liquefier. He made a conceptual study of building a medium-capacity hydrogen liquefier with a helium refrigeration cycle; however, it only produced a slight improvement from the Ingolstadt plant's efficiency.

4.5. *MR refrigeration by Stang et al. [5]*

A hydrogen liquefaction prototype laboratory unit was developed by NTNU–SINTEF. The process was based on using an MR process for pre-cooling, as shown in the figure of Stang et al. [5]. The rig is under experiment by the author of this paper. With the initial test, the hydrogen gas could be cooled by the MR refrigeration system from an ambient temperature of 25 °C down to near −193 °C with the highest efficiency. Detailed experimental results will be reported by the author in a future paper.

4.6. *Helium refrigeration cycle by Shimko and Gardiner [6]*

This is the design and construction of an estimated $2.6 million small-scale pilot plant (20 kg/h) that will be used for hardware demonstration (will be finished in 2011) and as a model for scaling to an estimated $39 million larger plant (50 TPD) [6]. Simulations were performed using EXCEL and REFPROP. Nevertheless, the efficiency is still lower than the proposed NTNU–SINTEF system. Moreover, helium is not suitable (hydrogen has better heat transfer properties) for cooling GH_2 from −193 to −253 °C. If used, every component such as compressors, expanders, and heat exchangers will have to be bigger.

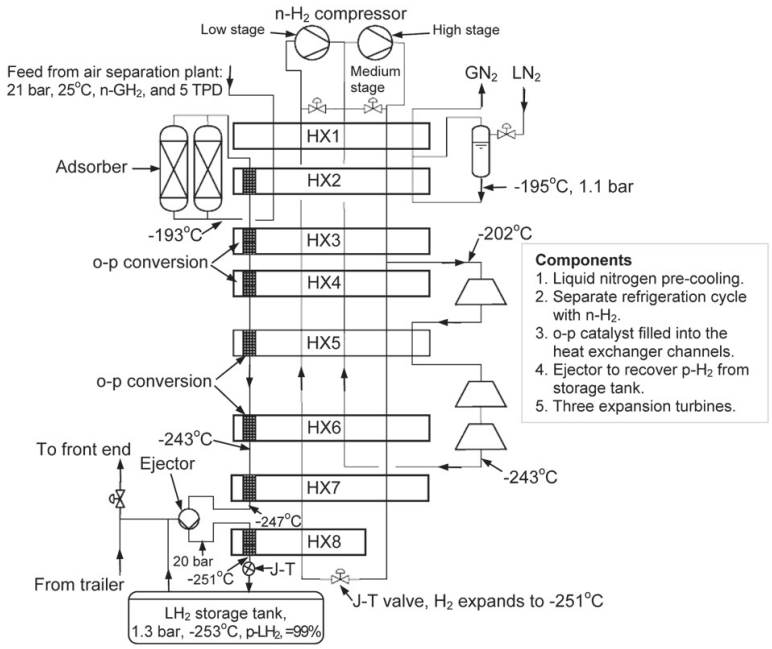

Fig. 4 – Process flow sheet of hydrogen liquefaction plant in Leuna [1].

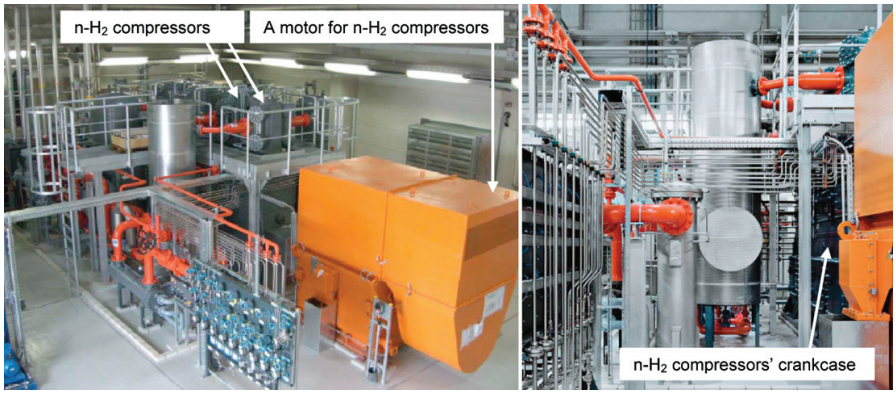

Fig. 5 – Piston compressors of hydrogen liquefaction plant in Leuna (adapted from Finanzberichte.Linde.com, 2008).

4.7. *Helium Joule–Brayton cascade system by Valenti [7]*

Valenti [7] proposed an innovative, high-efficiency, large-scale hydrogen liquefier that utilizes four cascaded helium Joule–Brayton cycles. However, helium is not suitable for cooling GH_2 from 25 to −193 °C and from −193 to −253 °C due to its inferior heat transfer properties compared to hydrogen. Moreover, the cycle's configuration itself to cool GH_2 from 25 °C to near −193 °C makes it impossible to have low exergy efficiency as reported. Also, internal simulation tests run in PROII by NTNU-SINTEF indicated that the system is not guaranteed to have a high-efficiency.

5. Development potential of large-scale LH_2 plants

A potential efficiency increase in future hydrogen liquefaction plants can be realized by the following means:

- Replacement of the J–T valve at the liquefaction stage by an expansion turbine. An increase in the number and quality of expansion turbines can minimize exergy losses.
- Reduction of the circulating mass flow or using a single H_2 feed stream as used by the Leuna plant, Quack [3], and Valenti [7]. By doing this, the last heat exchanger must be designed to cool the hydrogen to the lowest possible temperature, e.g. near −253 °C, so there is no vapor fraction after the expansion at the last J–T valve. A small ejector is recommended to recover p-GH_2 from the storage tank, the same as the plant in Leuna.
- Operating with a refrigerant mixture for pre-cooling hydrogen gas from 25 to −193 °C. This way, pre-cooled hydrogen gas and cold Multi-component Refrigerant (MR) streams get closer. This new system is currently being studied at NTNU–SINTEF [5], and the results will be published soon.
- Another major factor influencing liquefier efficiency is the feed gas input pressure. One alternative is to raise the hydrogen output pressure of the preceding hydrogen production plant, e.g. a high-pressure electrolysis process or a steam reforming plant. A good example is the 21 bar feed n-H_2 at the LH_2 plants in Ingolstadt and Leuna. The higher the feed pressure, the greater the liquefier's efficiency. The minimum liquefaction work is in conjunction with feed pressure. The minimum feed pressure must not be below 15 bars because there could be hydrogen condensation during the cooling process. If it is below 15 bars, more energy is needed in liquefaction, and there will be more exergy loss.
- Most of the exergy losses in the hydrogen liquefaction processes are dissipated through compressors. Therefore, it is recommended for manufacturers to design new high-efficiency compressors and expanders and design all compressors in a way such that the suction temperatures are reduced as done by Quack [3]. Also, it is recommended to ventilate heat from the compressors as much as possible during the compression process to reduce the exergy loss.
- Use aluminum plate-fin heat exchangers with maximum effectiveness to reduce the exergy losses.
- If possible, construct plants near seaports for delivering LNG to be used in the pre-cooling process. This will help significantly reduce the plant size and energy consumption as recommended by Kramer et al. [16] and Keundig et al. [1].
- A cost overview for the specific investment costs of conventional liquefaction plants. When designing a large-scale plant, the cost must be compared with other existing plants. Inflation should be accounted for in current and old plants. Companies who can offer cheap, large-scale hydrogen liquefaction plants are Linde, Air Products, and Praxair. Praxair has the largest hydrogen plant in the USA with the lowest investment cost.
- Krewitt and Schmid [19] say that costs for liquefaction are driven primarily by capital costs (today: 63%), then energy costs (29%), and finally, O&M [14]. Energy costs on the other hand are strong functions of the liquefier efficiency and are less dependent on the production rate. In small plants, energy and non-energy costs are comparable. In large-scale plants, the energy costs become more important. Krewitt and Schmid [19] also derived the following equation for the specific investment costs: Specific investment cost for liquefier (€2000/kg/h) = 828 313 × (production capacity, kg/h)$^{-0.48}$.

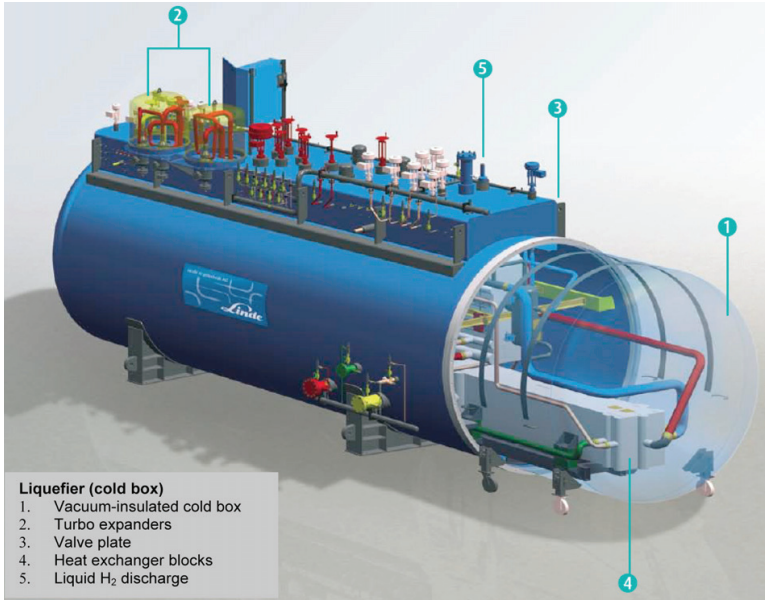

Fig. 6 – A Linde hydrogen (cold box) liquefier in Leuna (adapted from Linde-kryotechnik.ch, 2008).

- A method to decrease capital costs is to build plants on a larger scale and use the effect of building multiple plants of the same design. The following challenges for more cost effective LH_2 production systems are [14] system modularization for traditional sized units, large-scale equipment, higher efficiency compressors and expanders, more efficient refrigeration, and lower cost high-efficiency insulation.

The conclusions are the following:

- The problem with the current liquefaction systems is their high-energy consumption. Every large-scale hydrogen liquefaction plant is based on the pre-cooled Claude system, which is still the same as 50 years ago with little improvement. If it is possible to reduce from today's energy usage of 10 kW h/kg_{LH2} to around 5 kW h/kg_{LH2} which will reduce electrical power consumption of the plant to be half in the future, all of the compressors and motors in the plant, which constitute the most expensive components, could be reduced by 50%, which will also lead to cheaper plants.
- Methods to resolve the challenges include proposing completely new configurations and efficient systems coupled with improved efficiencies of the main system components such as compressors, expanders, and heat exchangers.
- The development trend is that a lot of people have tried to propose new better systems [1–7], but they are still neither more efficient nor realistic. Furthermore, compressor and expander manufacturers must invent more efficient machines.

6. Summary and comparison of hydrogen liquefaction process efficiencies

Table 2 gives the summary and comparison. Feed hydrogen flow is normal hydrogen at 1 atm, 25 °C. FOM × 100% = (Ideal liquefaction power/Actual system liquefaction power) × 100% or Exergy efficiency. The efficiencies of systems 3, 5, and 6 are from Nandi and Sarangi [13]; the same systems have different energy consumptions and exergy efficiencies because it depends on the assumptions of the efficiencies of compressors and expanders used in the systems. When making a comparison between several different cycles and liquefiers, Berstad et al.'s [20] comparison method is recommended. This method, which is a direct comparison of liquefiers based on the overall exergy efficiency and specific power consumption, favors those with a higher portion of pre-compression. The feed stream was assumed and calculated at 21 bars and 25 °C before going into any cycle/liquefier, which is identical to the Ingolstadt plant. Every system is directly compared with the Ingolstadt plant at a modified feed stream pressure of 21 bars. The energy consumptions and exergy efficiencies of the Ingolstadt, WE-NET, and Quack systems as shown in Table 2 were calculated by Berstad et al. [20].

The compression power reductions of the third, fourth, fifth, and sixth hydrogen liquefaction systems in Table 2 are 0.9167, 0.9167, 0.2313, and 0.1026 kW h/kg_{LH2}, respectively. These are from the ideal H_2 feed exergy reduction of 0.55, 0.55, 0.1388, and 0.0616 kW h/kg_{LH2}, respectively. Make-up gas is reversibly and isothermally (ideally) compressed from the feed at 21 bars and 25 °C to each cycle's high side. This was all calculated assuming a compression exergy efficiency of 60%.

Table 2 – Summary and comparison of hydrogen liquefaction process efficiencies.

System with modified feed state: normal hydrogen @21 bars, 25 °C	Original energy consumption (kW h/kg$_{LH2}$)	Modified energy consumption (kW h/kg$_{LH2}$)	Modified exergy efficiency (%)
1. The thermodynamically ideal liquefaction system			
Feed: 21 bars, 25 °C, n-GH_2			
Output: 1 bar, −253 °C, n-LH_2	–	2.178	100
Output: 1 bars, −253 °C, 99.8% p-LH_2	–	2.890	100
2. Theoretical simple Linde–Hampson system [8]. *Cannot liquefy hydrogen	–	–	–
3. Theoretical pre-cooled Linde–Hampson [8,13]. *Output*: 1 bar, −253 °C, n-LH_2	64.5–71.7	63.6–70.8	3.0–3.4
4. Theoretical Claude system [8,13]. *Output*: 1 bar, −253 °C, n-LH_2	Less than the pre-cooled Claude		
5. Theoretical pre-cooled Claude system [8,13]. *Output*: 1 bar, −253 °C, n-LH_2	24.8–35.0	24.6–34.8	6.2–8.8
6. Theoretical helium-refrigerated system [8,13]. *Output*: 1 bar, −253 °C, *n*-LH_2	29.3–49.5	29.2–49.4	4.4–7.4
7. Large-scale Praxair plant system [14]. *Output*: ≈1 bar, −253 °C, 95% p-LH_2	≈12–15		19–24
8. Large-scale Air Products plant system [14]. *Output*: ≈1 bar, −253 °C, 95% p-LH_2			
9. Large-scale Air Linde plant system [14]. *Output*: ≈1 bar, −253 °C, 95% p-LH_2			
10. Large-scale plant, Claude system in Ingolstadt on stream in 1994 by Bracha et al. [10]. *Output*: 1.3 bars, −253 °C, 95% p-LH_2	13.58		21.0
11. WE-NET: Nitrogen pre-cooled large-scale Claude plant by Matsuda and Nagami [2] *Output*: 1.3 bars, −253 °C, 95% p-LH_2			
1) Hydrogen Claude	≈8.5	N/A	N/A
2) Helium Brayton			
3) Basic neon			
4) Neon with cold pump		7.0	41.3
12. Large-scale conceptual plant by Quack [3] *Output*: 1 bar, −253 °C, 99.8% p-LH_2			
1) Without pressure drop in calculation	7.0	5.49	52.6
2) With pressure drop in calculation	≈7.3	N/A	N/A
13. Four helium Joule–Brayton cascade cycle by Valenti [7]. *Output*: 1.5 bars, −253 °C, 99.8% p-LH_2	5.04	5.76	50.2

For cycles 7–9, the hydrogen feed pressure was 21 bars, the same as Ingolstadt's. Thus the energy consumption was the same. With Valenti's system, GH_2 compression must be made from 21 bar supply feed to 60 bars; therefore, there is an increased consumption of 0.72 kW h/kg$_{LH2}$ with an assumed 60% exergy efficiency from the ideal H_2 feed exergy increase of 0.43 kW h/kg$_{LH2}$. Finally, all of the system exergy efficiencies were calculated by comparing with an ideal energy consumption of 2.89 kW h/kg$_{LH2}$; however, systems 3–6 were calculated using an ideal energy consumption of 2.178 kW h/kg$_{LH2}$.

Fig. 7 contains the information shown in Table 2. From the data, the theoretical pre-cooled Linde–Hampson system was the first imaginary system invented a long time ago, and its exergy efficiency is the lowest. After that, the second was the theoretical helium-refrigerated system, which is followed by the theoretical pre-cooled Claude system. All have a very low yield: e.g. 10% after expansion. The theoretical systems mentioned have never been used to liquefy hydrogen on a large-scale production. They were just small-scale laboratory systems. Next, Ingolstadt and Praxair brought this concept to invent real plants. Today, actual large-scale hydrogen liquefaction plants, e.g. Praxair, Air Products, and Air Liquids plants in the USA, energy consumptions are reported to be between 12 and 15 kW h/kg$_{LH2}$ [14]. Baker and Shaner's [21] was the first conceptual plant, and it had the lowest efficiency. The conceptual large-scale systems proposed by Matsuda and Nagami [2], Quack [3], and Valenti [7] were designed later. Recently, the efficiency of the Leuna plant (with energy consumption less than 13.58 kW h/kg$_{LH2}$) is a little better than Ingolstadt is assumed here. Quack's process reports the best cycle exergy efficiency at 5.76 kW h/kg$_{LH2}$. The best plant in the USA today is reported to require 10 kW h/kg$_{LH2}$ [14], but it is not known where. A simulated 50 TPD large-scale Shimko plant, which is a helium refrigeration system with a hydrogen feed at 21 bars, is reported at 8.7 kW h/kg$_{LH2}$. The proposed large-scale MR system is 5.35 kW h/kg$_{LH2}$ as depicted. The ideal theoretical minimum value is 2.89 kW h/kg$_{LH2}$. For the process with LNG for pre-cooling studied by Kuendig et al. [1], the power consumption is reported by Kramer et al. [16] to be 4 kW h/kg$_{LH2}$. Thus, the overall

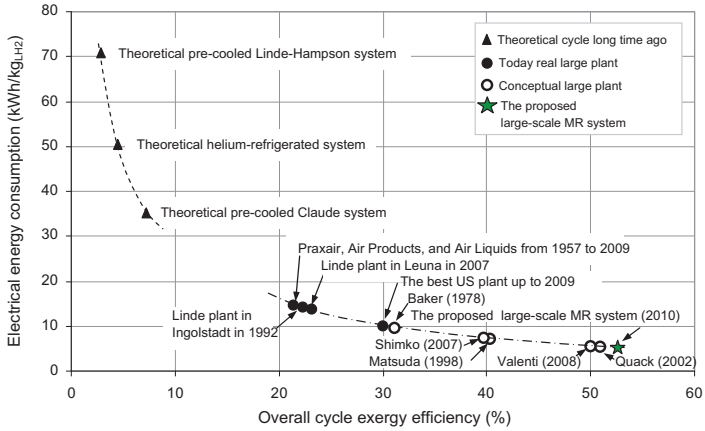

Fig. 7 – Comparison of hydrogen liquefaction process efficiencies by assuming that all processes are with uniform feed pressure equal to that of Ingolstadt plant at 21 bars.

efficiency, compared with the ideal process, is [(2.89 kW h/kg_{LH2})/(4 kW h/kg_{LH2})] × 100 = 72%, which is the highest with respect to all current systems. However, this is not shown in Fig. 7 because the process is cooled by free LNG, not by the system itself. Completely new approaches for low temperature refrigeration are magnetic refrigerators and acoustic refrigerators. Magneto caloric cooling may reduce liquefaction energy to 5.0 kW h/kg_{LH2} [22]; however, this may only be for small-scale to medium-scale plants. All of the literature related to magnetic cooling has been reorted on small-scale hydrogen plants. Nobody thinks such a system is realistic in large-scale systems.

7. Conclusion

Today large hydrogen liquefaction plants have exergy efficiencies of just 20–30%; thus, there is potential for improvement. From 1998 to 2008, some conceptual plants have been proposed with reported efficiencies of 40–50%. Finally, in the year 2010, NTNU and SINTEF Energy Research AS will propose a new MR system with an efficiency greater than 50%. Details of the proposed system will be reported in upcoming papers.

Acknowledgements

The author wishes to thank the Department of Energy and Process Engineering, Norwegian University of Science and Technology for a research fellow grant.

REFERENCES

[1] Kuendig A, Loehlein K, Kramer GJ, Huijsmans J. Large scale hydrogen liquefaction in combination with LNG re-gasification. Available from: http://www.cder.dz/A2H2/Medias/Download; 2006 [accessed 05.06.09].

[2] Matsuda H, Nagami M. Study of large hydrogen liquefaction process. Kanagawa, Japan: Nippon Sanso Corp. WE-NET: summary of annual reports. Available from: http://www.enaa.or.jp/WE-NET/ronbun/1997/e5/sanso1997.html; 1998 [accessed 05.06.09].

[3] Quack H. Conceptual design of a high efficiency large capacity hydrogen liquefier. Adv Cry Eng 2002;47:255–63.

[4] Kuzmenko IF, Morkovkin IM, Gurov EI. Concept of building medium-capacity hydrogen liquefiers with helium refrigeration cycle. Chem Pet Eng 2004;40(Nos: 1–2).

[5] Stang J, Neksa P, Brendeng E. On the design of an efficient hydrogen liquefaction process. WHEC 2006; 16/13–16 June 2006 – Lyon France.

[6] Shimko M, Gardiner M. Innovative hydrogen liquefaction cycle. Available from: http://www.hydrogen.energy.gov/pdfs/progress08/iii_7_shimko.pdf; 2007 [accessed 14.06.09].

[7] Valenti G. Proposal of an innovative, high-efficiency, large-scale hydrogen liquefier. Int J Hydrogen Energy 2008;33(12):3116–21.

[8] Dewar J. Liquid hydrogen. Science 1898;8(183):3–6.

[9] Barron RF. Cryogenic systems. Oxford, United Kingdom: Oxford University Press; 1966.

[10] Bracha M, Lorenz GA, Wanner M. Large-scale hydrogen liquefaction in Germany. Int J Hydrogen Energy 1994;19(1):53–9.

[11] Foerg W. History of cryogenics: the epoch of the pioneers from the beginning to the year 1911. Int J Refrig 2002;25(3):283–92.

[12] Timmerhaus KD, Flynn TM. Cryogenic process engineering. New York: Springer; 1989.

[13] Nandi TK, Sarangi S. Performance and optimization of hydrogen liquefaction cycles. Int J Hydrogen Energy 1993;18(2):131–9.

[14] Drnevich R. Hydrogen delivery – liquefaction & compression. Praxair, strategic initiatives for hydrogen delivery workshop – May 7, 2003. Available from: http://www1.eere.energy.gov/hydrogenandfuelcells/pdfs/liquefaction_comp_pres_praxair.pdf [accessed 20.5.09].

[15] Franser D. Solutions for hydrogen solutions for hydrogen storage and distribution by dynetek industries Ltd. The PEI Wind-Hydrogen Symposium June 22–24, 2003. Available from: http://www.gov.pe.ca/photos/original/dev_solutions.pdf [accessed 04.03.08].

[16] Kramer GJ, Huijsmans J, Austgen D. Clean and green hydrogen. 16th World hydrogen energy conference, 16/13–16

June 2006 – Lyon, France. Available from: http://www.shell.com/static/hydrogen-en/downloads/speeches/speech_clean_green_hydrogen_1.pdf [accessed 05.06.09].
[17] Mitsugi C, Harumi A, Kenzo F. WE-NET: Japanese hydrogen program. Int J Hydrogen Energy 1998;23(3):159–65.
[18] Beljakov V, Krakovsky BD, Popov OM. Low capacity hydrogen liquefier with helium cycle. In: Proc Cryogenics 2000; Praha: p. 158–61.
[19] Krewitt W, Schmid S. Common information database – fuel cell technologies and hydrogen production/distribution options. Available from: http://www.dlr.de/fk/Portaldata/40/Resources/dokumente/publikationen/2005-09-02_CASCADE_D1.1_fin.pdf; 2005 [accessed 14.06.09].
[20] Berstad D, Stang J, Neksa P. Comparison criteria for large-scale hydrogen liquefaction processes. Int J Hydrogen Energy 2009;34(3):1560–8.
[21] Baker CR, Shaner RL. A study of the efficiency of hydrogen liquefaction process. Int J Hydrogen Energy 1978;3(3):321–34.
[22] Dutton G. Hydrogen transitions – a UK perspective; 2003.

Krasae-in S, Stang J, Neksa P. Exergy analysis on the simulation of a small-scale hydrogen liquefaction test rig with a multi-component refrigerant refrigeration system. Int J Hydrogen Energy 2010;35(15):8030-42.

INTERNATIONAL JOURNAL OF HYDROGEN ENERGY 35 (2010) 8030–8042

Available at www.sciencedirect.com

ScienceDirect

journal homepage: www.elsevier.com/locate/he

Exergy analysis on the simulation of a small-scale hydrogen liquefaction test rig with a multi-component refrigerant refrigeration system

Songwut Krasae-in [a,*], *Jacob H. Stang* [b,1], *Petter Neksa* [b,2]

[a] *Norwegian University of Science and Technology, Kolbjorn Hejes vei 1d, NO-7491, Trondheim, Norway*
[b] *SINTEF Energy Research AS, Kolbjorn Hejes vei 1d, NO-7465, Trondheim, Norway*

ARTICLE INFO

Article history:
Received 11 March 2010
Received in revised form
8 May 2010
Accepted 9 May 2010
Available online 11 June 2010

Keywords:
Exergy efficiency
Hydrogen liquefier
Hydrogen liquefaction
Cryogenic process
Refrigeration

ABSTRACT

This study investigates the simulation of a proposed small-scale laboratory liquid hydrogen plant with a new, innovative multi-component refrigerant (MR) refrigeration system. The simulated test rig was capable of liquefying a feed of 2 kg/h of normal hydrogen gas at 21 bar and 25 °C to normal liquid hydrogen at 2 bar and −250 °C. The simulated power consumption for pre-cooling the hydrogen from 25 °C to −198 °C with this new MR cycle was 2.07 kWh/kg_{GH2} from the ideal minimum of 0.7755 kWh per kilogram of feed hydrogen gas. This was the lowest power consumption available when compared to today's conventional hydrogen liquefaction cycles, which are approximately 4.00 kWh/kg_{GH2}. Hence, the MR cycle's exergy efficiency was 38.3%. Exergy analysis of the test rig's cycle, which is required to find the losses and optimize the proposed MR system, was evaluated for each component using the simulation data. It was found that the majority of the losses were from the compressors, heat exchangers, and expansion valves. Suggestions are provided for how to reduce exergy in each component in order to reduce the exergy loss. Finally, further improvements for better efficiency of the test rig are explained to assist in the design of a future large-scale hydrogen liquefaction plant.

1. Introduction

Because hydrogen has shown promise as an important energy vector for use in future transportation vehicles, several hydrogen research projects have been conducted since 1980 and in particular, since 2000. One of the challenges in creating a hydrogen economy is the low efficiencies of the current hydrogen liquefaction plants' cycles. Currently, large hydrogen liquefaction plants, e.g., the plant in Ingolstadt as described by Bracha et al. [1], have exergy efficiencies of just 20–30%. These efficiencies are very low. The plant consumes 4.86 kWh per kilogram of hydrogen gas using a nitrogen refrigeration system to pre-cool normal hydrogen gas from 25 °C to equilibrium hydrogen gas at −198 °C. From 1998 through 2008, some conceptual plants were proposed with reportedly improved efficiencies of 40–50% [2–7]. A literature review for the development of large-scale hydrogen liquefaction processes throughout the world from 1898 to 2009 is given by Krasae-in et al. [8]. Finally, in the year 2010, the Norwegian University of Science and Technology (NTNU) and the Scandinavian Research Foundation (SINTEF) Energy Research AS proposed a new large-scale MR system with efficiency in

* *Corresponding author*. Tel.: +47 735 92991; fax: +47 735 97214.
E-mail addresses: songwut.krasaein@ntnu.no, krasaein@hotmail.com (S. Krasae-in), jacob.stang@sintef.no (J.H. Stang), petter.neksa@sintef.no (P. Neksa).
[1] Tel.: +47 735 98109.
[2] Tel.: +47 735 93923.

0360-3199/$ – see front matter © 2010 Professor T. Nejat Veziroglu. Published by Elsevier Ltd. All rights reserved.
doi:10.1016/j.ijhydene.2010.05.049

excess of 50%. Detailed results will be reported by the author in an upcoming paper.

Refrigeration systems thermodynamically release heat into the environment. The first law governs the conservation of energy only; it gives no information on how, where, and how much the system performance is degraded. Exergy analysis is a powerful tool in the design, optimization, and performance evaluation of energy systems. The principles and methodologies of exergy analysis are well established [9–14]. Exergy analysis of a complex system can be performed by analyzing the components of the system separately. Identifying the main sites of exergy destruction shows the direction for potential improvements.

Baker and Shaner [15] studied the exergy analysis of a hydrogen liquefaction system. Dincer and Rosen [16] and Chiu and Newton [17] conducted interesting discussions about the exergy analysis of cryogenic systems. Similarly, with a focus on the analysis of a hydrogen liquefaction cycle, Kanoglu [18] and Remeljej and Hoadley [19] presented methodologies for the exergy analysis of refrigeration cycles and obtained the minimum work relation for the liquefaction of natural gas.

Before the initial experiment, the test rig was redesigned and optimized by simulation and exergy analysis. In this paper, the operation of the small-scale laboratory liquid hydrogen plant is described first. Multi-component refrigerant was used in the cycle. This concept of a mixed refrigerant in gas liquefaction was discovered in the past few years and has resulted in reduced energy consumption compared to conventional liquefaction cycles. This reduction is similar to what was explained by Bottura [20], Chrz [21], and Mafi et al. [22], and Bosma and Nagelvoort [23]. The differences involve the new modified cycle and the new optimized refrigerant mixture that was specially designed for pre-cooling hydrogen gas from 25 °C to −198 °C. An exergy analysis was performed on the individual components in the cycle as well as on the entire cycle of the test rig. The coefficient of performance (COP) and second law efficiency for the entire cycle were obtained. Finally, a process is described for how to reduce exergy loss in each component and to obtain optimization of the minimum work required for the liquefaction process of the test rig—i.e., the specific objective of this paper.

2. System description

The simulation model was built in PRO/II. For the equation of state, Redlich–Kwong–Soave (SRK) was selected for use in this PRO/II simulation package because of its popularity, simplicity, and fast computation. Ortho–para conversion reactors were not included because the experimental rig could not contain the catalyst needed for the ortho–para conversion. The laboratory test rig pictured in Fig. 1 was designed by SINTEF Energy Research AS to use the MR containing more complex of composition. The concept of multi-component refrigerants (also known as mixed refrigerants) [20–23] has been widely used in the liquefaction of natural gas for decades because of the reduced energy consumption compared to other conventional liquefaction cycles. SINTEF has worked with this type of refrigeration cycles for several years. The novelty of this mixed refrigerant system is described very well by Flynn [24]. Before the startup of the rig, a decision was made to use a less complex refrigerant during the start up period. To help obtain a theoretically optimized refrigerant mix, a model of the liquefaction rig was made in the flow sheet of the PRO/II simulation program.

Table 1 contains design and assumption data. Ambient temperature, capacity, GH_2 feed, and LH_2 product were the design values. No pressure drop was assumed because the plant was a relatively small-scale system. Good low-temperature heat exchangers for cryogenic system were generally recommended by Barron [25] to have a 1–2 °C temperature approach. The compressors' efficiencies were estimated from the manufacturers' product catalogues, which generally contained small-size gas compressors. Hydrogen gas compression ratio was higher than that of MR gas, thus lower efficiency of H_2 compressor was assumed.

As shown in Fig. 1, feed hydrogen gas was first compressed from a suction pressure in a two-stage hydrogen piston compressor with inter- and after cooling. The outlet temperature of the aftercooler (both H_2 and MR circuit) was designed to be 25 °C. Next, the hydrogen was cooled in a series of 5 heat exchangers. In the first 4 heat exchangers, the hydrogen gas was cooled by the MR refrigeration system. In the last heat exchanger, the hydrogen gas was cooled by a liquid helium circuit. After cooling, a Joule–Thompson valve was used to throttle the hydrogen gas from 21 bar to 2 bar. Finally, most of hydrogen gas was liquefied to be 98% liquid hydrogen at stream 10 and 2% return flash hydrogen gas at stream 11.

The objective function was to minimize the MR compressor power by optimizing the following variables:

1. A suitable H_2 compressor discharge pressure:
The discharge pressure needed to be above 15 bar (supercritical pressure) to avoid condensation. For the test rig, the discharge pressure was designed to be 21 bar, equivalent to that of the feed at Ingolstadt. High feed pressures result in minimal work liquefaction as described by Matsuda and Nagami [2], Quack [3], and Valenti et al. [6] who used values of 50, 80, and 60 bar. On a larger scale, if the feed is 1–2 bar, it is recommended to compress the feed discharge to 21 bar instead of a higher value because of the increased energy requirement.

2. A suitable H_2 compressor suction pressure:
This pressure must be a slightly above ambient pressure (1 bar) to be kept in a liquid tank before supply. Ingolstadt uses 1.3 bar. For this test rig, the compressor suction pressure could be anywhere between 1.3 and 2 bar. For control simplicity, a value of 2 bar was selected.

3. A suitable MR compressor discharge pressure:
Several simulation trials were performed using PRO/II to determine an optimized composition for different suction pressures. An optimized and simplified 5-component mixture, consisting of 4% neon, 12% nitrogen, 26% methane, 30% ethane, and 28% butane, was satisfied with different suction and discharge MR pressures for all cases. The suitable MR compressor discharge pressure was 18 bar, which resulted in an MR compressor power of 4.55 kW. If the pressure was lower than that, e.g., 15, 16, or 17 bar, it was impossible for the MR system to cool the hydrogen.

In addition, a solid phase of the MR flow could form inside the heat exchangers if the pressure was much lower than

18 bar. However, if the discharge pressure was higher than 18 bar, the system would work, but it would result in a higher MR compressor power. Moreover, if the pressure was too high, there would be more exergy losses at the expansions valves: EX1, EX2, and EX3.

4. A suitable MR compressor suction pressure:
Too high or too low of a suction pressure would make it impossible to sufficiently cool down the hydrogen gas to a specified, designed temperature (−198 °C) flowing out of $\overline{HX}4$. The suitable pressure was 2 bar, which resulted in the minimum (theoretical) brake horse power (4.55 kW) of the MR compressor. The suction pressure could not be lower than 1 bar because it would result in a higher MR compressor power; additionally, it could not be higher than 2 bar because that would lead to a system that could not sufficiently cool down the hydrogen gas.

5. Hot-stream hydrogen outlet temperatures from HX1, HX2, HX3, HX4, and HX5:
Trial and error was used to find the optimum temperatures.

6. The suitable composition of the MR cycle:
Trial and error was performed to find the optimal composition. For simplicity, a reduced number of mixture components were used to complete the initial experiment as explained above. Thus, simulation of the test rig with the 5-component mixture was done first. After that, simulation of the test rig with a more complex 10-component mixture was also done to see the difference from the simplified 5-component mixture. The optimized complex MR composition, discovered through trial and error, was: 1.3% neon, 14.4% nitrogen, 14.4% methane, 16.1% R14, 17.1% ethane, 12.0% propene, 6.8% propane, 1.8% Ibutane, 8.7% butane, and 7.4% pentane. Simulation results of both 5-component and 10-component mixtures of the rig, as depicted in Fig. 1, are shown in Tables 3–5.

3. Analysis

All energy balance equations of all components, as depicted in Fig. 1, are shown in Table 5.

3.1. Heat removed from pre-cooling process

The heat removed from the hydrogen gas during the pre-cooling process from 25 °C to −198 °C in the test rig was determined by the following formula:

$$\dot{Q}_{\text{pre-cooling}} = \dot{m}_{H_2}(h_{\text{feed}} - h_{\text{pre-cooled}}) = \dot{m}_{H_2}(h_3 - h_7) \quad (1)$$

where $\dot{m}_{H_2}$ is the mass flow rate of hydrogen gas (kg/s), h_{feed} is the enthalpy of hydrogen gas at the feed (kJ/kg), which is at stream 3 (h_3), and $h_{\text{liquefied}}$ is the enthalpy of pre-cooled hydrogen (kJ/kg), which is at stream 7 (h_7). From the simulation of the test rig, $\dot{Q}_{\text{pre-cooling}} = 0.000571$ kg/s × (175.87 to −3038.81 kJ/kg) = 1.8356 kW, which was the same for both mixtures. For heat removed from the hydrogen gas during the liquefaction process, $h_{\text{liquefied}}$ was the enthalpy of liquefied hydrogen (kJ/kg) which was at stream 9 (h_9). Thus,

$$\dot{Q}_{\text{liquefaction}} = \dot{m}_{H_2}(h_{\text{feed}} - h_{\text{liquefied}}) = \dot{m}_{H_2}(h_3 - h_9) = 2.4949\ \text{kW}.$$

3.2. Energy efficiency (first law efficiency)

Coefficient of performance (COP) of the test rig may be expressed as:

$$\text{COP}_{\text{liquefaction}} = \eta_I = \frac{\dot{Q}_{\text{liquefaction}}}{\dot{W}_{BH,\ COM}} \quad (2)$$

$\dot{W}_{BH,\ COM} = \dot{W}_{BH,\ MR\ COM} + \dot{W}_{BH,\ H_2\ COM}$ was the brake horsepower of the test rig's compressors or the actual work rate input to the cycle (kW) that consisted of the compressor brake horsepower from both the MR compressor and the hydrogen compressor. Thus, COP of the test rig was $\text{COP}_{\text{liquefaction}} = \dot{Q}_{\text{liquefaction}}/\dot{W}_{BH,COM} = 2.4949\ \text{kW}/7.92\ \text{kW} = 0.3150$ for the 5-component mixture and 2.4949 kW/7.51 kW = 0.3322 for the 10-component mixture. COP of the MR cycle only was $\text{COP}_{\text{MR cycle}} = \dot{Q}_{\text{pre-cooling}}/\dot{W}_{BH,\ MR\ COM} = 1.8356\ \text{kW}/4.55\ \text{kW} = 0.4034$ for the 5-component mixture and 1.8356 kW/4.1426 kW = 0.4431 for the 10-component mixture.

3.3. Exergy efficiency (second law efficiency)

The exergy efficiency for the liquefaction process of the test rig maybe defined as:

$$\epsilon = \eta_{II} = \frac{\dot{W}_{\text{min, cycle}}}{\dot{W}_{BH,\ COM}} = \frac{\dot{W}_{BH,\ COM} - \dot{I}_{\text{total}}}{\dot{W}_{BH,\ COM}} = \frac{\dot{W}_{BH,\ COM} - (\dot{E}_{x,\ \text{in}} - \dot{E}_{x,\ \text{out}})}{\dot{W}_{BH,\ COM}} \quad (3)$$

where $\dot{W}_{\text{min, cycle}}$ is the minimum work rate input to the test rig's cycle (kW). For η_{II}, the analysis is given in Section 4.1, Results. The ideal minimum power consumption to pre-cool normal hydrogen gas from 25 °C to −198 °C at 2 kg/h and 21 bar was the ideal minimum power consumption of the MR cycle: $\dot{W}_{\text{min, MR cycle}} = \dot{E}_{x,\ 7} - \dot{E}_{x,\ 3} = 1.59$ kW. Exergy efficiency of the MR refrigeration cycle only was $\eta_{II,\ MR\ \text{cycle}} = \dot{W}_{\text{min, MR cycle}}/\dot{W}_{BH,\ MR\ COM} = 1.59\ \text{kW}/4.55\ \text{kW} = 0.3494$ for the 5-component mixture and 1.59 kW/4.1426 kW = 0.3838 for the 10-component mixture.

3.4. System exergy analysis of the test rig

The easiest approach to a thermodynamic analysis of a system is to introduce exergy as additional information for each state point. Exergy, the maximal available specific work (kJ/kg), is defined as:

$$e_x = h - Ts \quad (4)$$

where h is the enthalpy (kJ/kg), T is the temperature (K), s is the entropy (kJ/kg-K). Otherwise:

$$de_x = dh - Tds \quad (5)$$

or, integrated:

$$e_x = (h - h_o) - T_o(s - s_o) \quad (6)$$

where e_x is the specific exergy or the maximum available specific work (kJ/kg) that can be obtained from a periodic process between a state and the ambient condition or reference state. Usually, the reference state at ambient condition is at 1 bar, 25 °C (≈300 K) for the values of h_o, T_o and s_o. In general, when substituting values into Eq. (6), T_o is replaced by 300 K, not 25 °C, although any conditions, temperatures, or pressures can be inserted, given the user's specifications. As shown in Tables

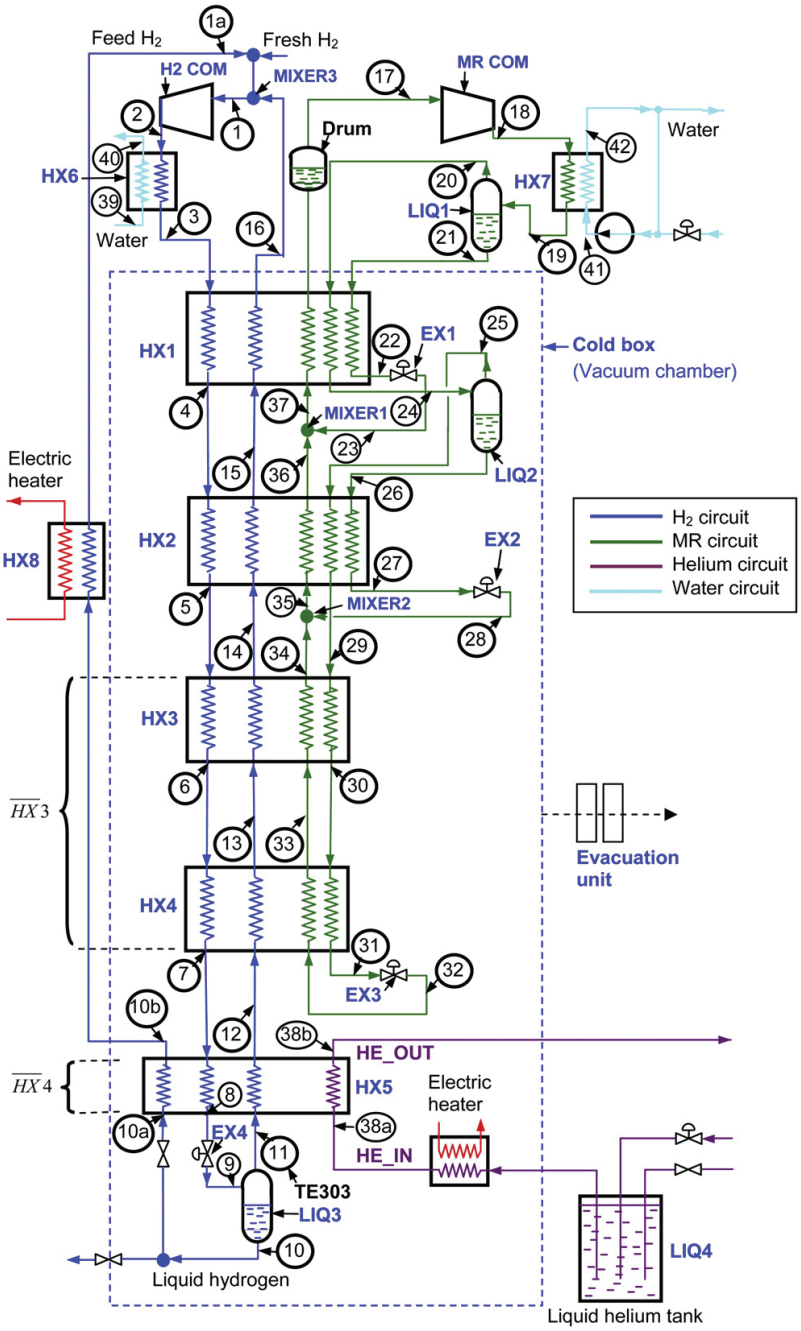

Fig. 1 – Schematic diagram of the laboratory MR hydrogen liquefaction system.

3 and 4, 25 °C was the ambient temperature where specific exergy (or maximum available specific work or stream exergy flow as in (Eqs. (4) and (7)) was assumed to be zero. This setting was used for comparison (as shown in Table 2) with other conventional systems that all use specified reference temperatures of 25 °C. In fact, when the reference temperature was varied, the exergy efficiency remained the same. However, if ambient temperature was increased, then exergy efficiency

Table 1 – Boundary conditions of the test rig's simulation.

Parameter	The test rig's process from the simulation
Ambient temperature	25 °C
Capacity of liquefied hydrogen	2 kg/h
GH_2 feed	1 bar and 25 °C
LH_2 product	2.0 bar, saturated liquid normal hydrogen
Pressure drop in system	No
Temperature approach in heat exchangers Isentropic efficiency:	1–2 °C (arbitrarily selected for high effectiveness)
H_2 compressor	65% (selected similar to actual machinery)
MR compressor	70% (selected similar to actual machinery)

decreased because less heat rejection at the condenser (HX7) resulted in a higher MR compressor power consumption.

Then:

$$\dot{E}_x = \dot{m} e_x \tag{7}$$

$\dot{E}_x$ = stream exergy flow (kW) and $\dot{m}$ is the mass flow rate (kg/s) of the stream. For the whole system as well as its individual parts, thermodynamic efficiencies can be calculated as ratios of the minimum exergy necessary to the exergy actually applied. For a system analysis, however, it was more reasonable to calculate the exergy loss occurring in a component and to compare it to the exergy input to the system. For the hydrogen liquefier test rig considered, an exergy flow diagram was plotted showing the exergy losses. Heat leaks into the liquefier were not taken into account.

Fig. 2 depicts a simple exergy flow diagram of the test rig system. The power input into the electric motor drives of the H_2 compressor and the MR compressor is only part of the exergy input to the liquefier. We assumed that other electrical devices, such as fan motors, air blowers, and water pumps, were relatively small compared to the two compressors. The percentage of the total exergy input was therefore given. Additionally, there were only three throttling valves within the plant causing a small loss, namely the Joule–Thomson valve in the cooling cycle. The exergy losses in the "cold box", a vacuum chamber (as depicted in Figs. 1 and 2) that contains low-temperature heat exchangers, liquid separators, expansion valves, and mixers, are due to inefficiencies of the heat exchangers, valves, separators, mixers, and the process itself.

A large amount of the overall exergy was dissipated (see Fig. 2 for each component) due to inefficiencies of the following components:

1. Compressors: H_2 COM, and MR COM
2. Gas cooler: HX7
3. Liquid separators: LIQ1, LIQ2, and LIQ3
4. Heat exchangers: HX1, HX2, HX3, HX4, and HX5
5. Expansion valves: EX1, EX2, and EX3
6. Mixers: MIXER1, MIXER2, and MIXER3.

Fig. 2 shows that a major part of the losses was due to the process design and would occurred even if ideal heat exchangers were used. Therefore, the total exergy destruction in the cycle was simply the sum of the exergy destructions described above and can be expressed by the following equation:

$$\dot{I}_{\text{total}} = \dot{E}_{x,\ \text{in}} - \dot{E}_{x,\ \text{out}} \tag{8}$$

For this case, $\dot{W}_{BH,\ COM} = \dot{E}_{x,\ \text{in}}$ and for this test rig, $\dot{E}_{x,\ 10b} = \dot{E}_{x,\ \text{out}}$. Thus,

$$\begin{aligned}\dot{I}_{\text{total}} = {} & \left(\dot{I}_{H2\ COM} + \dot{I}_{MR\ COM}\right) + \left(\dot{I}_{LIQ1} + \dot{I}_{LIQ2} = \dot{I}_{LIQ3}\right) \\ & + \left(\dot{I}_{EX1} + \dot{I}_{EX2} + \dot{I}_{EX3}\right) + \left(\dot{I}_{HX1} + \dot{I}_{HX2} + \dot{I}_{HX3} + \dot{I}_{HX4}\right) \\ & + \left(\dot{I}_{MIXER1} + \dot{I}_{MIXER2} + \dot{I}_{MIXER3}\right)\end{aligned} \tag{9}$$

In conclusion, the calculation of exergy losses was a very powerful means of identifying the sources of irreversibility, their portion of the total loss, the potential for improvement, and their effect on power input and operating costs of the plant.

4. Results and discussion

4.1. Results

First, the specific exergy and exergy flow were calculated from the simulation results of each stream as shown in Tables 3 and 4. In these two tables, it is noted that the reference state of hydrogen is the feed at 2 bar and 25 °C; thus, $h_o = 171.30$ kJ/kg and $s_o = 85.84$ kJ/kg-K. The reference state of the MR side was stream 19 at 18 bar and 25 °C; thus, $h_o = 348.04$ kJ/kg and $s_o = 9.24$ kJ/kg-K. For cooling water circuit, at streams 41 and 42, and the reference state was at 1 bar and 25 °C; thus, $h_o = 105.65$ kJ/kg and $s_o = 0.37$ kJ/kg-K. Stream numbers 2, 6, 13, 30, 33, 38a, 38b, 39, and 40 were blank and were not included in the calculation because they were not needed. The calculation of irreversibility/exergy loss of each component is shown in Table 5.

The liquefier can be operated by making the MR refrigerant more complex. Complex components mean that there are more components in the mixture than are found with simplified components of mixture. From Table 5, with change from the 5-component mixture to the 10-component mixture, exergy losses were reduced in most of the components. This reduction was especially evident in the decreased losses at the heat exchangers (HX1, HX2, and $\overline{HX}3$) due to the reduction in the temperature difference between the pre-cooling hydrogen gas and the complex MR refrigerant. This improved temperature difference allowed adaptation to the pre-cooling curve, absorption of more heat, and better boiling heat-transfer properties than the simplified mixture. The reduction in exergy loss at the MR compressor was also due to the lower complex–mixture-MR flow rate needed in the cycle. Finally, the actual work was 7.51 kW, and the liquefier exergy efficiency was 21.06%. This result demonstrates a slight improvement in exergy efficiency. Note that $\dot{W}_{BH,\ COM} = \dot{W}_{\min,\ \text{cycle}} + (\dot{I}_{\text{total}} + \dot{I}_{\text{unknown}})$, or 7.51 kW = 1.59 kW + (5.4195 kW + 0.5005 kW). In short, there was a potential improvement for the overall system efficiency when using the proposed complex 10-component mixture compared to the simplified 5-component mixture.

In Table 4, the simulation data from PRO/II is collected. The return flash hydrogen gas stream (stream 11) was relatively small compared to the main feed (stream 3). Thus, the ideal minimum

Table 2 – Comparison of the energy and exergy efficiencies of an MR refrigeration system with other conventional and conceptual refrigeration systems.

Refrigeration systems	Inventor	Energy consumption	Energy efficiency	Exergy efficiency
MR refrigeration	Propose in this paper	2.07 kWh/kg_{GH2}	44.3%	38.3%
N_2 refrigeration	Matsuda and Nagami [2]	≈4.00 kWh/kg_{GH2}	≈22.3%	≈19.4%
	Ingolstadt plant in 1992 by Bracha et al. [1]	4.00 kWh/kg_{GH2}	22.3%	19.4%
	Leuna plant in 2007 [8]	≈4.00 kWh/kg_{GH2}	≈22.3%	≈19.4%
	Praxair since 1957 [8]	≈4.00 kWh/kg_{GH2}	≈22.3%	≈19.4%
Helium refrigeration	Valenti et al. [6]	A lot higher than 4.00 kWh/kg_{GH2}	A lot lower than 22.3%	A lot lower than 19.4%
	Shimko and Gardiner [5]	Higher than 4.00 kWh/kg_{GH2}	Lower than 22.3%	Lower than 19.4%
Propane + helium refrigeration	Quack [3]	Higher than 4.00 kWh/kg_{GH2}	Lower than 22.3%	Lower than 19.4%

energy consumption to cool down a single feed through normal hydrogen gas from 21 bar to 25 °C to normal hydrogen gas at −193 °C at the same pressure was $w_{MR\ cycle,\ ideal} = e_{x,\ 7} - e_{x,\ 3} =$ 2791.84 kJ/kg_{GH2} = 0.7755 kWh/kg_{GH2}. The ideal minimum energy consumption to further cool the hydrogen down to −253 °C was $w_{Helium,\ ideal} = e_{x,\ 8} - e_{x,\ 7} =$ 7210.20 kJ/kg_{GH2} = 2.07 kWh/kg_{GH2} as shown in Fig. 3.

Table 2 shows that the efficiency and energy consumption of the proposed 10-component MR system (used to pre-cool normal hydrogen gas at 21 bar from 25 °C to be −198 °C of normal hydrogen gas at the same pressure) were less than other conventional (Ingolstant, Leuna, and Praxair) and conceptual (Matsuda, Valenti, Shimko, and Quack) pre-cooling systems. The feed pressure of every refrigeration system was the same at 21 bar and 25 °C. In the table, Valenti's, Shimko's, and Quack's cycles, which were simulated in PRO/II by the author, have higher energy consumptions than 4.00 kWh/kg_{GH2}. The proposed MR system had a lower energy consumption (2.07 kWh/kg_{GH2}) and a higher exergy efficiency (38.3%) relative to the ideal minimum of 0.7755 kWh/kg_{GH2} (ηII, MR cycle = $w_{MR\ cycle,\ ideal}/w_{BH,\ MR\ COM}$ = 0.7755 kWh/kg GH2/2.07 kWh/kg_{GH2} ≈ 0.383). This system offered the best performance when compared to the aforementioned conventional and conception systems. For example, the conventional system had an exergy efficiency of 19.4%. It was assumed that 4.00 kWh/kg_{GH2} was the approximate amount of required energy as simulated in PRO/II by the author. Ortho–para conversion was not included. Actually, at the Ingolstadt plant (as reported by Bracha et al. [1] and recalculated by Kuzmenko et al. [4]), 4.86 kWh/kg_{GH2} was the amount of energy required, including ortho–para conversion. Specific heat removal from the pre-cooling process was $\dot{Q}_{pre-cooling}/\dot{m}_{H_2} = (h_{feed} - h_{pre-cooled}) = (h_3 - h_7) =$ 3214.68 kJ/kg_{GH2} = 0.8929 kWh/kg_{GH2}. Thus, energy efficiency of the MR cycle was 44.3%, whereas the conventional cycle at the Ingolstadt plant had an efficiency of 22.3%. This result indicates that at the same refrigeration or pre-cooling load, the power consumption of the MR cycle was around half that of the conventional cycle. This finding corresponds to the energy consumptions shown in the table. In short, a comparison

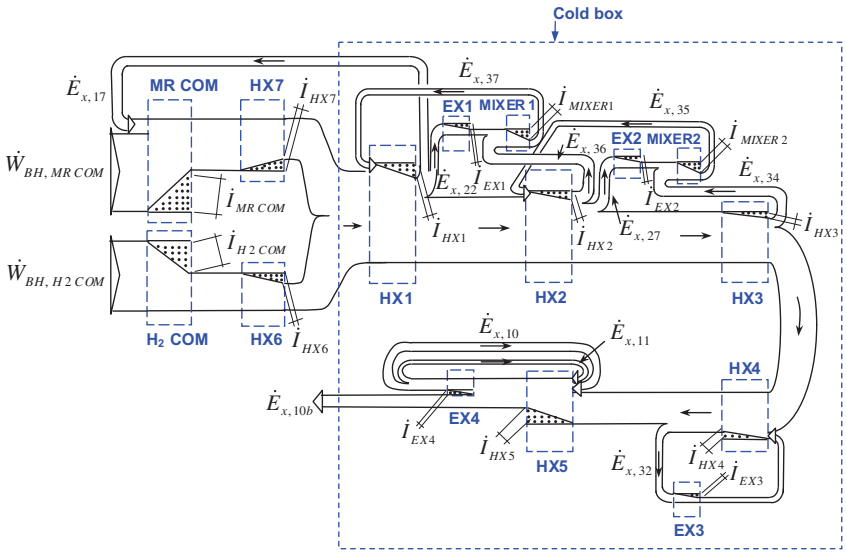

Fig. 2 – Exergy flow diagram of the system.

Table 3 – Thermodynamic properties of each stream: enthalpy, entropy, specific exergy, and exergy flow of the proposed simplified 5-component mixture.

Stream number	Pressure P	Temp. T	Flow rate $\dot{m}$	Enthalpy h	Entropy s	Exergy e_x	Exergy flow $\dot{E}_x$	Phase	Description
	(bar)	(C)	(kg/s)	(kJ/kg)	(kJ/kg-K)	(kJ/kg)	(kW)		
1	2	24.6	0.000571	165.79	85.82	0.04	0.00	Superheated vapor	H_2 cool gas
1a	2	25.0	0.000556	171.30	85.84	0.00	0.00	Superheated vapor	H_2 cool gas
2									
3	21	25.0	0.000571	175.87	76.12	2921.68	1.67	Superheated vapor	H_2 cool gas
4	21	−46.1	0.000571	−837.64	72.23	3073.19	1.75	Superheated vapor	H_2 cold gas
5	21	−103.1	0.000571	−1650.18	68.11	3497.42	2.00	Superheated vapor	H_2 cold gas
6									
7	21	−198.1	0.000571	−3038.81	56.09	5713.52	3.26	Superheated vapor	H_2 cold gas
8	21	−250.0	0.000571	−4193.52	28.21	12 923.72	7.38	Superheated vapor	H_2 cold gas
9	2	−250.2	0.000571	−4193.52	29.30	12 596.59	7.19	Mixture	H_2 cold mixture
10	2	−250.2	0.000556	−4206.16	28.75	12 749.28	7.09	Saturated liquid	H_2 cold liquid
10a	2	−250.2	0.000556	−4206.16	28.75	12 749.28	7.09	Saturated liquid	H_2 cold liquid
10b	2	−201.8	0.000556	−3038.81	65.60	2860.63	1.59	Superheated vapor	H_2 cold gas
11	2	−250.2	0.000016	−3744.47	48.88	7172.87	0.11	Superheated vapor	H_2 cold gas
12	2	−201.8	0.000016	−3038.81	65.59	2866.19	0.04	Superheated vapor	H_2 cold gas
13									
14	2	−107.2	0.000016	−1678.36	77.68	599.29	0.01	Superheated vapor	H_2 cold gas
15	2	−53.8	0.000016	−945.19	81.49	187.96	0.00	Superheated vapor	H_2 cold gas
16	2	10.9	0.000016	−29.66	85.15	6.18	0.00	Superheated vapor	H_2 cold gas
17	2	10.9	0.016818	319.52	8.98	51.62	0.87	Superheated vapor	MR cold gas
18	18	158.7	0.016818	590.32	9.21	253.08	4.26	Superheated vapor	MR hot gas
19	18	25.0	0.016818	213.14	8.12	202.12	3.40	Saturated liquid	MR warm liquid
20	18	25.0	0.011543	282.90	8.59	130.02	1.50	Saturated vapor	MR warm gas
21	18	25.0	0.005274	60.46	7.08	359.91	1.90	Saturated liquid	MR warm liquid
22	18	−46.1	0.005274	−106.68	6.45	384.08	2.03	Compressed liquid	MR cold liquid
23	2	−50.4	0.005274	−106.68	6.47	378.67	2.00	Mixture	MR cold mixture
24	18	−46.1	0.011543	−40.51	7.36	175.93	2.03	Superheated vapor	MR cold mixture
25	18	−46.1	0.005505	54.06	8.29	−9.30	−0.05	Mixture	MR cold gas
26	18	−46.1	0.006038	−126.74	6.51	344.81	2.08	Saturated liquid	MR cold liquid
27	18	−103.1	0.006038	−256.73	5.85	412.34	2.49	Compressed liquid	MR cold liquid
28	2	−106.3	0.006038	−256.73	5.87	405.76	2.45	Mixture	MR cold mixture
29	18	−103.1	0.005505	−209.91	6.95	130.69	0.72	Superheated vapor	MR cold gas
30									
31	2	−198.1	0.005505	−579.65	3.94	664.32	3.66	Saturated liquid	MR cold liquid
32	2	−199.7	0.005505	−579.65	4.03	635.38	3.50	Mixture	MR mixture
33									
34	2	−105.8	0.005505	−69.70	8.40	−163.28	−0.90	Superheated vapor	MR cold gas
35	2	−102.8	0.011543	−167.53	7.08	132.66	1.53	Mixture	MR cold gas
36	2	−53.8	0.011543	65.57	8.30	0.32	0.00	Superheated vapor	MR cold gas
37	2	−53.4	0.016818	11.55	7.73	118.90	2.00	Mixture	MR cold mixture
38a, b									
39, 40									
41	1	25.0	0.002229	105.65	0.37	0.00	0.00	Compressed liquid	Liquid water
42	1	150.0	0.002229	2775	7.619	494.65	0.50	Superheated vapor	Hot steam

between energy and exergy efficiencies (as shown in Eq. (2) and Eq. (3)) highlighted the importance of exergy and showed that the exergy efficiency indicated the proximity to the ideal minimum, whereas the energy efficiency did not.

From Table 5, for the 5-component mixture, the majority of exergy losses were from the H_2 compressor and aftercooler, $\overline{HX}4$, the MR compressor, HX1, $\overline{HX}3$, HX7, EX3, and HX2. The large loss from $\overline{HX}4$ occurred because this was not the correct way to cool down the hydrogen gas. The temperature difference between the pre-cooling hot-stream hydrogen gas and the cold, liquid helium from LIQ4 was very large. HX1, HX2, and $\overline{HX}3$, however, performed very well and produced little exergy loss. Note that $\dot{W}_{BH,\ MR\ COM} = \dot{W}_{min,\ cycle} + (\dot{I}_{total} + \dot{I}_{unknown})$, or 7.92 kW = 1.59 kW + (5.8490 kW + 0.491 kW). Finally, the minimum liquefaction work, $\dot{W}_{min,\ cycle} = \dot{X}_{10b} - \dot{X}_{1a}$, was 1.59 kW; the actual work, $\dot{W}_{BH,\ COM} = \dot{W}_{BH,\ MR\ COM} + \dot{W}_{BH,\ H_2\ COM}$, was 7.92 kW; and the liquefier second law or exergy efficiency, $\eta_{II} = (\dot{W}_{min,\ cycle}/\dot{W}_{BH,\ COM}) \times 100\%$, was 20.06%.

4.2. *Comments on how to reduce exergy loss in each component*

1. Hydrogen compressor and MR compressor (shown in numbers by PRO/II in Table 6):

Table 4 – Thermodynamic properties of each stream: enthalpy, entropy, specific exergy, and exergy flow of the proposed 10-component mixture.

Stream number	Pressure P (bar)	Temp. T (C)	Flow rate $\dot{m}$ (kg/s)	Enthalpy h (kJ/kg)	Entropy s (kJ/kg-K)	Exergy e_x (kJ/kg)	Exergy flow $\dot{E}_x$ (kW)	Phase	Description
1	2	25.0	0.000571	171.14	85.84	0.00	0.00	Superheated vapor	H_2 cool gas
1a	2	25.0	0.000556	171.30	85.84	0.00	0.00	Superheated vapor	H_2 cool gas
2									
3	21	25.0	0.000571	175.87	76.12	2921.68	1.67	Superheated vapor	H_2 cool gas
4	21	−46.1	0.000571	−837.64	72.23	3073.19	1.76	Superheated vapor	H_2 cold gas
5	21	−103.1	0.000571	−1650.18	68.11	3497.42	2.00	Superheated vapor	H_2 cold gas
6									
7	21	−198.1	0.000571	−3038.81	56.09	5713.52	3.26	Superheated vapor	H_2 cold gas
8	21	−250.0	0.000571	−4193.52	28.21	12 923.72	7.38	Superheated vapor	H_2 cold gas
9	2	−250.2	0.000571	−4193.52	29.30	12 596.59	7.20	Mixture	H_2 cold mixture
10	2	−250.2	0.000556	−4206.16	28.75	12 749.28	7.08	Saturated liquid	H_2 cold liquid
10a	2	−250.2	0.000556	−4206.16	28.75	12 749.28	7.08	Saturated liquid	H_2 cold liquid
10b	2	−201.9	0.000556	−3038.81	65.59	2866.19	1.59	Superheated vapor	H_2 cold gas
11	2	−250.2	0.000016	−3744.47	48.88	7172.87	0.11	Superheated vapor	H_2 cold gas
12	2	−201.9	0.000016	−3038.81	65.59	2866.19	0.04	Superheated vapor	H_2 cold gas
13									
14	2	−107.2	0.000016	−1698.12	77.56	615.10	0.01	Superheated vapor	H_2 cold gas
15	2	−58.5	0.000016	−1011.20	81.19	213.23	0.00	Superheated vapor	H_2 cold gas
16	2	24.5	0.000016	165.39	85.82	0.04	0.00	Superheated vapor	H_2 cold gas
17	2	24.5	0.019929	263.40	6.66	37.68	0.75	Superheated vapor	MR cold gas
18	18	166.1	0.019929	471.27	6.84	193.37	3.85	Superheated vapor	MR hot gas
19	18	25.0	0.019929	173.77	5.99	149.08	2.97	Saturated liquid	MR warm liquid
20	18	25.0	0.015497	207.69	5.81	238.31	3.69	Saturated vapor	MR warm gas
21	18	25.0	0.004432	55.18	6.64	−162.90	−0.72	Saturated liquid	MR warm liquid
22	18	−46.1	0.004432	−101.74	6.04	−140.21	−0.62	Compressed liquid	MR cold liquid
23	2	−50.4	0.004432	−101.74	6.06	−145.17	−0.64	Mixture	MR cold mixture
24	18	−46.1	0.015497	−33.68	4.89	273.69	4.24	Superheated vapor	MR cold mixture
25	18	−46.1	0.008085	32.83	4.67	403.77	3.26	Mixture	MR cold gas
26	18	−46.1	0.007412	−106.23	5.12	131.80	0.98	Saturated liquid	MR cold liquid
27	18	−103.1	0.007412	−215.16	4.57	188.27	1.40	Compressed liquid	MR cold liquid
28	2	−106.3	0.007412	−215.16	4.58	182.79	1.35	Mixture	MR cold mixture
29	18	−103.1	0.008085	−139.35	3.79	497.69	4.02	Superheated vapor	MR cold gas
30									
31	2	−198.1	0.008085	−349.49	2.09	798.29	6.45	Saturated liquid	MR cold liquid
32	2	−198.4	0.008085	−349.49	2.11	789.59	6.38	Mixture	MR mixture
33									
34	2	−107.2	0.008085	−43.84	4.69	323.87	2.62	Superheated vapor	MR cold gas
35	2	−105.0	0.015497	−125.78	4.64	255.69	3.96	Mixture	MR cold gas
36	2	−58.3	0.015497	45.41	5.53	158.93	2.46	Superheated vapor	MR cold gas
37	2	−55.6	0.019929	12.69	5.65	90.62	1.81	Mixture	MR cold mixture
38a, b									
39, 40									
41	1	25.0	0.002229	105.65	0.37	0.00	0.00	Compressed liquid	Liquid water
42	1	150.0	0.002229	2775.00	7.62	494.65	0.50	Superheated vapor	Hot steam

- Reduce the suction temperature. From experience, (which can also be verified by calculations) the compressor power is also reduced when the suction temperature is reduced. In this test rig, the hydrogen feed temperature was decreased by turning off the HX8 electric heater. The hydrogen recycled temperature and MR suction temperature were reduced by designing the right MR composition. The right composition, e.g., enough ethane inside the MR cycle, requires enough to boil and cool down HX2 and finally, HX1. Sufficient methane and neon are needed to cool down HX4 and HX3. If all heat exchangers can be cooled down low enough, then the temperature of the suction compressors will be low. Moreover, discharge temperature will also decrease, resulting in the reduction of compressor fatigue, corrosion, and temperature, thereby extending compressor life.
- Reduce or increase the term of equation: $\dot{I}_{MR\ COM} = \dot{E}_{x,\ 17} - \dot{E}_{x,\ 18} + \dot{W}_{BH,\ MR\ COM}$. From the equation, when the suction temperature is reduced, $\dot{E}_{x,\ 17}$ is reduced. Reduction of the suction temperature causes a reduction in $\dot{W}_{BH,\ MR\ COM}$. For the reasons mentioned above, irreversibility (or loss) is decreased.
- Decrease the mass flow rate. Because the largest exergy loss (compared to other losses) is at the compressor, reducing the mass flow rate or making a smaller compressor will reduce the power consumption and exergy loss. For this

Table 5 – Calculation of exergy loss in each process's component of the 5-component and the 10-component mixtures.

Component	Energy equation	Exergy equation	5-component mixture		10-component mixture	
			$\dot{I}$	Percent loss	$\dot{I}$	Percent loss
			(kW)	%	(kW)	%
MR COM	$\dot{W}_{BH,\ MR\ COM} = \dot{m}_{17}(h_{18} - h_{17})$	$\dot{I}_{MR\ COM} = \dot{E}_{x,\ 17} - \dot{E}_{x,\ 18} + \dot{W}_{BH,\ MR\ COM}$	1.1662	19.94	1.0392	19.18
H_2 COM	$\dot{W}_{BH,\ H_2\ COM} = \dot{m}_1(h_2 - h_1)$	$\dot{I}_{H_2\ COM} = \dot{E}_{x,\ 1} - \dot{E}_{x,\ 3} + \dot{W}_{BH,\ H_2\ COM}$	1.7012	29.09	1.7012	31.39
HX1	$\dot{m}_3h_3 + \dot{m}_{15}h_{15} + \dot{m}_{37}h_{37} + \dot{m}_{20}h_{20} + \dot{m}_{21}h_{21} = \dot{m}_4h_4 + \dot{m}_{16}h_{16} + \dot{m}_{17}h_{17} + \dot{m}_{24}h_{24} + \dot{m}_{22}h_{22}$	$\dot{I}_{HX1} = (\dot{E}_{x,\ 3} + \dot{E}_{x,\ 15} + \dot{E}_{x,\ 37} + \dot{E}_{x,\ 20} + \dot{E}_{x,\ 21}) - (\dot{E}_{x,\ 4} + \dot{E}_{x,\ 16} + \dot{E}_{x,\ 17} + \dot{E}_{x,\ 24} + \dot{E}_{x,\ 22})$	0.3905	6.68	0.3228	5.96
HX2	$\dot{m}_4h_4 + \dot{m}_{14}h_{14} + \dot{m}_{35}h_{35} + \dot{m}_{25}h_{25} + \dot{m}_{26}h_{26} = \dot{m}_5h_5 + \dot{m}_{15}h_{15} + \dot{m}_{36}h_{36} + \dot{m}_{29}h_{29} + \dot{m}_{27}h_{27}$	$\dot{I}_{HX2} = (\dot{E}_{x,\ 4} + \dot{E}_{x,\ 14} + \dot{E}_{x,\ 35} + \dot{E}_{x,\ 25} + \dot{E}_{x,\ 26}) - (\dot{E}_{x,5} + \dot{E}_{x,\ 15} + \dot{E}_{x,\ 36} + \dot{E}_{x,\ 29} + \dot{E}_{x,\ 27})$	0.1133	1.94	0.0856	1.58
$\overline{HX}3$	$\dot{m}_5h_5 + \dot{m}_{12}h_{12} + \dot{m}_{32}h_{32} + \dot{m}_{29}h_{29} = \dot{m}_7h_7 + \dot{m}_{14}h_{14} + \dot{m}_{34}h_{34} + \dot{m}_{31}h_{31}$	$\dot{I}_{\overline{HX}3} = (\dot{E}_{x,\ 5} + \dot{E}_{x,\ 12} + \dot{E}_{x,\ 32} + \dot{E}_{x,\ 29}) - (\dot{E}_{x,\ 7} + \dot{E}_{x,\ 14} + \dot{E}_{x,\ 34} + \dot{E}_{x,\ 31})$	0.2290	3.92	0.1043	1.93
$\overline{HX}4$	$\dot{m}_{10a}h_{10a} + \dot{m}_7h_7 + \dot{m}_{11}h_{11} + \dot{m}_{38a}h_{38a} = \dot{m}_{10b}h_{10b} + \dot{m}_8h_8 + \dot{m}_{12}h_{12} + \dot{m}_{38b}h_{38b}$	$\dot{I}_{\overline{HX}4} = (\dot{E}_{x,\ 10a} + \dot{E}_{x,\ 7} + \dot{E}_{x,\ 11} + \dot{E}_{x,\ 38a}) - (\dot{E}_{x,\ 10b} + \dot{E}_{x,\ 8} + \dot{E}_{x,\ 12} + \dot{E}_{x,\ 38b})$	1.4483	24.76	1.4395	26.56
HX7	$\dot{m}_{18}h_{18} + \dot{m}_{41}h_{41} = \dot{m}_{19}h_{19} + \dot{m}_{42}h_{42}$	$\dot{I}_{HX7} = (\dot{E}_{x,\ 18} + \dot{E}_{x,\ 41}) - (\dot{E}_{x,\ 19} + \dot{E}_{x,\ 42})$	0.3570	6.10	0.3827	7.06
LIQ1	$\dot{m}_{19}h_{19} = \dot{m}_{20}h_{20} + \dot{m}_{21}h_{21}$	$\dot{I}_{LIQ1} = (\dot{E}_{x,\ 20} + \dot{E}_{x,\ 21}) - \dot{E}_{x,\ 19}$	0.0002	0.00	0.0000	0.00
LIQ2	$\dot{m}_{24}h_{24} = \dot{m}_{25}h_{25} + \dot{m}_{26}h_{26}$	$\dot{I}_{LIQ2} = (\dot{E}_{x,\ 25} + \dot{E}_{x,\ 26}) - \dot{E}_{x,\ 24}$	0.0001	0.00	0.0000	0.00
LIQ3	$\dot{m}_9h_9 = \dot{m}_{10}h_{10} + \dot{m}_{11}h_{11}$	$\dot{I}_{LIQ3} = (\dot{E}_{x,\ 11} + \dot{E}_{x,\ 10}) - \dot{E}_{x,\ 9}$	0.0078	0.13	0.0000	0.00
EX1	$h_{22} = h_{23}$	$\dot{I}_{EX1} = \dot{E}_{x,\ 22} - \dot{E}_{x,\ 23}$	0.0285	0.49	0.0220	0.41
EX2	$h_{27} = h_{28}$	$\dot{I}_{EX2} = \dot{E}_{x,\ 27} - \dot{E}_{x,\ 28}$	0.0397	0.68	0.0406	0.75
EX3	$h_{31} = h_{32}$	$\dot{I}_{EX3} = \dot{E}_{x,\ 31} - \dot{E}_{x,\ 32}$	0.1593	2.72	0.0703	1.30
EX4	$h_8 = h_9$	$\dot{I}_{EX3} = \dot{E}_{x,\ 8} - \dot{E}_{x,\ 9}$	0.1868	3.19	0.1868	3.45
MIXER1	$\dot{m}_{23}h_{23} + \dot{m}_{36}h_{36} = \dot{m}_{37}h_{37}$	$\dot{I}_{MIXER\ 1} = \dot{E}_{x,\ 36} + \dot{E}_{x,\ 23} - \dot{E}_{x,\ 37}$	0.0011	0.02	0.0135	0.25
MIXER2	$\dot{m}_{28}h_{28} + \dot{m}_{34}h_{34} = \dot{m}_{35}h_{34}$	$\dot{I}_{MIXER\ 2} = \dot{E}_{x,\ 34} + \dot{E}_{x,\ 28} - \dot{E}_{x,\ 35}$	0.0199	0.34	0.0110	0.20
MIXER3	$\dot{m}_{1a}h_{1a} + \dot{m}_{16}h_{16} = \dot{m}_1h_1$	$\dot{I}_{MIXER\ 3} = \dot{E}_{x,\ 1a} + \dot{E}_{x,\ 16} - \dot{E}_{x,\ 1}$	0.0001	0.00	0.0000	0.00
Total		$\dot{I}_{total}$	**5.8490**	**100.00**	**5.4195**	**100.00**

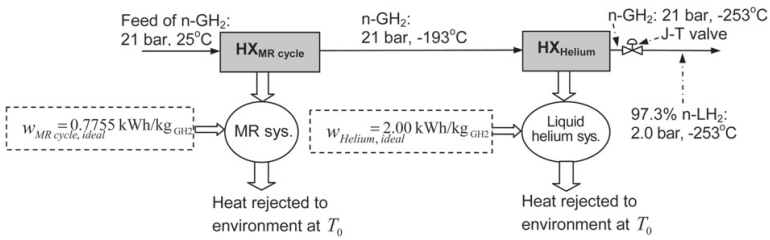

Fig. 3 – Ideal minimum energy consumptions calculated from the PRO/II simulation data.

test rig, reducing the MR compressor rotational speed will reduce the MR mass flow rate. But it should also be noted that too low of a MR mass flow rate will cause an insufficient flow to pre-cool the hydrogen gas.

- Additionally, there is the exergy flow due to heat transfer from the compressor. Cooling down the compressor by any means (water-cooled or aircooled) is recommended before the compressed gas comes out of the compressor. For this test rig, a two-stage hydrogen compressor was already designed by the manufacturer to include water cooling between the stages. For the MR compressor, heat was ventilated from the compressor by an aircooled fan system.
- For a large liquefaction system, a good example is the arrangement of hydrogen compressors and pre-cooling propane compressors connected in series. This setup is the same as Quack [3]'s conceptual plant, which cools down both the suction and discharge gas temperatures by cooling and exchanging heat with a low-temperature propane heat exchanger. Therefore, the suction temperature of a hydrogen compressor and propane compressor is around 0 °C. Moreover, it is highly recommended for a large compressor manufacturer to design a product with a water cooling system that wraps around the compressor case to transfer heat or make the outer surface temperature as low as possible (the same as a car engine water cooling system). Alternatively, high-flow oil injection cooling can be used in a screw refrigeration compressor. In short, any means of ventilating as much heat as possible somewhere around the compressor is highly recommended. A high efficiency compressor can also be used. The final recommendation is to avoid designing a system that results in too large of a difference between the suction and discharge pressure.

2. Gas coolers: HX6 and HX7
   - For HX6 and HX7: Increase or make the size of the heat exchanger as large as possible to reduce the temperature difference between the two streams and between the inlet and outlet. However, this will increase the cost of material, so the appropriate size should be considered. For this test rig, gas coolers were already selected and installed. Alterations were not possible.
   - For HX6, *Hydrogen aftercooler*: Consider the equation: $\dot{I}_{HX6} = (\dot{E}_{x,\ 2} + \dot{E}_{x,\ 39}) - (\dot{E}_{x,\ 3} + \dot{E}_{x,\ 40})$ and $(T_2 - T_{40})$ should be as close as possible to transfer all heat or to have high heat exchange effectiveness. For example, at HX6, the temperature of stream 40 should be close to or the same as that of stream 2. Likewise, the temperature of stream 39 should be close to or the same as that of stream 3. Also, the cooling water flow rate should be increased as much as possible, but the inlet and the outlet water should not be colder than the outlet hydrogen discharge or the inlet hydrogen suction.
   - For HX7, *MR water-cooled condenser*: The following equation, $\dot{I}_{HX7} = (\dot{E}_{x,\ 18} + \dot{E}_{x,\ 41}) - (\dot{E}_{x,\ 19} + \dot{E}_{x,\ 42})$, indicates that the term $(\dot{E}_{x,\ 18} + \dot{E}_{x,\ 41})$ must be a low value, while the term $(\dot{E}_{x,\ 19} + \dot{E}_{x,\ 42})$ must be a high value. Thus, it is recommended to have a low discharge MR temperature, a low water inlet temperature, a high outlet MR temperature (close to water inlet temperature), and a high water outlet temperature (close to MR discharge temperature). The temperature of stream 42 should be close to or the same as that of stream 18, and the temperature of stream

Table 6 – Methods to reduce MR compressor's exergy loss/irreversibility of the test rig's 5 components.

Numbers in bold italics are the changed values. Numbers in bold were simulated from PRO/II.	Suction			Discharge			$\dot{W}_{BH,\ MR\ COM}$	$\dot{I}_{MR\ COM}$
	P_{17}	T_{17}	$\dot{E}_{x,\ 17}$	P_{18}	T_{18}	$\dot{E}_{x,\ 18}$		
Unit	(bar)	(°C)	(kW)	(bar)	(°C)	(kW)	(kW)	(kW)
Suppose that the reference state is at: =>	1.4	25	**−2.94**	22	**194**	**1.74**	**6.09**	**1.41**
1. Reduce suction temperature	1.4	**10.9**	**−2.92**	22	**178**	**1.49**	**5.81**	**1.40**
2. Increase suction pressure	**2.0**	25	**−2.49**	22	**173**	**1.42**	**5.15**	**1.24**
3. Reduce discharge pressure	1.4	25	**−2.94**	**18**	**181**	**1.32**	**5.58**	**1.32**
4. Reduce mass flow rate from 1.8 to 1.58 kg-mol/hr	1.4	25	**−2.58**	22	**194**	**1.52**	**5.34**	**1.24**
5. Ventilate heat from compressor	1.4	25	**−2.94**	22	**190**	**1.70**	**6.00**	**1.36**

Table 7 – Methods to reduce HX3 and HX4's exergy loss/irreversibility of the test rig's 5 components of composition.

Numbers in bold italics are the changed values. Numbers in bold were simulated from PRO/II.	Inlet flow				Outlet flow				$\dot{Q}_{HX3}$	$\dot{I}_{HX3}$
	T_5	T_{12}	T_{29}	T_{32}	T_7	T_{14}	T_{31}	T_{34}		
Unit	(°C)	(°C)	(°C)	(°C)	(°C)	(°C)	(°C)	(°C)	(kW)	(kW)
Reference state	−103	−201	−103	−199	−198	−105	−198	−105	**2.828**	**3.92**
1. High HXs effectiveness	−103	***−199***	−103	***−199***	−198	***−104***	−198	***−104***	**2.880**	**1.50**
2. MR 10 components instead of 5	−103	−201	−103	−198	−198	−107	−198	***−107***	**2.489**	**1.93**

41 should be close to or the same as that of stream 19. In short, a high effectiveness *MR water-cooled condenser* is recommended. A large heat exchanger with a lower water-cool flow rate is better than a small heat exchanger with a high water-cool flow rate and a very low water inlet temperature.

3. Expansion valves: EX1, EX2, and EX3
   - From equations: $\dot{I}_{EX1} = \dot{E}_{x,\ 22} - \dot{E}_{x,\ 23}$, $\dot{I}_{EX2} = \dot{E}_{x,\ 27} - \dot{E}_{x,\ 28}$, and $\dot{I}_{EX3} = \dot{E}_{x,\ 31} - \dot{E}_{x,\ 32}$; a decrease in exergy loss means making the difference between the inflow and outflow exergy rate, $\dot{E}_x$ as small as possible.
   - The only way to reduce exergy loss in the expansion device is by reducing the pressure difference. This reduction may involve avoiding too large of a pressure difference between the suction and discharge pressure of the MR cycle. Also, this may mean trying to maintain the suction MR pressure at the designed 2.0 bar, with a low discharge MR pressure.
   - The last way to reduce exergy loss is to reduce the temperature difference between an incoming fluid temperature and an out-going fluid temperature.
4. Heat exchangers: HX1, HX2, HX3, HX4, and HX5 (shown in numbers by PRO/II in Table 7)
   - Increase heat transfer or increase the size of the heat exchanger as much as possible to enhance the surface area between the two streams (hydrogen and MR) and the decreased temperature difference between the inlet and outlet. For example, from HX3, consider the equation: $\dot{I}_{\overline{HX3}} = (\dot{E}_{x,\ 5} + \dot{E}_{x,\ 12} + \dot{E}_{x,\ 32} + \dot{E}_{x,\ 29}) - (\dot{E}_{x,\ 7} + \dot{E}_{x,\ 14} + \dot{E}_{x,\ 34} + \dot{E}_{x,\ 31})$; $(T_5 - T_{14})$, $(T_6 - T_{13})$, $(T_{29} - T_{34})$, and $(T_{30} - T_{33})$ should be as close as possible to transfer all heat or to have a high heat exchange effectiveness (an almost perfect heat exchanger). For example, at $\overline{HX}3$, the temperatures of streams 14 and 34 should be close to those of streams 5 and 29, and the temperatures of streams 12 and 32 should be close to those of streams 5 and 29. Other heat exchangers, HX1, HX2, HX4, and HX5, are all the same. The results from attempting to make the temperature difference between the hydrogen and MR as low as possible while pre-cooling are shown in Fig. 4. Finally, it is recommended that more components of the MR composition, e.g., a complex composition instead of simplified one, have a smaller temperature gap between the pre-cooled hydrogen and the MR cooling mixture. This is to increase the heat exchanger size or enhanced surface area; however, this will increase the cost of material, so the appropriate size should be considered. In the actual large plant design, the heat exchanger should be inside a vacuum chamber to attempt to reduce the temperature difference. However, a vacuum will cause it to be too big to fit inside. Therefore, consultations should be made with the heat exchanger manufacturer. From the energy and exergy balances above, it should be noted that the amount of heat transfer from the feed hydrogen gas to the MR cold stream in HX1–HX4 was not directly related to how much exergy was lost.
   - The right substance, capable of both flowing and boiling (to take heat away from each heat exchanger) is recommended. Because boiling involves latent heat of phase change, it can absorb more heat per kg of mass flow. Thus, only a small amount of fluid flow is needed. Less energy is required to drive the smaller fluid flow, which results in a smaller compressor size. Thus, the heat exchanger size is reduced. Moreover, a small temperature difference between the two fluid streams reduces the exergy loss in the heat exchanger. It should be noted that the author tried to have a high concentration of methane in $\overline{HX}3$, ethane in HX2, and butane in HX1 to boil and thus take heat away from each heat transfer. This boiling heat-transfer method is the best way to remove as much heat as possible. In short, the right MR mixture will make this successful.
5. Mixers: MIXER1 and MIXER2

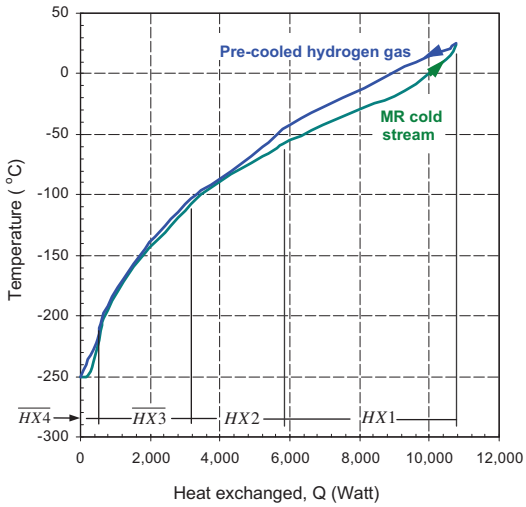

Fig. 4 – Hydrogen pre-cooling curve of the proposed 10-component mixture.

Reducing the exergy loss at fluid mixer is difficult. It should be noted that trying to avoid too large of temperature difference between the two incoming–mixing streams and the exit stream will reduce exergy loss at the fluid mixer. On the test

rig, this can be done by adjusting the MR compressor speed and modifying the MR composition.

6. Liquid separators: LIQ1, LIQ2, and LIQ3

Reduce the pressure drop by avoiding pressure differences, temperature differences, and a high liquid level over the inlet. Reducing the exergy loss at the fluid gas separators is important. Insulation must be made for the low-temperature *LIQ2* and *LIQ3* segments of the test rig to prevent heat. Finally, it should be noted that the separation of two phases in equilibrium is nearly reversible.

Before designing a large system, improvements must be made. For the exergy analysis, some development must be done to reduce the exergy loss in each component as recommended. A concise conclusion of these recommendations follows:

1. H_2 compressor and MR compressor: use the highest efficiency compressor, e.g., 80–95 percent.
2. More improvement to reduce exergy loss at HX1, e.g., a better MR composition to cool down HX1.
3. No $\overline{HX}4$ in a real large system.
4. For a real large system, use turbines to replace EX3 and EX4 (and maybe EX1 and EX2).
5. Use an additional liquid separator, e.g., LIQ4, after EX3 as a buffer to maintain volatile components.
6. More improvements in MIXER1 and MIXER2, if possible.
7. Use a complex composition, if possible.
8. In MR mixture, replace neon with hydrogen because of its higher specific heat capacity.
9. Improvements to reduce exergy loss at HX7.

In short, in order to improve the test rig to be a more highly efficient future large-scale plant, replace the components with higher efficiency compressors, almost perfect heat exchangers with complex MR refrigerant compositions, and higher efficiency expanders.

5. Conclusions

Because of its higher efficiency, a new innovative MR refrigeration system is proposed in this paper as a pre-cooling system to cool down hydrogen gas in a small-scale laboratory hydrogen liquefaction plant. This paper presents a simulation of a test rig capable of liquefying 2 kg/h of normal hydrogen gas at 21 bar and 25 °C to normal liquid hydrogen at 2 bar and −250 °C. The simulated power consumption of the MR compressor in the MR refrigeration system was 2.07 kWh per kilogram of feed hydrogen gas (to pre-cool it from 25 °C to −198 °C), which was the lowest power consumption compared to today's conventional hydrogen liquefaction cycles (with power consumptions around 4 kWh per kilogram of feed hydrogen gas). The energy efficiency of the MR cycle was 44.3%, compared to 22.3% for the conventional cycle such as the Ingolstadt plant. The proposed MR system had a higher exergy efficiency at 38.3% from the ideal minimum at 0.77 kWh/kg_{GH2}, whereas the conventional system had a lower exergy efficiency of 19.4%. The main purpose of this paper was to find where and how exergy losses occurred and to optimize the test rig's overall performance through a reduction in exergy loss in each component. It was found that major losses resulted from the compressors, heat exchangers, and expansion valves. To highlight the importance of exergy, the exergy efficiency indicated the proximity to the ideal minimum, whereas energy efficiency did not. Importantly, exergy analysis was needed to find the losses and optimize the MR system proposed in the paper. Finally, comparison of the simulation data presented in this paper to experimental data of the test rig will be reported by the author in an upcoming paper.

Acknowledgement

The author wishes to thank the Department of Energy and Process Engineering at the Norwegian University of Science and Technology for a research fellow grant.

Nomenclature

Symbols and abbreviations

COP	coefficient of performance, –
$\dot{E}$	rate of exergy (stream flow exergy) when used with subscript *x*, kW
e	specific exergy when used with subscript *x*, kJ/kg
h	enthalpy, kJ/kg
$\dot{I}$	exergy loss/irreversibility, kW
$\dot{m}$	mass flow rate, kg/s
$\dot{Q}$	refrigeration load/the heat removed from the hydrogen gas during the pro-cooling process of the test rig, kW
s	entropy, kJ/kg-K
T	temperature, K or °C
w	specific work/energy requirement, kJ/kg
$\dot{W}$	power/rate of work, kW

Greek letters

ϵ	exergy efficiency, –
η	efficiency, –

Subscripts

I	of the first law, –
II	of the second law, –
0	at reference/dead state, –
1 up to 38	stream number of the test rig process depicted in Fig. 1, –
BH	brake/shaft horse, –
elec	electrical, –
EX	at expansion valve, –
feed	of the feed flow at 21 bar and 25 °C, –
GH_2	hydrogen gas, –
in	input or at inlet, –
H_2	of feed hydrogen, –
H_2 *COM*	of hydrogen compressor, –
Helium	of liquid helium system, –
HX	of heat exchanger, –
LIQ	at liquid separator, –
liquefaction	due to hydrogen liquefaction process of the test rig, –

liquefied liquefied hydrogen, –
min minimum, –
MIXER at mixer, –
MR COM of MR compressor, –
MR cycle of MR refrigeration cycle, –
out at outlet, –
pre-cooled of pre-cooled hydrogen gas, –
pre-cooling of hydrogen gas pre-cooling process from 25 °C to −198 °C, –
total of total, –

REFERENCES

[1] Bracha M, Lorenz GA, Wanner M. Large-scale hydrogen liquefaction in Germany. Int J Hydrogen Energy 1994;19(1):53–9.
[2] Matsuda H, Nagami M. Study of large hydrogen liquefaction process. Kanagawa, Japan: Nippon Sanso Corp. WE-NET: Summary of annual reports. Available from: http://www.enaa.or.jp/WE-NET/ronbun/1997/e5/sanso1997.html; 1998 [accessed 14.06.2009].
[3] Quack H. Conceptual design of a high efficiency large capacity hydrogen liquefier. Adv Cry Eng 2002;47:255–63.
[4] Kuzmenko IF, Morkovkin IM, Gurov EI. Concept of building medium-capacity hydrogen liquefiers with helium refrigeration cycle. Chem and Petro Eng 2004;40(1–2).
[5] Shimko M, Gardiner M. Innovative hydrogen liquefaction cycle. Available from: http://www.hydrogen.energy.gov/pdfs/progress08/iii_7_shimko.pdf; 2007 [accessed 14.06.2009].
[6] Valenti G. Proposal of an innovative, high-efficiency, large-scale hydrogen liquefier. Int J Hydrogen Energy 2008;33(12):3116–21.
[7] Berstad D, Stang J, Neksa P. Large-scale hydrogen liquefier utilising mixed-refrigerant pre-cooling. Int J Hydrogen Energy 2010;35(10):4512–23.
[8] Krasae-in S, Stang J, Neksa P. Development of large-scale hydrogen liquefaction processes from 1898 to 2009. Int J Hydrogen Energy 2010;35(10):4524–33.
[9] Gaggioli RA. Available energy and exergy. Internat. J. Appl. Thermodyn 1998;1(1–4):1–8.
[10] Wark KJ. Advanced thermodynamics for engineers. New York: McGraw-Hill; 1995.
[11] Bejan A. Advanced engineering thermodynamics. New York: Wiley; 1988.
[12] Moran MJ. Availability analysis: a Guide to efficient energy use. Englewood Cliffs, NJ: Prentice-Hall; 1982.
[13] Bejan A. Entropy Generation through heat and fluid flow. New York: Willey; 1982.
[14] Kotas TJ. The exergy method of Thermal plant analysis. Florida: Kreiger; 1995.
[15] Baker CR, Shaner RL. A study of the efficiency of hydrogen liquefaction process. Int J Hydrogen Energy 1978;3(3):321–34.
[16] Dincer I, Rosen M. Exergy analysis of cryogenic systems. Exergy Energy Environ Sustainable Dev; 2007:277–89.
[17] Chiu CH, Newton CL. Second law analysis in cryogenic processes. Energy 1980;5(8–9):899–904.
[18] Kanoglu M. Exergy analysis of multi-stage cascade refrigeration cycle used for natural gas liquefaction. Int J Energy Res 2002;26:763–74.
[19] Remeljej CW, Hoadley AFA. An exergy analysis of small-scale liquefied natural gas (LNG) liquefaction processes. Energy 2006;31(12):2005–19.
[20] Bottura L. Cryogenic mixed refrigerant processes. Cryogenics 2009;49(12):745–6.
[21] Chrz V. Cryogenic mixed refrigerant processes. Int J Refrigeration 2010;33(3):648–9.
[22] Mafi M, Amidpour M, Mousavi Naeynian SM. Development in mixed refrigerant cycles used in olefin plants. In: Proceedings of the first annual gas processing symposium, 10–12 January 2009, Doha, Qatar 2009. p. 154–61.
[23] Bosma P, Nagelvoort RB. Liquefaction technology; developments through history. In: Proceedings of the first annual gas processing symposium, 10-12 January 2009, Doha, Qatar 2009. p. 19–31.
[24] Flynn TM. Cryogenic engineering. 2nd ed. NY: Marcel Dekker Press; 1997.
[25] Barron RF. Cryogenic systems. Oxford, United Kingdom: Oxford University Press; 1966.

Krasae-in S, Bredesen A, Stang J, Neksa P. Simulation and experiment of a hydrogen liquefaction test rig using a multi-component refrigerant refrigeration system. Int J Hydrogen Energy 2010;36(1):907-919.

INTERNATIONAL JOURNAL OF HYDROGEN ENERGY 36 (2011) 907–919

Available at www.sciencedirect.com

ScienceDirect

journal homepage: www.elsevier.com/locate/he

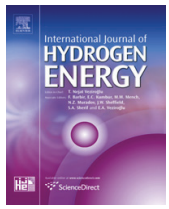

Simulation and experiment of a hydrogen liquefaction test rig using a multi-component refrigerant refrigeration system

Songwut Krasae-in [a,*], *Arne M. Bredesen* [a,1], *Jacob H. Stang* [b,2], *Petter Neksa* [b,3]

[a] *Norwegian University of Science and Technology, Kolbjorn Hejes vei 1d, NO-7491 Trondheim, Norway*
[b] *SINTEF Energy Research AS, Kolbjorn Hejes vei 1d, NO-7465, Trondheim, Norway*

ARTICLE INFO

Article history:
Received 12 March 2010
Received in revised form
31 July 2010
Accepted 1 September 2010
Available online 12 October 2010

Keywords:
Liquid hydrogen
Hydrogen liquefier
Large hydrogen liquefaction
Exergy efficiency

ABSTRACT

A small-scale laboratory hydrogen liquefaction plant that contains a new innovative MR (multi-component refrigerant) refrigeration system is proposed. A test rig was constructed to verify the simulation of this system. Initial experiments indicated that the rig were able to adequately cool normal hydrogen gas from 25 °C to −158 °C at a flow rate of 0.6 kg/h using a simplified five-component MR mixture refrigeration system. The power consumption of pre-cooling from the MR compressor was 1.76 kW h per kilogram of feed hydrogen gas. After two weeks, the lowest temperature was about −180 °C when a few additional grams of nitrogen gas were charged into the rig. The simulation and experimental data were in good agreement, and the primary conclusion was that pre-cooling hydrogen gas with the MR refrigeration system resulted in a lower energy consumption per kilogram of feed hydrogen gas compared to conventional refrigeration systems.

1. Introduction

Hydrogen has good potential as an energy vector for future use in transportation vehicles, and several hydrogen research activities have been conducted since 1980 and especially since 2000. One of the major obstacles for the future hydrogen economy is the large amount of hydrogen liquefaction work. There are several existing simple hydrogen liquefaction processes [1–4]. Baker and Shaner [5] proposed the first conceptual plant with the lowest efficiency. Today, large hydrogen liquefaction plants, such as the Ingolstadt plant described by Bracha et al. [6], have exergy efficiencies of only 20–30%, which is considered to be very low. The plant consumes 4.86 kW h per kilogram of hydrogen gas using a nitrogen refrigeration system to pre-cool normal hydrogen gas from 25 °C to equilibrium hydrogen gas at −198 °C. Therefore, it is possible to improve this efficiency. From 1998 until 2008, some conceptual plants were proposed that reported improved efficiencies of 40–50%: Matsuda [7] under WE-NET's project [8], Quack [9], Kuzmenko et al. [10], Shimko and Gardiner [11], and Valenti [12]. Different cycles were compared by Berstad et al. [13]. Later on, a literature review for the development of large-scale hydrogen liquefaction processes throughout the world from 1898 to 2009 was conducted by Krasae-in et al. [14]. Finally, in 2009, NTNU (Norwegian University of Science and Technology) and SINTEF (The Scientific and Industrial Research Froundation) Energy Research AS proposed a new

* *Corresponding author*. Tel.: +47 735 92991; fax: +47 735 97214.
E-mail addresses: songwut.krasaein@ntnu.no, krasaein@hotmail.com (S. Krasae-in), arne.m.bredesen@ntnu.no (A.M. Bredesen), jacob.stang@sintef.no (J.H. Stang), petter.neksa@sintef.no (P. Neksa).
[1] Tel.: +47 73593744; fax: +47 735 97214.
[2] Tel.: +47 735 98109.
[3] Tel.: +47 735 93923.
0360-3199/$ – see front matter
doi:10.1016/j.ijhydene.2010.09.005

large-scale MR refrigeration system with an efficiency greater than 50%.

Multi-component refrigerant was used in the test rig cycle. This concept of mixed refrigerant in gas liquefaction (which was discovered in recent years) results in reduced energy consumption compared to conventional liquefaction cycles, which is in agreement with the work by Bottura [15], Chrz [16], Mafi et al. [17], and Bosma et al. [18]. In this paper, the differences are as follows: A new modified cycle and a new optimized refrigerant mixture designed for pre-cooling hydrogen gas from 25 °C to −198 °C were used, as proposed by Stang et al. [19].

In this paper, simulations and experiments of a small-scale laboratory test rig were performed. The simulation was conducted to design the rig, whereas the experiments were performed to verify the simulation data. First, a determination of the correct simplified mixture and the operation of the small-scale laboratory liquid hydrogen plant are described. Then, the simulation, optimization, experiment, comparison, and discussion of the results are presented.

2. Test rig description

A schematic diagram of the test rig is shown in Fig. 7, and the rig is further explained in Section 3.2. Fig. 1(a) shows the outside of the test room, i.e., an overview of the test rig. All of the compressors, heat exchangers, and instruments were located inside of the test room. The room is designed to protect personnel in case of a fire, hydrogen leak, or explosion.

Fig. 1(b) shows a portion of the inside of the test room. The vacuum chamber contains all of the heat exchangers: HX1, HX2, HX3, HX4, and HX5. The heat exchangers are handmade copper spiral tube-in-tube type that were internally designed and manufactured. The vacuum chamber also contains LIQ2, EX1, EX2, and EX3. The hydrogen compressor unit (bottom left of Fig. 1(b)) is equipped with a Mehrer TZL 20/80/65/S4-4Ex compressor, which is an open-type two stage reciprocating unit with two cylinders with a rotational speed of 485 RPM. The compressor is used to compress hydrogen gas from 25 °C at a suction pressure of 2 (abs) bar to an outlet pressure of 21 (abs) bar, and the expected hydrogen flow rate is 2 kg/h. The unit is water cooled between stages. The power of the motor is 4 kW. The MR compressor unit is a Blackmer HD162C compressor, which is an open-type single-stage reciprocating unit with one cylinder. The rotational speed is 350/825 RPM. The compressor is used to compress MR gas at 25 °C at a suction pressure of 2.0 (abs) bar to an outlet pressure of 20 (abs) bar, and the expected gas flow rate is 44 kg/h. The compressor always operates at its maximum speed; thus, the maximum braking horsepower is 7.5 kW. The hydrogen flow rate meter is a Brook Instruments 5863 E (with an accuracy of ±1%), and the mass flow meter for the MR circuit is an Endress + Hauser − Promass 83 F (with an accuracy of ±0.35%). The temperature sensors are Lake Shore Silicon diodes DT-470-CO-13 (with an accuracy of ±0.5 K for a temperature range of 2–30 K, ±0.25 K for 30–60 K, and ±0.15 K for 60–345 K). The liquid level sensors are Endress PMD75 (with accuracy ±0.05%), and the pressure sensors are Endress PMD71 (with an accuracy up to ±0.075% of the set span).

3. Preliminary rig simulation

3.1. Determination of the correct components

Fig. 2 presents the boiling curves for arbitrarily selected components: neon, nitrogen, methane, R14, ethylene, ethane, propene, propane, I-butane, butane, I-pentane, and pentane. These curves were obtained from the boiling temperature and pressure of each substance and were plotted using PRO/II. The designed working temperatures of the four heat exchangers are shown as dashed blue lines, whereas the boiling pressure of the MR mixture in the MR cycle at 2.0 bar is shown as a red horizontal line. For each of the selected components in the mixture, the partial pressure (0.1–1 bar) at the boiling point temperature is slightly below this value. Although it is difficult to use these curves to directly calculate the optimal composition of the MR, they were used to indicate the components that must be included. For example, at heat exchanger 1 (HX1), one or two volatile substances such as propane, I-butane, butane, I-

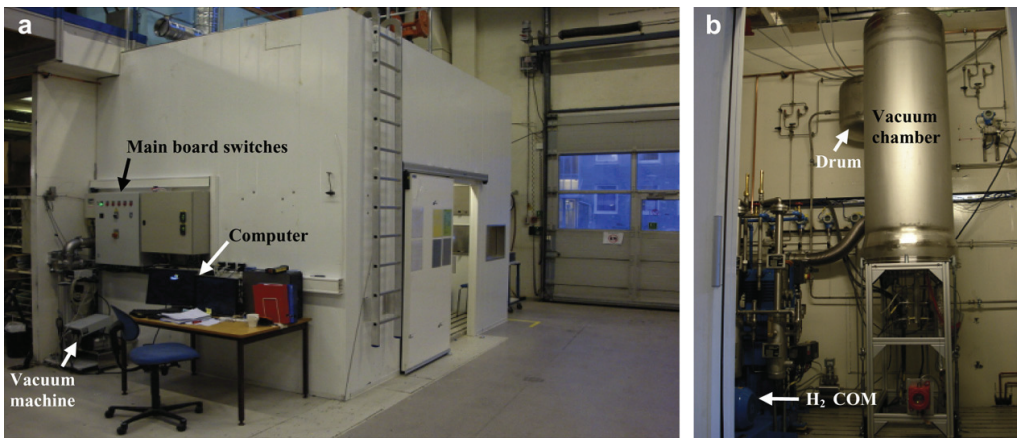

Fig. 1 – Complete construction of: (a) the test room, and (b) inside the test room.

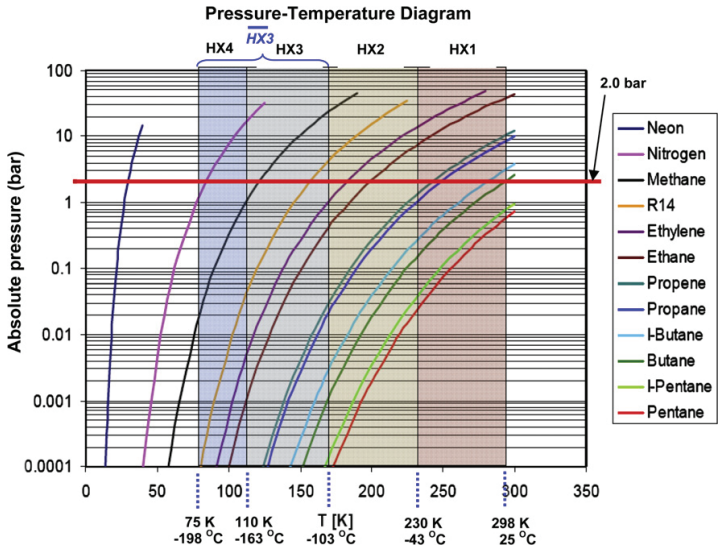

Fig. 2 – Boiling curves for different components (PRO/II, v.8.1).

pentane, or pentane should be selected. At HX3 and HX4, methane and nitrogen should be selected to boil and transfer heat from the hydrogen gas. Additionally, the flow rate of each substance should be high enough to boil and transfer heat in each of the heat exchangers. Neon was also used in the refrigerant because its lower temperature could be used to cool HX4. (For interpretation of the references to colour in text, the reader is referred to the web version of this article).

3.2. *Design conditions*

The simulation model was built in PRO/II. Ortho-para conversion reactors were not included because the experimental rig did not contain a catalyst for ortho-para conversion. The laboratory test rig shown in Fig. 7 was designed to use a complex multi-component refrigerant with 10 components. The concept of multi-component refrigerants (or mixed refrigerants) [15–18] are widely used in the liquefaction of natural gas because of their reduced energy consumption compared to conventional liquefaction cycles. SINTEF Energy Research AS has worked with these types of refrigeration cycles for several years. During the startup period of the rig, a less complex five-component composition of the MR was used. To obtain a theoretically optimized refrigerant mix, a flow chart was used to model the liquefaction rig using the PRO/II simulation program. The design conditions for the test rig are shown in Table 1.

From Figs. 3 and 7, feed hydrogen gas was first compressed from a suction pressure in a two stage hydrogen piston compressor with inter- and after-cooling. The outlet temperature of the aftercooler (both H_2 and MR circuit) was set to 25 °C.

Table 1 – Assumptions in the simulation model.

Hydrogen flow rate	2 kg/h	–	–	–
Compressors	Inlet abs. pressure [bar]	Outlet abs. pressure [bar]	Isentropic efficiency	Outlet temperature (°C)
H_2 compressor	2 bar at stream 1	21 bar at stream 2	0.65	25
MR compressor	2 bar at stream 18	18 bar at stream 18	0.70	25
Heat exchangers	Hot stream outlet temperature [°C]	Cold stream outlet temperature [°C]	Pressure drop [bar]	Heat leak [W]
HX1	−46.15 °C at stream 4	–	0	0
HX2	−103.15 °C at stream 5	–	0	0
HX3	−163.15 °C at stream 6	–	0	0
HX4 ($\overline{HX3}$)	−198.15 °C at stream 7	–	0	0
HX5 ($\overline{HX4}$)	−250.00 °C at stream 8	–	0	0
JT valves	Outlet pressure [bar]	–	–	–
H_2: (EX4)	2	–	–	–
MR: (EX1, EX2, EX3)	2	–	–	–
Flash drums	Pressure drop [bar]	Duty [W]	–	–
LIQ1	0	0	–	–
LIQ2	0	0	–	–
LIQ3	0	0	–	–

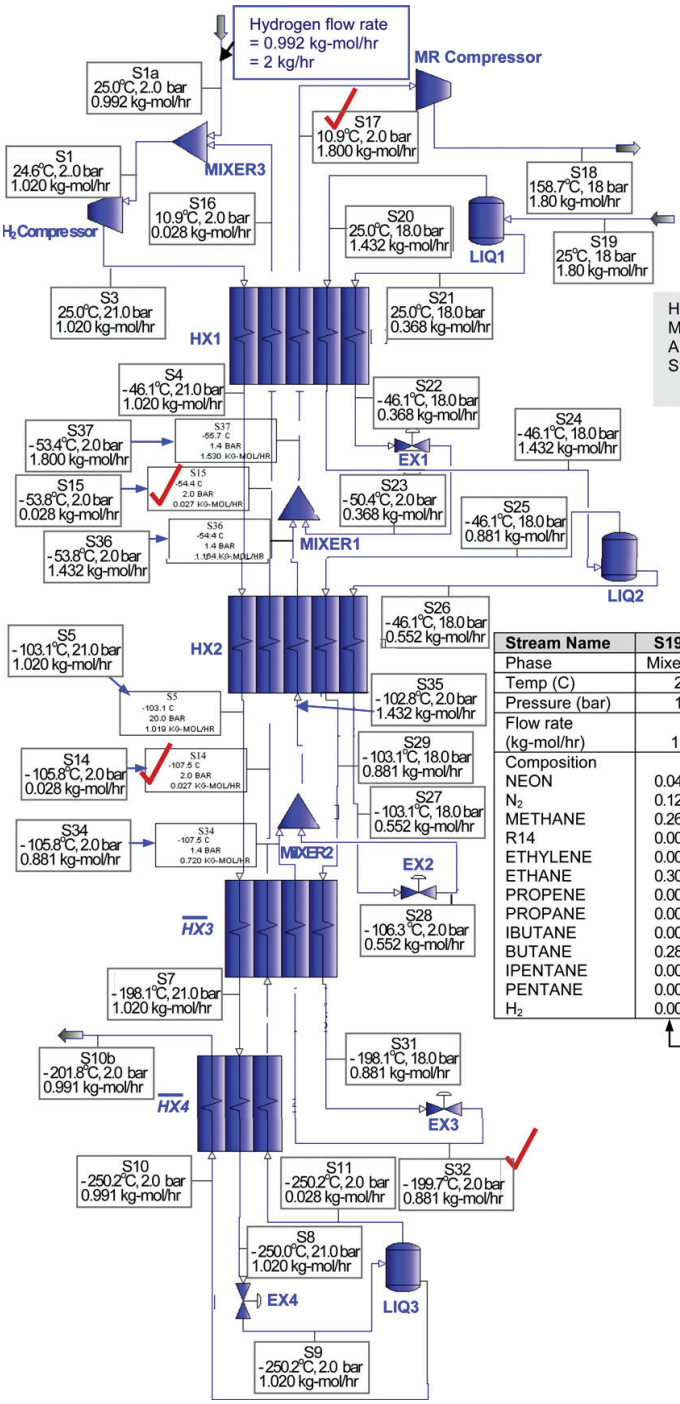

Stream Name	S19	S20	S21	S23	S28	S31
Phase	Mixed	Vapor	Liquid	Mixed	Mixed	Mixed
Temp (C)	25	25	25	-50.3	-106.3	-198.1
Pressure (bar)	18	18	18	2.0	2.0	18
Flow rate (kg-mol/hr)	1.8	1.432	0.368	0.368	0.552	0.881
Composition						
NEON	0.040	0.050	0.001	0.001	0.001	0.081
N_2	0.120	0.149	0.005	0.005	0.010	0.237
METHANE	0.260	0.318	0.035	0.035	0.095	0.457
R14	0.000	0.000	0.000	0.000	0.000	0.000
ETHYLENE	0.000	0.000	0.000	0.000	0.000	0.000
ETHANE	0.300	0.333	0.171	0.171	0.513	0.221
PROPENE	0.000	0.000	0.000	0.000	0.000	0.000
PROPANE	0.000	0.000	0.000	0.000	0.000	0.000
IBUTANE	0.000	0.000	0.000	0.000	0.000	0.000
BUTANE	0.280	0.150	0.787	0.787	0.381	0.005
IPENTANE	0.000	0.000	0.000	0.000	0.000	0.000
PENTANE	0.000	0.000	0.000	0.000	0.000	0.000
H_2	0.000	0.000	0.000	0.000	0.000	0.000

Proposed composition

Fig. 3 – PRO/II simulation flow-sheet of the proposed five-component composition.

The hydrogen gas was subsequently cooled in five heat exchangers. In the first four heat exchangers, the hydrogen was pre-cooled by the MR circuit and hydrogen flash gas from the Joule–Thompson valve. In the last heat exchanger, the hydrogen flash gas and product were used to cool the hydrogen feed, but no helium was used in the simulation. For the final cooling of the hydrogen to −251 °C, a Joule–Thompson valve was used to throttle the hydrogen down to the suction pressure. In a large-scale hydrogen liquefaction plant, an expansion machine can be used; however, its use was not economically feasible for this small-scale laboratory plant. The Redlich–Kwong–Soave (SRK) equation of state was selected as the fluid package for the simulation software because of its popularity, simplicity, and computational efficiency. The goal was to minimize the MR compressor power by optimizing the following variables:

1. Suitable H_2 compressor discharge pressure:
   The discharge pressure must be greater than 15 bar (supercritical pressure) to avoid condensation. For the test rig, the discharge pressure was designed to be 21 bar, which is equivalent to the pressure of the feed at Ingolstadt. Higher feed pressures result in minimal work liquefaction, which was reported by Matsuda [7], Quack [9], and Valenti et al. [12] who used values of 50, 80, and 60 bar, respectively. At the large-scale, if the feed is 1–2 bar, then it is recommended to compress the feed discharge to 21 bar instead of a higher value because of the increased energy requirement.

2. Suitable H_2 compressor suction pressure:
   The suction pressure must be a slightly above the ambient pressure (1 bar) to be stored in a liquid tank before it is supplied. Ingolstadt uses 1.3 bar. For this test rig, the pressure could be anywhere between 1.3 and 2 bar. For the simplicity of the controls, a value of 2 bar was selected.

3. Suitable MR compressor discharge pressure:
   Several simulation trials were performed using PRO/II to determine the optimal composition for different suction pressures. An optimized, simplified, five-component mixture that consisted of 4% neon, 12% nitrogen, 26% methane, 30% ethane, and 28% butane was adequate with different suction and discharge MR pressures for all of the cases. A suitable MR compressor discharge pressure was 18 bar, which resulted in a MR compressor power of 4.55 kW. If the pressure was lower than 18 bar, e.g., 15, 16, or 17 bar, then it was impossible for the MR system to cool the hydrogen. In addition, solid phase MR flow could form inside of the heat exchangers if the pressure was much lower than 18 bar. However, if the discharge pressure was higher than 18 bar, then the system would function, but it would result in an increase in MR compressor power. Furthermore, if the pressure was too high, then there would be more exergy losses at expansions valves EX1, EX2, and EX3.

4. Suitable MR compressor suction pressure:
   A very high or low suction pressure would not be allowed. The hydrogen gas can be cooled sufficiently to the specified design temperature (−198 °C) flowing out of $\overline{HX}4$. A suitable pressure was 2 bar, which resulted in the minimum (theoretical) brake horsepower (4.55 kW) of the MR compressor. The suction pressure should not be lower than 1 bar because that would increase the MR compressor power; additionally, the pressure should not be higher than 2 bar because this would result in a system that could not sufficiently cool the hydrogen gas.

5. Hot stream hydrogen outlet temperatures from HX1, HX2, HX3, HX4, and HX5:
   Trial and error was used to determine the optimal temperatures.

6. Suitable composition of the MR cycle:
   Trial and error was used to determine the optimal composition as shown in Table 2.

3.3. *The proposed simplified five components of composition for the initial experiment*

For simplicity, a reduced number of components for the mixture were required to perform the initial experiment. The simulation results proposed an optimized composition of 4% neon, 12% nitrogen, 26% methane, 30% ethane, and 28% butane, as shown in Table 2. Neon could be replaced by hydrogen or helium with similar results. The experiments were performed on the test rig, and trial and error was used to obtain the composition. Finally, the simulation result for this composition is shown in Fig. 3 and is detailed in Krasae-in et al. [20].

The possibility of having three components of the mixture, e.g., 26% methane, 30% ethane, and 28% butane, without nitrogen was investigated. In this case, the pre-cooled hydrogen gas at stream 7 leaving $\overline{HX}3$ could only be cooled to −150 °C but not to the designed −198.15 °C. Therefore, the presence of nitrogen in the mixture was required to sufficiently cool the hydrogen gas because nitrogen has a lower boiling temperature than methane after expanding at EX3. In conclusion, the mixture must have at least five-components, and more components result in a better liquefier. The simulation results are shown in Fig. 3 for an energy consumption of 3.96 kW h/kg of the hydrogen liquefied/feed. The MR flow rate was 1.8 kg mol/h, which is the minimum flow rate. The flow rate must be maintained above this minimum rate; otherwise,

Table 2 – - Choice of the proposed five-component MR mixture.

Option No.	1	2	3
Component	%Mol	%Mol	%Mol
Hydrogen	–	4	–
Helium	–	–	4
Neon	4		–
Nitrogen	12	12	12
Methane	26	26	26
Ethylene	–	–	–
Ethane	30	30	30
Propene	–	–	–
Butane	28	28	28

Table 3 – Amount of heat transfer from the two hot streams to the MR cold stream (Q), Watts.

HX	From H_2 gas hot stream (W)	From MR hot stream (W)	Total (W)
HX1	578	3760	4338
HX2	464	1783	2247
HX3	793	1625	2418

the low-temperature liquefaction system cannot be produced because there would not be enough MR fluid flowing to transfer heat. Fig. 3 shows a hydrogen pre-cooling curve. Table 3 shows that most of the heat from the MR hot stream is transferred to the MR cold stream.

Fig. 4 indicates that the MR pre-cooling performs better than N_2 pre-cooling because, in the latter case, a large amount of heat is transferred to the N_2 at a constant temperature (roughly 80 K), whereas, in the former case, heat is transferred to the MR at a variable temperature. In addition, the MR can better track the H_2 cooling curve.

4. Initial experimental results

This section expands on Section 3, *Preliminary rig simulation*; it provides a detailed description of the experimental procedure, experimental results, and analysis of the test rig. All of the data were automatically collected using LABVIEW while running the experiments.

4.1. *Initial experiment*

Table 4 provides a detailed composition of the MR mixture used in the initial experiments; the simulated and experimental compositions are compared. Butane has the highest molecular weight, which causes the flow to be heavier at a higher flow rate.

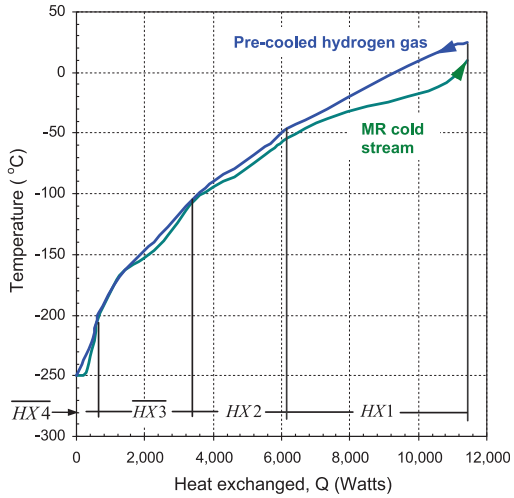

Fig. 4 – Hydrogen pre-cooling curve for the proposed five-component mixture depicted in Table 2 and Fig. 3.

Table 4 – Composition of the mixture.

Component	Molecular weight (kg/kmol)	%Mole by simulation	Measured %mole by experiment
Neon	420.18	44.0	1.0
Nitrogen	28.01	12.0	10.0
Methane	16.04	26.0	33.0
Ethane	30.07	30.0	38.0
Butane	58.12	28.0	18.0
Total		100%	100%

First, each component (neon, nitrogen, methane, ethane, and butane) contained in the high pressure cylinder tank was discharged directly into the test rig at the MR cycle. This discharge was done by measuring the mass reduction of the gas tank, which is equivalent to the amount of the gas filled in the rig at the MR cycle. The simulated and measured compositions shown in Table 4 are located in the MR flow at stream 19. Each component was then charged into the rig at the suction of the MR compressor when it was switched on. Each cylinder tank had a higher pressure than the suction pressure of the MR compressor. Thus, the gas mixture was forced to flow from the inside of the tank into the MR circuit of the rig until it achieved a satisfactory MR composition. The measured composition shown in Table 4 (at stream 19) can be achieved directly by reading the gas chromatography instrument, which can be positioned at three different points, as shown in Fig. 7. This process describes the process for creating the MR mixture in the test. Before the last initial experiment of the cycle was performed, as shown in Figs. 5–7, a preliminary test run was performed, which included several tests. Some experiments were performed multiple times to allow the rig to cool the temperature of the flowing hydrogen gas as much as possible. This cooling was done by adjusting the MR composition, suction and discharge pressures, and MR flow rate until the temperature was optimized. The final total amounts of neon, nitrogen, methane, ethane, and butane completely charged into the rig were 0.080, 0.330, 0.900, 2.160, and 4.790 kg, respectively. However, these values are not exact due to the presence of multiple leakages. As a result, the exact composition inside the test rig remained unknown.

4.2. *Initial experimental results*

Fig. 5 shows the pressure and temperature characteristics of the MR cycle side. Fig. 6 shows the pressure and temperature characteristics of the H_2 cycle side. As shown on the x-axis of the two figures, the experiment began on 08.09.2009 at 10:08:01 and ended at 17:10:03.

- At 10:08:01, logging began on all of the measuring instruments. The computer then began to collect the temperatures, pressures, flow rates, and other parameters.
- At 10:30:03, the MR compressor was switched on. In Fig. 5(a), the MR discharge pressure was raised to 8 bar within a few minutes. The low side pressure decreased to 2 bar within a few minutes.
- Between 11:30:03 and 14:10:03, ethane, methane, and nitrogen were charged into the MR side. This increased both

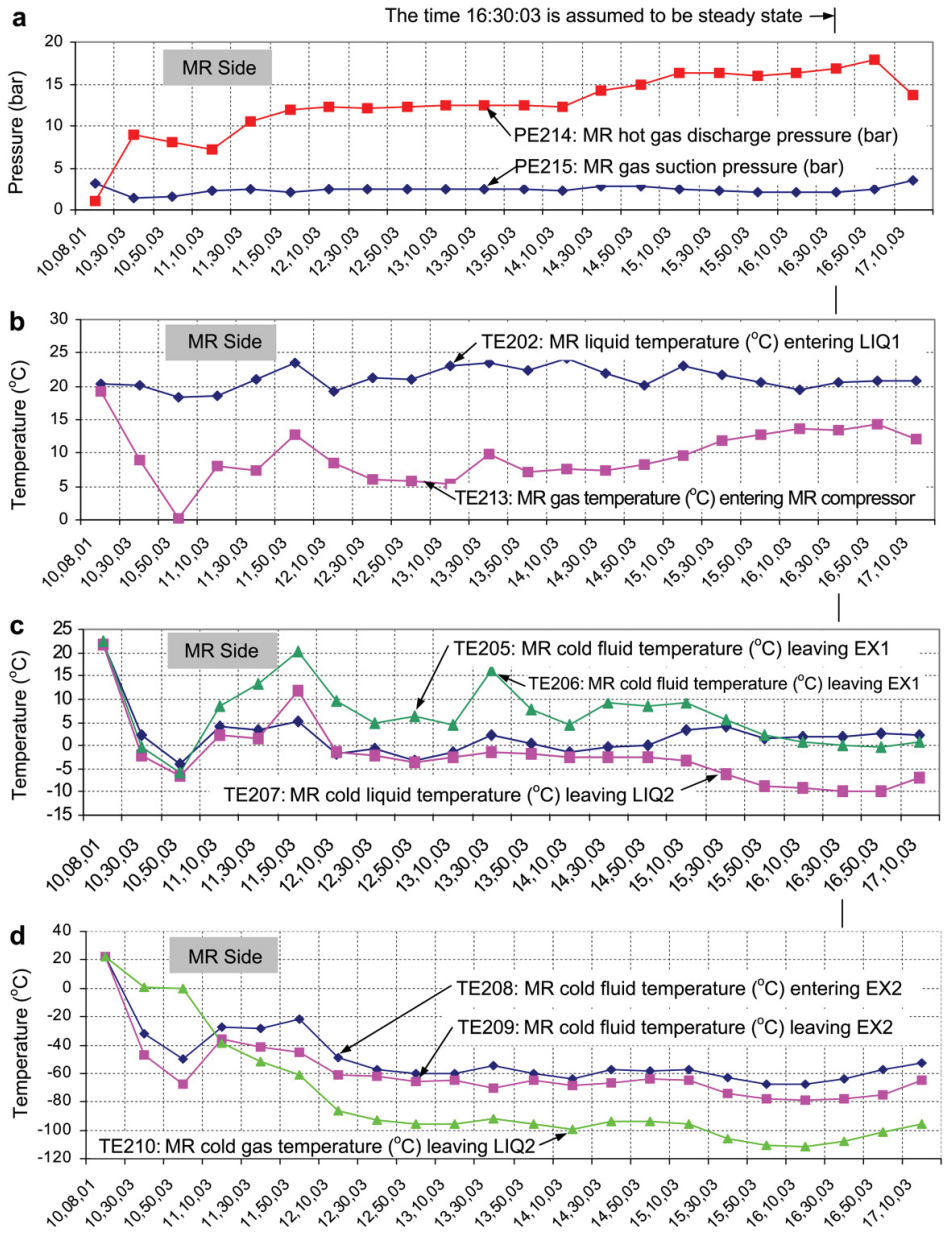

Fig. 5 – Final transient experimental results of the MR side: pressures and temperatures as a function of time.

the MR discharge and the suction pressures. However, the MR suction pressure was maintained at 2 bar by an additional closure of expansion valves EX1, EX2, and EX3. Therefore, the MR discharge pressure gradually increased to 18 bar, as shown in Fig. 5(a).

- At 14:50:03, the helium side was turned on, as shown in Fig. 5(a). Helium gas at −256 °C and 1 bar was used to cool down HX5. Each temperature reading began to decrease, especially on the H_2 side, as shown in Fig. 6(c) and (d). This decrease was due to the helium cooling HX5, which was connected to and near HX4. Furthermore, the helium gas cooled the hydrogen gas that was leaving HX4 towards HX5. The cold recycled hydrogen gas that returned to the H_2 compressor from HX5 cooled HX4, HX3, HX2, and HX1.
- At 15:10:03, the H_2 compressor was turned on, as shown in Fig. 6(b).

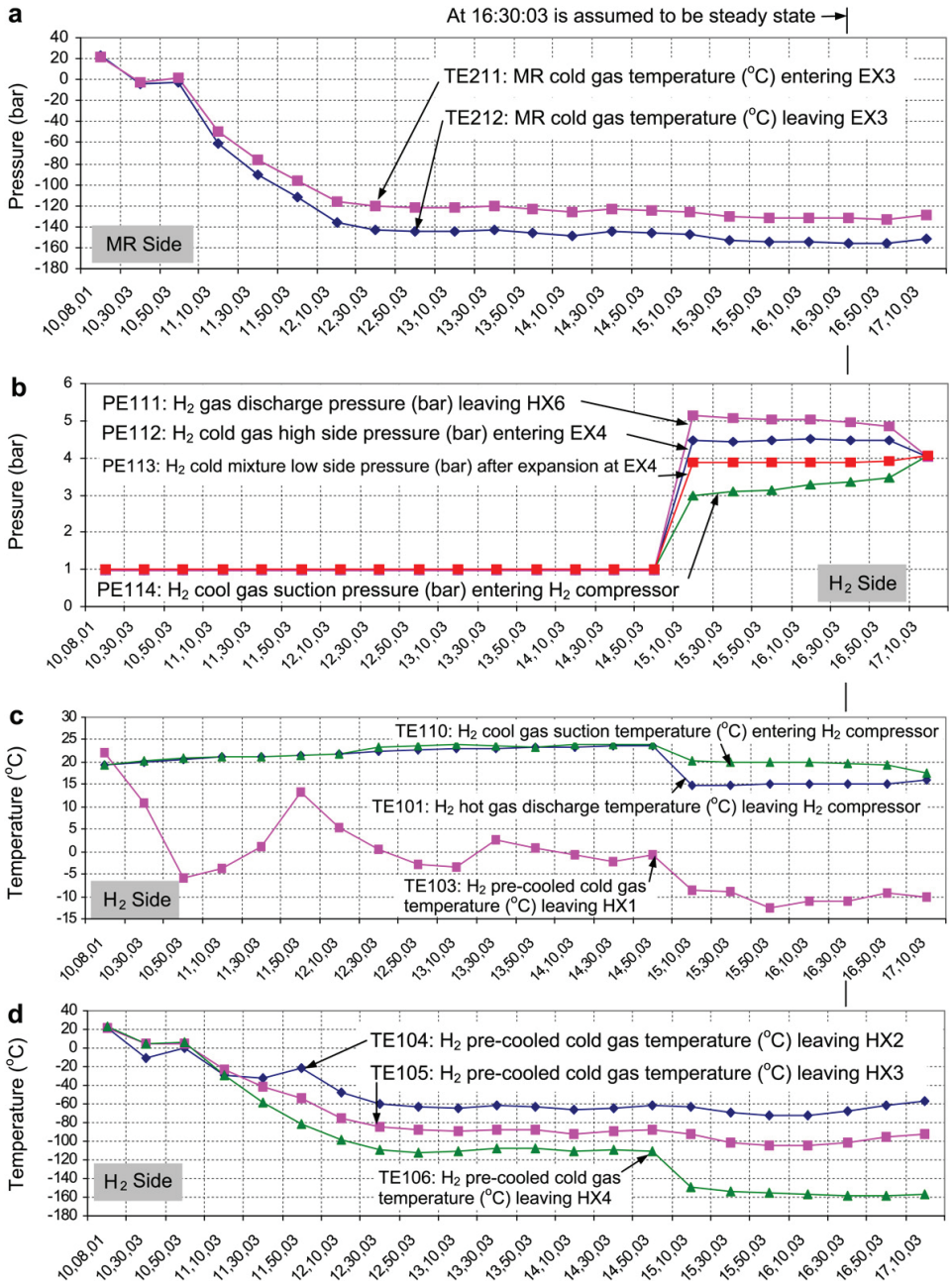

Fig. 6 – Final transient experimental results of the H_2 side: pressures and temperatures as a function of time.

- From 15:50:03 until 16:50:03, particularly at 16:30:03, a steady state was reached, as shown in Fig. 7. The MR side, H_2 side, and helium side were all opened, and all of the temperatures and pressures were stable. The most interesting temperature was TE106, *H_2 pre-cooled cold gas temperature (°C) leaving HX4*, as shown in Fig. 6(d). At TE106, hydrogen could only be cooled to −158 °C, whereas the simulation predicted a temperature of −198 °C, as shown in Fig. 3. It was assumed that an inadequate amount of the MR mixture was charged into the system (particularly the volatile components such as nitrogen and neon) in the initial experiment and that the 2 h opening of the system was insufficient. However, the final

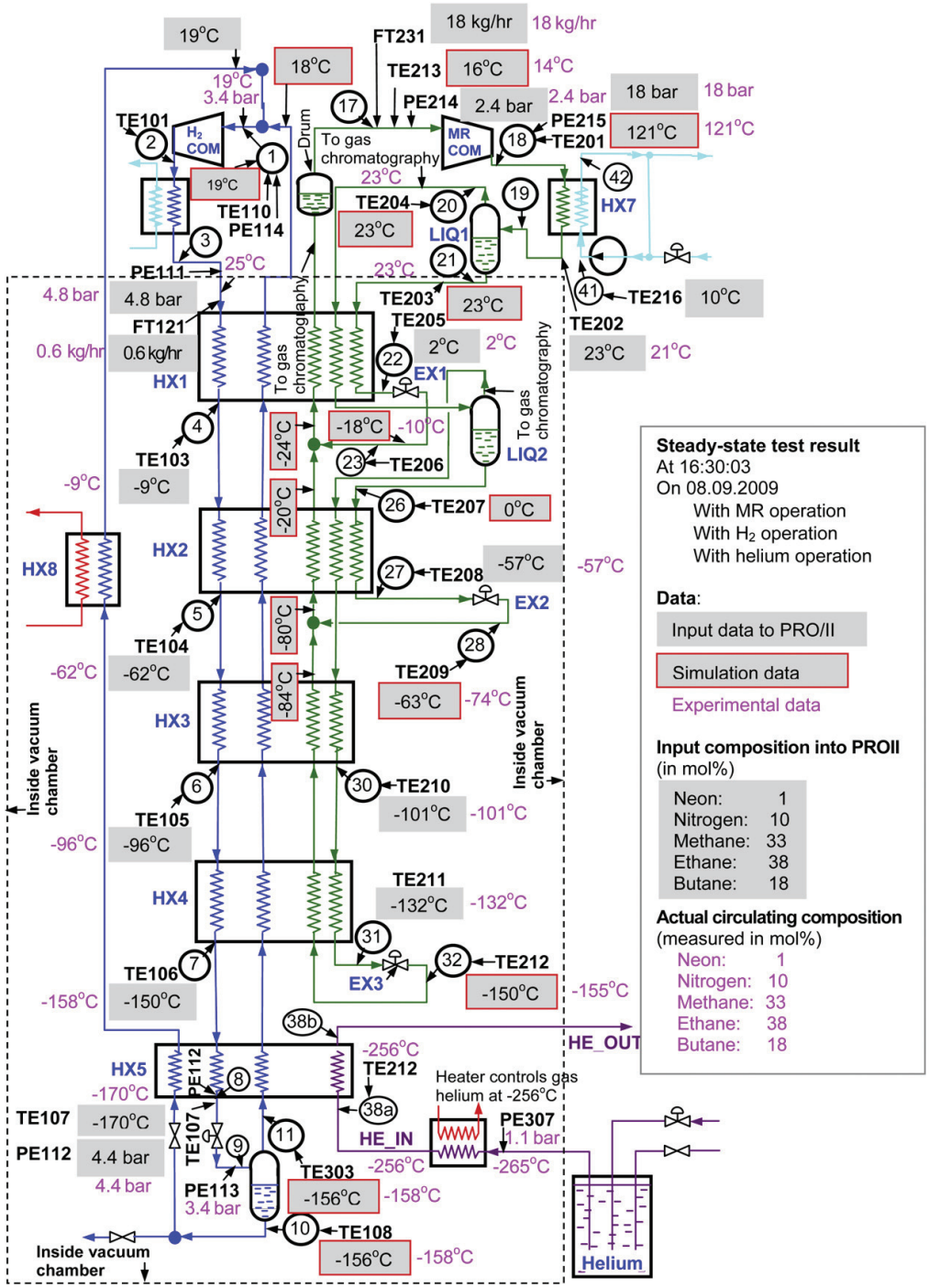

Fig. 7 – Simulation data of the laboratory test rig with the proposed simplified composition compared to the experimental data with H_2 and helium operation at steady state. The experimental data reached steady state at 14:50:03 on 08.09.2009.

experiment exhibited an improvement over the first experiment that was performed several months prior; the hydrogen gas could be cooled to a lower temperature. When helium was used, more refrigerant was charged into the rig at appropriate MR suction and discharge pressures. The other interesting temperatures were cooling the MR flow at, for example, TE206, TE209, TE210, TE211, and TE212 as shown in Figs. 5(c), (d) and 6(a). In Fig. 5(a): the MR high side pressure (PE215) was maintained at 18 bar, which is the same as the simulation result. The MR compressor speed was maintained at the highest speed. The low side pressure (PE214) was set to 2 bar, which is the same as the simulation result, by the further closure of expansion valves EX1, EX2, and EX3 to maintain the MR suction pressure at 2 bar.

- At 16:50:03, the H_2 compressor was switched off, as shown in Fig. 6(b).
- At the same time, 16:50:03, the MR compressor was finally switched off, as shown in Fig. 5(a).

5. Comparison

5.1. *Comparison of the experimental data to the simulation data*

Fig. 7 shows the steady state experimental data at 16:30:03 when both the H_2 and helium sides were on. The simulation was used to design the test (i.e., to select a composition) and to compare the test; thus, the simulation was used at two different times (as illustrated in Fig. 3 for the preliminary design of the rig and Fig. 7 for comparison to the experimental results). After both the H_2 and MR sides were switched on, the helium circuit was opened to allow cold helium gas from the liquid helium storage tank to cool HX5. This was an important time to record and compare the measured experimental data to the simulation data. Cold helium gas was flowing to cool HX5. As a result, all of the temperatures, especially TE211 and TE212, decreased further. Thus, the feed hydrogen gas could be cooled to −158 °C after leaving HX4 and remain at the same temperature at LIQ3. If more time was available, then HX5 could almost cool to the feed helium temperature, and liquid hydrogen would exist at LIQ3. As shown in Fig. 7, changes in the simulation data were required to obtain the measured hydrogen flow rate from the experiment. The simulated H_2 flow rate shown in Fig. 3 was adjusted from 2.0 kg/h (i.e., every 2 kg of hydrogen requires 50 kg of MR flow rate) to 0.6 kg/h, and the MR flow rate was set to 18 kg/h. From the simulation, 18 kg/h of MR flow rate was required to cool 0.6 kg/h of hydrogen gas. The hydrogen flow rate was too low because all of the expansion valves were closed to maintain a low suction pressure of 2 bar. All of the simulated temperatures were still the same as in Fig. 3. The final composition that was measured using gas chromatography in the rig also remained the same; it consisted of: 1% neon, 10% nitrogen, 33% methane, 38% ethane, and 18% butane. The neon content appeared to be too low, which prevented a further decrease in the temperature at TE212 following the expansion at EX3. In summary, the simulation and experimental data are nearly equivalent.

Table 5 indicates that the simulation and experimentally measured power consumptions of the two compressors were equal because the simulation data was calculated using the experimental data. The compressor power was calculated from the flow rate, inlet and outlet pressures, and temperatures. According to the law of conservation of energy, the calculated brake horsepower was the same as the measured one. The hydrogen gas flow rate from the measurement was only 0.6 kg/h instead of the initially designed 2.0 kg/h, as shown in Fig. 3. The flow rate was adjusted to account for the small flow of the MR, which enabled the liquefier to cool the hydrogen gas. The measured MR suction gas flow rate was only 18 kg/h at the maximum MR compressor speed instead of the designed 55 kg/h. However, this is not significant because the flow rate can be increased by increasing the rotational speed of the motor. There may have also been solidification of the MR after expansion, e.g., at EX3. Therefore, more time and experiments were performed to correct these problems. Another possibility was freezing due to moisture; in this case, a refrigeration filter dryer should be installed after the condenser. However, freezing was not a problem because the refrigerant was of high

Table 5 – Simulation and initial experimental data of the proposed simplified five-component mixture from Fig. 7.

Values	Equations/Symbol	Simulation data[a]	Experimental data[a]
H_2 mass flow rate at S3	$\dot{m}_{H_2}$ in kg mol/h	0.3 kg mol/h[a]	N/A kg mol/h[b]
	$\dot{m}_{H_2}$ in kg/hr	0.6 kg/h[c]	0.6 kg/h[d]
MR mass flow rate at S17	$\dot{m}_{MR}$ in kg mol/h	0.474 kg mol/h[a]	N/A kg mol/h[b]
	$\dot{m}_{MR}$ in kg/h	18.0 kg/h[c]	18.0 kg/h[d]
H_2 compressor power	$\dot{W}_{H_2\ Com,\ BH}$	0.067 kW[a]	0.067 kW[d]
Isentropic efficiency of H_2 compressor	$\eta_{ISEN,\ H_2\ Com}$	80%[b]	80%[b]
MR compressor power	$\dot{W}_{MR\ Com,\ BH}$	1.06 kW[b]	1.06 kW[b]
Isentropic efficiency of MR compressor	$\eta_{ISEN,\ MR\ Com}$	85%[b]	85%[b]
Actual work	$\dot{W}_{Com,\ BH} = \dot{W}_{MR\ Com,\ BH} + \dot{W}_{H_2\ Com,\ BH}$	1.127 kW = 1.06 kW + 0.067 kW[c]	1.127 kW = 1.06 kW + 0.067 kW[b]

a From Fig. 7, Simulation data of the laboratory test rig with the proposed simplified composition compared to the experimental data with H_2 and helium operation at steady state.
b Experimental data: mass flow rates, inlet and outlet pressures, and temperatures of compressors were used to simulate the values in PRO/II.
c Values assumed to be the same as in the experiment
d Values measured directly from the experiment at the test rig.

quality and there was no moisture. It is important to note that the measured MR compressor power consumption should be the same as the simulation value. Compressor powers of 0.067 kW for the hydrogen compressor and 1.06 kW for the MR compressor were obtained from the measured pressures and temperatures of both the suction and discharge together with the measured flow rate. The isentropic efficiencies of the two compressors were 80% and 85%, which are quite high; this may have been due to the small mass flow rates. The final overall test rig power consumption was 1.12 kW.

In Fig. 7, regarding the flow rate of the MR and hydrogen streams, the simulation and experimental results are exactly the same because the experimental data were input into the simulation software. In contrast, there are small discrepancies in the temperatures because the SRK model used in the commercial software is only an approximation.

5.2. *Uncertainty analysis*

5.2.1. *Simulation data*

The main thermophysical properties of hydrogen gas at 4.8 bar and between −150 °C and 0 °C, as shown in Fig. 7, were compared to REFPROP 8 by NIST [21] as a reference. The average uncertainties for n-H_2 of some important properties such as ρh, s, and c_P were found to be 0.7%, 2.2%, 0.6%, and 7.1%, respectively. However, the MR side is very complicated; thus, an uncertainty analysis is difficult to perform due to its complex composition.

5.2.2. *Parameters calculated from the simulation data*

An uncertainty analysis for the calculated parameters of the proposed system was performed using the method by Moffat [22]. According to that method, the function R is calculated from a set of N simulated data (independent variables), which is represented by $R = R(X_1, X_2, X_3, \ldots, X_N)$. Then, the uncertainty of the result R can be determined by combining the uncertainties of individual terms by using a root-sum-square method, i.e.,

$$\delta R = \left\{ \sum_{i=1}^{N} \left(\frac{\partial R}{\partial X_i} \delta X_i \right)^2 \right\}^{1/2}$$

Using the accuracies as simulation variables, the uncertainties of the parameters calculated by PRO/II, such as $\dot{W}_{H_2\ Com,\ BH}$, and $\eta_{ISEN,\ H_2\ Com}$ as shown in Table 5, estimated by the analysis are 0.3% and 0.3%, respectively.

5.2.3. *Measured data*

The uncertainty of the measured data, such as temperatures, pressures, and flow rates of both hydrogen and MR sides, due to errors in the measuring devices are reported and were given above in Section 2, *Test rig description*.

5.3. *Differences betweem simulation and experimental data*

The main conclusion is that the compressor power and liquefier efficiency were the same as the simulation data. Although the test rig was capable of cooling hydrogen gas using the MR refrigeration system, it was only able to reach a temperature of −158 °C instead of the designed value of −198 °C. Even for the final experimental results, the MR cycle was not well adjusted, meaning it was very successful. However, additional experimental work is required to study, identify, and resolve the problems. Several factors can explain why the temperature could not be decreased to −198 °C, and some differences between the simulation and experimental data are as follows:

- Correct MR composition:
  Most of the flow was directed to EX3; therefore, the composition consisted of methane and nitrogen. It was not known if there was an adequate amount of liquid methane and nitrogen after EX3 to boil and cool HX3 and HX4 or if a LIQ (liquid separator) was present after EX3. Thus, the temperature at TE212 could not reach 198 °C. The chromatography measured the composition of the test rig, which was compared to the simulated composition. However, that was not more important than determining if there was an adequate amount of liquid in each liquid separator to boil, absorb heat, and cool each heat exchanger. Additionally, before steady state, the temperature of the MR flow was higher after expanding at EX3. According to the simulation, this indicates that more volatile components such as methane, nitrogen, and especially neon were required in the composition. If the MR composition was not correct, then it would not be able to reach the desired temperature, regardless of the flow rate of the MR refrigerant.

- Correct amount of MR refrigerant charged into the rig:
  If the quantity of refrigerant is not sufficient, then both the suction and discharge pressures will be low. In the opposite case, both pressures will be high. Therefore, it is difficult to control the appropriate pressures.

- Correct MR compressor suction and discharge pressures:
  The discharge pressure should be about 18 bar or higher, and higher pressures are more favorable because they result in lower temperatures after the expansion valves. The pressure could be as high as 22–24 bar according to the simulation results. This higher pressure could be achieved by using a faster compressor speed, closing more expansion valves, and charging more refrigerant. However, more power consumption is required for the MR compressor for a high discharge pressure. Additionally, according to the simulation, the MR compressor suction pressure should be about 2 bar. However, the simulation can only predict the qualitative behavior; the actual values could be slightly lower or higher. Additional experiments should be performed to determine the optimal suction and discharge pressures of the MR cycle.

- Correct flow rate of the MR refrigerant:
  If there is not sufficient flow, it will not transfer heat, and the liquefier will be too warm. The control must to be adjusted during the experiment to ensure that the flow is sufficient to produce the desired temperature.

- Helium must be in operation:
  The helium was always turned on to cool HX5, which was the lowest temperature heat exchanger. Because HX5 was

connected to HX4, heat conduction occurred to HX4. If there was no helium flow to cool it down, then it would be too warm. Also, the recycled hydrogen that flowed back from HX5 would be warm. Therefore, the other heat exchangers, HX1, HX2, HX3, and HX4, would be warmer. For HX5, it always had to be cooled by helium to produce the coolest exchanger as explained above.

- Flow rate of feed hydrogen gas:
  If the MR flow rate was too low, but the feed hydrogen gas was too high, then there would not be enough MR flow to cool the heat exchangers. The correct hydrogen flow rate should correspond to the correct MR flow rate.

6. Conclusion

From the simulation, a simplified five-component mixture that consisted of 4% neon, 12% nitrogen, 26% methane, 30% ethane, and 28% butane was developed for the new MR refrigeration system. Suitable MR compressor suction and discharge pressures were found as 2 bar and 18 bar, respectively, which yielded the lowest MR compressor power of 4.55 kW. Initial experiments showed that the test rig could cool 0.6 kg/h normal hydrogen gas from 25 °C to 158 °C with a measured simplified five-component mixture similar to the simulated composition: 1% neon, 10% nitrogen, 33% methane, 38% ethane, and 18% butane. The power consumption required to pre-cool the feed hydrogen gas was 1.76 kW h per kilogram. After two weeks, the lowest temperature was about −180 °C with a few more grams of nitrogen gas charged into the rig. More volatile components such as neon and nitrogen must be charged into the rig to further decrease the temperature to −200 °C. The resulting power consumption was nearly equal to that of the initial experiment, and the simulated and experimental power consumption were nearly equal. The main conclusion was that pre-cooling hydrogen gas with the new MR refrigeration system resulted in a lower energy consumption compared to conventional refrigeration systems. This lower energy consumption was due to the higher heat transfer coefficient of boiling MR for a lower mass flow rate of compression at the MR compressor. Currently, an actual hydrogen liquefaction plant at Ingolstadt consumes 4.86 kW h per kilogram using a nitrogen refrigeration system. Therefore, it is highly recommended to design this new refrigeration system to pre-cool feed normal hydrogen gas from an ambient temperature of 25 °C down to equilibrium hydrogen gas at −200 °C in the future large-scale hydrogen liquefaction plant.

Acknowledgements

The authors would like to thank the Department of Energy and Process Engineering at the Norwegian University of Science and Technology for a research fellow grant. Also, financial support provided by the Shell Global International Company and the Research Council of Norway (project 164494) for the construction of the test rig and subsequent experiments is greatly appreciated.

Nomenclature

Symbols and abbreviations

c_P	specific heat, kJ/kg K
h	enthalpy, kJ/kg
$\dot{I}$	exergy loss/irreversibility, W
N	total number of independent variables in the function R, –
R	function of independent variables, –
s	entropy, kJ/kg K
$\dot{W}$	power, W
X	independent variable, –
$\dot{X}$	stream exergy flow, W
$\dot{m}$	mass flow rate, kg/h

Greek letters

η	efficiency, –
ρ	density, kg/m^3

Subscripts

1–38	stream number of the process depicted in Figs: 2 and 6, –
BH	brake/shaft horse, –
H_2	of hydrogen, –
$H_{2\ Com}$	of hydrogen compressor, –
ISEN	isentropic, –
min	minimum, –
MR	of MR, –
MR Com	of MR compressor, –

REFERENCES

[1] Dewar J. Liquid hydrogen. Science 1898;8:3–6.
[2] Barron RF. Cryogenic systems. Oxford: Oxford University Press; 1966.
[3] Timmerhaus KD, Flynn TM. Cryogenic process engineering. New York: Springer; 1989.
[4] Nandi TK, Sarangi S. Performance and optimization of hydrogen liquefaction cycles. Int J Hydrogen Energy 1993;18:131–9.
[5] Baker CR, Shaner RL. A study of the efficiency of hydrogen liquefaction process. Int J Hydrogen Energy 1978;3:321–34.
[6] Bracha M, Lorenz GA, Wanner M. Large-scale hydrogen liquefaction in Germany. Int J Hydrogen Energy 1994;19:53–9.
[7] Matsuda H, Nagami M. Study of large hydrogen liquefaction process. WE-NET: Summary of annual reports Available from:. Kanagawa, Japan: Nippon Sanso Corp http://www.enaa.or.jp/WE-NET/ronbun/1997/e5/sanso1997.html; 1998 [accessed 14.06.2009].
[8] Mitsugi C, Harumi A, Kenzo F. WE-NET: Japanese hydrogen program. Int J Hydrogen Energy 1998;23:159–65.
[9] Quack H. Conceptual design of a high efficiency large capacity hydrogen liquefier. Adv Cryog Eng 2002;47:255–63.
[10] Kuzmenko IF, Morkovkin IM, Gurov EI. Concept of building medium-capacity hydrogen liquefiers with helium refrigeration cycle. Chem Petro Eng 2004;40:94–8.
[11] Shimko M, Gardiner M. Innovative hydrogen liquefaction cycle. Available from: http://www.hydrogen.energy.gov/pdfs/progress08/iii_7_shimko.pdf; 2007 [accessed 14.06.2009].

[12] Valenti G. Proposal of an innovative, high-efficiency, large-scale hydrogen liquefier. Int J Hydrogen Energy 2008;33:3116–21.
[13] Berstad D, Stang J, Neksa P. Large-scale hydrogen liquefier utilising mixed-refrigerant pre-cooling. Int J Hydrogen Energy 2010;35:4512–23.
[14] Krasae-in S, Stang J, Neksa P. Development of large-scale hydrogen liquefaction processes from 1898 to 2009. Int J Hydrogen Energy 2010;35:4524–33.
[15] Bottura L. Cryogenic mixed refrigerant processes. Cryogenics 2009;49:745–6.
[16] Chrz V. Cryogenic mixed refrigerant processes. Int J Refrig 2010;33:648–9.
[17] Mafi M, Amidpour M, Mousavi Naeynian SM. Development in mixed refrigerant cycles used in olefin plants. In: Proc first Annu Gas Process Symp 10–12 January 2009, Doha, Qatar, p. 154–61.
[18] Bosma P, Nagelvoort RB. Liquefaction technology; developments through history. In: Proc first Annu Gas Process Symp. 10–12 January 2009, Doha, Qata, p. 19–31.
[19] Stang J, Neksa P, Brendeng E. On the design of an efficient hydrogen liquefaction process. WHEC 16/13–16, June 2006 – [Lyon, France].
[20] Krasae-in S, Stang J, Neksa P. Exergy analysis on the simulation of a small-scale hydrogen liquefaction test rig with a multi-component refrigerant refrigeration system. Int J Hydrogen Energy 2010;35:8030–42.
[21] National Institute of Standards and Technology (NIST). Thermophysical Properties Division, Chemical Science and Technology Laboratory. Thermophysical properties of hydrogen. Available from: http://www.boulder.nist.gov/div838/Hydrogen/Properties/Properties.htm [accessed 19.05.10].
[22] Moffat RJ. Describing the uncertainties in experimental results. Exp Thermal Fluid Sci 1988;1:3–17.

Krasae-in S, Stang J, Neksa P. Simulation on a proposed large-scale liquid hydrogen plant using a multi-component refrigerant refrigeration system. Int J Hydrogen Energy 2010;35(22):12531-44.

INTERNATIONAL JOURNAL OF HYDROGEN ENERGY 35 (2010) 12531–12544

Available at www.sciencedirect.com

ScienceDirect

journal homepage: www.elsevier.com/locate/he

Simulation on a proposed large-scale liquid hydrogen plant using a multi-component refrigerant refrigeration system

Songwut Krasae-in [a,*], *Jacob H. Stang* [b,1], *Petter Neksa* [b,2]

[a] *Norwegian University of Science and Technology, Kolbjorn Hejes vei 1d, NO-7491 Trondheim, Norway*
[b] *SINTEF Energy Research AS, Kolbjorn Hejes vei 1d, NO-7465 Trondheim, Norway*

ARTICLE INFO

Article history:
Received 9 June 2010
Received in revised form
17 August 2010
Accepted 17 August 2010
Available online 9 September 2010

Keywords:
Liquid hydrogen
Hydrogen liquefier
Large hydrogen liquefaction
Exergy efficiency

ABSTRACT

A proposed liquid hydrogen plant using a multi-component refrigerant (MR) refrigeration system is explained in this paper. A cycle that is capable of producing 100 tons of liquid hydrogen per day is simulated. The MR system can be used to cool feed normal hydrogen gas from 25 °C to the equilibrium temperature of −193 °C with a high efficiency. In addition, for the transition from the equilibrium temperature of the hydrogen gas from −193 °C to −253 °C, the new proposed four H_2 Joule–Brayton cascade refrigeration system is recommended. The overall power consumption of the proposed plant is 5.35 kWh/kg_{LH2}, with an ideal minimum of 2.89 kWh/kg_{LH2}. The current plant in Ingolstadt is used as a reference, which has an energy consumption of 13.58 kWh/kg_{LH2} and an efficiency of 21.28%: the efficiency of the proposed system is 54.02% or more, where this depends on the assumed efficiency values for the compressors and expanders. Moreover, the proposed system has some smaller-size heat exchangers, much smaller compressor motors, and smaller crankcase compressors. Thus, it could represent a plant with the lowest construction cost with respect to the amount of liquid hydrogen produced in comparison to today's plants, e.g., in Ingolstadt and Leuna. Therefore, the proposed system has many improvements that serve as an example for future hydrogen liquefaction plants.

1. Introduction

Because hydrogen has shown promise as an important energy vector for use in future transportation vehicles, several hydrogen research projects have been conducted since 1980 and in particular, since 2000. One of the challenges in creating a hydrogen economy is the low efficiencies of the current hydrogen liquefaction plant cycles. Currently, large hydrogen liquefaction plants, e.g., the plant in Ingolstadt as described by Bracha et al. [1], have exergy efficiencies of just 20–30%. These efficiencies are very low. The plant consumes 4.86 kWh per kilogram of hydrogen gas using a nitrogen refrigeration system to pre-cool normal hydrogen gas from 25 °C to equilibrium hydrogen gas at −198 °C. From 1998 through 2008, some conceptual plants were proposed with reportedly improved efficiencies of 40–50% [2–7]. A literature review for the development of large-scale hydrogen liquefaction processes throughout the world from 1898 to 2009 is given by Krasae-in et al. [8]. Finally, in the year 2010, the Norwegian University of Science and Technology (NTNU) and the Scandinavian Research Foundation (SINTEF) Energy Research AS proposed a new large-scale MR system with efficiency in excess of 50%. The details of this new system are reported in this paper.

* *Corresponding author*. Tel.: +47 735 92991; fax: +47 735 97214.
E-mail addresses: songwut.krasaein@ntnu.no, krasaein@hotmail.com (S. Krasae-in), jacob.stang@sintef.no (J.H. Stang), petter.neksa@sintef.no (P. Neksa).
[1] Tel.: +47 735 98109; fax: +47 735 93950.
[2] Tel.: +47 735 93923; fax: +47 735 93950.
0360-3199/$ – see front matter
doi:10.1016/j.ijhydene.2010.08.062

2. The proposed 100 ton per day LH_2 plant with the MR refrigeration system

For a larger metropolitan area with 100,000–200,000 hydrogen vehicles, the automotive consumption rate will be in the magnitude of 100 tons/day (TPD) [9]. Therefore, a large-scale LH_2 plant of that size will be proposed in this section. From a preliminary study, single MR refrigeration alone cannot be used to cool down n-GH_2 from 25 °C to −253 °C because there will be solidification of the mixed heavy component between −193 °C and −253 °C. MR refrigeration can be used with a very high efficiency to cool down the gas from 25 °C to only −193 °C, as shown in Fig. 1. Then, to cool equilibrium hydrogen gas from −193 °C to −253 °C, a four H_2 Joule–Brayton cascade system is recommended in this paper. It is noted that w_A is the net power for system A, while w_B is the net power for system B.

2.1. *Choice of refrigeration systems for the proposed plant*

Refrigeration systems such as MR, nitrogen, helium, and propane can be used to cool hydrogen gas from 25 °C to −193 °C (see Table 1). MR, which is a cycle under research at NTNU-SINTEF, was selected first because it has the lowest power consumption.

MR cycle has been used for decades in the Liquefied Natural Gas (LNG) sector. This concept of mixed refrigerant in gas liquefaction [10–13] discovered in the past few years results in reduced energy consumption compared to conventional liquefaction. The novelty of this mixed refrigerant system is described very well by Flynn [14]. The differences involve the new modified cycle and the new optimized refrigerant mixture that was specially designed for pre-cooling hydrogen gas from 25 °C to −198 °C explained in Section 2.3.

Today, large-scale plants that use nitrogen refrigeration systems [1] have a power consumption of 4.86 kWh/kg_{LH2}. From a simulation test run in a commercial software package, SimSci-PRO/II, the helium system of Valenti and Macchi [6] has a very high energy consumption. Propane in combination with a helium refrigeration system [3] cannot achieve a high efficiency because it only has one or two refrigerants and its own system cycle. For cooling hydrogen gas from −193 °C to −253 °C, either hydrogen or helium can be used as a refrigerant in refrigeration systems because they do not freeze in this low temperature range. Hydrogen freezes at temperatures below −259 °C, while helium freezes below −272 °C. Helium is widely used as a refrigerant in cryocoolers because it remains in the gas phase at extremely low temperatures. The Matsuda and Nagami [2] under a Japanese hydrogen program [16] and Praxair cycles are quite similar to the Ingolstadt and Leuna cycles. Since they are all hydrogen refrigeration systems; in particular, Ingolstadt's cycle requires 8.65 kWh/kg_{LH2} of power to cool hydrogen gas from −193 °C to −253 °C [4], which is a high power consumption. Thus, we will now consider the helium system [3], which is too simple. However, from a simulation test that was run with a 64-bar discharge and a 2.7-bar suction pressure in the Joule–Brayton cycle, it is impossible to have a high efficiency system. Kuz'menko et al. [4]'s helium system has a power consumption of 7.84 kWh/kg_{LH2}, which is a little better than the hydrogen refrigeration's power consumption of 8.65 kWh/kg_{LH2}. However, it is still very high due to the complexity of the helium liquefaction process. For Shimko and Gardiner [5]'s helium system, the preliminary simulation/test run in PRO/II indicates that it is still not good in comparison to the proposed four H_2 Joule–Brayton cascade system. Finally, the performance of the reversed helium/neon Brayton cycle by Berstad et al. [7] is may be lower because helium gas has inferior heat transfer properties to hydrogen gas used in the cycle proposed in this paper. The researchers aforementioned have developed the systems with plenty of the best efforts; more explanations of remodeling those conceptual plants are made by Krasae-in et al. [8]. This paper proposes completely new configurations and systems. The MR refrigeration system is selected to cool from 25 °C to −193 °C in combination with the four H_2 Joule–Brayton cascade system, which cools from −193 °C to −253 °C. The proposed MR system consumes only 1.36 kWh/kg_{LH2} in comparison to the ideal of 0.51 kWh/kg_{LH2}. In addition, the proposed four H_2 Joule–Brayton cascade system consumes 3.99 kWh/kg_{LH2} in comparison to the ideal of 2.38 kWh/kg_{LH2}. Finally, comparison of the energy consumption of the proposed MR refrigeration system and the proposed four H_2 Joule–Brayton cascade system to other conventional and the conceptual refrigeration systems, is detailed in Table 1.

2.2. *The whole process plant*

In Fig. 2, the flow sheet was developed from the PRO/II simulation flow sheet that was modified from a laboratory test rig based on research at NTNU-SINTEF. Experiments were conducted. The simulation data and experimental data matched

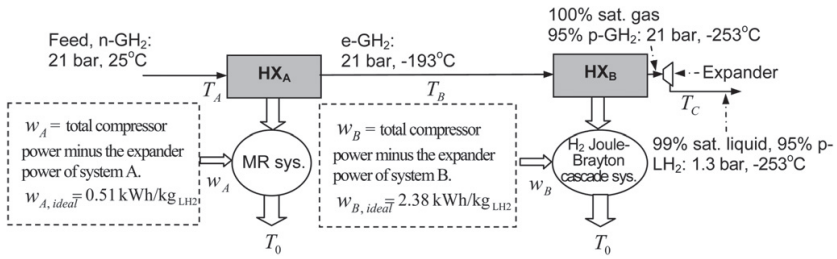

Fig. 1 – MR refrigeration system in combination with the four H_2 Joule–Brayton cascade refrigeration system.

Table 1 – Choice of refrigeration systems for the proposed 100-TPD H_2 liquefaction plant.

System	Refrigeration system	Inventor	Energy consumption
HX_A	MR refrigeration	Propose in this paper	1.30 kWh/kg_{LH2}
	N_2 refrigeration	Matsuda and Nagami [2]	≈4.86 kWh/kg_{LH2}
		Ingolstadt plant in1992 [1]	4.86 kWh/kg_{LH2}
		Leuna plant in 2007 [8]	≈4.86 kWh/kg_{LH2}
		Praxair since 1957 [8]	≈4.86 kWh/kg_{LH2}
	Helium refrigeration	Valenti and Macchi [6]	Extremely higher than 4.86 kWh/kg_{LH2}
	Propane + helium refrigeration	Shimko and Gardiner [5]	Higher than 4.86 kWh/kg_{LH2}
		Quack [3]	Higher than 4.86 kWh/kg_{LH2}
HX_B	H_2 refrigeration	Matsuda and Nagami [2]	A little ≤8.65 kWh/kg_{LH2}
		Ingolstadt plant in 1992 [1]	8.65 kWh/kg_{LH2}
		Leuna plant in 2007 [8]	A little ≤8.65 kWh/kg_{LH2}
		Praxair since 1957 [8]	A little ≤8.65 kWh/kg_{LH2}
	Helium refrigeration	Valenti and Macchi [6]	Higher than 8.65 kWh/kg_{LH2}
		Shimko and Gardiner [5]	Higher than 8.65 kWh/kg_{LH2}
		Quack [3]	Higher than 8.65 kWh/kg_{LH2}
		Kuz'menko et al. [4]	7.84 kWh/kg_{LH2}
	Reversed helium/neon Brayton cycle	Berstad et al. [7]	≈5.18 kWh/kg_{LH2}
	Four H_2 Joule–Brayton cascade refrigeration	Propose in this paper	3.80 kWh/kg_{LH2}

well, and the main discovery was that pre-cooling hydrogen gas with this new MR refrigeration system resulted in a lower energy consumption per kilogram of feed hydrogen gas compared to conventional refrigeration systems. Details of the results will be reported in an upcoming paper.

For simplicity, it is assumed that there is no pressure drop in the simulation because the exact components' sizes such as heat exchangers and pipings are not known. The single hydrogen feed-through stream is at: a pressure of 21 bar (which is the same condition as the Ingolstadt plant [1]), a temperature of 25 °C, and a flow rate of 1.157 kg/s for 24 h a day in operation or 100-TPD. The large-scale isentropic efficiency for every compressor and expander is assumed to be 80% (usually 90% found in large-scale refrigeration compressors) for the worst case; thus, it has already compensated for the no pressure drop assumption and the temperature difference, which is too small, between the pre-cooled hydrogen gas stream and the MR pre-cooling stream. Moreover, if the three or more number of stages required in compression are used which means more number of compressors, the overall system's efficiency will be better. However, it will be more expensive than a single compression (only single big compressor) and two-stage compression (two compressors). It is not known how much it costs for each compressor. This information is needed to investigate the number of stages required in the compressors as well as in the expanders to think of the payback period of investment. A frequently applied approximation for optimum intermediate pressure of ideal gas compression or expansion, in this case which possibly applicable to MR and hydrogen gases that for simplicity are assumed to be ideal, is given by: $P_{opt\ int} = \sqrt{P_L P_H}$. Where $P_{opt\,int}$ represents an estimate of the optimum intermediate pressure, P_L is the low pressure, and P_H is the high pressure. In addition, due to the large volume of mass flow rates and low compression ratios, MR compressors and hydrogen compressors must be dynamic. On the other hand, because of lower mass flow rates at expanders in the MR cycle proposed have two-phase inlets and outlets, thus volumetric machines that have margin for two-phase flows are recommended. The manufacturers should be consulted about the machinery. In this paper, at least two-stage compression with inter-cooling between stages is recommended as an example. More than two-stage compression of MR is used just because lower compression power. But, compression of hydrogen gas in the four H_2 Joule–Brayton cascade cycle, more than two-stage compression must be used, because, besides lower energy consumption, a single stage compression results in very high outlet temperature. The condensers must be evaporative cooling towers. Mechanical conversion of work from the expander is assumed to be 98%. For cooling n-H_2 from 25 °C to e-H_2 around −193 °C, the MR refrigeration system is proposed. For cooling from −193 °C to −253 °C, as a preliminary design, a combination of the four H_2 cascade and the Brayton refrigeration system is proposed due to the improved efficiency. In fact, the whole 100-TPD-capacity plant flow sheet can be split into subsystems with the exact same cycle, e.g., 50/50, 33/33/33, 25/25/25/25 TPD, or more. This depends on the limitations, e.g., the sizes of the compressors, expanders, and heat exchangers that are available in the market; installation areas; etc.

Table 2 lists the boundary conditions that were used to simulate the process depicted in Fig. 2. It contains design and assumption data. Ambient temperature, capacity, GH_2 feed, and LH_2 product were the design values. For simplicity, no pressure drop was assumed. Good low temperature heat exchangers for cryogenic system were generally recommended by Barron [15] to have a 1–2 °C temperature approach. The compressors' efficiencies were estimated from the manufacturers' product catalogues, which generally contained large size gas compressors. The process was simulated with the PRO/II software package. For the equation of state, Redlich-Kwong-Soave (SRK) was selected for use because of its popularity, simplicity, and fast computation.

In PRO/II simulation software, the component models of heat exchangers, compressors, and expanders are absolutely correct. But investigation the accuracy of the modeling of all the working fluids in the cryogenic region of interest must be performed. The thermodynamic model must be validated first. Regarding hydrogen, one may use as a comparison either

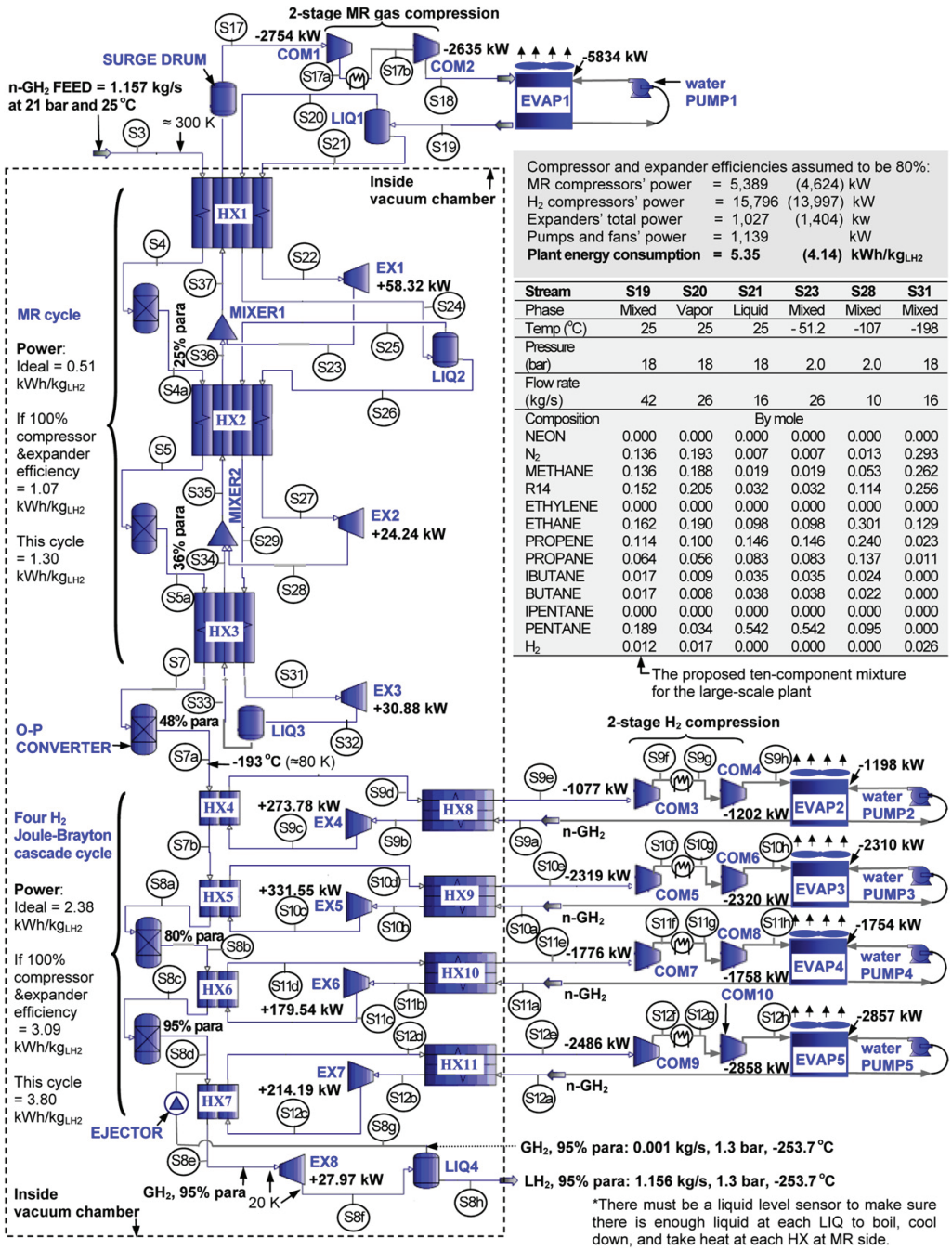

Stream	S19	S20	S21	S23	S28	S31
Phase	Mixed	Vapor	Liquid	Mixed	Mixed	Mixed
Temp (°C)	25	25	25	-51.2	-107	-198
Pressure (bar)	18	18	18	2.0	2.0	18
Flow rate (kg/s)	42	26	16	26	10	16
Composition	By mole					
NEON	0.000	0.000	0.000	0.000	0.000	0.000
N_2	0.136	0.193	0.007	0.007	0.013	0.293
METHANE	0.136	0.188	0.019	0.019	0.053	0.262
R14	0.152	0.205	0.032	0.032	0.114	0.256
ETHYLENE	0.000	0.000	0.000	0.000	0.000	0.000
ETHANE	0.162	0.190	0.098	0.098	0.301	0.129
PROPENE	0.114	0.100	0.146	0.146	0.240	0.023
PROPANE	0.064	0.056	0.083	0.083	0.137	0.011
IBUTANE	0.017	0.009	0.035	0.035	0.024	0.000
BUTANE	0.017	0.008	0.038	0.038	0.022	0.000
IPENTANE	0.000	0.000	0.000	0.000	0.000	0.000
PENTANE	0.189	0.034	0.542	0.542	0.095	0.000
H_2	0.012	0.017	0.000	0.000	0.000	0.026

Fig. 2 – PRO/II simulation flow sheet for the proposed large-scale 100-TPD LH_2 plant with MR and four H_2 Joule–Brayton cascade cycles.

Table 2 – Boundary conditions.

Parameter	The proposed 100-TPD process plant from the simulation
Ambient temperature	25 °C
Capacity	100-TPD (in 24 h) = 4166 kg/h = 1.157 kg/s
GH_2 feed	21 bar and 25 °C
LH_2 product	1.3 bar, saturated liquid with 95% para
Ortho-para conversion	Stepwise
Pressure drop in system	No
Temperature approach in heat exchangers	1–2 °C (arbitrarily selected for high effefectiveness)
Isentropic efficiency:	
Compressors	80% (arbitrarily selected for the worst case)
Expanders	80% (selected similar to actual machinery)

the monography R. McCarty, J. Hord, H. Roder, selected properties of hydrogen (Engineering Design Data), Tech. Rep. Monograph 168, U.S. National Bureau of Standards (now NIST) (1981) or the software REFPROP 8. Recently, the best paper about hydrogen properties is given by Leachman et al. [17]. All data about thermo-physical properties of fluid hydrogen from the same researchers mentioned, found at the software REFPROP 8, can also be checked at NIST [18].

However, after investigating the accuracy of the modeling of all the working fluids in the region of interest especially hydrogen gas at temperature between −193 °C to −253 °C, it is found that SRK model is quite the same as that of the model from REFPROP 8. This is also in temperature range between 25 °C to −193 °C. It is especially the given values of pressure and temperature, then the simulated density will be exactly the same. Even though there are some differences regarding simulated enthalpy and entropy, this is because the references used in the two models are not the same; but the simulated enthalpy and entropy increments (Δh and Δs) are the same which indicate the two values are correct. These two values are important in energy and exergy analyses of the overall plant. Moreover, even if there are some extremely small deviations of specific heat coefficients, but this is acceptable. The other thermo-physical properties are not important. In short, the SRK model is adequate for the cryogenic region and the simulation results are near the reality.

2.3. *MR refrigeration system for cooling feed normal hydrogen gas from 25 °C to the equilibrium temperature of −193 °C*

When designing a large MR refrigeration system, there are various ways to improve efficiency. Briefly, these improvements include the following: to use 21-bar single n-GH_2 feed-through, to use a high isentropic efficiency MR compressor, to replace every expansion valve with a high efficiency expander, to use a ten-component mixture of MR refrigerant, to add another liquid separator after EX3, and to improve the condenser. The flow sheet is depicted in Fig. 2.

The MR compressor power must be minimized. Thus, the variables that must be optimized were determined from trial and error in PRO/II and are arranged below:

1. First, the suitable feed pressure of the H_2 compressor must be determined:
   The feed pressure must be above 15 bar, which is the supercritical pressure to avoid condensation. The pressure of 18 bar may still be too close to 15 bar. For the proposed plant, the discharge pressure is designed to be 21 bar, which is equal to the feed at Ingolstadt (see Fig. 1). However, for the real large-scale process, if the feed is 1–2 bar, it is recommended to compress it to 21 bar.
2. Then, the hot stream hydrogen outlet temperatures from HX1, HX2, and HX3 should be determined:
   This is determined from trial and error for the minimum MR compressor in the simulation software. In addition, the MR mass flow rate at HX1 is the largest, while HX3 is the smallest. Thus, HX1 should cool and remove heat from the hydrogen gas more than HX3.
3. Next, a suitable discharge pressure for the MR compressor should be determined:
   The discharge pressure cannot be lower than 18 bar because it will be impossible to cool the system. In addition, it should not be more than 22 bar because there will be too much compression power.
4. After that, a suitable suction pressure for the MR compressor must be determined:
   The suction pressure cannot be lower than 1 bar because of the MR compressor's high power. The suction should not be more than 2 bar because it will be insufficient or impossible to cool the hydrogen gas.
5. Finally, a suitable composition for the MR mixture and the flow rate should be determined:
   This is also found from trial and error. This step is more complex, e.g., up to a ten-component mixture is needed for the large-scale plant's process.

Previously, Krasae-in et al. [19] made the design and simulation of a small-scale test rig. The new, optimized MR has been particularly modified for large-scale processes with heat conversion by catalysts and has the following composition: 1.2% hydrogen, 13.6% nitrogen, 13.6% methane, 15.2% R14, 16.2% ethane, 11.4% propene, 6.4% propane, 1.7% Ibutane, 1.7% butane, and 18.9% pentane. A better efficiency is attained when neon is replaced with 1.3% hydrogen. All of these results were determined from trial and error by the simulation in PRO/II. In fact, the catalysts should be filled inside of the heat exchangers to improve efficiency, but this cannot be simulated in the PRO/II software. There is a liquid separator, LIQ3, that acts as a buffer to maintain enough volatile components, such as nitrogen, methane, R14, and hydrogen (or not). They are almost in the liquid phase after expansion at stream 32 (S32). If they are not charged enough, the HX3 will not be able to cool the hydrogen gas to the designed value at −193 °C. There will not be enough of the volatile mixture to cool down the HX3. If they are charged too much, there is no problem; they will be kept in the liquid phase while in operation at LIQ4. Moreover, there is no energy loss from having the liquid separator, LIQ3. A surge drum acts as a buffer to keep liquid MR refrigerant when the plant stops for

maintenance and to protect MR compressors while in operation. The simulation's net power, w_A is 1.36 kWh/kg$_{LH2}$ in comparison to the ideal of 0.51 kWh/kg$_{LH2}$. In Fig. 2, electricity consumptions for the cooling loads due to water pumps and air-cooled fans in the after coolers and evaporative condensers are very relatively small compared to compressors and expanders. However, they are assumed to be around 5% of power consumption from compressors as calculated in Table 7. From the simulation's calculations, second law analysis was conducted. The exergy losses are dissipated mainly through the following components: compressors 55%, evaporative condenser 19%, heat exchangers 18%, expanders 5%, mixers 1%, and liquid separator 1% as calculated in Table 5. In fact, the loss due to evaporative condenser may not be included because it seems not important to know. It is impossible to avoid all those losses aforementioned. However, this proposed MR cycle is the best system in comparison to the nitrogen, helium, and propane refrigeration systems, as shown in Table 1.

In Table 3, air flowing into evaporative condenser is assumed to be ambient at 25 °C with 50% relative humidity as a reference. This temperature and humidity is in summer time usually used for the peak heating load to design conventional refrigeration systems. And air flowing out, from experience, is assumed to be 32 °C with 100% relative humidity. Thus, air flow rate, $\dot{m}_{air}$, of each evaporative condenser can be calculated by a simple energy balance equation: $\dot{m}_{air}(h_{air,\ out} - h_{air,\ in}) = \dot{m}_{MR,\ S18}(h_{MR,\ S18} - h_{MR,\ S19})$. Air enthalpy and entropy values are from psychrometric chart or from HumidAirWeb [20]. This method used is also the same as what calculated in Table 4.

The proposed MR system is quite mature now with respect to process configuration. A little more research is needed for small improvements. This is just a preliminary design; it is not really a real one. More information from future studies on the MR ten-component mixture or the more complex mixtures is needed to better simulate the size of each MR heat exchanger. The information is as follows:

- The temperature of each pre-cooled hydrogen gas stream that leaves each heat exchanger, e.g., HX1, HX2, and HX3 from the experiment. Those temperatures depend on the information below.
- The optimized MR composition for the complex mixture from the test rig experiment.

Table 3 – Thermodynamic properties of each stream: enthalpy, entropy, specific exergy, and exergy flow of the proposed MR cycle.

Stream number	Pressure	Temp.	Flow rate	Specific enthalpy	Specific entropy	Specific exergy	Exergy flow	Phase	Description
	P	T	$\dot{m}$	h	s	e_x	$\dot{E}_x$		
	(bar)	(°C)	(kg/s)	(kJ/kg)	(kJ/kg- K)	(kJ/kg)	(kW)		
3	21	25	1.157	175.87	76.12	2920.57	3379.10	Superheated vapor	H_2 cool gas
4	21	−46.15	1.157	−837.64	72.23	3074.06	3556.69	Superheated vapor	H_2 cold gas
4a	21	−46.15	1.157	−552.78	75.14	2485.92	2876.21	Superheated vapor	H_2 cold gas
5	21	−103.15	1.157	−1377.43	70.95	2918.27	3376.44	Superheated vapor	H_2 cold gas
5a	21	−103.15	1.157	−1373.83	70.98	2912.87	3370.19	Superheated vapor	H_2 cold gas
7	21	−198.15	1.157	−2776.45	58.84	5152.25	5961.15	Superheated vapor	H_2 cold gas
7a	21	−194.75	1.157	−2183.80	61.75	4871.90	5636.79	Superheated vapor	H_2 cold gas
7b	21	−213.15	1.157	−2481.86	57.42	5872.84	6794.88	Superheated vapor	H_2 cold gas
17	2	6	42.07	227.16	6.69	−92.05	−3872.48	Superheated vapor	MR cool gas
17a	6	39	42.07	292.62	6.74	−41.59	−1749.62	Superheated vapor	MR warm gas
17b	6	25	42.07	216.76	6.49	−42.45	−1785.80	Superheated vapor	MR cool gas
18	18	62	42.07	279.41	6.53	8.20	345.04	Superheated vapor	MR hot gas
19	18	25	42.08	140.73	6.10	0.00	0.00	Saturated liquid	MR cool liquid
20	18	25	26.01	194.38	5.70	172.02	4475.86	Saturated vapor	MR cool gas
21	18	25	16.06	53.81	6.73	−278.10	−4465.51	Saturated liquid	MR cool liquid
22	18	−46.15	16.05	−100.77	6.13	−251.98	−4044.25	Compressed liquid	MR cool liquid
23	2	−51.55	16.05	−104.41	6.14	−258.62	−4150.83	Mixture	MR cold mixture
24	18	−46.15	26.02	−17.62	4.88	206.17	5364.59	Mixture	MR cold mixture
25	18	−46.15	15.95	38.47	4.75	301.26	4805.12	Saturated vapor	MR cool gas
26	18	−46.15	10.07	−106.44	5.09	54.35	547.32	Saturated liquid	MR cool liquid
27	18	−103.15	10.07	−215.98	4.53	112.81	1136.01	Compressed liquid	MR cool liquid
28	2	−107.30	10.07	−218.40	4.54	107.39	1081.43	Mixture	MR cold mixture
29	18	−103.15	15.94	−142.50	3.82	399.29	6364.71	Mixture	MR cold mixture
31	18	−198.15	15.94	−350.50	2.13	697.93	11124.93	Mixture	MR cold mixture
32	2	−199.10	15.94	−352.43	2.14	694.10	11063.89	Mixture	MR cold mixture
34	2	−107.06	15.94	−42.65	4.73	226.14	3604.70	Mixture	MR cold mixture
35	2	−105.20	26.02	−110.67	4.66	179.12	4660.74	Mixture	MR cold mixture
36	2	−52.50	26.02	79.32	5.64	75.11	1954.40	Mixture	MR cold mixture
37	2	−50.20	42.08	9.02	5.83	−52.19	−2196.09	Mixture	MR cold mixture
EVAP1: air in	1	25 °C, 50% RH	95.15	50.760	0.1858	0.00	0.00	Air and water vapor	Moist air Saturated
EVAP1: air out	1	32 °C, 100% RH	95.15	112.07	0.3918	−0.5000	−47.57	Air and water vapor	moist air

Table 4 – Thermodynamic properties of each stream: enthalpy, entropy, specific exergy, and exergy flow of the proposed four H_2 Joule–Brayton cascade cycle.

Stream number	Pressure	Temp.	Flow rate	Specific enthalpy	Specific entropy	Specific exergy	Exergy flow	Phase	Description
	P	T	$\dot{m}$	h	s	e_x	$\dot{E}_x$		
	(bar)	(°C)	(kg/s)	(kJ/kg)	(kJ/kg-K)	(kJ/kg)	(kW)		
8a	21	−233.15	1.157	−2887.82	48.43	8163.88	9445.61	Superheated vapor	H_2 cold gas
8b	21	−232.08	1.157	−2591.49	48.84	8337.21	9646.15	Superheated vapor	H_2 cold gas
8c	21	−243.15	1.157	−2994.12	38.43	11057.58	12793.62	Superheated vapor	H_2 cold gas
8d	21	−243.15	1.157	−2782.80	37.56	11529.90	13340.09	Superheated vapor	H_2 cold gas
8e	21	−253.15	1.157	−2998.93	28.88	13917.77	16102.86	Superheated vapor	H_2 cold gas
8f	21	−253.71	1.157	−3023.10	28.88	13893.60	16074.90	Mixture: 99% liquid	H_2 mixture
8g	21	−253.71	0.001	−2509.85	53.07	7149.85	7.15	Superheated vapor	H_2 cold gas
8h	21	−253.71	1.156	−3023.10	28.88	13893.60	16061.00	Superheated vapor	H_2 cold liquid
9a	40	25.00	1.283	178.90	73.42	3733.60	4790.21	Superheated vapor	H_2 cold gas
9b	40	−195.15	1.283	−3036.41	53.61	6461.29	8289.84	Superheated vapor	H_2 cold gas
9c	14	−213.24	1.283	−3249.83	54.52	5974.87	7665.76	Superheated vapor	H_2 cold gas
9d	14	−195.54	1.283	−2980.96	58.46	5061.74	6494.21	Superheated vapor	H_2 cold gas
9e	14	24.00	1.283	159.80	77.75	2415.50	3099.09	Superheated vapor	H_2 cold gas
9f	23	87.44	1.283	1076.50	78.48	3113.20	3994.24	Superheated vapor	H_2 cold gas
9g	23	25.00	1.283	176.40	75.74	3035.10	3894.03	Superheated vapor	H_2 cold gas
9h	40	89.48	1.283	1113.19	76.26	3815.89	4895.79	Superheated vapor	H_2 cold gas
10a	40	25.00	1.633	181.06	73.43	3732.76	6095.60	Superheated vapor	H_2 cold gas
10b	40	−213.15	1.633	−3347.23	49.06	7515.47	12272.76	Superheated vapor	H_2 cold gas
10c	8	−234.11	1.633	−3550.20	50.42	6904.50	11275.05	Superheated vapor	H_2 cold gas
10d	8	−215.73	1.633	−3262.50	56.48	5374.20	8776.07	Superheated vapor	H_2 cold gas
10e	8	24.00	1.633	159.80	80.42	1614.50	2636.48	Superheated vapor	H_2 cold gas
10f	17.8	129.67	1.633	1686.60	81.15	2922.30	4772.12	Superheated vapor	H_2 cold gas
10g	17.8	25.00	1.633	175.06	76.80	2715.76	4434.84	Superheated vapor	H_2 cold gas
10h	40	122.71	1.633	1596.07	77.54	3914.77	6392.82	Superheated vapor	H_2 cold gas
11a	20	25.00	1.924	175.62	76.32	2860.32	5503.26	Superheated vapor	H_2 cold gas
11b	20	−233.15	1.924	−3661.50	43.88	8755.20	16845.00	Superheated vapor	H_2 cold gas
11c	6.8	−244.32	1.924	−3754.81	44.69	8418.89	16197.94	Superheated vapor	H_2 cold gas
11d	6.8	−232.43	1.924	−3512.60	51.94	6486.10	12479.26	Superheated vapor	H_2 cold gas
11e	6.8	24.00	1.924	158.10	80.73	1519.80	2924.10	Superheated vapor	H_2 cold gas
11f	11.6	99.58	1.924	1247.62	81.79	2291.32	4408.50	Superheated vapor	H_2 cold gas
11g	11.6	25.00	1.924	173.53	78.57	2183.23	4200.53	Superheated vapor	H_2 cold gas
11h	20	88.26	1.924	1087.28	79.09	2940.98	5658.45	Superheated vapor	H_2 cold gas
12a	2.2	25.00	2.099	171.35	85.44	120.05	251.98	Superheated vapor	H_2 cold gas
12b	2.2	−245.15	2.099	−3667.88	51.54	6450.82	13540.27	Superheated vapor	H_2 cold gas
12c	0.5	−253.57	2.099	−3769.91	52.90	5940.79	12469.72	Superheated vapor	H_2 cold gas
12d	0.5	−245.33	2.099	−3650.77	57.98	4535.93	9520.92	Superheated vapor	H_2 cold gas
12e	0.5	24.00	2.099	156.69	91.51	−1715.61	−3601.07	Superheated vapor	H_2 cold gas
12f	1.0	108.54	2.099	1372.85	92.25	−721.45	−1514.32	Superheated vapor	H_2 cold gas
12g	1.0	25.00	2.099	171.08	88.69	−855.22	−1795.11	Superheated vapor	H_2 cold gas
12h	2.2	119.54	2.099	1532.50	89.41	290.20	609.13	Superheated vapor	H_2 cold gas
EVAP2: air in	1	25 °C, 50% RH	19.55	50.760	0.1858	0.00	0.00	Air and water vapor	Moist air
EVAP2: air out	1	32 °C, 100% RH	19.55	112.07	0.3918	−0.5000	−9.77	Air and water vapor	Saturated moist air
EVAP3: air in	1	25 °C, 50% RH	37.69	50.760	0.1858	0.00	0.00	Air and water vapor	Moist air
EVAP3: air out	1	32 °C, 100% RH	37.69	112.07	0.3918	−0.5000	−18.84	Air and water vapor	Saturated moist air
EVAP4: air in	1	25 °C, 50% RH	28.61	50.760	0.1858	0.00	0.00	Air and water vapor	Moist air
EVAP4: air out	1	32 °C, 100% RH	28.61	112.07	0.3918	−0.5000	−14.30	Air and water vapor	Saturated moist air
EVAP5: air in	1	25 °C, 50% RH	46.60	50.760	0.1858	0.00	0.00	Air and water vapor	Moist air
EVAP5: air out	1	32 °C, 100% RH	46.60	112.07	0.3918	−0.5000	−23.30	Air and water vapor	Saturated moist air

2.4. *Cooling the feed equilibrium hydrogen gas from −193 °C to −253 °C by the four H_2 Joule–Brayton cascade refrigeration system*

Initially, Brayton Quack's [3] and Valenti and Macchi's [6] helium systems with optimized discharge and suction pressures were selected by a preliminary test run in PRO/II. However, from trial and error, it was found that replacing helium with hydrogen as a refrigerant in the four Joule–-Brayton cascade cycle that was proposed by Valenti and Macchi [6] is better than helium when cooling hydrogen gas from −193 °C to −253 °C. One disadvantage of helium is the high discharge temperature when it is compressed, which is due to the lower heat transfer properties. Hydrogen has much better heat transfer properties than helium. For that reason, the size of the heat exchangers will be smaller. In addition, the

Table 5 – Calculation of exergy loss in each process's component of the proposed MR cycle.

Component	Energy equation	Exergy equation	$\dot{I}$ (kW)	Percent loss %
COM1	$\dot{W}_{BH,\ COM1} = \dot{m}_{17}(h_{17a} - h_{17})$	$\dot{I}_{COM1} = \dot{E}_{x,\ 17} - \dot{E}_{x,\ 17a} + \dot{W}_{BH,\ COM1}$	631.05	30.93
COM2	$\dot{W}_{BH,\ COM2} = \dot{m}_{17}(h_{18} - h_{17b})$	$\dot{I}_{COM2} = \dot{E}_{x,\ 17b} - \dot{E}_{x,\ 18} + \dot{W}_{BH,\ COM2}$	504.84	24.75
HX1	$\dot{m}_3 h_3 + \dot{m}_{20} h_{20} + \dot{m}_{21} h_{21} + \dot{m}_{37} h_{37} = \dot{m}_4 h_4 + \dot{m}_{17} h_{17} + \dot{m}_{22} h_{22} + \dot{m}_{24} h_{24}$	$\dot{I}_{HX1} = (\dot{E}_{x,\ 3} + \dot{E}_{x,\ 20} + \dot{E}_{x,\ 21} + \dot{E}_{x,\ 37}) - (\dot{E}_{x,\ 4} + \dot{E}_{x,\ 17} + \dot{E}_{x,\ 22} + \dot{E}_{x,\ 24})$	188.82	9.26
HX2	$\dot{m}_{4a} h_{4a} + \dot{m}_{25} h_{25} + \dot{m}_{26} h_{26} + \dot{m}_{35} h_{35} = \dot{m}_5 h_5 + \dot{m}_{27} h_{27} + \dot{m}_{29} h_{29} + \dot{m}_{36} h_{36}$	$\dot{I}_{HX2} = (\dot{E}_{x,\ 4a} + \dot{E}_{x,\ 25} + \dot{E}_{x,\ 26} + \dot{E}_{x,\ 35}) - (\dot{E}_{x,5} + \dot{E}_{x,\ 27} + \dot{E}_{x,\ 29} + \dot{E}_{x,\ 36})$	57.83	2.83
HX3	$\dot{m}_{5a} h_{5a} + \dot{m}_{29} h_{29} + \dot{m}_{32} h_{32} = \dot{m}_7 h_7 + \dot{m}_{31} h_{31} + \dot{m}_{34} h_{34}$	$\dot{I}_{HX3} = (\dot{E}_{x,\ 5a} + \dot{E}_{x,\ 29} + \dot{E}_{x,\ 32}) - (\dot{E}_{x,\ 7} + \dot{E}_{x,\ 31} + \dot{E}_{x,\ 34})$	108.01	5.29
LIQ1	$\dot{m}_{19} h_{19} = \dot{m}_{20} h_{20} + \dot{m}_{21} h_{21}$	$\dot{I}_{LIQ1} = \dot{E}_{x,\ 19} - (\dot{E}_{x,\ 20} + \dot{E}_{x,\ 21})$	10.35	0.51
LIQ2	$\dot{m}_{24} h_{24} = \dot{m}_{25} h_{25} + \dot{m}_{26} h_{26}$	$\dot{I}_{LIQ2} = \dot{E}_{x,\ 24} - (\dot{E}_{x,\ 25} + \dot{E}_{x,\ 26})$	12.14	0.60
LIQ3	$\dot{m}_{32} h_{32} = \dot{m}_{33} h_{33}$	$\dot{I}_{LIQ3} = \dot{E}_{x,\ 32} - \dot{E}_{x,\ 33} = 0$	0.00	0.00
EX1	$\dot{m}_{22} h_{22} = \dot{m}_{23} h_{23} + \dot{W}_{EX1}$	$\dot{I}_{EX1} = \dot{E}_{x,\ 22} - \dot{E}_{x,\ 23} - \dot{W}_{EX1}$	48.25	2.37
EX2	$\dot{m}_{27} h_{27} = \dot{m}_{28} h_{28} + \dot{W}_{EX2}$	$\dot{I}_{EX2} = \dot{E}_{x,\ 27} - \dot{E}_{x,\ 28} - \dot{W}_{EX2}$	30.34	1.49
EX3	$\dot{m}_{31} h_{31} = \dot{m}_{32} h_{32} + \dot{W}_{EX3}$	$\dot{I}_{EX3} = \dot{E}_{x,\ 31} - \dot{E}_{x,\ 32} - \dot{W}_{EX3}$	30.16	1.48
MIXER1	$\dot{m}_{23} h_{23} + \dot{m}_{36} h_{36} = \dot{m}_{37} h_{37}$	$\dot{I}_{MIXER\ 1} = \dot{E}_{x,\ 23} + \dot{E}_{x,\ 36} - \dot{E}_{x,\ 37}$	0.33	0.02
MIXER2	$\dot{m}_{28} h_{28} + \dot{m}_{34} h_{34} = \dot{m}_{35} h_{35}$	$\dot{I}_{MIXER\ 2} = \dot{E}_{x,\ 28} + \dot{E}_{x,\ 34} - \dot{E}_{x,\ 35}$	25.39	1.24
EVAP1	$\dot{m}_{18} h_{18} + \dot{m}_{air,\ in} h_{air,\ in} = \dot{m}_{19} h_{19} + \dot{m}_{air} h_{air,\ out}$	$\dot{I}_{EVAP1} = (\dot{E}_{x,\ 18} + \dot{E}_{x,\ air,\ in}) - (\dot{E}_{x,\ 19} + \dot{E}_{x,\ air,\ out})$	392.62	19.24
Total		$\dot{I}_{total}$	2040.13	100

power consumption from the compressor is less when using hydrogen because of less mass flow rate compared to helium. To cool hydrogen from −243 °C to −253 °C, the hydrogen Brayton cycle is better. Currently, all large-scale plants use hydrogen refrigeration systems; nobody uses helium. Thus, it is recommended to use hydrogen. To improve efficiency, the four cycles may also be replaced by up to six cycles: −193 to −203 °C, −203 to −213 °C, −213 to −223 °C, −223 to −233 °C, −233 to −243 °C, and −243 to −253 °C. However, a larger number of heat exchangers results in a greater exergy loss; there will be more compressors and the system will be more complicated. The choice of pressure levels or temperature levels in the hydrogen Joule–Brayton cascade sub plant is all from trial and error to get optimum. Finally, the feed hydrogen gas at −253 °C is depressurized by the expander from 21 bar to 1.3 bar. By simulation, this is a 100% yield 95% p-LH_2. But in reality there might be a small fraction of vapor, thus 99% liquid (stream 8h) and 1% vapor (stream 8g) is assumed. Actually, para content at 95% of LH_2 output is enough to be kept for use, the same as Ingolstadt plant's. If it is more than this value, more conversion energy is needed which is not necessary. By doing this, the last heat exchanger must be designed to cool the hydrogen to the lowest possible temperature, e.g. near −253 °C, so there is no vapor fraction after the expansion at the last expander. A small ejector is recommended to recover p-GH_2 from the storage tank (LIQ4) the same as the plant in Leuna. In short, the sum of the simulation's net power, w_B, for the proposed system is 3.39 kWh/kg_{LH2} in comparison to the ideal of 2.38 kWh/kg_{LH2}. According to second law analysis, the exergy losses are dissipated through the following: compressors 32%, expanders 33%, heat exchangers 21%, and evaporative condensers 14% as calculated in Table 6. Exergy losses are much especially at expanders that two-stage expanders might be used. The losses due to evaporative condensers may also not be included because it seems not important to know. This proposed four H_2 Joule–Brayton cascade cycle is best compared to the nitrogen and helium refrigeration systems, as shown in Table 1. However, if anyone has suggestions or different opinions for more improvement, they can be proposed later. Unfortunately, the proposed four H_2 Joule–-Brayton cascade system is still not the best; each H_2 Joule–-Brayton cascade cycle is the Linde Hampson system, which is the world's first air liquefaction system, but with the expander to replace the Joule-Thomson (J-T) valve for work recovery. To improve the efficiency of the proposed large-scale system, each H_2 Joule–Brayton cascade cycle can be replaced with a pre-cooled Linde Hampson, a Claude, or a pre-cooled Claude systems, respectively. The pre-cooled Claude may be the best because of its own proven efficient cycle. Moreover, the helium-refrigerated or hydrogen-refrigerated hydrogen systems may be good as well. However, the system with pre-cooling needs an additional nitrogen pre-cooled system that makes the overall system complicated due to the additional compressors and heat exchangers for the nitrogen liquefaction system. The Claude system may also be good since it has a compressor power reduction around 5–10%, which was found in a preliminary test run in PRO/II; however, a greater number of heat exchangers and a high-priced expander are needed. For simplicity, it can be a J-T valve instead of an

Table 6 – Calculation of exergy loss in each process's component of the proposed four H_2 Joule–Brayton cascade cycle.

Component	Energy equation	Exergy equation	$\dot{I}$ (kW)	Percent loss %
COM3	$\dot{W}_{BH,\ COM3} = \dot{m}_{9e}(h_{9f} - h_{9e})$	$\dot{I}_{COM3} = \dot{E}_{x,\ 9e} - \dot{E}_{x,\ 9f} + \dot{W}_{BH,\ COM3}$	181.85	2.56
COM4	$\dot{W}_{BH,\ COM4} = \dot{m}_{9e}(h_{9h} - h_{9g})$	$\dot{I}_{COM4} = \dot{E}_{x,\ 9g} - \dot{E}_{x,\ 9h} + \dot{W}_{BH,\ COM4}$	200.25	2.82
COM5	$\dot{W}_{BH,\ COM5} = \dot{m}_{10e}(h_{10f} - h_{10e})$	$\dot{I}_{COM5} = \dot{E}_{x,\ 10e} - \dot{E}_{x,\ 10f} + \dot{W}_{BH,\ COM5}$	357.41	5.03
COM6	$\dot{W}_{BH,\ COM6} = \dot{m}_{10e}(h_{10h} - h_{10g})$	$\dot{I}_{COM6} = \dot{E}_{x,\ 10g} - \dot{E}_{x,\ 10h} + \dot{W}_{BH,\ COM6}$	100.20	1.41
COM7	$\dot{W}_{BH,\ COM7} = \dot{m}_{11e}(h_{11f} - h_{11e})$	$\dot{I}_{COM7} = \dot{E}_{x,\ 11e} - \dot{E}_{x,\ 11f} + \dot{W}_{BH,\ COM7}$	286.99	4.04
COM8	$\dot{W}_{BH,\ COM8} = \dot{m}_{11e}(h_{11h} - h_{11g})$	$\dot{I}_{COM8} = \dot{E}_{x,\ 11g} - \dot{E}_{x,\ 11h} + \dot{W}_{BH,\ COM8}$	300.09	4.22
COM9	$\dot{W}_{BH,\ COM9} = \dot{m}_{12e}(h_{12f} - h_{12e})$	$\dot{I}_{COM9} = \dot{E}_{x,\ 12e} - \dot{E}_{x,\ 12f} + \dot{W}_{BH,\ COM9}$	399.26	5.62
COM10	$\dot{W}_{BH,\ COM10} = \dot{m}_{12e}(h_{12h} - h_{12g})$	$\dot{I}_{COM10} = \dot{E}_{x,\ 12g} - \dot{E}_{x,\ 12h} + \dot{W}_{BH,\ COM10}$	453.76	6.39
HX4	$\dot{m}_{7a}h_{7a} + \dot{m}_{9c}h_{9c} = \dot{m}_{7b}h_{7b} + \dot{m}_{9d}h_{9d}$	$\dot{I}_{HX4} = (\dot{E}_{x,\ 7a} + \dot{E}_{x,\ 9c}) - (\dot{E}_{x,\ 7b} + \dot{E}_{x,\ 9d})$	13.46	0.19
HX5	$\dot{m}_{7b}h_{7b} + \dot{m}_{10c}h_{10c} = \dot{m}_{8a}h_{8a} + \dot{m}_{10d}h_{10d}$	$\dot{I}_{HX5} = (\dot{E}_{x,\ 7b} + \dot{E}_{x,\ 10c}) - (\dot{E}_{x,\ 8a} + \dot{E}_{x,\ 10d})$	151.75	2.14
HX6	$\dot{m}_{8b}h_{8b} + \dot{m}_{11c}h_{11c} = \dot{m}_{8c}h_{8c} + \dot{m}_{11d}h_{11d}$	$\dot{I}_{HX6} = (\dot{E}_{x,\ 8b} + \dot{E}_{x,\ 11c}) - (\dot{E}_{x,\ 8c} + \dot{E}_{x,\ 11d})$	571.22	8.04
HX7	$\dot{m}_{8d}h_{8d} + \dot{m}_{12c}h_{12c} = \dot{m}_{8e}h_{8e} + \dot{m}_{12d}h_{12d}$	$\dot{I}_{HX7} = (\dot{E}_{x,\ 8d} + \dot{E}_{x,\ 12c}) - (\dot{E}_{x,\ 8e} + \dot{E}_{x,\ 12d})$	185.72	2.61
HX8	$\dot{m}_{9a}h_{9a} + \dot{m}_{9d}h_{9d} = \dot{m}_{9b}h_{9b} + \dot{m}_{9e}h_{9e}$	$\dot{I}_{HX8} = (\dot{E}_{x,\ 9a} + \dot{E}_{x,\ 9d}) - (\dot{E}_{x,\ 9b} + \dot{E}_{x,\ 9e})$	104.50	1.47
HX9	$\dot{m}_{10a}h_{10a} + \dot{m}_{10d}h_{10d} = \dot{m}_{10b}h_{10b} + \dot{m}_{10e}h_{10e}$	$\dot{I}_{HX9} = (\dot{E}_{x,\ 10a} + \dot{E}_{x,\ 10d}) - (\dot{E}_{x,\ 10b} + \dot{E}_{x,\ 10e})$	211.62	2.98
HX10	$\dot{m}_{11a}h_{11a} + \dot{m}_{11d}h_{11d} = \dot{m}_{11b}h_{11b} + \dot{m}_{11e}h_{11e}$	$\dot{I}_{HX10} = (\dot{E}_{x,\ 11a} + \dot{E}_{x,\ 11d}) - (\dot{E}_{x,\ 11b} + \dot{E}_{x,\ 11e})$	100.00	1.41
HX11	$\dot{m}_{12a}h_{12a} + \dot{m}_{12d}h_{12d} = \dot{m}_{12b}h_{12b} + \dot{m}_{12e}h_{12e}$	$\dot{I}_{HX11} = (\dot{E}_{x,\ 12a} + \dot{E}_{x,\ 12d}) - (\dot{E}_{x,\ 12b} + \dot{E}_{x,\ 12e})$	166.30	2.34
EX4	$\dot{m}_{9b}h_{9b} = \dot{m}_{9c}h_{9c} + \dot{W}_{EX4}$	$\dot{I}_{EX4} = \dot{E}_{x,\ 9b} - \dot{E}_{x,\ 9c} - \dot{W}_{EX4}$	350.21	4.93
EX5	$\dot{m}_{10b}h_{10b} = \dot{m}_{10b}h_{10c} + \dot{W}_{EX5}$	$\dot{I}_{EX5} = \dot{E}_{x,\ 10b} - \dot{E}_{x,\ 10c} - \dot{W}_{EX5}$	666.16	9.37
EX6	$\dot{m}_{11b}h_{11b} = \dot{m}_{11c}h_{11c} + \dot{W}_{EX6}$	$\dot{I}_{EX6} = \dot{E}_{x,\ 11b} - \dot{E}_{x,\ 11c} - \dot{W}_{EX6}$	467.52	6.58
EX7	$\dot{m}_{12b}h_{12b} = \dot{m}_{12c}h_{12c} + \dot{W}_{EX7}$	$\dot{I}_{EX7} = \dot{E}_{x,\ 12b} - \dot{E}_{x,\ 12c} - \dot{W}_{EX7}$	856.36	12.05
EX8	$\dot{m}_{8c}h_{8e} = \dot{m}_{8f}h_{8f} + \dot{W}_{EX8}$	$\dot{I}_{EX8} = \dot{E}_{x,\ 8e} - \dot{E}_{x,\ 8f} - \dot{W}_{EX8}$	≈ 0.00	≈ 0.00
EVAP2	$\dot{m}_{9h}h_{9h} + \dot{m}_{air}h_{air,\ in} = \dot{m}_{9a}h_{9a} + \dot{m}_{air}h_{air,\ out}$	$\dot{I}_{EVAP\ \ 2} = (\dot{E}_{x,\ 9h} + \dot{E}_{x,\ air\ in}) - (\dot{E}_{x,\ 9a} + \dot{E}_{x,\ air\ out})$	115.35	1.62
EVAP3	$\dot{m}_{10h}h_{10h} + \dot{m}_{air}h_{air,\ in} = \dot{m}_{10a}h_{10a} + \dot{m}_{air}h_{air,\ out}$	$\dot{I}_{EVAP\ \ 3} = (\dot{E}_{x,\ 10h} + \dot{E}_{x,\ air\ in}) - (\dot{E}_{x,\ 10a} + \dot{E}_{x,\ air\ out})$	316.06	4.45
EVAP4	$\dot{m}_{11h}h_{11h} + \dot{m}_{air}h_{air,\ in} = \dot{m}_{11a}h_{11a} + \dot{m}_{air}h_{air,\ out}$	$\dot{I}_{EVAP\ \ 4} = (\dot{E}_{x,\ 11h} + \dot{E}_{x,\ air\ in}) - (\dot{E}_{x,\ 11a} + \dot{E}_{x,\ air\ out})$	169.49	2.39
EVAP5	$\dot{m}_{12h}h_{12h} + \dot{m}_{air}h_{air,\ in} = \dot{m}_{12a}h_{12a} + \dot{m}_{air}h_{air,\ out}$	$\dot{I}_{EVAP\ \ 5} = (\dot{E}_{x,\ 12h} + \dot{E}_{x,\ air\ in}) - (\dot{E}_{x,\ 12a} + \dot{E}_{x,\ air\ out})$	380.44	5.35
Total		$\dot{I}_{total}$	7106.00	100

expander. Thus, it depends on the overall liquefier's size, suitability, cost, etc. The proposed system (see Fig. 2) is an optimistic preliminary design process. However, it is still not very mature. The designer should take this into account when in the design process. Finally, more time and work is needed to find the best system to cool hydrogen gas from −193 °C to −253 °C. *In short, it is possible to obtain a cycle that has a better efficiency than what is mentioned. However, a better efficiency means a more complicated and more expensive system. Thus, the following information is needed to design the real plant: machinery from the manufacturers, cost of the materials, size of the heat exchangers, and so on.*

2.5. *Comparison of the proposed system to Ingolstadt liquefier*

In Table 7, the types of hydrogen liquefiers are the following: 1. Ingolstadt system, 2. the proposed system (MR system + four H_2 Joule–Brayton cascade system). The Ingolstadt system is from a paper by Kuz'menko et al. [4], *Comparison of thermodynamic efficiencies with Ingolstadt liquefier*. The proposed plant is from a simulation that is shown in Fig. 2. The system's net power consumptions to cool n-GH_2 from 25 °C to e-GH_2 at −193 °C and then e-GH_2 at −193 °C to e-GH_2 at −253 °C are $w_A = 1.36$ and $w_B = 3.99$ kWh/kg_{LH2}, respectively. Therefore, the overall power is $w_A + w_B = 5.35$ kWh/kg_{LH2}. Finally, the efficiency of the proposed plant is 54.02%, in comparison to the ideal liquefaction power of 2.89 kWh/kg_{LH2}; this efficiency is a lot better than Ingolstadt's, which is used as a reference (21.28%). Moreover, it is better than WE-NET's hydrogen liquefaction project [14] by Matsuda and Nagami. [2]. However, Quack's [3], and Valenti and Macchi's [6] systems do not explicitly mention whether they have high efficiencies. If not, the proposed system is the most efficient. Therefore, the proposed system has a great potential for improvement and can be used as a reference for future hydrogen liquefaction plants.

3. Economic analysis of the proposed plant with MR refrigeration

The cost of liquid hydrogen production consists of the following:

Drnevich et al. [21] states that:
LH_2 manufacturing cost ($/kg) = Capital cost + Energy cost + Operation and maintenance.
Kramer et al. [9] also states that:
Hydrogen cost ($/kg) = LH_2 manufacturing cost + Distribution cost + Retail site operations.

The energy cost is measured by the overall liquefier efficiency. The low efficiency liquefier consumes a lot of electrical power. In addition, when constructing a LH_2 plant, the capital cost should also be considered. It must be determined how the MR pre-cooling process is superior to the other pre-cooling cycles of Ingolstadt, Leuna, Quack, and Valenti and Macchi. Similarly, it must be determined how cooling hydrogen gas with multi-component refrigerant is different from the others, e.g., nitrogen and hydrogen (Ingolstadt, Leuna, Praxair, and

Table 7 – Comparison of the proposed system's to Ingolstadt liquefier's thermodynamic efficiency.

Parameter		System	
		Ingolstadt[a]	The proposed new cycle[b]
Capacity referred to liquid hydrogen	Ton per day	4.4 TPD	100 TPD
	kg/h	180	4166
	kg/s	0.05	1.1572
Para form content in the product, %		95	95
Pressure of liquid hydrogen, bar		1.3	1.3
Flow rates of streams in the cycle, kg/h:			
MR		–	151,473
hydrogen		1440	4618/5878/6926/7557
helium		–	–
nitrogen (liquid nitrogen requirement, kg/h)		1750	–
Compression pressure in the cycle, bar:			
MR		–	18/2
hydrogen		22	40/20/14/8.0/6.8/0.5
helium		–	–
nitrogen		1.4	–
Power consumption, kW:			
of MR compressor		–	5389
of all hydrogen compressors		1557	15,796
of all helium compressors		–	–
of all nitrogen compressors		–	–
of other equipments[f] at the MR cycle		–	291[f]
of other equipments[f] at the four H_2 J-B cascade cycle		–	848[f]
All expander power, kW:		N/A	1,027[c]
Total energy consumption with due regard for the consumption for liquid nitrogen from an air separation plant at the rate of 0.5 kWh/kg of liquid nitrogen, kWh		2432	–
Net $\dot{W}_A$, kW		875	5680
Net $\dot{W}_B$, kW		1557	16,644
Net w_A, kWh/kg$_{LH2}$		4.86	1.36
Net w_B, kWh/kg$_{LH2}$		8.65	3.99
Overall cycle specific energy consumption for liquefaction, kWh/kg$_{LH2}$		≈13.58[d]	5.35
The thermodynamically ideal liquefaction system, kWh/kg$_{LH2}$		2.89[e]	2.89[e]
Thermodynamic efficiency with due regard for ortho-para conversion, %		21.28	54.02

a Information is from Kuzmenko et al. [4].
b Info from Fig. 2, PRO/II simulation flow sheet of the proposed large-scale 100-TPD LH_2 plant with MR and four H_2 Joule–Brayton cascade cycles.
c The sum of all expander powers, kW: mechanical conversion is 98% from the expanders.
d This is modified from Kuz'menko et al. [4]: 4.86 + 8.65 = 13.51 kWh/kg$_{LH2}$.
e Minimum theoretical exergy consumption from feed 21 bar, 25 °C, n-GH_2 to: 1.3 bar, −253 °C, 95% p-LH_2.
f Electricity consumptions for the cooling loads due to water pumps and air-cooled fans in the after coolers and evaporative condensers. They are assumed to be around 5% of power consumption from compressors.

WE-NET), propane (Quack), and helium (Valenti and Macchi). The overall size of the compressor and the heat exchanger is a measure. It reflects the capital or construction cost of the entire plant.

3.1. *Comparison of compressor's size to other refrigeration systems*

This section compares the compressor's swept volumes. From Table 8, the ratio between the suction volumetric flow rate of the MR and the hydrogen, $\dot{V}_{MR}/\dot{V}_{H2}$ is less than with nitrogen, $\dot{V}_{N2}/\dot{V}_{H2}$. Ingolstadt uses both gas and liquid nitrogen to cool the hydrogen feed stream. Even though hydrogen has the smallest suction volumetric flow rate when it is used in refrigeration systems to cool hydrogen gas, it is impossible to use because of its high power consumption. Therefore, the overall MR compressor's size for the proposed large-scale MR system is smaller than closed liquid nitrogen system with recondensation such as WE-NET's nitrogen refrigeration system.

3.2. *Comparison of the heat exchanger's size to other refrigeration systems*

The right way to size the heat exchanger is by (1) using the LMTD or NTU to find the approximate size, or by (2) dividing the whole heat exchanger into many small finite volumes/pieces together with the computational balance equations (mass, momentum, and energy) to find the actual size. The plate fin heat exchangers are widely used in cryogenic applications due to their compactness, low weight, and high effectiveness, and their use is proposed here. Aluminum is the most commonly used material, but stainless steel construction is employed for high pressure and high temperature applications. Fin geometries can be plain, offset strip, perforated, wavy, pin, or louvered.

Table 8 – Comparison of the proposed large-scale plant to the MR refrigeration system's overall compressor swept volume, together with the overall heat exchanger's size in comparison to the Ingolstadt/Leuna liquefier (nitrogen refrigeration) and the Valenti liquefier (helium refrigeration).

Parameter	Unit	Refrigerant				
		MR_{HX1}[a]	G-Hydrogen	G-Nitrogen[b]	L-Nitrogen	G-Helium[c]
$\dot{m}_i/\dot{m}_{H2}$	–	25.70	1	$\frac{1{,}750\ kg/h}{180\ kg/h} = 9.70$	9.70	$\frac{27.35\ kg/s}{10.00\ kg/s} = 2.75$
$\dot{V}_i/\dot{V}_{H2}$	–	12.9	1	$\frac{1{,}400\ m^3/hr}{100\ m^3/hr} = 14.31$	14.31	$\frac{161.83\ m^3/s}{5.43\ m^3/s} = 29.80$
α_i/α_{H2}	–	Gas MR: 0.522 Liquid MR: 1.26 Boiling MR: 1.89	Gas: 1	Gas: 0.2892	0.2490 Boiling: ≈0.28–0.4	Gas: 0.9723
$A_{HX,\,i}/A_{HX,\,MR}$	–	The smallest	Bigger than MR	The largest	Bigger than G-Helium	Bigger than G-Hydrogen
Thermo-physical properties below are at 1 bar and 0 °C. Data are from SRK simulation model in PRO/II.						
c_P	kJ/kg-°C	1.02/2.01[d]	14.34	1.04	2.04[e]	5.19
k	kW/m-°C	0.02/0.13[d]	0.16	0.02	0.02[e]	0.142
Latent heat of vaporization	kJ/kg	N/A	446	–	199[e]	20
ρ	kg/m^3	4.5/655[d]	0.085	1.25	808[e]	0.169
μ	Pa.s	0.00001/0.00033[d]	0.00001	0.00002	0.00018[e]	0.00002
Pr	–	0.51/5.10[d]	0.89625	1.04	18.36	0.73098
Gas price	–	Most expensive	Expensive	The cheapest		Very expensive

a The proposed large-scale plant with MR refrigeration system; in particular, the analysis is at the top MR heat exchanger.
b Ingolstadt liquefier.
c Valenti liquefier. $\dot{m}_{H2}$ is the mass flow rate of the feed hydrogen gas into the liquefier at 21 bar and 25 °C.
d Properties of the MR at stream 37 between gas/liquid at 2 bar and −50 °C.
e Properties of liquid nitrogen at 1 bar and −200 °C. $\dot{V}_{H2}$ is the volumetric flow rate (m^3/s) of the feed hydrogen gas into the liquefier at 21 bar and 25 °C. α_i/α_{H2} is the ratio between the refrigerant heat transfer coefficient (kW/m^2-°C) and the hydrogen gas coefficient (kW/m^2-°C). A_i/A_{MR} is the ratio between the refrigerant heat transfer area (m^2) and the MR heat transfer area (m^2).

Among these, the offset strip fin is frequently adopted for its high heat transfer coefficient. It is the most widely used finned surface, particularly in high effectiveness heat exchangers that are employed in cryogenic applications.

Fig. 3 (a) explains that a small heat transfer $d\dot{Q}$ from the hot stream hydrogen gas (node i to $i+1$ and $i-1$) can be cooled with a cold gas that is generally in the liquefaction process, e.g., hydrogen, nitrogen, or helium. It is a small finite volume inside of the heat exchanger, as depicted in Fig. 3(b).The heat exchanger has a stack arrangement. The gases are compared with the MR to determine which one can best reduce the heat exchanger's size. In Fig. 3(c), the heat transfer is from both the hot stream hydrogen and the MR hot stream to the MR cold mixture stream (node to $i+1$ and $i-1$ to i). Fig. 3(d) depicts the possible arrangement of the streams in the MR heat exchangers (HX1, HX2, and HX3) for the proposed large-scale system, as in Fig. 2. The heat transfer and flow friction characteristics of the plate fin surfaces are presented in terms of the Colburn factor, j, and the Fanning friction factor, f, versus the Reynolds number, Re; the relationships are different for the different surfaces. Usually, turbulent flow (approximately 3000 to 10,000) is mandatory for most heat exchangers to attain a better heat transfer coefficient and for a compact size. However, with more turbulence, the pressure drop increases. Thus, an optimization should be done to compute the velocity, pressure, and temperature fields to determine the over appropriate range of the Reynolds number and the geometric dimensions. In order to compare the size of the heat exchanger for different fluids, we will first start with the heat transfer coefficient for any flow in a channel.

$$\alpha = \frac{jGc_P}{Pr^{2/3}} \tag{1}$$

Manglik and Bergles [22] proposed the Colburn factor, j, in Eq. (1) to describe the right trend of the heat transfer behavior for a single phase flow and a channel with offset strip fins in the laminar, transition, and turbulent flow regimes:

$$j = 0.6522 Re_{Dh}^{-0.5403} \beta^{-0.1541} \delta^{0.1499} \gamma^{0.0678} \times \left[1 + 5.269 \times 10^{-5} Re_{Dh}^{1.34} \beta^{0.504} \delta^{0.456} \gamma^{-1.055}\right]^{0.1} \tag{2}$$

where $Re_{Dh} = (GD_h)/\mu$. β, δ, and γ are geometrical descriptions of the typical offset strip fin core inside of the heat exchanger's channel. Then, the ratio of the heat transfer coefficient (α_i) for a flowing gas (hydrogen, nitrogen, or helium) to that of hydrogen's (α_{H2}) is used as a comparison. It is assumed that all of the channel sizes and fin dimensions of the pre-cooled hydrogen and cooling medium are the same. By eliminating the offset strip fin's geometrical descriptions that are all assumed to be the same, Eq. (1) can be expressed as follows:

$$\frac{\alpha_i}{\alpha_{H2}} = \left(\frac{\mu_{H2}}{\mu_i} \cdot \frac{\dot{m}_i}{\dot{m}_{H2}}\right)^{-0.5403} \left(\frac{\dot{m}_i}{\dot{m}_{H2}}\right) \left(\frac{c_{Pi}}{c_{PH2}}\right) \left(\frac{Pr_{H2}}{Pr_i}\right)^{2/3} \tag{3}$$

where $\dot{m}_i/\dot{m}_{H2}$, μ, c_P, and Pr are from Table 8. For simplicity, it is assumed that the fluid's thermo-physical properties at different temperatures (from −250 °C to 0 °C) are quite the same at 0 °C. Thus, the comparison of the heat transfer coefficients for flowing hydrogen, nitrogen, or helium gas to that of hydrogen's in the heat exchanger is calculated and shown in Table 8. It seems that hydrogen gas has the highest heat transfer coefficient in comparison to hydrogen gas itself.

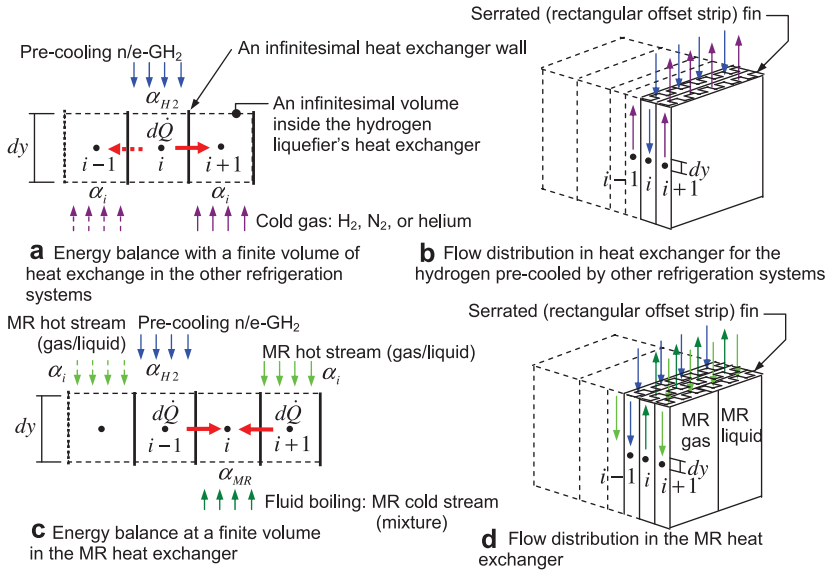

Fig. 3 – Proposed plate fin heat exchanger for the proposed hydrogen liquefaction system.

Then, it is followed by helium gas, liquid nitrogen, and nitrogen gas ($\alpha_{H2}>\alpha_{Helium}>\alpha_{LN2}>\alpha_{GN2}$).

Next, the analysis compares the heat exchanger's size or area, A_{HX}. Actually, the *LMTD* is used if all of the outlet and inlet stream temperatures are known as below:

$$\dot{Q}_{HX} = FU_{HX}A_{HX}(LMTD_{HX}) \tag{4}$$

where $\dot{Q}_{HX}$ is the overall heat transfer for the whole heat exchanger (kW). F is the correction factor. When the fin efficiency and the wall resistance are neglected for simplicity, U_{HX} can be expressed in dominant terms, e.g., α_{H2} and α_i, as follows:

$$\frac{1}{U_{HX}} = \frac{1}{\alpha_{H2}} + \frac{1}{\alpha_i} \tag{5}$$

α_i is a cold fluid (hydrogen gas, helium gas, liquid nitrogen, or nitrogen gas) that cools hydrogen gas in a heat exchanger. Finally, Eq. (5) in combination with Eq. (4) gives a comparison of the heat transfer area of the gas (hydrogen gas, helium gas, liquid nitrogen, or nitrogen gas) as a cooling media to that of the MR, which is expressed in an inverse relation between its heat transfer coefficient as follows:

$$\frac{A_{HX,i}}{A_{HX,\ MR}} \propto \frac{\alpha_{MR}}{\alpha_i} \tag{6}$$

The MR fluid in the MR refrigeration system and the liquid nitrogen at Ingolstadt and Leuna, which flows inside of the heat exchanger, are two-phase flows. The others are single phase flows. Boiling inside of the heat exchanger is dominated by two phenomena: convective boiling and nucleated boiling. Thus, the local boiling heat transfer coefficient, as in this case, can be formulated by using superposition (which includes both nucleated and convective boiling effects) and is commonly represented as follows [23]:

$$\alpha_{TP} = \alpha_{nb} + \alpha_{cb} \tag{7}$$

where α_{TP} is the local two-phase flow heat transfer coefficient (kW/m^2-°C). α_{nb} is the nucleated heat transfer coefficient (kW/m^2-°C) and α_{cb} is the heat transfer coefficient (kW/m^2-°C). It seems to have been accepted that at high heat fluxes or low qualities, nucleated boiling has a larger influence than convective boiling. For the considered condition, the effect of nucleated boiling is small and the dominant heat transfer mechanism is two-phase forced convection. If noticed from Eq. (1) for the same flow rate of any fluid, in most cases, a single phase flow of liquid has a higher heat transfer coefficient than that of the gas due to the higher c_p. A study from Feldman et al. [24] seems to imply that boiling heat transfer inside of the plate fin heat exchanger usually has a boiling coefficient around 1.5–2 times greater than the liquid flow.

At last, the values of $A_{HX,i}/A_{HX,MR}$ are calculated in Table 8. In the table, the most important thing is boiling heat transfer coefficient of MR refrigerant in the MR cycle is the highest when compared to feed hydrogen gas's as a reference (Eq. (3): $\alpha_{MR}/\alpha_{H2} = 1.89$ of Boiling MR). For that reason, it can be concluded that if the feed hydrogen gas is cooled by hydrogen gas, helium gas, liquid nitrogen, or nitrogen gas; the size of the heat transfer area or heat exchanger is the smallest when using hydrogen gas because it has the highest heat transfer coefficient. It is then followed by helium gas and liquid nitrogen. Eq. (6) proves this statement. *In summary, it seems that MR has the highest heat transfer coefficient due to boiling; thus, the trend is that it may offer the smallest heat exchanger size in comparison to using other fluids to cool the hydrogen liquefaction system.*

4. Conclusion

For cooling n-GH$_2$ from 25 °C to be e-GH$_2$ around −193 °C, the MR refrigeration system is recommended with the simulation's net

power at 1.36 kWh/kg_{LH2}, in comparison to the ideal of 0.51 kWh/kg_{LH2}. The compressor and expander efficiencies are assumed to be 80%, which is close to the actual values for general large sizes that are available in the general market. With 100% efficiencies for ideal compression and expansion, the power consumption of the MR system is 1.07 kWh/kg_{LH2}. The largest loss is from the compressors and expanders. The other loss is from the heat exchangers of the MR system. It is the best in comparison to the nitrogen, helium, and propane refrigeration systems. In addition, for cooling from −193 °C e-GH_2 to −253 °C e-GH_2, the four H_2 Joule–Brayton cascade refrigeration system is recommended due to its improved efficiency. The net power for the proposed system is 3.99 kWh/kg_{LH2}, in comparison to the ideal of 2.38 kWh/kg_{LH2}. Similarly, the losses are from the compressors, expanders, and heat changers. It is the best in comparison to the nitrogen and helium refrigeration systems. The overall power consumption of the whole system is 1.36 kWh/kg_{LH2} + 3.99 kWh/kg_{LH2} = 5.35 kWh/kg_{LH2}. Usually, the liquefier at Ingolstadt is a reference with an energy consumption of 13.58 kWh/kg_{LH2} and an efficiency of 21.28%. *While the proposed system is 54.02% or more, it depends on the assumption of the compressor and expander efficiencies*. The efficiency of the proposed system can reach very close to the ideal's if the compressors, expanders, and heat exchangers are ideal and if there is no pressure drop. Moreover, the system has some smaller-size heat exchangers, a much smaller compressor motor, and a smaller crankcase compressor for both the MR and the four H_2 Joule–Brayton cascade cycles, which is due to the smaller energy consumption and hydrogen mass flow rates in the heat exchangers. Nitrogen pre-cooled systems that are designed for very large-scale systems (like Ingolstadt's) will require an additional nitrogen liquefaction cycle to liquefy nitrogen gas back (like WE-NET's). It will be a much larger size plant. Thus, the proposed new system could possibly be the lowest specific construction cost plant in comparison to Ingolstadt and Leuna. Therefore, the proposed system has a great potential for improvement and is recommended as a reference for future hydrogen liquefaction plants.

Acknowledgement

The author wishes to thank the Department of Energy and Process Engineering, Norwegian University of Science and Technology for a research fellow grant.

Nomenclature

Symbols

A	area/heat transfer area, m^2
c_P	specific heat capacity, kJ/kg-°C
e_x	specific exergy, kJ/kg
$\dot{E}_x$	rate of exergy flow = $\dot{m}e_x$, kW
F	correction factor
f	friction factor
G	mass flow rate, kg/m^2-s
h	specific enthalpy, kJ/kg
$\dot{I}$	rate of irreversibility, kW
j	Colburn factor, $j = St.Pr^{2/3}$ or $Nu/(Re.Pr^{1/3})$
k	thermal conductivity, kW/m-°C
$LMTD$	Log Mean Temperature Difference, °C
$\dot{m}$	mass flow rate, kg/s
$\dot{Q}$	rate of heat transfer, kW
P	pressure, bar
Pr	Prandtl number
Re	Reynolds number
s	specific entropy, kJ/kg-K
T	temperature, °C
U	overall heat transfer coefficient, kW/m^2-°C
v	specific volume, m^3/kg
V	volume, m^3
$\dot{V}$	volumetric flow rate, m^3/s
w	specific work/energy requirement, kJ/kg_{LH2} or kWh/kg_{LH2}, kJ/kg_{LH2}
$\dot{W}$	power, kW

Abbreviations

COM	compressor
EVAP	evaporative condenser
EX	expander
GH_2	gas hydrogen
HX	heat exchanger
J-B	Joule–Brayton
LH_2	liquid hydrogen
LIQ	liquid separator
n-	normal
MIXER	mixer of streams
MR	multi-component refrigerant/multi-mixed refrigerant
O-P	ortho-para
p-	para
RH	relative humidity
TPD	ton per day

Greek letters

α	heat transfer coefficient, kW/m^2-°C
β, δ, γ	fin geometric parameters
ρ	density, kg/m^3

Subscripts

1, 2,…to n	of the numbers: 1, 2,… to n/of stream numbers: 1, 2,… to n
air	of flowing air
A	of system A
B	of system B
BH	brake horse power
cb	convective boiling
D_h	hydraulic diameter, m
EX	of expander
i	of a single phase fluid: nitrogen, hydrogen, helium, or MR
in	inlet
$isen$	isentropic
H	high
$H2$	of hydrogen stream
$H2\ Com$	of hydrogen compressor
HX	of heat exchanger
L	low
MR	of MR stream
$MR\ Com$	of MR compressor

nb	of nucleate boiling
net	net of cycle power consumption = compressors − expanders
opt int	optimum intermediate
out	outlet
TP	of two-phase flow
V	volumetric

REFERENCES

[1] Bracha M, Lorenz G, Patzelt A, Wanner M. Large-scale hydrogen liquefaction in Germany. Int J Hydrogen Energy 1994;19(1):53–9.

[2] WE-NET: Summary of annual reports Matsuda H, Nagami M. Study of large hydrogen liquefaction process. Available from. Kanagawa, Japan: Nippon Sanso Corp., http://www.enaa.or.jp/WE-NET/ronbun/1997/e5/sanso1997.html; 1998 [accessed 14.06.09].

[3] Quack H. Conceptual design of a high efficiency large capacity hydrogen liquefier. Adv Cry Eng 2002;47:255–63.

[4] Kuz'menko IF, Morkovkin IM, Gurov EI. Concept of building medium-capacity hydrogen liquefiers with helium refrigeration cycle. Chem Petro Eng 2004;40(1–2):94–8.

[5] Shimko M, Gardiner M. Innovative hydrogen liquefaction cycle. Available from, http://www.hydrogen.energy.gov/pdfs/progress08/iii_7_shimko.pdf; 2007 [accessed 14.06.09].

[6] Valenti G, Macchi E. Proposal of an innovative, high-efficiency, large-scale hydrogen liquefier. Int J Hydrogen Energy 2008;33(12):3116–21.

[7] Berstad D, Stang JH, Neksa P. Large-scale hydrogen liquefier utilising mixed-refrigerant pre-cooling. Int J Hydrogen Energy 2010;35(10):4512–23.

[8] Krasae-in S, Stang JH, Neksa P. Development of large-scale hydrogen liquefaction processes from 1898 to 2009. Int J Hydrogen Energy 2010;35(10):4524–33.

[9] Kramer GJ, Huijsmans J, Austgen D. Clean and green hydrogen. In: 16th world hydrogen energy conference, 16/13-16 June 2006 Lyon, France. Available from:http://www.shell.com/static/hydrogen-en/downloads/speeches/speech_clean_green_hydrogen_1.pdf [accessed 05.06.2009]

[10] Bottura L. Cryogenic mixed refrigerant processes. Cryogenics 2009;49(12):745–6.

[11] Chrz V. Cryogenic mixed refrigerant processes. Int J Refrigeration 2010;33(3):648–9.

[12] Mafi M, Amidpour M, Naeynian SMM. Development in mixed refrigerant cycles used in olefin plants. In: Proceedings of the first annual gas processing symposium. Doha, Qatar; 10–12 January 2009. p. 154–61.

[13] Bosma P, Nagelvoort RB. Liquefaction technology; developments through history. In: Proceedings of the first annual gas processing symposium. Doha, Qatar; 10–12 January 2009. p. 19–31.

[14] Flynn TM. Cryogenic engineering. 2nd ed. NY: Marcel Dekker Press; 1997.

[15] Barron RF. Cryogenic systems. Oxford, United Kingdom: Oxford University Press; 1966.

[16] Mitsugi C, Harumi A, Kenzo F. WE-NET: Japanese hydrogen program. Int J Hydrogen Energy 1998;23(3):159–65.

[17] Leachman JW, Jacobsen RT, Penoncello S, Lemmon EW. Fundamental equations of state for para hydrogen, normal hydrogen, and ortho hydrogen. J Phys Chem Reference Data 2009;38(3):721–48.

[18] National Institute of Standards and Technology (NIST). Thermophysical properties of hydrogen, http://www.boulder.nist.gov/div838/Hydrogen/Properties/Properties.htm. Available from[accessed 19.05.10].

[19] Krasae-in S, Stang JH, Neksa P. Exergy analysis on the simulation of a small-scale hydrogen liquefaction test rig with a multi-component refrigerant refrigeration system. Int J Hydrogen Energy 2010;35(15):8030–42.

[20] HumidAirWeb: online psychrometric calculator by MegaWatSoft. Available from, http://www.psychrometric-calculator.com [accessed 28.05.10].

[21] Drnevich R. Hydrogen delivery – liquefaction & compression. Praxair, strategic initiatives for hydrogen delivery workshop. Available from, http://www1.eere.energy.gov/hydrogenandfuelcells/pdfs/liquefaction_comp_pres_praxair.pdf; May 7, 2003 [accessed 20.05.09].

[22] Manglik RM, Bergles AE. Heat transfer and pressure drop correlations for the rectangular offset strip fin compact heat exchangers. Exp Thermal Fluid Sci 1995;10(2):171–80.

[23] Kim B, Sohn B. An experimental study of flow boiling in a rectangular channel with offset strip fins. Int J Heat Fluid Flow 2006;27(3):514–21.

[24] Feldman A, Marvillet C, Lebouche M. Nucleate and convective boiling in plate fin heat exchangers. Int J Heat Mass Transfer 2000;43(18):3433–42.